Program and Abstract Volume

LUNAR AND PLANETARY INSTITUTE

LPI Contribution No. 1483

LUNAR RECONNAISSANCE ORBITER SCIENCE TARGETING MEETING

Arizona State University, Tempe, Arizona

June 9–11, 2009

Conveners

Steve Mackwell
USRA/Lunar and Planetary Institute

Mark Robinson
Arizona State University

Richard Vondrak
NASA Goddard Space Flight Center

Jennifer Heldmann
NASA Headquarters, Science Mission Directorate (SMD)

Michael Wargo
NASA Headquarters, Exploration System Mission Directorate (ESMD)

Organizing Committee

Mark Robinson, *Arizona State University*
Bradley Thomson, *Johns Hopkins University/Applied Physics Laboratory*
Lisa Gaddis, *U.S. Geological Survey*
Brad Jolliff, *Washington University*
John Keller, *NASA Goddard Space Flight Center*
Samuel Lawrence, *Arizona State University*
Steve Mackwell, *USRA/Lunar and Planetary Institute*
Wendell Mendell, *NASA Johnson Space Center*
Clive Neal, *University of Notre Dame*
Harrison Schmitt, *University of Wisconsin/Madison*
Dave Smith, *NASA Goddard Space Flight Center*
Jeff Taylor, *University of Hawaii*

Local Organizing Committee

Carmen Salas, *Arizona State University*
Nicki Staab, *Arizona State University*

Lunar and Planetary Institute 3600 Bay Area Boulevard Houston TX 77058-1113

LPI Contribution No. 1483

Compiled in 2009 by
LUNAR AND PLANETARY INSTITUTE

The Lunar and Planetary Institute is operated by the Universities Space Research Association under a cooperative agreement with the Science Mission Directorate of the National Aeronautics and Space Administration.

Abstracts in this volume may be cited as

Author A. B. (2009) Title of abstract. In *Lunar Reconnaissance Orbiter Science Targeting Meeting*, p. XX. LPI Contribution No. 1483, Lunar and Planetary Institute, Houston.

This volume is distributed by

ORDER DEPARTMENT
Lunar and Planetary Institute
3600 Bay Area Boulevard
Houston TX 77058-1113, USA
Phone: 281-486-2172
Fax: 281-486-2186
E-mail: order@lpi.usra.edu

A limited number of copies are available for the cost of shipping and handling.
Visit the LPI Online Store at https://www.lpi.usra.edu/store/products.cfm.

ISSN No. 0161-5297

Preface

This volume contains abstracts that have been accepted for presentation at the Lunar Reconnaissance Orbiter Science Targeting Meeting, June 9–11, 2009, Tempe, Arizona.

Administration and publications support for this meeting were provided by the staff of the Publications and Program Services Department at the Lunar and Planetary Institute.

Contents

Program

Tuesday, June 9, 2009
WELCOME AND OPENING PLENARY
8:00 a.m.

8:00 a.m. Robinson M. S. Hodges K.
Welcome and Introduction

8:10 a.m. Robinson M. S. *
Agenda Overview and Logistics

8:20 a.m. Schmitt H. H. *
LRO Science Measurements from Jack's Perspective

9:00 a.m. Vondrak R. *
LRO Mission Overview: Instrument Capabilities and Science Objectives

9:30 a.m. Jolliff B. L. *
LRO Science Measurements: Targeting Strategy and Constraints

10:00 a.m. BREAK

10:15 a.m. Gruener J. E. * Joosten B. K.
NASA Constellation Program Office Regions of Interest on the Moon: A Representative Basis for Scientific Exploration, Resource Potential, and Mission Operations **[#6036]**

10:30 a.m. Lucey P. G. * Gillis-Davis J. T. Hawke B. R. Taylor L. A. Duke M. B. Brady T. Mosher T.
LEAG Review of Constellation Program Regions of Interest for Human Exploration of the Moon **[#6022]**

10:45 a.m. Paige D. *
LRO Diviner Imaging Strategies

11:15 a.m. Nozette S. *
Mini-RF Capabilities and Limitations for Science Measurements

11:45 a.m. Pieters C. M. * Boardman J. Buratti B. Clark R. Combe J.-P. Green R. Head J. W. III Hicks M. Isaacson P. Klima R. Kramer G. Lundeen S. Malaret E. McCord T. B. Mustard J. Nettles J. Petro N. Runyon C. Staid M. Sunshine J. Taylor L. Tompkins S. Varanasi P. [INVITED]
Characterization of Lunar Mineralogy: The Moon Mineralogy Mapper (M^3) on Chandrayaan-1 **[#6002]**

12:15 p.m. LUNCH

Tuesday, June 9, 2009
LUNAR REGOLITH
1:15 p.m. Basha Family Library

Chair: **Michael Duke**

1:15 p.m. Mendell W. W. * [INVITED]
The Lunar Regolith as a Remote Sensing Target for the Lunar Reconnaissance Orbiter (LRO) **[#6018]**

1:45 p.m. McKay D. S. * [INVITED]
Do Lunar Pyroclastic Deposits Contain the Secrets of the Solar System? **[#6014]**

2:15 p.m. Plescia J. B. * [INVITED]
Understanding the Physical Evolution of the Lunar Regolith Using LRO Data **[#6032]**

2:45 p.m. Nozette S. * Bussey D. B. J. Butler B. Carter L. Gillis-Davis J. Goswami J. Heggy E. Kirk R. Misra T. Patterson G. W. Robinson M. Raney R. K. Spudis P. D. Thompson T. Thompson B. Ustinov E.
Joint LROC — Mini-RF Observations: Opportunities and Benefits **[#6041]**

3:05 p.m. BREAK

3:15 p.m. Crawford I. A. * Joy K. H. Fagents S. A. Rumpf M. E.
The Importance of Lunar Palaeoregolith Deposits and the Role of Lunar Reconnaissance Orbiter **[#6007]**

3:35 p.m. Greenhagen B. T. * Paige D. A.
Diviner Lunar Radiometer Targeting Capabilities **[#6028]**

3:55 p.m. Plenary Discussion of Target Priorities

5:15 p.m. END OF SESSION

Tuesday, June 9, 2009
VOLCANISM: TIMING, FORM, AND COMPOSITION
1:15 p.m. Carson

Chair: Ronald Greeley

1:15 p.m. Greeley R. * [INVITED]
Lunar Volcanism: Timing, Form, and Composition **[#6001]**

1:45 p.m. Head J. W. III* Wilson L. [INVITED]
Lunar Volcanism in Space and Time: Range of Eruption Styles and Implications for Magma Ascent and Emplacement **[#6024]**

2:15 p.m. Gaddis L. R. * Robinson M. S. Hawke B. R. Giguere T. Gustafson O. Lawrence S. J. Stopar J. D. Jolliff B. L. Bell J. F. III [INVITED]
LRO Targeting of Lunar Pyroclastic Deposits **[#6025]**

2:45 p.m. Shearer C. K. * [INVITED]
Lunar Basalts as Probes of the Moon's Mantle and Recorders of Crustal Growth **[#6021]**

3:15 p.m. BREAK

3:25 p.m. Keszthelyi L. P. *
Imaging Rilles and Flood Lavas with LROC **[#6029]**

3:45 p.m. Williams D. A. * Garry W. B. Keszthelyi L. P. Kerr R. C. Jaeger W. L.
Lunar Sinuous Rilles: Reassessing the Role of Erosion by Flowing Lava **[#6008]**

4:05 p.m. Plenary Discussion of Target Priorities

5:15 p.m. END OF SESSION

Tuesday, June 9, 2009
POSTER SESSION
6:00 p.m. Carson

Crawford I. A. Smith A. Gowen R. A. Joy K. H. UK Penetrator Consortium
MoonLITE: Science Case and Targeting Considerations **[#6006]**

Foing B. H. Koschny D. Grieger B. Josset J.-L. Beauvivre S. Grande M. Huovelin J. Keller H. U. Mall U. Nathues A. Malkki A. Noci G. Sodnik Z. Kellett B. Pinet P. Chevrel S. Cerroni P. de Sanctis M. C. Barucci M. A. Erard S. Despan D. Muinonen K. Shevchenko V. Shkuratov Y. Ellouzi M. Peters S. Borst A. Baxkens F. Boche-Sauvan L. Mahapatra P. Almeida M. Frew D. Volp J. Heather D. McMannamon P. Camino O. Racca G.
SMART-1 Results and Targets for LRO **[#6049]**

Joy K. H. Grindrod P. M. Crawford I. A. Lintott C. T. Smith A. Roberts D. Fortson L. Bamford S. Cook A. C. Bugiolacchi R. Balme M. R. Gay P.
Moon Zoo: Utilizing LROC Lunar Images for Outreach and Lunar Science **[#6035]**

Beyer R. A. Archinal B. Li R. Mattson S. McEwen A. Robinson M.
LROC Stereo Observations **[#6046]**

Cloutis E. Norman L.
Reflectance Spectroscopy of Single Mineral Grains: Implications for Lunar Remote Sensing **[#6020]**

Hiesinger H. Klemm K. van der Bogert C. H. Reiss D. Head J. W.
Lunar Mare Basalts: Scientifically Important Targets for LROC **[#6038]**

Stopar J. D. Hawke B. R. Lawrence S. J. Robinson M. S. Giguere T. Gaddis L. R. Jolliff B. L.
LROC Targeting of Lunar Domes, Cones, and Associated Volcanic Features **[#6039]**

Bell J. F. III Pritchard M. E. Schiff A. C. Gustafson J. O. Williams N. R. Watters T. R.
LRO Targeting of Lunar Tectonic Features **[#6011]**

Wyatt M. B. Donaldson Hanna K. L. Pieters C. M. Helbert J. Maturilli A. Greenhagen B. T. Paige D. A. Lucey P. G.
Diviner Constraints on Plagioclase Compositions as Observed by the Spectral Profiler and Moon Mineralogy Mapper **[#6026]**

Conrad A. R. Lyke J. E. Wooden D. Woodward C. Lucey P.
Acquisition and Tracking of the LCROSS Impact Site with Keck-II **[#6023]**

Wingo D. R. Lundquist C. A.
Coordinating LOIRP Enhanced Lunar Orbiter and Lunar Reconnaissance Orbiter High Resolution Images for Selected Science and Exploration Targets **[#6044]**

Crotts A.
High Resolution Imaging of Sites of Rapid Changes on the Lunar Surface **[#6013]**

Chaufray J.-Y. Retherford K. D. Gladstone G. R. Hurley D. M. Hodges R. R.
Lunar Argon Cycle Modeling **[#6015]**

Wright S. P. Newsom H. E.
Targeted Search near Lunar Poles for Potential Alteration Resulting from Impact Cratering into Volatile-"rich" Terrains **[#6045]**

Retherford K. D. Gladstone G. R. Stern S. A. Kaufmann D. E. Parker J. Wm. Egan A. F. Greathouse T. K. Versteeg M. H. Slater D. C. Davis M. W. Steffl A. J. Miles P. F. Hurley D. M. Pryer W. R. Hendrix A. R. Feldman P. D.
LRO/LAMP Expected Data Products: Overview of FUV Maps and Spectra **[#6047]**

Wednesday, June 10, 2009
COMPOSITION OF THE CRUST AND CLUES TO THE INTERIOR
8:00 a.m. Carson

Chair: **Paul Lucey**

8:00 a.m. Announcements

8:10 a.m. Jolliff B. L. * [INVITED]
Lunar Crustal Rock Types, Global Distribution, and Targeting **[#6040]**

8:40 a.m. Korotev R. L. * [INVITED]
Lunar Surface Geochemistry and Lunar Meteorites **[#6005]**

9:10 a.m. Norman M. D. * [INVITED]
Lunar Anorthosites as Targets for Exploration **[#6012]**

9:40 a.m. Johnson C. L. Watters T. R. Mackwell S. J. [INVITED]
What New can LRO Tell Us About Lunar Thermal Evolution, Interior Structure and Dynamics? **[#6051]**

10:10 a.m. BREAK

10:20 a.m. Hood L. L. * [INVITED]
Lunar Magnetism **[#6004]**

10:50 a.m. Lucey P. G. * Lawrence S. J. Robinson M. R. Greenhagen B. T. Paige D. A. Wyatt M. B. Hendrix A. R. [INVITED]
The Compositional Contribution of LRO **[#6019]**

11:20 a.m. Plenary Discussion of Target Priorities

12:00 p.m. LUNCH

Wednesday, June 10, 2009
HABITATION AND LUNAR RESOURCES
8:00 a.m. Basha Family Library

Chair: Jeff Plescia

8:00 a.m. Announcements

8:10 a.m. Duke M. B. * [INVITED]
Lunar Resources and LRO **[#6033]**

8:40 a.m. Gertsch L. S. * [INVITED]
Lunar Mining: Knowns, Unknowns, Challenges, and Technologies **[#6031]**

9:10 a.m. Schwadron N. * [INVITED]
Lunar Radiation Environment

9:40 a.m. Lawrence, S. * [INVITED]
LRO and Remote Observations of Lunar Resources

10:10 a.m. BREAK

10:20 a.m. Taylor L. A. * [INVITED]
How In-Situ Resource Utilization (ISRU) Fits into Lunar Outpost Concepts and Requirements on LRO Target Selection

10:50 a.m. Mitrofanov I. G. * Sanin A. S. Mokrousov M. I. Litvak M. L. Kozyrev A. S. Malakhov A. A. Trety'akov V. I. Vostrukhin A. V. Shvetsov V. N. Sagdeev R. Boynton W. Harshman K. Enos H. Trombka J. McClanahan T. Evans L. Starr R.
Lunar Exploration Neutron Detector for NASA LRO Mission **[#6050]**

11:10 a.m. Plenary Discussion of Target Priorities

12:00 p.m. LUNCH

Wednesday, June 10, 2009
IMPACT CRATERING AND HISTORY
1:00 p.m. Basha Family Library

Chair: **Barbara Cohen**

1:00 p.m. Kring D. A. * [INVITED]
Targeting Complex Craters and Multi-Ring Basins to Determine the Tempo of Impact Bombardment While Simultaneously Probing the Lunar Interior **[#6037]**

1:30 p.m. Bray V. J. * Tornabene L. L. McEwen A. S. [INVITED]
The Moon as a Laboratory for Understanding Impact Processes **[#6034]**

2:00 p.m. Cohen B. A. * [INVITED]
The Lunar Cataclysm and How LRO Can Help Test It **[#6048]**

2:30 p.m. Cuk M. * [INVITED]
The Dynamics Behind Inner Solar System Impacts — Past and Present **[#6042]**

3:00 p.m. BREAK

3:10 p.m. Oberst J. * Wählisch M. Hempel S. Knapmeyer M.
Locations and Morphology of Spacecraft Impact Craters for Re-Calibration of Apollo Seismic Data **[#6003]**

3:30 p.m. Koeberl C.
Central Uplift Formation in Complex Impact Craters — Comparison of Lunar and Terrestrial Craters **[#6030]**

3:50 p.m. Plenary Discussion of Target Priorities

5:15 p.m. END OF SESSION

Wednesday, June 10, 2009
LUNAR VOLATILES: POLAR AND EXOSPHERIC
1:00 p.m. Carson

Chair: **David Lawrence**

1:00 p.m. Feldman W. C. * [INVITED]
Our Current Understanding of Lunar Polar Hydrogen Deposits **[#6009]**

1:30 p.m. Hurley D. M. * [INVITED]
Current Understanding of Lunar Volatile Transport and Segregation **[#6027]**

2:00 p.m. Gladstone G. R. * Retherford K. D. [INVITED]
The Lunar Atmosphere and Its Study by LRO **[#6010]**

2:30 p.m. Bussey D. B. J. * [INVITED]
A Review of Lunar Polar Lighting Condiitons: What We Know Now, and What We Will Learn Soon **[#6043]**

3:00 p.m. BREAK

3:10 p.m. Bart G. D. * Colaprete A.
The Importance of LRO Observations to the LCROSS Mission **[#6016]**

3:30 p.m. Plenary Discussion of Target Priorities

5:00 p.m. END OF SESSION

Thursday, June 11, 2009
PANEL DISCUSSION OF LRO TARGETING, CLOSING PLENARY
8:00 a.m. Carson

8:00 a.m.	Announcements
8:10 a.m.	Report on Panel Sessions, Discussion of Targeting Priorities (Moderators, All)
10:40 a.m.	BREAK
10:50 a.m.	Summary of Targeting Priorities (Moderators, All)
12:00 p.m.	LUNCH
1:00 p.m.	Synthesis and Final Report Preparation (Moderators, Invitees)
5:00 p.m.	MEETING ADJOURNS

THE IMPORTANCE OF LRO OBSERVATIONS TO THE LCROSS MISSION. G. D. Bart[1], A. Colaprete[2], [1]*University of Idaho, Department of Physics, PO Box 440903, Moscow, ID 83843, USA. (gbarnes@uidaho.edu)*, [2]*NASA Ames Research Center, M/S 245-3, Moffett Field, CA 94035, USA..*

The LCROSS Mission: LCROSS, the Lunar CRater Observation and Sensing Satellite, will be launched on the same rocket as the Lunar Reconnaissance Orbiter (LRO) later this year (`http://lcross.arc.nasa.gov`).

The LCROSS scientific objectives are: (1) Confirm the presence or absence of water ice in a permanently shadowed region on the Moon. (2) Identify the form/state of hydrogen observed by at the lunar poles. (3) Quantify, if present, the amount of water in the lunar regolith, with respect to hydrogen concentrations. (4) Characterize the lunar regolith within a permanently shadowed crater on the Moon. The presence of water ice is hypothesized based on evidence found by the Lunar Prospector neutron spectrometer for hydrogen in permanently shadowed regions at the poles [1].

The LCROSS spacecraft will set the rocket's Centaur Earth departure upper stage (EDUS) on an impact trajectory with the Moon. Once the trajectory is set, the spacecraft will release the EDUS, which will then impact the Moon in a permanently shadowed region characterized by high concentrations of hydrogen according to the Lunar Prospector neutron spectrometers. Following four minutes behind the EDUS, LCROSS will fly through the impact plume, using its 5 cameras (1 visible, 2 Near IR, 2 Mid IR), three spectrometers (1 visible, 2 NIR), and one photometer to search for water ice.

Impact Site Candidates: Four south-pole regions are currently candidates for the LCROSS impact (Fig. 1): Shoemaker crater (88.1 S, 44.9 E, 50.9 km diameter), Shackleton crater (89.9 S, 0.0 E, 19 km diameter), Faustini crater (87.3 S, 77.0 E, 39 km diameter), and Cabaeus (85 S, 35 E) (Fig. 1). Several north pole craters are currently under consideration as well (A-F, Fig. 2).

Site Criteria and Characterization:

Target selection will be key to the success of this mission. The constraints on the impact site selection are: (1) The ejecta plume must be observable by ground-based and orbital observatories. (2) The ejecta must be illuminated by sunlight, since the instruments primarily measure reflected light. (3) The target should have known surface properties (low roughness and slopes, deep regolith cover.) (4) The target should be in a permanently shadowed region with an observed concentration of increased hydrogen, which could indicate the presence of water (Fig. 3) [2].

The first two criteria depend on the angles between the moon and the earth, and the moon and the sun, respectively. These criteria are set by the orbital motion of the bodies, and thus are determined at any given site by the impact date and time. Some impact dates will not provide acceptable viewing and lighting conditions for any impact sites. Other dates will provide acceptable viewing and lighting conditions for some sites and not others.

The third criteria, characterizing the expected terrain within the crater, is more challenging to achieve because the target impact site is required to be permanently shadowed. Because of lack of high resolution visible imaging at the poles, we use high resolution Earth-based radar data [3], which can directly observe some parts of the permanently shadowed regions. In addition, the "KAGUYA" (SELENE) team at JAXA has kindly provided us with some of their data for internal project use only. Once the tools and analysis methods are established, we will be ready to quickly assess new data provided by the instruments on LRO, which will begin taking data 2-3 months prior to the LCROSS impact.

LRO Targeting

LRO's targeting of the impact site, both before and after the impact, will be critical to achieving the LCROSS mission. Targeting before impact will aid both with target selection and target characterization. Because the final impact site can be tweaked a small amount up to 30 days before impact, data received early from LRO could allow us to optimize the impact site to avoid previously undetected hazards or to impact in a site that is more likely to harbor H_2O.

Furthermore, pre-impact LRO data will allow the impact site to be well characterized prior to impact. Estimates of preexisting regolith depth, rockiness, and small scale slopes, as seen by LRO, will be helpful in interpreting the impact's ejecat plume and resulting crater.

Finally, data taken by LRO post-impact will allow us to better understand impact cratering processes. The resulting impact flash, the crater depth/diameter ratio, the crater morphology, and the ejecta pattern will all be analyzed given all the known parameters of the impactor (mass, shape, density, impact velocity, impact angle.) We expect the Centaur crater to be 20-25 meters across and 3-4 meters deep. The crater that will form when the shepherding spacecraft impacts crater will be 13-15 meters across and about 2 meters deep.

Conclusion:

This study is critical to providing the best scientific return from the LCROSS mission. Understanding the target as well as possible will both optimize the quality of data return and improve the analysis of the data. Although this study is critical to the success of the LCROSS mission, it will also return scientific results relevant to:

- NASA lunar exploration initiatives
- Future landing site selection
- Understanding cratering processes
- Dry craters (Moon) vs. possibly wet craters (Mars)
- Ice deposits elsewhere, such as Mercury

References:

[1] Feldman W.C., Maurice S., Binder A.B., Barraclough B.L., et al. (1998) *Science*, *281* 1496–1500.

[2] Elphic R.C., Eke V.R., Teodoro L.F.A., Lawrence D.J., et al. (2007) *Geophys Res Lett*, *34* L13,204.

[3] Campbell B.A. and Campbell D.B. (2006) *Icarus*, *180* 1–7.

[4] Margot J.L., Campbell D.B., Jurgens R.F., and Slade M.A. (1999) *Science*, *284* 1658–1660.

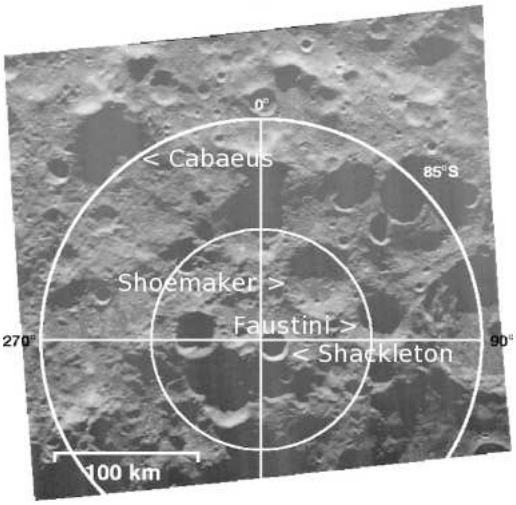

Figure 1: South Pole: Illustration of the location of candidate impact locations for LCROSS, superimposed on a radar backscatter map of the lunar south pole from [4].

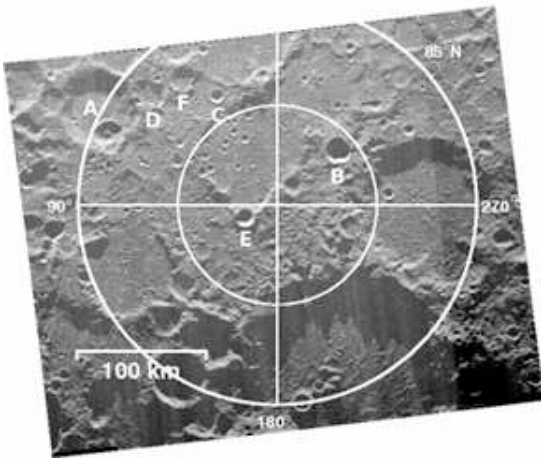

Figure 2: North Pole: Illustration of the location of candidate impact locations for LCROSS, superimposed on a radar backscatter map of the lunar north pole from [4]. Labels B-F are placed directly beneath the corresponding crater.

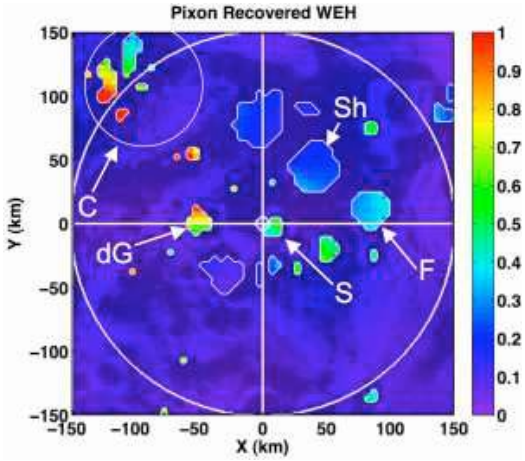

Figure 3: Water-equivalent hydrogen (WEH) in wt% corresponding to the epithermal count rates. Large circle denotes 85S. *C* = Cabaeus, *Sh* = Shoemaker, *dG* = de Gerlache, *S* = Shackleton, *F* = Faustini. From [2].

LRO TARGETING OF LUNAR TECTONIC FEATURES. J.F. Bell III[1], M.E. Pritchard[1], A.C. Schiff[1], J.O. Gustafson[1], N.R. Williams[1], and T.R. Watters[2], [1]Cornell University, Ithaca, NY; [2]NASM/Smithsonian Institution, Washington, DC; (jfb8@cornell.edu)

Introduction: The global-scale, high-resolution imaging survey to be conducted by the Lunar Reconnaissance Orbiter Camera (LROC) Narrow Angle Camera (NAC) subsystem will enable significant advances in our understanding of lunar tectonism, as well as possible testing of competing hypotheses for the early evolution of the Moon. This abstract describes the science rationale and status of LRO targets being entered as part of a global survey of lunar tectonic features.

Science Rationale: The ddds presence or absence of global-scale faults on the Moon has implications for the origin of the Moon and the early history of the Earth. If the Moon formed almost completely molten and cooled monotonically throughout history, the lunar radius would contract, building up stress in the lunar lithosphere and creating global-scale thrust faults [*e.g.,* 1,2]. Such global-scale faults on Mercury were long thought to indicate global contraction of that planet [*e.g.,* 3], although more recent work has questioned whether these faults were, in fact, global in extent [4]. Although thrust faults have been found in the lunar highlands [*e.g.,* 5,6], no global network of thrust faults have been found on the Moon. The lack of a global network of faults on the Moon has been used to place tight constraints on the lunar radius change since formation and on the initial thermal state of the Moon [*e.g.,* 2,7]. According to these models, the Moon must have started out so cold that the constrained initial thermal state might be inconsistent with current scenarios for the giant impact origin for the Moon that involve rapid accretion [*e.g.*, 8, 9].

However, there are several reasons to suspect that the absence of global-scale faults on the Moon does not rule out the giant impact theory of lunar origin [9, and references therein]. One reason is that lunar highland faults have not been completely characterized because only portions of the Moon have been imaged with the low solar illumination angle necessary to reveal low relief scarps [10]. Binder and Gunga [10] used Apollo high-resolution photographs to document some highland scarps, but they estimated that scarps could only be visible when the solar illumination angle was between 5 and 45 degrees. Only 4.4% of the lunar surface could be imaged with their available imagery within this range of illumination angles. Extrapolating the limited data to the rest of the Moon indicates that more than 2000 highland scarps could exist. Thus, it cannot be ruled out that there are numerous low-amplitude global-scale faults on the Moon. Such numerous small faults might, in fact, be expected to form in the highly comminuted lunar breccia and could accommodate significant radius change [*e.g.,* 11].

We are planning to use LROC to search for low-amplitude faulting, particularly in the lunar highlands. We are working with the LROC targeting team to select the camera viewing geometries that would be most favorable to detection of these scarps, focusing mostly on choosing low Sun illumination angles during dedicated "morphology" campaigns primarily during the Science Mission Phase (such as the 60°-80° incidence angle imaging campaign described by [12]), but also capitalizing on any Exploration Mission Phase inherently low Sun angle imaging in the polar regions (which are separately a major focus of LROC observations overall) and any opportunities during either mission phase that might be identified for off-nadir spacecraft slews to provide additional perspectives on possible candidate faults. To test for the global nature of these faults, a significant sampling of the Moon will need to be imaged

under the most favorable geometries. If we are able to detect highland fault scarps, we will characterize their length, orientation and offset. The offset of the faults can be measured by properties of the shadows (photoclinometry) and by stereographic imaging [*e.g.*, 13], calibrated where data is available with topography measured by LOLA. The measurements of offset, length, location, and orientation will be essential for determining if the faults are of regional or global origin [*e.g.*, 4].

In addition to our search for highlands faults, we are also planning to use LROC to conduct a global-scale survey of catalogued and uncatalogued lunar tectonic features in general. High resolution stereo imaging of ridges, rilles, fractures, scarps, and transitional structural landforms will provide new, quantitative data on morphology and topography that will help us better understand the mechanical properties of and stresses in the lunar crust and lithosphere, with implications for their origin and evolution.

Targeting Strategy:

We have a two-part strategy for targeting regions of interest in our lunar tectonic survey. First, for our overall survey of lunar tectonic features, we are targeting all of the major named lunar tectonic features in the USGS Planetary Nomenclature Database [14], as well as structural features identified in the recent lunar tectonics review chapter by Watters and Johnson [15] and references therein. We are also targeting uncatalogued lunar tectonic features found during our examination of the newly-digitized Apollo Metric Image collection [16].

Second, our strategy for searching for evidence of highlands scarps involves targeting of a random subset of the lunar highlands. To begin to make this search as extensive as possible, we are starting with 500 randomly-distributed (lat,lon) coordinates in the highlands, using an albedo threshold to distinguish between highlands and mare. Our target list will be biased towards the lunar farside, because of the higher relative fraction of highlands material in that hemisphere. Because of the prior finding that highland scarps are most detectable in low solar illumination conditions [10], images of our random highlands scarp search images will be constrained to an incidence angle range of ~70 to 85 degrees. In addition, we will not initially request stereo imaging of these target regions. Rather, we will examine the images taken by LROC, and if potential evidence for interesting structural landforms or candidate highlands scarps is identified, we will resubmit a companion stereo target request for that region.

Images for our overall survey of lunar tectonic features will be targeted as Priority 3 (with 1 being highest and 5 being lowest), while images for our random highlands scarp search will be targeted as Priority 4.

References: [1] MacDonald, *Planet. Space Sci*., 2, 249-255, 1960; [2] Solomon and Chaiken, *Proc. Lunar Sci. Conf. 7th*, 3229-3243, 1976; [3] Strom *et al., J. Geophys. Res*., 80, 2478-2507, 1975; [4] Watters *et al., Geophys. Res. Lett*., 31, doi: 10.1029/2003GL019171, 2004 [5] Howard and Muehlberger, *Apollo 17 Preliminary Science Report*, NASA SP-330, 31-22 to 31-25, 1973; [6] Lucchitta, *Proc. Lunar Sci. Conf. 7th*, 2761-2782, 1976; [7] Kirk & Stevenson, *J. Geophys. Res*., 94, 12133-12144, 1989; [8] Ida *et al*., *Nature*, 389, 353-357, 1997; [9] Pritchard & Stevenson, Thermal aspects of a lunar origin by giant impact, in *Origin of the Earth and Moon*, eds. R. Canup and K. Righter, U. Arizona Press, 179-196, 2000; [10] Binder and Gunga, *Icarus*, 63, 421-441, 1985; [11] Weisberg & Hager, *Origin of the Earth and Moon Conference*, Abstract #4052, Monterey, CA, 1998; [12] Robinson *et al.,* 36th Annual Lunar and Planetary Science Conference, Abstract #1576. 2005; [13] Watters & Robinson, *J. Geophys. Res., 102,* 10889, 1997; [14] http://planetarynames.wr.usgs.gov/ [15] Watters & Johnson, "Lunar Tectonics," in *Planetary Tectonics* (T.R. Watters and R.A. Schultz, eds.), Cambridge, 2008. [16] http://apollo.sese.asu.edu/

LROC Stereo Observations. Ross A. Beyer[1,2], Brent Archinal[3], Ron Li[5], Sarah Mattson[6], Alfred McEwen[6], and Mark Robinson[7]. [1]Carl Sagan Center at the SETI Institute, [2]NASA Ames Research Center, MS 245-3, Moffett Field, CA, USA (Ross.A.Beyer@nasa.gov), [3]United States Geological Survey, [4]Ohio State University, [5]The University of Arizona, and [6]Arizona State University

The Lunar Reconnaissance Orbiter Camera (LROC) [1, 2] will obtain two types of multiple overlapping coverage to enable derivation of high-resolution terrain models of the lunar surface. LROC has two Narrow Angle Cameras (NACs), and they work together to provide a wider (in the cross-track direction) field of view for each observation. They do not view the surface at different emission angles like the Terrain Cameras on SELENE [3] or the Terrain Mapping Cameras on Chandrayaan-1 [4]. In order to derive dense topographic information from LROC images, multiple observations on different orbits are required, similar to stereo observations from the Mars Orbiter Camera (MOC) or the High Resolution Imaging Science Experiment (HiRISE). The Lunar Reconnaissance Orbiter's (LRO's) orbit precesses (is not Sun-synchronous), and the same target can be viewed at different solar azimuth and incidence angles providing the opportunity to acquire 'photometric stereo' observations in addition to traditional 'geometric stereo' data.

Geometric Stereo

We use the term 'geometric stereo' to refer to traditional two-look stereo pairs. To obtain the data for geometric stereo, LROC must acquire two separate observations of a target. These observations must have different emission angles to provide a reasonable stereo convergence angle such that the resultant images have enough parallax for a reasonable stereo solution. The lighting at the target must not be radically different. If shadows move between observations, it is very difficult to correlate the images.

The majority of NAC geometric stere observations will be acquired with one nadir (emission angle of zero degrees) and one off-pointed image. The off-naidr image will be obtained with the spacecraft rolled (normal limits are 20°) to one side or the other. For equatorial targets, where the orbital tracks have their greatest spacing, or for target terrain with a particularly low relief, both halves of the stereo pair could be obtained with a spacecraft roll (one to the left and one to the right, providing a stereo convergence angle of up to 40°).

Cook, et al. [5] provide general guidelines that solar altitude not differ more than 10° and solar azimuth not differ more than 45° between the two images. Therefore, the two halves of a stereo pair must either be taken within a few orbits of one another, or obtained when the orbit precesses around such that the target has similar lighting conditions as when the first observation was acquired. In addition, the orbits must be such that the right convergence angle between the two observations is achieved. Since most of LRO's other instruments require a nadir-pointed orientation for acquiring data, the number of off-nadir rolls that LROC can request is limited to three per day. Not all off-nadir rolls will be used for geometric stereo acquisition, many will be used to extend narrow angle coverage in selected areas. All of these constraints limit the total number of geometric stereo pairs which LROC will be able to acquire and the speed with which matching pairs can be obtained [6].

Although this abstract focuses onthe NACs, the Wide Angle Camera (WAC) will also yield data suitable for geometric stereo analysis. The WAC has a 90° field-of-view and will provide sufficient overlap at useful viewing angles from nominal naidr mapping observations (in monochrome mode). However, at an image scale of $\sim$ 75 m/pixel results in 200 m/post (or greater) terrain, thus only proving an incremental improvement over Lunar Obiter Laser Altimeter (LOLA) data.

Photometric Stereo

Photometric stereo was first described by Woodham [7] and refers to multiple-look observations of the same target under different lighting conditions. To obtain data for photometric stereo, LROC will acquire at least three (ideally five) observations of a target. These observations should have near identical emission angles (ideally nadir-looking), but with varying solar aziumth and incidence angles. Photometric stereo does not require any particular spacecraft motions (because the default nadir-looking arrangement is ideal), it only requires that LROC image the target multiple times under the right variety of lighting conditions. Such images sets can be correlated and aligned so that the only change from image to image is the location of shadows.

Gaskell, et al. [8] discuss using a technique they call stereophotoclinometry which combines elements of both geometric and photometric stereo techniques, and can make use of any and all observations of a particular target. This technique does not require particular convergence angles nor near-identical emission angles. Therefore it enables terrain and albedo model creation from a collection of overlapping imagery that does not conform to either the strict 'geometric stereo' or 'photometric stereo' described above, as long as three or more images of the area of interest are available with signifi-

cantly different lighting and emission angles. Although qualitatively showing great promise, the stereophotoclinometry method has not been rigorously compared to results from the other methods or from altimetry. Once LROC has obtained the planned multiple coverages, it will finally be possible to do such comparisons between all of these methods.

Jitter Correction

For any of these techniques, images must be coregistered to sub-pixel accuracy to obtain reliable results. Pushbroom images are distorted by small variations in the orientation of the spacecraft, induced by motions of the reaction wheels, gimbals on the high-gain antenna and solar arrays, and possibly by motions of other instruments. Fortunately, due to the geometry of the two NACs, we may be able to sample and partially correct this jitter.

The NACs have an overlap of about 150 pixels so that the individual images can be mosaicked together for each observation (providing a final 'image' that is twice as wide as what a single narrow angle camera can obtain). However, the CCDs are arranged with one ahead of the other, such that a particular point in the overlap region on the ground is first imaged by the leading NAC, and then miliseconds later by the trailing camera. This offset in time, but overlap in space allows for certain jitter frequencies to be resolved, characterized, and minimized, thereby reducing the impact of the jitter on the final topographic estimates. This correction technique is employed successfully in HiRISE imagery which has similar (but not identical) detector offsets [9].

Summary

The LROC targeting system allows for the designation of targets as either geometric or photometric stereo observations. Once the first observation (either the first of two for a geometric set, or the first of three to five for a photometric set) of a stereo target is acquired, the LROC Stereo Planner system automatically calculates the best lighting and observation conditions to acquire the subsequent observations, ensuring that LROC captures high quality data for the purpose intended.

Geometric stereo techniques result in terrain models with a post spacing of a few times the pixel scale. For LRO's primary mission phase, the expected LROC narrow angle imagery will be at a scale of 50 cm/pixel, resulting in terrain models with post spacings of a few meters per post. Photometric stereo and stereophotoclinometry techniques, under the right conditions, can provide models with post-spacings at $2\times$ the image scale, or better. The vertical precision of both techniques is expected to be $\sim$ 20 cm for images acquired during the primary mission [5].

The LROC team is not funded to systematically produce terrain models from all acquired data, but is instead focused on acquiring the highest quality data. The LROC team will build some example terrain models for certain ESMD-requested sites and a small number of other test locations.

References

[1] M. S. Robinson, et al. LROC – Lunar Reconnaissance Orbiter Camera. In S. Mackwell and E. Stansbery, editors, *Lunar and Planetary Science XXXVI*, #1576. Lunar and Planetary Institute, Houston (CD-ROM), 2005.

[2] G. Chin, et al. Lunar Reconnaissance Orbiter Overview: The Instrument Suite and Mission. *Space Science Reviews*, 129:391–419, 2007. doi:10.1007/s11214-007-9153-y.

[3] J. Haruyama, et al. Global lunar-surface mapping experiment using the Lunar Imager/Spectrometer on SELENE. *Earth, Planets, and Space*, 60:243–255, 2008.

[4] A. S. Kiran Kumar and A. Roy Chowdhury. Terrain mapping camera for Chandrayaan-1. *Journal of Earth System Science*, 114:717–720, 2005. doi:10.1007/BF02715955.

[5] A. C. Cook, et al. Clementine imagery: selenographic coverage for cartographic and scientific use. *Planetary and Space Science*, 44:1135–1148, 1996.

[6] S. J. Lawrence, et al. Preparing to Scout the Next Frontier: Hardware and Operational Constraints Encountered During Targeting of the Lunar Reconnaissance Orbiter Camera Narrow Angle Cameras. In S. Mackwell and E. Stansbery, editors, *Lunar and Planetary Science XL*, #2316. Lunar and Planetary Institute, Houston, 2009.

[7] R.J. Woodham. Photometric method for determining surface orientation from multiple images. *Optical Engineering*, 19(1):139–144, 1980.

[8] R. W. Gaskell, et al. Characterizing and navigating small bodies with imaging data. *Meteoritics and Planetary Science*, 43:1049–1061, 2008.

[9] R. L. Kirk, et al. Ultrahigh resolution topographic mapping of Mars with MRO HiRISE stereo images: Meter-scale slopes of candidate Phoenix landing sites. *Journal of Geophysical Research (Planets)*, 113, 2008. doi: 10.1029/2007JE003000.

THE MOON AS A LABORATORY FOR UNDERSTANDING IMPACT PROCESSES. V. J. Bray, L. L. Tornabene and A. S. McEwen. Lunar and Planetary Lab., University of Arizona, Tucson, AZ 85721, USA. vjbray@lpl.arizona.edu

Introduction: Due to the diverse nature of planetary crusts in our solar system, impact craters and their ejecta blankets display a variety of different morphologies, some thought to be directly associated with specific target composition or structure such as central pit craters, rampart craters and anomalous domes [1, 2, 3]. Before the crater characteristics produced as a result of atmospheric interactions, target volatiles and later alteration by surface processes can be discerned from those produced as an inherent part of the cratering process, the mechanics of crater formation itself must be better understood.

The current study of impact cratering combines observational data, including images of planetary surfaces and geophysical information from terrestrial craters, with small-scale hypervelocity laboratory and explosion experiments, and with computer models that can simulate planetary-scale impacts. Although theoretically able to model impact crater formation on any solar system body, hydrocodes require accurate material models to recreate a material's response to impact, and validation of results by comparison with observational data for fresh craters.

The Moon is one of the few bodies in the solar system from which we have obtained documented samples, providing information on the composition, strength properties and volatile content of a portion of lunar surface rock. Additionally, due to the lack of lunar atmosphere, and the associated erosional and depositional processes, fresh lunar craters provide an ideal observational dataset with which to compare the surface morphology of pristine craters produced by computer modeling. The Moon thus provides a unique opportunity to further the study of impact crater formation, as we possess both actual material samples, and observational data for relatively pristine craters.

Targeting Rational: We will discuss the ways in which new data from the Lunar Reconnaissance Orbiter (LRO) may advance our understanding of the impact process, and conversely, the ways in which we can utilize our current understanding of impact cratering to investigate the lunar crust. Here we present our rationale for a selection of our intended LRO Camera (LROC) targets, chosen to facilitate the investigation of both the lunar surface and the impact process itself.

1. Small Fresh Craters and Regolith Thickness

A large proportion of our narrow angle camera (NAC) targets to date concentrate on imaging small (D < 5 km) craters, identified as relatively fresh due to their extensive and distinct ejecta blankets (Fig. 1). The ejecta blankets of fresh craters are distinctive in albedo and color due to exposure of immature soils, although excavation of distinct sub-surface mineralogy is also possible. Imaging these new craters will provide us with a better idea of relatively pristine crater morphology and impact melt generation for small craters on the Moon. Resultant morphometric data can then be used to further our understanding of the cratering process, as (for example) comparison to the dimensions of fresh craters is a vital test of any numerical model of crater formation.

These fresh, and presumably 'simple' (bowl-shaped), craters can also be used to investigate regolith thickness, as their internal morphology and ejecta characteristics will change depending on whether they have excavated into coherent bedrock. 'Nested' craters and/or those with blocky ejecta close to their rims can be used to estimate regolith thickness (Fig. 2), as these characteristics indicate excavation into a more resistant substrate [1, 4]. Depending on regolith coverage and thickness, these craters and their ejecta, also offer an important opportunity to image exposed bedrock in the crater walls, providing compositional and structural information for the lunar surface.

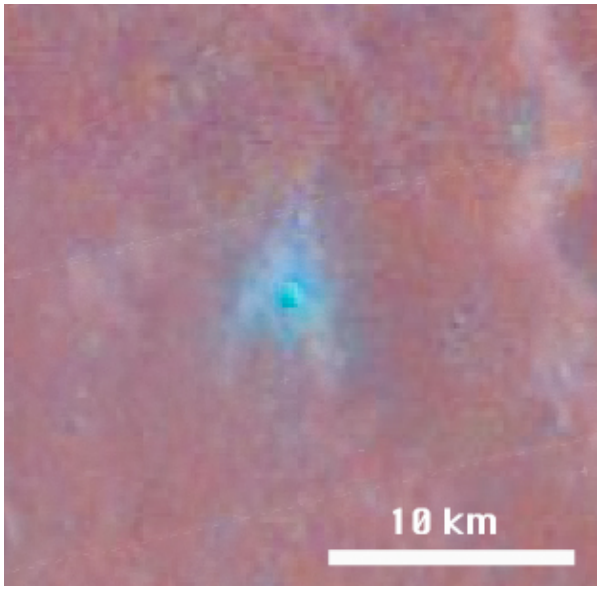

Figure 1: Clementine UVVIS mineral ratio over a Lunar Orbiter global mosaic image showing a fresh crater with a distinct ejecta blanket.

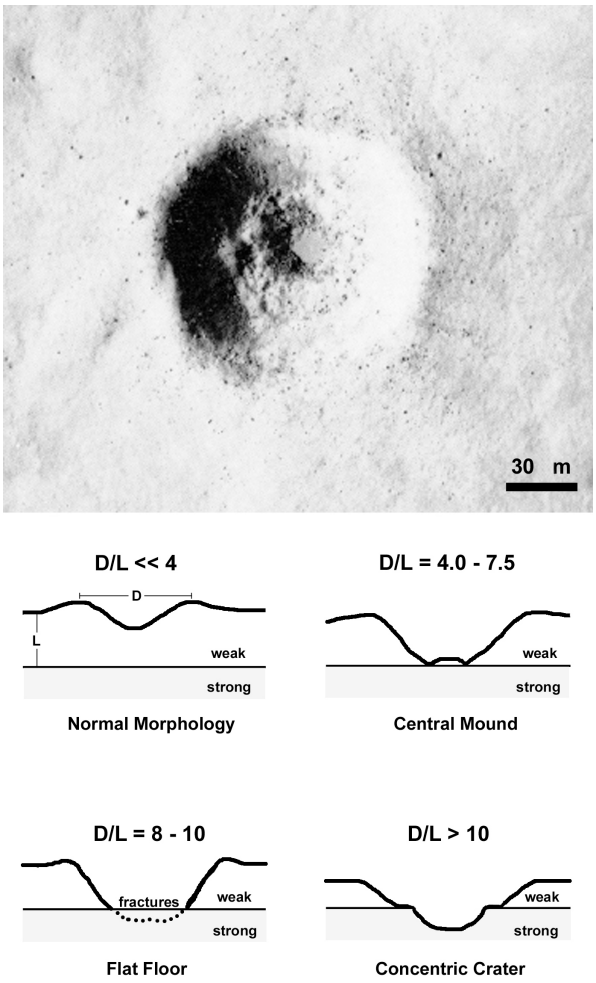

Figure 2: (top) Image of a 1.2 km simple crater on the Moon. The wide bench on its interior wall has been used to infer that the Moon's surface in this area consists of a weak layer about 100 m thick overlying a more resistant rock unit. Apollo Panoramic Photograph AS15-9287. (Bottom) Sketches of different crater morphologies produced when the ratio of crater diameter and the thickness of the upper weak layer changes. From [1], after [4].

2. Larger Fresh Craters and Impact Melt Bodies

Central peak craters are characterized by terraced rims, flat floors and a central peak, thought to be uplifted from depth. The resultant bedrock exposures at central peak, and other complex craters, provide insight into the lunar subsurface, allowing us to discern its composition via spectral analysis [5]. High resolution imaging of these central peaks will also allow assessment of the nature of the bedrock exposure (e.g. massive, layered, megabreccia) which in turn provides information on the cratering and central peak formation process.

The High Resolution Imaging Science Experiment (HiRISE) onboard the Mars Reconnaissance Orbiter has provided a closer look at fresh martian craters, revealing alluvial fans, viscous flow features and ponded regions of pitted materials containing breccia clasts, interpreted to be melt-bearing breccias [6, 7]. The presence of impact melt on Mars, and the role of sub-surface volatiles in facilitating its production, despite the relatively low impact velocity (10km/s), are topics of ongoing research.

We are targeting relatively fresh lunar craters with LROC for comparison to HiRISE imagery, so that crater morphology and melt volume in dry silicate-rich targets (the Moon) can be compared to those in relatively volatile rich silicate targets (e.g. Mars and the Earth). Such comparison will also shed light on the formation mechanism of the small scale pitting seen on martian melt ponds, as they are currently thought to form due to the presence of target volatiles; if significant ponded-pitted material is revealed in lunar craters by LROC, this paradigm will have to be revised.

3. The Simple-to-Complex Transition

The progression of crater morphology from simple bowl shaped depressions, to more complex structures with terraced rims and additional internal features is controlled by the gravity of the planetary body, and also affected by the strength of the local target material [1]. Understanding the mechanism of crater collapse at different crater sizes is pivotal for our understanding of crater formation as a whole. The different terrains, and their variable volatile contents, complicate the size-morphology progression on the Earth and Mars. The Moon offers a comparatively homogeneous, volatile and atmosphere free environment in which to study the natural progression in the extent of crater collapse with crater diameter. We are targeting craters between 10 and 30 km in diameter with LROC so that the changing degree of wall slump and central uplift may be more closely examined.

References: [1] Melosh (1989), Impact Cratering: a geological process. Oxford Univ. Press, London [2] Passey and Shoemaker (1982), In Satellites of Jupiter, Morrison, D. Ed., UofA Press, pp. 379-434. [3] Carr et al., 1977 J. Geophys. Res 82:4055-4065. [4] Quaide and Oberbeck (1968), Icarus 9:446-465. [5] Tompkins and Pieters, (1999), Meteorit. and Planet. Sci. 34(1):25-41. [6] McEwen et al., (2007), Science 317. [7] Tornabene et al. (2007) *Mars 7*, abs. 3288.

A REVIEW OF LUNAR POLAR LIGHTING CONDITIONS: WHAT WE KNOW NOW, AND WHAT WE WILL LEARN SOON. D. B. J. Bussey[1], [1]The Johns Hopkins University Applied Physics Laboratory, Laurel MD 20723 (ben.bussey@jhuapl.edu)

Introduction: The moon's spin axis is nearly perpendicular to the ecliptic plane. This results in illumination conditions that are likely unique in the solar system. Were one to stand at a lunar pole the Sun would traverse around the horizon once every 708 hours with the center of the Sun never deviating more than ±1.5° from the nominal horizon. Therefore topographically low areas; such as the floors of impact craters have the possibility of being errantly shadowed. Conversely topographic high regions near the pole may be in sunlight far more than the lunar average 50%.

Current Knowledge: Both image data and illumination simulations using topography have provided information on the lunar polar illumination conditions

Clementine-derived quantitative illumination maps: The Clementine mission gave us our first comprehensive look at the lunar poles. It imaged both poles approximately once every 10 hours for 71 days. The data were acquired during summer for the northern hemisphere. From these data quantitative maps were produced for both poles [1,2]. The main conclusions from this work were that no areas near the south pole are constantly illuminated although several regions exist that receive >50% sunlight in winter. Two of these regions, one on the rim of Shackleton and the other approximately 15 km away on a ridge, were collectively illuminated for ~98% of the time (Figure 1). At the north pole, several areas on the rim of Peary crater were constantly illuminated for an entire summer day (Figure 2). It was not possible to claim if these areas would be constantly illuminated but they represent the best candidate sites. Comparing the low spatial-resolution illumination maps with high-resolution imaging data revealed that the areas that receive the most illumination were associated with relatively small topographic highs (Figure 3).

Topographic Simulations: Analysis of images has pros and cons. The advantages are that an image definitively shows which portion of the surface is illuminated or shadowed for a given Sun position. However it shows it only for an instant in time. Two images taken a few hours apart may show the same region to be illuminated in both. But one has to infer that it was illuminated for the entire time in between images. Illumination simulations permit the investigation of all possible lighting conditions. The ideal scenario involves using real lunar topographic data. In the 90's there were two primary lunar-polar topographic data sets available, Goldstone radar-derived [3] and Clementine stereo [4,5]. Margot used a 600 m/pixel Digital Elevation Model (DEM) he generated using Goldstone radar data to map out areas of permanent shadow near both lunar poles.

Bussey compared simulations using the Margot data and Cook stereo with actual images [6]. He concluded that the radar-derived DEM produce the more realistic simulations but that neither data set was sufficiently accurate to produce quantitative illumination maps. Both data sets yield errors in simulations, either predicted areas to be dark when the image shows it to be light, or vice-versa. As an alternative approach Bussey used realistically shaped craters to investigate the amount of permanently shadowed regions within simple craters [7]. He concluded that simple craters as far away as 12° latitude from the pole can contain permanent shadow, and that the total amount of permanent shadow was far larger than previously predicted (Figure 4).

SMART-1 AMIE data: ESA's SMART-1 spacecraft orbited the Moon for more than a year and was thus able to observe the entire seasonal illumination variation at the poles. Analysis of AMIE image data revealed the location of a small hill close to Shackleton crater (an area previously identified as having high illumination from the Clementine data) that appeared to be constantly illuminated during a southern summer day [8].

Kaguya Laser-derived topography: The JAXA Kaguya spacecraft carried a laser altimeter which produced a DEM of both lunar poles. These data were used to produce quantitative illumination maps for the area within 5° of both poles [9]. They conclude that no areas of permanent sunlight exist at either pole.

Future Data: Data from ongoing and soon-to-launch missions raise the possibility of thoroughly characterizing the polar illumination conditions. The LROC instrument on Lunar Reconnaissance Orbiter will take a snapshot at a spatial scale of 100 m/pixel, of the illumination conditions of each pole every two hours. At the same time NAC images at 50 cm/pixel will reveal surface illumination conditions in unprecedented detail.

The polar DEMs produced by the Kaguya, Chandrayaan-1 and LRO missions will be of much higher fidelity than is currently available and will permit very detailed illumination studies to be conducted.

References: [1] Bussey D. B. J. et al. (1999) *GRL,* 26, 1187 [2] Bussey D. B. J. et al. (2005) *Nature* 434, 842 [3] Margot J. L. (1999) *Science,* 284, 1658. [4] Cook A. C. et al. (2000) *JGR,* 105, 12023, [5] Rosiek M. R. et al. (1999) *LPSC* XXX, #1853 [6] Bussey D. B. J. et al. (2001) *LPS XXXII,* Abstract #1907. [7] Bussey D. B. J. et al. (2003) *GRL*, V30 #6, 1278, [8] Josset J-L. et al. (2007) *ILEWG9*, #220 [9] Noda H. et al. {2008) *GRL*, 35, L24203

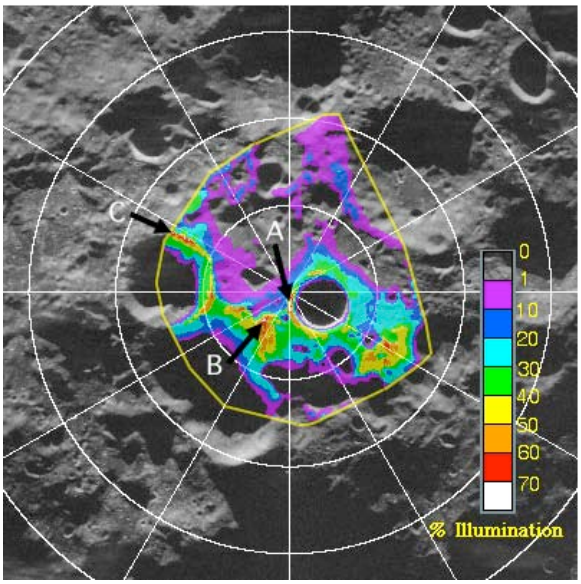

Figure 1. South pole quantitative illumination map derived from Clementine UVVIS data [1].

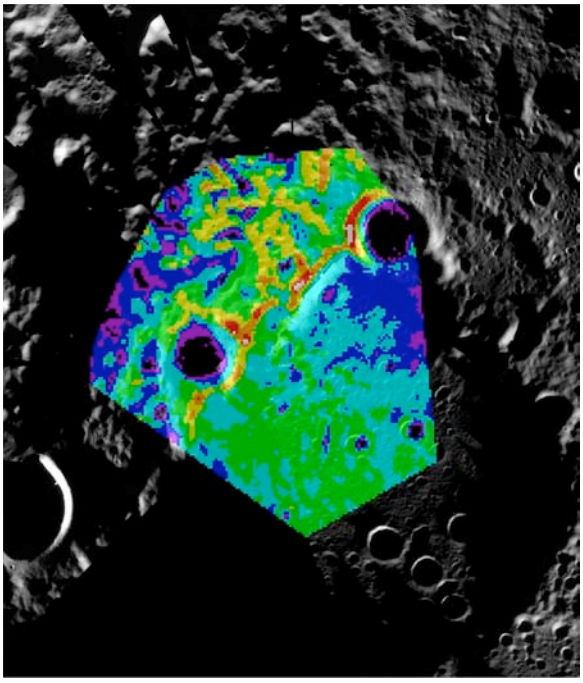

Figure 2. North pole quantitative illumination map [2].

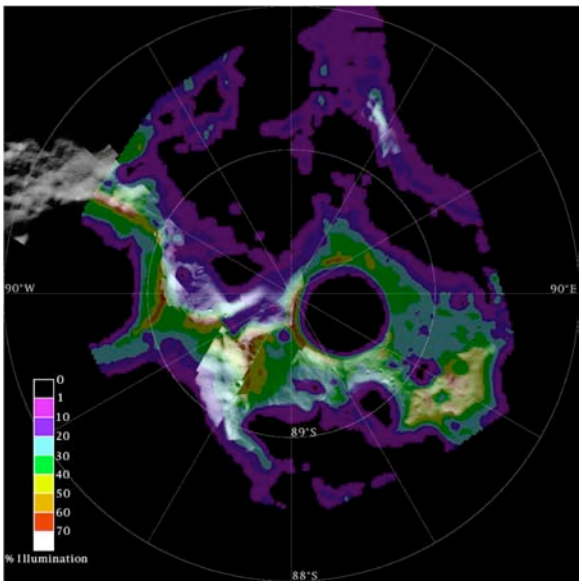

Figure 3. South pole illumination map overlaid on top of a Clementine hi-res mosaic.

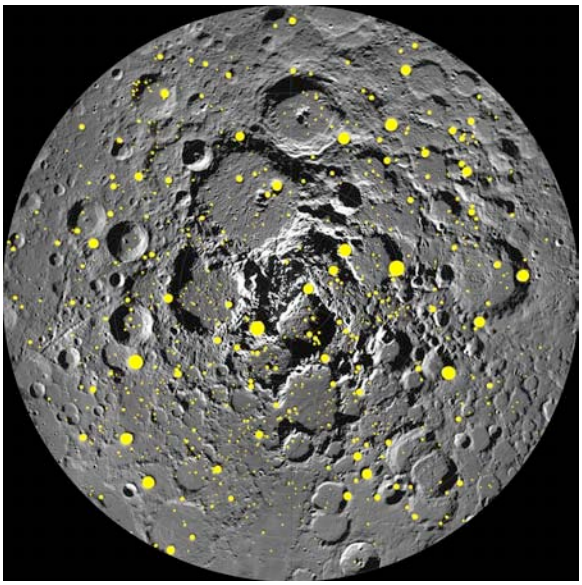

Figure 4. Map showing simple craters near the north pole that contain permanent shadow.

A Target for the Lunar Reconnaissance Orbiter near the Southwest Limb of the Moon

Charles J. Byrne, Image Again**,** 39 Brandywine Way, Middletown, NJ 07748, charles.byrne@verizon.net.

Introduction: My principle interest is in those targets that would either support or refute the Near Side Megabasin (NSM)[1, 2, 3]. The NSM is so large that any departure from the near side sites examined in the past would provide new and useful information. This contribution is intended to propose a particular site of interest to the NSM hypothesis, but the target is also of considerable other interest, both as a remote sensing target and as a potential landing site.

Proposed Target: The site is in the pre-Nectarian Mendel-Rydberg Basin, northeast of the Eratosthenian crater Hausen, at 52 Sº, 85,5º W. It is located on the segment of the rim of the NSM that is on the near side. As a landing site, it would allow continual communication with Earth, at least at favorable libration.

Figure: LO193H3, NASA, LPI, cleaned[4].

The target is in a very interesting area that has received ejecta from many impact features. It is on the outer ejecta blanket of Bailly and is just beyond the ejecta blanket of the Orientale Basin. It appears to have received molten material from Early Imbrian Orientale Basin, which provides smoothness to the proposed landing site. Ejecta from the Eratosthenian crater Hausen should be on the surface. The history of this area may be as follows:

1. A base of about 1000 meters of ejecta near the rim of the NSM, resting on pristine crust
2. About 150 meters of ejecta from the South Pole-Aitken Basin (SPA)
3. Modification by the Mendel-Rydber Basin
4. Possible Pingre-Hausen ejecta
5. Ejecta from the Bailley Basin
6. Orientale Basin ejecta, molten material and secondaries
7. Hausen ejecta. A traverse toward Hausen should encounter material from older layers, according to the principle of layer inversion in ejecta blankets.

High-resolution multispectral data may reveal differences among these materials. In-situ or sample return and analysis would add information on the formation and subsequent modification of this complex site. An objective should be to obtain sufficient resolution to certify the safety of a landing mission.

Other data of interest: All of the soft landing missions to date have been in the same unit of the NSM: the reconstituted crust of its flat floor. Data concerning the slope up to the rim, the rim itself, and the ejecta blanket that covers all of the far side beyond its rim are needed to fully describe the NSM.

Missions to either poles would be in the NSM slope, the area from the flat floor to the rim. Almost any mission to the far side beyond the SPA Basin would be in the NSM ejecta blanket. Any samples taken there would be characteristic of the pristine crust, reworked by the NSM, SPA Basin, and other basins and craters in the neighborhood.

One test of a hypothesis is to make a prediction, and see what happens. It may be that the seismically active zone on the near side is at the boundary of the NSM transient crater. If so, a seismometer network on the far side would see a similar active zone under the SPA Basin, but not under the northern hemisphere of the far side. If we are to deploy a seismic network on the far side, it would be well if it could distinguish such a pattern.

References: [1] Byrne, C.J., The Near Sde Megabasin of the Moon, LPSC 37, talk, Abstract 1930. [2] Byrne, C.J., Interior of the Near Side Megabasin of the Moon, LPSC 38. Abstract 1248. [3] Byrne, C.J., A large near side basin on the Moon, manuscript submitted to Earth, Moon, and Planets, October 4, 2006. [4] Byrne, C.J., Lunar Orbiter photographic atlas of the near side of the Moon, Springer, 2005.

LUNAR ARGON CYCLE MODELING

J-Y. Chaufray[1], K. D. Retherford[1], G. R. Gladstone[1], D. M. Hurley[2], and R. R. Hodges[3].
[1]Southwest Research Institute, 6220 Culebra Road, San Antonio, 78238-5166 TX, [2]John Hopkins University, Applied Physics Laboratory, 1110 John Hopkins Road, Laurel MD 20723-6099, [3]Laboratory for Atmospheric and Space Physics, University of Colorado, Boulder, CO 80309-0392.

Introduction: The idea of stable deposits of volatiles in cold permanently shaded regions (PSRs), first advanced by [1], has been revived since observations by Lunar Prospector suggested large amounts of hydrogen in the polar caps. Previous studies have mainly focused on hydrogen (and water) [2] but other important volatiles such as argon could also be trapped. Temperatures in the coldest regions (Amundsen and Nansen F craters) could reach 30 – 40 K [3], low enough to hold argon and create a reservoir of trapped argon [4]. Such deposits could explain a temporal enhancement of argon in the lunar exosphere observed by Apollo 17 mission which may have resulted from a seismic event releasing argon in a cold region [5]. Argon is unique because, contrary to water vapor, argon has been clearly identified in the lunar exosphere and measurements of its diurnal variation are available [5]. New measurements of the argon exosphere are planned with the LRO/LAMP instrument which will further characterize its spatial and temporal variations. In the following we present the goals and the method of a project, recently funded by NASA's LASER program, to describe the transport of argon from the lunar surface to the cold traps or to space and the possibility of argon frost in the coldest regions on the Moon.

1) Goals of the study: The main goal of this study is to investigate the possible accumulation of argon in PSRs and the potential for argon frost. Whether argon frost exposed to the surface would be detectable is unknown and will be investigated in terms of surface reflectance and thermal inertia. The argon exospheric density will be derived and used to make predictions of the Ar-1048Å emission line intensity. This study will be useful for interpreting future exospheric observations by LRO and LADEE, as well as PSRs soil properties deduced from LRO observations [6].

2) Models description: Our study will be based on two models:

- An exospheric model describing the transport of argon in the exosphere providing the argon flux to PSRs (Fig.1).

- A space weathering model describing the stability of the argon deposits in the PSRs taking into account the input rates (from the exospheric model) and loss rates (e.g: due to sputtering) (Fig.2).

The exospheric model will use Monte Carlo code to describe the movement of argon atoms from the lunar surface to the PSRs or to space. The main sources of argon are summarized in Fig. 1 Thermal desorption is likely the most important source, as indicated by the strong diurnal variation of the argon exospheric density [5] and will be the first source to be described. Sputtering could be a main source of non-thermal argon, capable of producing an extended argon corona. Finally, our model will be able to investigate the sudden release of a large amount of argon from PSRs or from other regions of transient outgassing from internally active regions and their exospheric signatures.

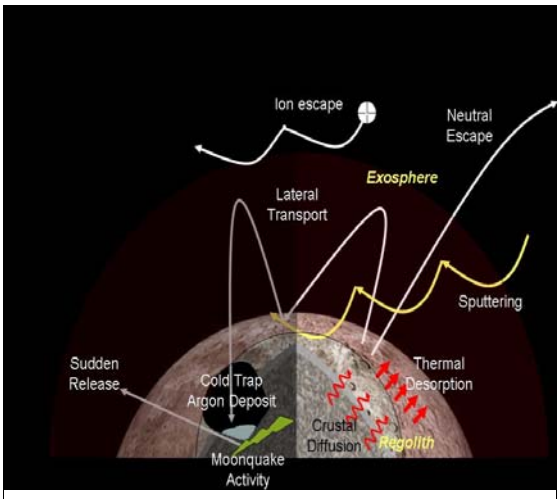

Fig.1: Schematic view of the main processes acting on the Moon's argon exosphere.

The space weathering of a PSR argon deposit in PSR will determine the stability of such deposit over billion year time scales. This model will mimic the approach used by [7], using the argon deposit flux given by the exospheric model and describing loss rates due to interplanetary Lyman-α radiation, thermal desorption, sputtering and soil gardening

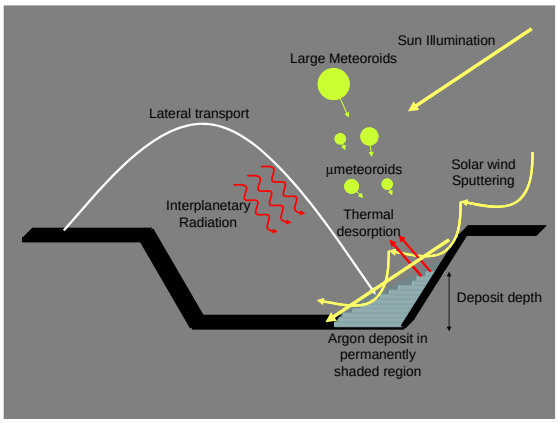

Fig.2: Schematic view of the main processes controlling the stability of argon deposits in permanently shaded regions.

by meteoroids, as summarized in Fig. 2. This model will be used to derive the mixing ratio of argon expected in the PSR

soil and the possibility of argon frost will be investigated. A first estimate can be done by using a deposit rate $\varphi = m_{Ar} n_{Ar} <V>/4 \sim 2.4 \times 10^{-5}$ kg Myr^{-1} cm^{-2}, and assuming that 10% of argon is stable. We derive a mass density $w_{Ar} = 0.1\ \varphi/(d\rho) \sim$ 7000 ppm, where $d \sim$ 2mm is the thickness gardened in 1 Myr [7] and ρ the density of the regolith (1.67 g cm^{-3}). The value concentration obtained is well above the highest concentration found in lunar samples ~ 1 ppm [8] and the soil of PSRs could be saturated in ^{40}Ar. Another more speculative possibility would be the presence of argon frost.

3) Driving science: Our study is expected to provide insight into several more general and complex subjects:

- *The evolution of other volatile components not yet observed in the lunar exosphere*. SO_2, CO_2, NH_3 and other nobles gases are expected but currently show with no detectable atmospheric trace.

- *The interaction between exospheric particles and regolith*. This problem concern not only the Moon environment but also many different objects of the solar system (e.g., Merucry, jovian satellites, asteroids, etc). Interactions between argon atoms and surface regolith and therefore adsorption properties are required to describe the exospheric transport. Enthalpy of adsorption needed to reproduce exospheric argon observations is larger than enthalpy measured for terrestrial analogs [9]. This difference could be due to a high degree of cleanliness of the lunar regolith. This high degree of cleanliness would require low abundance of water vapor and therefore be inconsistent with water exospheric transport [9].

- *Internal activity and radiogenic heating.* Most lunar argon is produced by radioactive decay of ^{40}K. The escape rate must be balanced by a high rate of leakage. If short-term trapped argon reservoirs exist, the rate of leakage should be reduced while if long-term trapped argon exist it should be increased. Transient Lunar Phenomena (TLPs) that could correspond to lunar outgassing are not distributed randomly and could be the residual effect of past massive eruptions. This activity as well as moonquakes could liberate argon into the exosphere [10].

- *Time history of the solar wind*. As noted by [11], the ratio between ^{40}Ar and ^{36}Ar is ~ 10 in the lunar exosphere, which is close to the high end of the range values observed for Ar trapped on grain surfaces and considerably larger than the mean ratio of ~ 1 in the regolith. Whether this ratio is diagnostic of solar wind activity versus depth in the regolith through time will be considered in our study.

4) Input expected for interpretation of LRO data:

New measurements of the argon exosphere are planned with the LRO/LAMP instrument. This instrument will observe the argon emission lines at 1048Å and 1067Å [12]. Coupling the exospheric model with a radiative transfer model will allow us to predict what LRO/LAMP would see and study quantitatively the existence of a hot argon population suggested by [13] to explain a controversed observation [14].

The reflectance of water ice is generally higher than that of the lunar regolith, and an absorption band exists in the FUV (Gladstone et al. 2005). Similarly the LRO/LROC instrument might observe higher reflectances at such sights using crater scattered sunlight and the LRO LOLA instrument may actively sound the surface to measure its reflectance [6]. Whether argon frost, exposed to the surface in the permanently shaded regions, would be detectable using similar techniques is unknown (at least to us) and will be investigated in this project.

If argon frost exists, the effect of such a frost on the thermal properties will be investigated. Using thermal conductivity, specific heat capacity and density of solid argon from [15], we estimate the thermal inertia ~ 700 J m^{-2} s$^{-1/2}$ K^{-1} (SI Units) at 40 K between the thermal inertia of lunar regolith (~ 43 SI) and rocks (~ 2500 SI).The thermal inertia measurements done by LRO-Diviner could identify possible argon frost.

References:

[1] Watson, K.B. et al (1961), *JGR., 66*, 3046-3303, [2] Arnold, J.R. (1979), *JGR, 84*, 5659-5668, [3] Vasavada, A.R. et al., (1999), *Icarus, 141*, 179-193, [4] Hodges, R.R. (1980), *PLPSC XI*, 2463-2477, [5] Hodges, R.R., and J.H. Hoffman, (1974), *PLPSC V*, 2955-2961, [6] Chin, G. et al, (2007), *Space Sci. Rev., 129*, 391-419, [7] Crider, D.H., and R.R. Vondrak, (2003), *JGR, 108(E7),* 5079, [8] Heymann, D. and A. Yaniv, (1970), *GeoCAS, 1*, 1247 [9] Hodges, R.R., (2002), *JGR, 107*, 5001, [10] Crotts, A.P.S, (2008), *ApJ, 687*, 692, [11] Wieler, R., and V.S. Heber (2002), *Space Sci. Rev., 106*, 197-210, [12] Gladstone, G.R. et al., (2005), *Proc.SPIE, 5906*, doi:10.1117/12.617778, [13] Flynn, B., (1998), *ApJ, 500*, L71, [14] Parker, J.W. et al. (1998), *ApJ, 509*, L61, [15] Dobbs E.R and G.O. Johns, (1957), *Rep. Prog. Phys., 20*, 516

REFLECTANCE SPECTROSCOPY OF SINGLE MINERAL GRAINS: IMPLICATIONS FOR LUNAR REMOTE SENSING. Ed Cloutis[1] and Leif Norman[1], [1]Department of Geography, University of Winnipeg, 515 Portage Avenue, Winnipeg, Manitoba, Canada; e.cloutis@uwinnipeg.ca.

Introduction: Interpretation of spectroscopic remote sensing data for the Moon has relied on a variety of materials, including bulk lunar samples, lunar mineral separates, and terrestrial analogues [e.g., 1]. Each type of sample provides valuable insights into lunar surface geology. Terrestrial samples, such as mineral separates have been invaluable for developing relationships between mineral composition, structure, and spectral variations [e.g., 2-3]. Bulk lunar samples have provided insights into how exposure of the lunar surface to space (space weathering) can affect spectral reflectance [4]. Some advances have also been made in measuring the spectral reflectance properties of lunar sample separates, such as constituent minerals and glass, but these studies have been of limited scope because of the difficulties inherent in producing pure fractions in sufficient quantities [1]. Given the compositional diversity of the lunar surface, it is desirable to expand the range of reflectance spectra of lunar minerals and other regolith constituents.

To date, only transmission spectroscopy has been applied to analysis of single grains of lunar materials [e.g., 5]. This is due to the long heritage of transmission compared to reflectance spectroscopy, and the perceived difficulties in conducting, and limitations of, single grain reflectance spectroscopy. Here we report the results of ongoing work to develop single grain reflectance spectroscopy techniques. This work is an outgrowth of a similar effort for characterization of diamond indicator minerals.

Experimental set-up: Work to develop a methodology for measuring single grain reflectance spectra, and to assess the validity of the resultant data for interpretation of remote sensing data, has been fraught with many false starts and disappointing results. The derived methodology presented here is based on the lessons learned during this investigation.

In our methodology development we were trying to balance signal-to-noise ratios, time for spectral acquisition, minimization of spurious spectral features, repeatability, and ease of use. The methodology that we found provided the best balance involves a 0.25” diameter well with a tapered bottom in an aluminum alloy (T6061) block (Figure 1). This set-up was developed specifically for use with single grains in the 250-1000 micron size range. With this configuration, a single grain is placed in the bottom of the well. For our spectroscopic measurements we are using both an Ocean Optics S2000 and ASD FieldSpecPro HR spectrometer. Both are equipped with a 0.25” diameter steel ferrule at the business end of bifurcated optical fiber assemblies. The fiber bundles direct light into the well from an external light source and reflected light to the spectrometer. The Ocean Optics fiber bundle consists of a ring of 6 illumination fibers surrounding a central pick-up fiber. The ASD fiber bundle consists of ~150 fibers with half providing illumination and the other half directing the reflected light to the three detectors. The illumination and pick-up fibers are randomly arranged in the bundle. The numerical aperture of each fiber is ~0.2, corresponding to a field of view of ~25°.

The steel ferrule is of the same diameter as the well, so that when it is inserted in the well, external ambient light is eliminated. The distance from the end of the fiber bundle to the bottom of the well is 0.75”. With the numerical aperture of the fiber and depth to the sample, most of the incident light interacts with the walls of the well, which are rough to facilitate light scattering. The bottom of the well is tapered (60° from normal); we found that a flat-bottomed well resulted in too little light interaction with a single grain, resulting in an essentially featureless spectrum. We also investigated an off-axis arrangement where the grain is not in the direct field of view (for either illumination or pick-up). We found that this resulted in too low a SNR and lack of strong mineral absorption features. Similarly we investigated a variety of integrating spheres with various sizes and arrangements of sample illumination and reflected light pick-up (direct, indirect). None of these performed as well as the vertical well set-up.

Our choice of an Al alloy for the sample block was a compromise between optical stability, high reflectance, and spectral neutrality. We investigated a wide variety of metals and found that while pure metals such as Ag or Al are spectrally quite featureless between 0.35 and 2.5 µm, they are prone to oxidation and changes in spectral properties. The Al alloy that we selected (T6061) was spectrally similar to other Al alloys that we investigated: a shallow absorption band near 0.8 µm and small narrow features near 1.35 and 1.8 µm (Figure 2). This material has shown excellent spectral stability over many months.

We also investigated the use of Spectralon/halon/PTFE for sample wells or integrating

spheres. We found that these materials, which are highly reflective due to scattering by grain boundaries, did not confine the light enough to provide featured spectra. By contrast, the metal well confines all the light within the well.

Our spectral measurement methodology uses the empty well as the standard, and well plus grain as the sample (dark currents are also subtracted). Given the size of a typical grain (250 µm = ~0.2 mm^2 of occluded well) compared to the area of the well sides and bottom (~400 mm^2), <<1% of the well's surface area is occluded by a grain. Scattering of the incident light by the walls and bottom of the well helps to provide a relatively uniform illumination of all facets of a grain.

Results: The quality of the single grain spectra was measured against standard powdered sample spectra (<45 µm, 250-500, and 500-1000 µm). Our most advanced work involves garnet and olivine.

Olivine offers a better test of the methodology than garnet because it is anisotropic. The relevant olivine reflectance spectra (acquired with the ASD spectrometer) are shown in Figure 3. The single grain spectra retain the characteristic spectral shape of olivine (the 3 grain spectra are for the same grain in different orientations in the base of the well). The broadness and depth of the 1-µm region absorption feature is also comparable to the coarse powder spectra. Some of the minor absorption bands in the 0.3-0.4 µm region are also preserved in the single grain spectra. Overall reflectance of the single grain spectra is higher than the powders, but this is not unexpected. Absolute reflectance also exceeds 100% in one of the single grain spectra, however these test results were also used to examine sensitivity to small variations in height of the probe above the well. The single grain spectra artifacts around 0.65 µm due to the ASD's order sorting filter.

Conclusions: We are currently expanding the range of minerals that we are investigating, to include the most important lunar minerals (ilmenite, plagioclase feldspar, pyroxenes). Preliminary results suggest that these minerals are also measurable with this single grain configuration and produce reflectance spectra comparable to conventional powder spectra in the same sense as the olivine results presented here, and applied to analysis of lunar spectra. This capability is important for lunar minerals which may be compositionally heterogenous, such as metal oxides. Thus a single lunar sample can be used as a probe of spectral variability – a capability which is not readily attainable for a conventional powder sample spectrum which may contain spectral contributions from heterogenous grains.

References: [1] Adams J.B. and Jones R.L. (1970) *Science*, 167, 737-739. [2] Cloutis E.A. and Gaffey M.J. (1991) *JGR*, *96*, 22809-22826. [3] Cloutis E.A. et al. (2004) *Meteoritics & Planet. Sci.*, *39*, 545-565. [4] Charette M.P. et al. (1974) *JGR*, *79*, 1605-1613. [5] Burns R.G. et al. (1973) *Proc. LSC*, *4*, 983-994.

Acknowledgments: This work was supported by grants and contracts from NSERC, CSA, and UW.

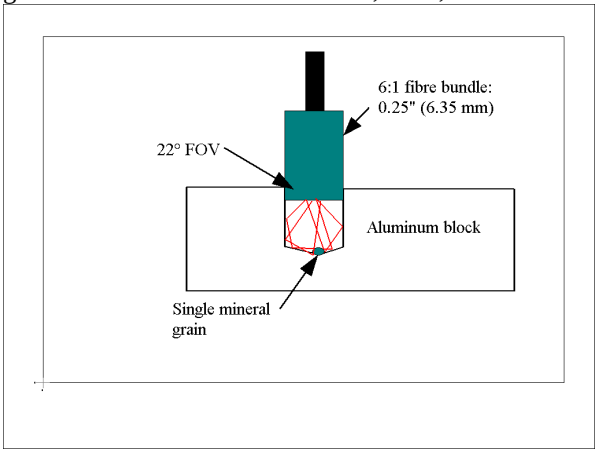

Fig. 1. Experimental set-up for single grain work.

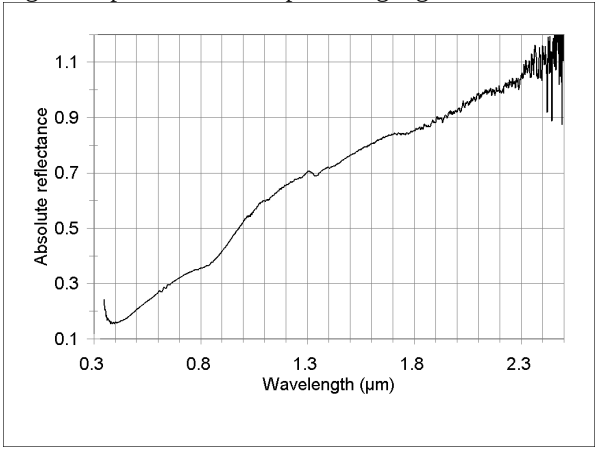

Fig. 2. Reflectance spectra of Al alloy sample well.

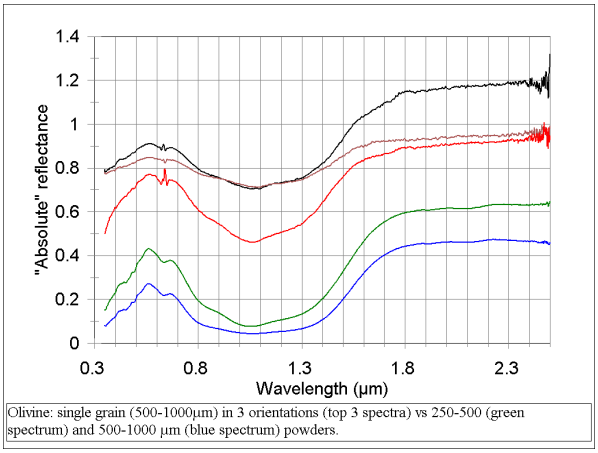

Fig. 3. Spectra of olivine single grains and powders.

THE LUNAR CATACLYSM AND HOW LRO CAN HELP TEST IT. B. A. Cohen, NASA Marshall Space Flight Center, Huntsville AL 35812 (Barbara.A.Cohen@nasa.gov)

Introduction: One of the important outstanding goals of lunar science is understanding the bombardment history of the Moon and calibrating the impact flux curve for extrapolation to the Earth and other terrestrial planets. The "terminal lunar cataclysm," a brief but intense period of bombardment about 3.9 billion years ago, is of particular scientific interest. Radiometric dating of lunar impact-melt rocks forms the backbone of the lunar cataclysm hypothesis. A histogram of precise age determinations of impact-melt rocks shows the characteristics of the classic formulation of the lunar cataclysm hypothesis: a sharp peak at 3.9 Ga, a steep decline after 3.9 Ga perhaps only 20-200 Myr long, and few rocks of impact origin prior to ~4.0 Ga [1-3]. The paucity of impact-melt rocks older than 3.9 Ga has been be variously interpreted as evidence that there was a low flux of impactors prior to ~3.9 Ga, creating few impact melt rocks [2], that the early impactor flux was so high that the lunar crust was reset and/or destroyed (the “stone wall” effect) [4], or that the dated samples may all be related to a single basin-forming event, Imbrium [5]. If the early lunar flux were much lower, then the apparent spike in impact rate would be a true "cataclysm.” If the flux were much higher, than the increased flux could be viewed as simply a bump or inflection on a generally declining post-accretionary impact rate.

Mass constraints on the amount of material needed to create the large lunar basins appears to support a low pre-Nectarian flux [6], and the population of planetesimals remaining from planetary accretion would have been insufficient to produce as many basins as late as Imbrium, Serenitatis, and Nectaris [7]. Instead, insights gleaned from our improved understanding of giant planet formation and migration in planetesimal disks suggest that the Jovian planets experienced a late, sudden instability as they crossed some mutual resonance. This triggered a rapid depletion of the trans-Neptunian planetesimal disk and caused an acceleration of the migration of Jupiter and Saturn, which in turn destabilized the majority of the asteroids in the main belt. The “Nice model” built on this idea not only explains the main characteristics of the impact spike in terms of delay, intensity and duration, but also the current orbital architecture of the giant planets, the existence and the orbital distribution of many populations of small bodies (trojans, KBOs, satellites) [8-10]. This class of dynamical models, that invokes secular sweeping of the asteroid main belt via resonances, has been bolstered by work on the size-frequency distribution of lunar craters mirrors that of the main belt [11]. The responsible impactor population, and the dynamics of its delivery, plays an important role in determining whether the impact flux history of the Moon should map onto the other terrestrial planets.

The lunar cataclysm hypothesis continues to be tested. Indeed, the top three science goals articulated in The Scientific Context for the Exploration of the Moon (SCEM) [12] relate to placing better constraints on the lunar impact flux. Because of the fine detail gleaned in terrestrial labs from existing samples, the level of precision needed to address some of the outstanding questions related to the cataclysm depends on sample return. However LRO could assist in meeting these goals in important ways:

(SCEM 1a) Test the cataclysm hypothesis by determining the spacing in time of the lunar basins. There is little recognizable pre-Nectarian terrain on the Moon for crater counting, stratigraphy, or association with rock ages. However, the timing of the large Imbrian-era basins can be constrained by using LRO high-resolution images to provide targeted crater counts of undisturbed ejecta surfaces from Orientale, Imbrium, Serenitatis, and Nectaris, as well as Imbrian-era farside basins. Identification and mapping of extant melt sheets in nearside basins such as Nectaris and in farside basins would be important in guiding future missions to sample such lithologies.

Another possibility for putting age constraints on ancient surfaces may be improved crater counting on the oldest basalt flows. In turn, stratigraphic relationships between such ancient basalt flows and basin ejecta may help bound basin formation ages. Some of these flows have been identified on the eastern limb by crater counting [13, 14]. Others may be identified based on their mineralogical or elemental affiliation with ancient basalt samples in our collection, such as the high-Al basalts and lunar meteorite Kalahari 009 [15-17]. In particular, farside flows may hold important clues. Model ages of mare deposits on the lunar farside using crater frequency distributions in 10 m/px images obtained by Kaguya’s Terrain Camera identified an ancient basalt flow in Mare Nishina, at ~3.85 Ga.[18].

(SCEM 1b) Anchor the early Earth-Moon impact flux curve by determining the age of the oldest lunar basin, the South Pole-Aitken (SPA) basin. The SPA basin, with a diameter of 2000 km, is the stratigraphically oldest lunar basin and probably created more impact melt than all other lunar craters combined.

Endogenous impact melt probably still resides on the basin floor and could be directly sampled by a robotic mission. Before that time, however, higher-resolution images to provide targeted crater counts on ejecta of basins within SPA would help bound the SPA formation age and provide constraints on the impact history provided by a scoop sample. Remote sensing of possible sample collection sites is also crucial to help determine the regional geologic context of future returned samples.

(SCEM 1c) Establish a precise absolute chronology. It is important to understand the inflections and changes in of the lunar flux throughout time so that we can judge whether a period, such as the Cataclysm, is truly anomalous. Are age-correlated changes in the apparent lunar crater size-frequency distribution due to of erasure of small craters or due to evolution of the production function? How do changes in the lunar crater size-frequency distributions reflect the impactor populations responsible for creating them? Higher-resolution images providing targeted crater counts on selected ejecta facies, such as Copernicus and Tycho, will be able to be correlated with radiometric ages. The very young end of the lunar flux curve can be examined by comparing new remote sensing data sets with Apollo-era data sets to detect formation of new craters.

References: [1] F. Tera et al. (1974) *Earth Planet Sci Lett* **22**, 1. [2] G. Ryder (1990) *Eos* **71**, 313. [3] B.A. Cohen et al. (2005) *Met Planet Sci* **40**, 755. [4] W.K. Hartmann (2003) *Met Planet Sci* **38**, 579. [5] L.A. Haskin et al. (1998), *Met Planet Sci* **33**, 959. [6] G. Ryder (2002) *J Geophys Res* **107**, DOI 10.1029/2001JE001583. [7] W.F. Bottke et al. (2007) *Icarus* **190**, 203. [8] R. Gomes et al. (2005) *Nature* **435**, 466. [9] A. Morbidelli et al. (2005) *Nature* **435**, 462. [10] K. Tsiganis et al. (2005) *Nature* **435**, 459. [11] R.G. Strom et al. (2005) *Science* **309**, 1847. [12] National Research Council (2007) *The Scientific Context for the Exploration of the Moon*, 120 pp, National Academies Press, Washington, DC. [13] H. Hiesinger et al. (2003) *J Geophys Res* **108**, 5065. [14] H. Hiesinger et al. (2000) *J Geophys Res* **105**, 29239. [15] C.R. Neal and G.Y. Kramer (2006) *Am Min* **91**, 1521. [16] G.Y. Kramer et al. (2008) *J Geophys Res* **113**, 01002. [17] A.K. Sokol et al. (2008) *Geochim Cosmochim Acta* **72**, 4845. [18] J. Haruyama et al. (2009) *Science* **323**, 905.

ACQUISITION AND TRACKING OF THE LCROSS IMPACT SITE WITH KECK-II. A. R. Conrad[1], J. E. Lyke[1], D. Wooden[2], C. Woodward[3], M. DiSanti[4], P. Lucey[5], [1]W.M. Keck Observatory, 65-1120 Mamalahoa Hwy, Kamuela, HI, 96743, [2]NASA Ames Research Center, Moffett Field, CA 94043, [3]Dept. of Astronomy, U. Minnesota, 116 Church St, SE, Minneapolis, MN 55455, [4]Planetary Systems Laboratory, NASA/GSFC, Code 693.0, Greenbelt, MD 20771, [5]Hawaii Institute of Geophysics and Planetology, University of Hawaii, 2525 Correa Road, Honolulu, Hawaii 96822

Introduction: We plan to use the Keck-II high-resolution, near-infrared, spectrograph (NIRSPEC) to measure the subliming water vapor in the LCROSS ejecta curtain [1]. The impact of the 2200 kg kinetic impactor will result in a ~6000 kg plume, ~30 kg of which is expected to be water ice [2]. We hope to detect the spectral signature of that water by keeping the NIRSPEC slit fixed on the plume for a sufficient length of time to acquire the needed spectra.

Tracking and Guiding: The Keck-II-NIRSPEC system provides two acquisition and guide cameras: an infrared, slit-viewing, camera sensitive out to 2.5 microns and with a field of view of 46 arcseconds on a side; and an optical-CCD annular guider with an outer diameter of 3.5 arcminutes (see fig. 1). On April 7th, 2009, during a half-night on Keck we proved that, by using both of these cameras for different aspects of acquisition and guiding, it will be possible to carry out the LCROSS observation. We will report on our methods for limiting lunar flux to levels detectable by the two NIRSPEC guiders; and on our methods for offset-guiding, in a rotating field, by locking on lunar features.

Future: We will also discuss briefly other possible observing modes for the moon, which, following our tests on April 7th, we now feel may be possible with Keck. This discussion will include a discussion of adaptive optics and, in particular, the challenges that make the use of that observing mode unlikely, but not out of the question, for Keck observations of the moon.

Acknowledgements: We gratefully thank and acknowledge the expert assistance of obeerving assistant Terry Stickel in performing the April 7th observation. Some of the data presented herein were obtained at the W.M. Keck Observatory, which is operated as a scientific partnership among the Cal Tech, Univ. California and NASA. Keck Observatory was made possible by the generous financial support of the W.M. Keck Foundation.

References: [1] McLean et al. 1998, SPIE, 3354, 566. [2] Ennico K. (2009) *LPS XL*, Abstract #1878.

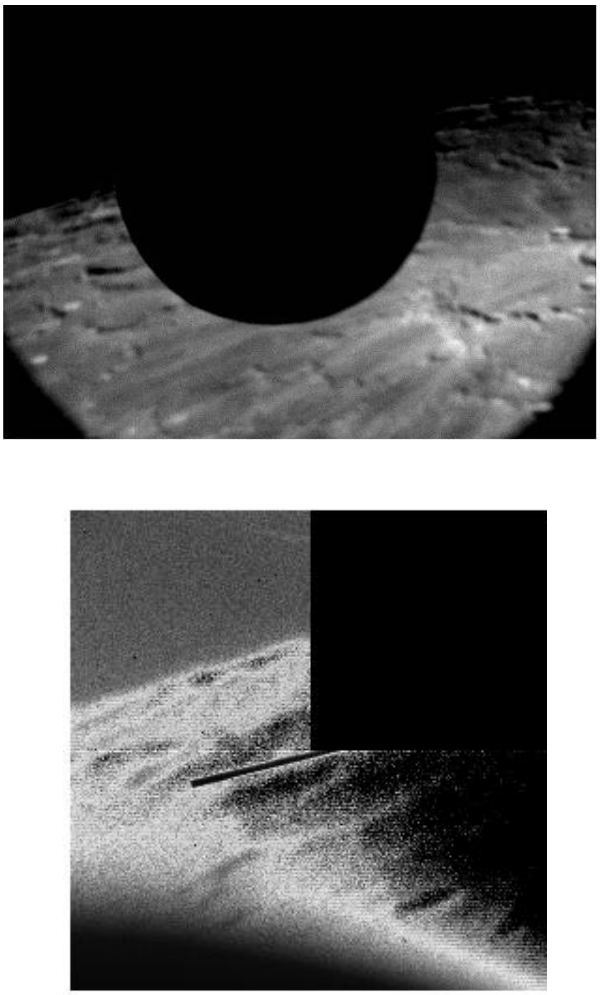

Figure 1. Representative images of the lunar surface taken with the annular guide camera (top) and the infrared, slit-viewing, guide camera (bottom).

THE IMPORTANCE OF LUNAR PALAEOREGOLITH DEPOSITS AND THE ROLE OF LUNAR RECONNAISSANCE ORBITER. I.A. Crawford[1] (i.crawford@ucl.ac.uk), K.H. Joy[1], S.A. Fagents[2] and M.E. Rumpf[2]. [1]School of Earth Sciences, Birkbeck College, London, WC1E 7HX, UK, [2]Institute of Geophysics and Planetology, University of Hawaii, 1680 East-West Road, Honolulu, HI 96822, USA.

Introduction: One of the principal scientific reasons for wanting to resume *in situ* exploration of the lunar surface is to access the record it contains of early Solar System history [1,2,3]. For example, studies of Apollo samples show that solar wind particles are efficiently implanted in the lunar regolith, which may therefore contain a record of the composition and evolution of the solar atmosphere [1,4]. Galactic cosmic ray particles may similarly be implanted, potentially leaving a record of galactic events. Samples of the Earth's early atmosphere may also be preserved [5], as well as samples of its early crust blasted off in large meteorite impacts [6]. However, as the present surficial regolith has been subject to comminution and overturning by meteorite impacts for the last three to four billion years, the record it contains will be an average over most of Solar System history. From the point of view of accessing ancient solar system history, it will be most desirable to find ancient regoliths (*palaeoregoliths*) that were formed, and buried, long ago.

Palaeoregolith Formation: A regolith will form when a fresh lunar surface is exposed to the flux of micrometeorites. Most exposed mare basaltic surfaces date from between about 3.8 Ga to 3.1 Ga, with relatively small-scale, geographically restricted, volcanism continuing to perhaps as recently as 1 Ga [7,8]. For example, the study by Hiesinger et al. [8] reveals a patchwork of discrete lava flows in Oceanus Procellarum with individual ages ranging from about 3.5 to 1.2 Ga. As younger lava flows are superimposed on older ones, we may expect to find layers of palaeoregoliths sandwiched between lava flows dating from within this age range. Support for the existence of such palaeoregolith layers is provided by recent results from the Kaguya radar sounder [9]. The archival value of palaeoregoliths will be enhanced by the fact that the under- and overlying basalt layers will lend themselves to radiometric dating, thereby defining the age of the geological record sandwiched between them.

Preserving a Record: A worthwhile geochemical record will only be preserved within a palaeoregolith layer if it survives the thermal consequences of burial by the initially molten overlying lava flow. In previous work [10,11] we have shown that, for lava flows ranging from 1 to 10 m thickness, solar wind and galactic cosmic ray particles should be preserved in palaeoregoliths at depths of greater than 0.1 to 1 m beneath an overlying lava flow, depending on the thickness of the latter. Given estimated regolith accumulation rates [12], individual lava flows would have to remain exposed for between 20 and 200 Myr to accumulate regoliths in this thickness range. The ages of individual basalt flows mapped by Hiesinger et al. [8] indicate that this is likely to have been a common occurrence, and sampling such palaeoregolith deposits would be an important objective of future exploration activities.

Importance of LRO: Geological mapping has already highlighted regions where palaeoregoliths may be expected (e.g. [7,8,13,14]), and the next step is to survey the boundaries of lava flows mapped as having different ages to identify localities where buried palaeoregoliths may be accessible to future exploration. We propose that targeted LROC NAC (50 cm/pixel) images be acquired of a number of such boundaries early in the mission in order to assess the feasibility of identifying potential outcrops. Identifying localities where small impact craters have excavated the surficial regolith to expose the boundaries, as may have occurred at the Apollo 15 Station 2 locality [15], will be of particular interest. Through studying the morphology of small impact craters [16] and/or spectral indicators that they have excavated buried lava flows [14], it may also be possible to identify localities where modest drilling (≤ 10m) would permit access to undisturbed palaeoregoliths. We note that while LROC images may also identify candidate palaeoregolith outcrops in the walls of rilles or large craters, these are likely to be less accessible than localities close to flow boundaries at the surface. The eventual aim would be to produce a catalogue of candidate outcrop localities which could inform the site selection of future surface missions.

References: [1] Spudis, P.D. (1996) *The Once and Future Moon*, Smith. Inst. Press. [2] Crawford, I.A. (2004) *Space Policy* 20, 91. [3] National Research Council (2006) *The Scientific Context for Exploration of the Moon*. [4] Wieler, R., et al. (1996) *Nature*, 384, 46. [5] Ozima, M., et al. (2005) *Nature*, 436, 655. [6] Armstrong, J.C., et al. (2002) *Icarus*, 160, 183. [7] Wilhelms, D.E. (1987) *The Geologic History of the Moon*, USGS Prof. Pap. 1348. [8] Hiesinger, H., et al. (2003) *JGR*, 108, E7, 1. [9] Ono, T. et al. (2009), Science, 323, 909. [10] Crawford, I.A., et al. (2007), LPSC, 38, 1323. [11] Rumpf, M.E., et al. (2008), LPSC, 39, 2259. [12] Horz, F., et al. (1991) in: *The Lunar Sourcebook*, CUP; p. 90. [13] Bugiolacchi, R., et al. (2006), MAPS, 41, 285. [14] Weider, S.Z. et al. (2009), LPSC, 40, 1573. [15] Spudis, P.D. & Taylor, G.J. (2009), LPSC, 40, 1039. [16] Wilcox, B.B., et al., *MAPS*, 40, 695, (2005).

MOONLITE*: SCIENCE CASE AND TARGETING CONSIDERATIONS. I. A. Crawford[1] (i.crawford@ucl.ac.uk), A. Smith[2], R. A. Gowen[2], K. H. Joy[1], and the UK Penetrator Consortium[3]. [1]School of Earth Sciences, Birkbeck College, London, WC1E 7HX, UK, [2]Mullard Space Science Laboratory, University College London, UK. (www.mssl.ucl.ac.uk/pages/general/news/UKLPC/UKLPC.pdf). *MoonLITE is a UK-led initiative which is currently the focus of a joint UK-NASA Phase-A study.

Introduction: MoonLITE is a proposal for a UK-led mission to the Moon that will place four instrumented scientific penetrators in the lunar surface to make geochemical and geophysical measurements that cannot be made from orbit [1,2]. It has the potential to make major contributions to lunar science, while at the same time providing knowledge that will be of central importance in the planning of future human missions to the Moon. In December 2008 the British National Space Centre (BNSC) announced that it would fund a Phase-A study for MoonLITE, and this is expected to start in April 2009. Following discussions with NASA, it is intended that there will be a significant US contribution to this study, in the expectation that MoonLITE will be a major vehicle for UK-US collaboration in lunar exploration (as envisaged by the 2007 NASA-BNSC Joint Working Group [3])

Scientific objectives: The principal scientific objectives of the MoonLITE penetrator mission are:

- To further our understanding of the origin, differentiation, internal structure and early geological evolution of the Moon;
- To obtain a better understanding of the origin and flux of volatiles in the Earth-Moon system;
- To obtain 'ground truth' geochemical data to complement orbital remote-sensing observations;
- To collect *in situ* surface data that will help in the planning of future lunar exploration.

As described in [2], these top-level science objectives require that the penetrators emplace instruments capable of contributing to several different areas of scientific investigation, including seismology, heat-flow, geochemistry, and volatile detection. These scientific objectives were reviewed by an International Peer Review Panel in July 2008, which found that "the scientific potential of the MoonLITE penetrator network concept to be exceptionally high in the context of the international exploration activities" [4].

Site targeting strategy: Current thinking calls for MoonLITE penetrators to be targeted as follows: one into a permanently shadowed south polar crater, one into a shadowed north polar crater, one into the central farside highlands, and one into the central nearside within the area covered by the Apollo network. Such a distribution would provide global coverage for the seismic, heatflow and geochemistry measurements, while at the same time sampling two permanently shadowed craters and providing some benchmarking against the earlier Apollo measurements. However, the nature of the MoonLITE mission, with penetrators being deployed from a polar orbiting spacecraft, ensures that it is very flexible with regard to site selection. This is a strength of the mission concept because it means that sites could, in principle, be chosen in response to the distribution of other surface assets (e.g. the nodes of the International Lunar Network, ILN) in such a way as to maximise the overall scientific return.

Importance of LRO: The high spatial resolution of the LROC WAC (75 m/pixel) and NAC (50 cm/pixel) cameras will be invaluable in the detailed planning of MoonLITE site selection. Whereas the regional locations of the impact sites can be defined by combining scientific considerations with the distribution of other surface networks, as discussed above, the final choice of specific target locality for each penetrator will require a detailed knowledge of the local terrain and associated hazards. The penetrator impact target ellipse is currently envisaged as having a width of 2-3 km, which means that relatively flat areas of this extent, free from surface boulders, and having local regolith depths of at least 5 m, will need to be identified to maximise the chance of penetrator survival. It is envisaged that LROC images will be able to contribute to impact site hazard assessment in each of these respects – the spatial resolution will be sufficient to map the distribution of surface boulders directly, and local regolith depth may be determined from a close analysis of small impact crater ejecta morphology [5]. Targeting within permanently shadowed craters will require special care, and we anticipate that LROC, and other LRO instruments, will be invaluable in this respect.

Conclusion: The UK-led MoonLITE mission provides an exciting opportunity to advance lunar science through UK-US collaboration. One aspect of this will be provided through the unique capabilities of LRO in selecting safe and scientifically valuable impact sites for the MoonLITE penetrators.

References: [1] Gao, Y., et al., *Planet. Space Sci*.,56, 368, (2008). [2] Crawford, I.A. & Smith, A., *Astron. Geophys*., 49, 3.11, (2008). [3] NASA-BNSC Joint Working Group Report, 2007 (http://www.bnsc.gov.uk). [4] MoonLITE IPR Report, 2008 (http://www.bnsc.gov.uk/7304.aspx). [5] Wilcox, B.B., et al., *MAPS*, 40, 695, (2005).

HIGH RESOLUTION IMAGING OF SITES OF RAPID CHANGES ON THE LUNAR SURFACE. A. Crotts[1] for the AEOLUS[2] collaboration; [1]Columbia University, [2]Atmosphere from Earth, Orbit and LUnar Surface

Introduction: There are several reasons why large, sudden, intrinsic changes might occur on the lunar surface, either temporarily or semi-permanently: cometary and meteoritic impacts, spacecraft impacts (or effects of other human activity), or the still unknown mechanism reported as Transient Lunar Phenomena (TLP or LTP). In the case of the latter, until 20 to 30 years ago, optical transients on the lunar surface were seen as an important, outstanding lunar mystery in need of study. [1,2,3] Since then, we have gained little understanding of TLPs, although recent work offers statistical evidence that they are at least highly correlated with lunar surface outgassing traced by ^{222}Rn. [4] The debate on even the reality of TLPs as a coherent physical effect (as opposed to observer error) has been limited to the popular literature, both pro and con. [5,6]

The primary difficulty with TLPs is the largely anecdotal nature of nearly all of the historical observational database. Although many TLP reporters were trained observers, and even though ^{222}Rn results above [4] were greatly expunged of many such effects, [7] this topic suffers from lack of an unbiased, objective data sample. We report on progress to produce such a dataset exploiting recent advances in robotic telescope technology, and follow-up studies to enhance the value of these observations, simultaneous to lunar satellite surveys bearing on outgassing. The *Kaguya*/ARD is in lunar polar orbit and designed to detect ^{222}Rn outbursts like those seen on Apollo and *Lunar Prospector*. Furthermore, *LRO* and other lunar satellites maintain orbit over the period 2005-2011, and will image repeatedly the lunar surface at high resolutions.

We are conducting a robotic imaging survey of the lunar surface from several ground-based monitors that image the entire Near Side every 20 seconds whenever the Moon is up, the Sun is down and weather permits. This monitoring will record the incandescent plasma flash from any impact large enough to create a permanent change on the order of 100 m or larger, corresponding to mpacts which might occur on the order of every few years (very roughly). This is also an excellent time sampling for the reported durations of TLPs.

Transient Monitoring Dataset: Since early 2008 we have monitored the Near Side with 0.25-meter telescopes imaging onto 16 Mpix CCDs. The two robotic telescopes are stationed at Cerro Tololo Inter-american Observatory near La Serena, Chile (70°.82W Long, 30°.16S Lat) and Rutherford Observatory in New York, NY (73°.96W Long, 40°.81N Lat). These allow possibly simultaneous observation of the same event at widely separated (~8000 km) sites, to help certify the lunar origin of a doubly-detected event.

Images produced by each monitor are nearly identical, corresponding to ~1.0 arcsec per pixel (~1.8 km). Since the historical database of TLP reports concentrate almost entirely in 1-100 minute durations, each monitor is programmed to take an exposure every 20 s, with a typical duration of 10 ms. As of 2009 April 16 these monitors have produced approximately 140,000 science images, equivalent to 1 month of continuous operation. Our goal is to at least triple this duration (based on several estimates from historical report rates, indicating intrinsic rates of several per month).

Data Reduction and Analysis. Once images are bias level subtracted and flat fielded, they are convolved with an image kernal that adjusts each image to a common image quality and subtracts the resulting flux from a reference image common to all exposures. This image subtraction residual has nearly all of the constant flux removed from each original image. In this case a change due a transient source is much easier to detect (by approximately a factor of 10 over what the eye detects as changes in the original image) to a level of order 1-2% of the original flux contained in a 1-arcsec point source (FWHM).

Results. At this point (2009 April 16) we have processed a test sample of 5000 images and found that we are approaching the photon-noise limit of sensitivity to flux changes. We are beginning analyze the entire dataset. We also continue to operate the two robotic stations. The summary of this effort is found at http://www.astro.columbia.edu/~arlin/TLP/ We will report at the meeting on the status of event detection.

Followup Observations: If TLP events are due to outgassing from the lunar surface, one plausible mechanism for these is the accumulation of gas below the regolith, leading to a localized blowout through the overlaying material as gas pressure increases. [8] One possible observable consequence beyond short-lived TLP events might be the quasipermanent change in the photometric properties of the regolith surface due to the age of dust indicated by the 0.95 micron Fe^{2+} band. [9,10] Not only is this band covered at high spatial resolution by current and future lunar missions, but we are conducting (approaching) diffraction-limited "Lucky Imaging" observations from the ground during this time with roughly 0.4-km resolution. [8] These are being made at the Calypso 1.2-meter imaging-optimized telescope over the period 2008-2011. In

addition to the 0.95 micron pyroxene band, the broadband reddening in the optical is a regolith maturity indicator; [11] these bands are covered by nearly all high-resolution imagers in lunar orbit, including LROC.

Potential Targets: There are several classes of sites that should be images at high resolution to further this study: 1) sites of reported TLPs, 2) sites of suspected, large historical impacts, and 3) sites of large spacecraft impacts. Consider these one at a time.

TLP Report Sites: Our survey's catalog of transient detections is still a work in progress, although we plan to report more results by the time of this Meeting. The previous, historical record of such reports is anecdotal, biased and likely contaminated by spurious reports, however there are some consistent patterns in reporting that are robust against various statistical sieves designed to reject spurious reports. [4,7] Craters Aristarchus, Plato, Grimaldi, Kepler, Tycho and Copernicus consistly survive these filters. (Note: Aristarchus, Plato and Kepler are also the only sites of reliable ^{222}Rn outgassing detections.) More than half of the robust sample lands on the Aristarchus Plateau. While it is true that the crater Aristarchus is a high-contrast feature which might be suspected to potentially mislead some visual observers into reporting false transients, a large fraction of these reports occur far from the crater in the Plateau interior. (See Figure 1.)

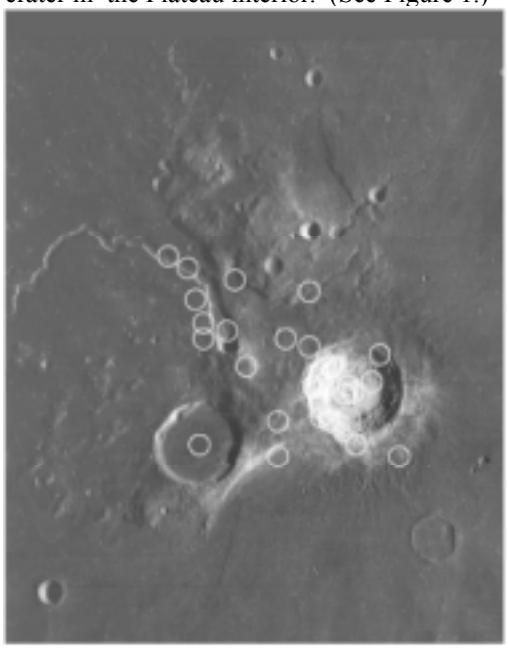

Figure 1: cleaned *Lunar Orbiter IV* photo of the Aristarchus Plateau with locations of detailed reports of TLPs from the most reliable (pre-1957) portion of the historical data base. Each is marked with a 10 km diameter circle. Some marks in Aristarchus and Vallis Schröteri represent multiple reports.

One prior limitation to such a study was the absence of a rectified, cleaned "before" image of this Aristarchus Plateau as would be required to reliably show any changes caused by TLP events or any other process; however, several 2-3 m resolution sequences of this region were taken with *Lunar Orbiter V*, and we are currently engaged in a funded effort to rectify and clean these images, among others. [12] If all else fails regarding the modern detection of events with the robotic monitors, some effort should be made to see if permanent changes are associated with the Aristarchus Plateau.

In terms of large impacts seen during historical periods, there are two still uncertain cases of possible events, from the years 1178 and 1953, the latter being recorded photographically. Several works have debated the interpretation of each event, and we will not discuss these further here.

Finally, all of the Saturn V third-stage S-IVB boosters which struck the Moon (except one) were tracked accurately to their impacts (and in most cases localized with seismometers). These serve as known calibrations for the effects of impacts on the lunar surface and should be observed at high resolution. In addition, the Apollo LM ascent stages and several other spacecraft impacts offer smaller features worthy of study.

References: [1] Lunar Geoscience Working Group (1986) *Status & Future of Lunar Geoscience*, NASA SP-484.; also Grant H. H., Vaniman D. T. & French B. M. (1986) *Lunar Sourcebook* (Cambridge U. Press), p. 654. [2] Geake J. E.. (1976) *Report of Ad Hoc Working Group, Comm. 17, IAU*, Proc. IAU Gen. Ass'y, 16, p. 150. [3] Various authors in TLP special issue (1977) *Phys. Earth & Planet. Interiors*, vol. 14. [4] Crotts A. P. S. (2008) *ApJ*, 687, 692. [5] Cameron W. S. (1991) *Sky & Tel.*, 81, 265. [6] Sheehan W. and Dobbins T. (1999) *Sky & Tel.*, 98, 118. [7] Crotts A.P.S. (2009) *ApJ*, in press (also http://arxiv.org/abs/0706.3947). [8] Crotts A.P.S. & Hummels C. (2008) *ApJ,* submitted (http://arxiv.org/abs/0706.3952 & 3954). [9] Charette M.P. et al. 1976, LPSC, 7, 2579. [10] Lucey P. *et al.* (2000) *JGR,* 105, 20,377. [11] Buratti B. et al. (2000) Icarus, 146, 98. [12] Byrne C. & Crotts A.P.S., in preparation.

THE DYNAMICS BEHIND INNER SOLAR SYSTEM IMPACTS - PAST AND PRESENT. M. Cuk[1], [1]Department of Earth and Planetary Sciences, Harvard University, 20 Oxford St, Cambridge, MA 02138. E-mail: cuk@eps.harvard.edu.

Introduction: Lunar impact history (which is our best proxy for that of the whole inner system) can be divided into three distinct eras. The last 3.5 Gyr have been dominated by bombardment due to NEAs ultimately derived from the asteroid belt. The bombardment in the first couple of hundred Myr was very likely dominated by the sweep-up of debris leftover from inner planet formation. Between these two eras, at 3.9-3.8 Gyr ago, the Moon apparently experienced a cataclysm known as the Late Heavy Bombardment (LHB) during which the impactor dynamics was likely very different from that before and after this event. Here I will present a review of what is (though to be) known about the dynamics of impactors during each of these eras.

Present Bombardment: Ever since Hartmann's original estimate of the age of lunar maria, researchers have accepted that the present rate of bombardment by near-Earth objects can be extrapolated as far back as 3.5 Gyr ago [1]. Modern view sees near-Earth asteroids as an order of magnitude more important source of impactors than the comets {2}. These NEAs are thought to have been derived from the asteroid belt through the action of various gravitational resonances [3, 4]. Now the prevailing view is that the new obects are fed to resonances by the Yarkovsky effect, rather than directly from asteroid collisions [5, 6]. While this process is roughly in a steady state, there is some uncertainty of how important individual family-forming events are for the bombardment rate on Earth and the Moon. It is plausible that the numbers of NEAs can increase by a factor of few for tens of Myr following a large family forming event in the main belt [7]. Alternatively, a long-term decline in bombardment has also been proposed based on some martian cratering and lunar meteorite data [8, 9], but this view is currently not supported by dynamics. There is also a question of interpretation of lunar spherule data peak since 400 Mya [10] and possible connection to meteorite ages and formation of certain main-belt asteroid families [11].

Post-Formation Bombardment: As the inner planets are thought to have formed by accretion of smaller bodies, it is all but certain that all bodies suffered very high rater of bombardment by accretion leftovers early in the Solar System's history. While there has been lots of uncertainty in the rate of this sweep-up, recent numerical work [12] has conclusively shown that the impacts due to post-formation debris decrease by at least two orders of magnitude within the first 200 Myr. Presently, it is a wide open question which (if any) of the visible lunar features might have been formed by this bombardment, as no sampled lunar units have widely agreed pre-LHB dates. There is also additional issue of geocentric debris leftover from lunar formation. While most of it is likely to be swept-up soon, other stable satellites could have formed [13]. However, fast tidal evolution of the Moon would have destabilized all other satellites in less than 100 Myr [14]. In principle, some of the oldest basins could have been produced in collisions with other geocentric objects, but their effects would be hard to distinguish from those of heliocentric leftover planetesimals.

The Lunar Cataclysm/ Late Heavy Bombardment: After being controversial for several decades, it is now likely that the Lunar Cataclysm 3.8-3.9 Gyr ago [15] was an event distinct from planet formation (see [16] for an an opposing view). The most solid evidence of the cataclysm is that the formation of Imbrium and Orientale basins too late and too close together in time to be explained either by formation leftovers or present NEA flux [12]. The controversy over the ages of Nectarian basins as well as meteoritic evidence is still ongoing (Dr. Cohen's and Dr. Kring's talks at this meeting), with wide-ranging implications for the extent of the LHB. While we know that the LHB ended relatively abruptly, it's beginning is not known [17], with a relatively short spike being dynamically most likely.

Currently, the most prominent dynamical explanation for the cataclysm is the so-called “Nice model” of outer planet migartion. One element of the model is the

hypothesis that the outer planet migration was delayed until the LHB [18]. During a short-lived migration phase the primordial Kuiper belt was destroyed, producing a large number of cometary impactors. However, more relevant for the known impact record might be main-belt asteroids destabilized at the same time by sweeping secular resonances [18, 19, 20]. Asteroids would be a more top-heavy impactor population than the comets, producing more basins, and would also impact the Moon and inner planets later, leaving more of a surviving record. This delay in the Nice model migration is dynamically possible, although not necessary and (to me at least) somewhat artificial. There are some possible issues with destabilization of inner planets during a late giant planet migration, but work on that is still in progress [21].

The size-distribution of lunar craters has been cited as an evidence of asteroidal impactors [22], although some of our recent work (Cuk, Gladman and Stewart 2009, under review) calls that into doubt.

In general, the immediate end-LHB impactors appear to have been on NEA-like orbits, at least according to the fall-off in lunar cratering recorded on the maria [23]. This argues against a geocentric source of impactors [24], which also are now though to be dynamically implausible [14, 25]. Apart from the destabilization of the asteroid belt [18, 26], a tidal or collisional break-up of a large inner solar system body [27] could lead to impactors on NEA-like orbits.

Conclusion: The present (post-3.5 Gya) bombardment of the Moon and the inner system is thought to be well-understood after recent advances in understanding radiation forces on asteroid and numerical modeling. The Late Heavy Bombardment, on the other hand, is still an area of intense theoretical work, and LRO observations could help us test some of the models. New photographic data could be used to determine (or confirm) crater size-distributions on different lunar stratigraphic units. In principle, the three epochs of lunar bombardment history should have had different SFDs of impactors, opening a possibility of distinguishing them using crater statistics. Of course, crater erasure and statistical limitations could interfere with this goal, but new, hypothesis-testing-oriented crater counts have a potential of advancing our knowledge of lunar history beyond the achievement of the Apollo era.

References: [1] Hartmann, W. K. (1966), Ph.D. Thesis, U. of Arizona. [2] Weissman, P. R. (1982) in *Geological Implications of Impacts of Large Asteroids and Comets on the Earth,* Silver and Schultz, eds, pp 15-24. [3] Wetherill, G. W. (1988) *Icarus,* 76, 1–18. [4] Bottke, W. F., et al. (2002) *Icarus* 156*,* 399-433. [5] Farinella, P., Vokrouhlicky, D. (1999). *Science* 283, 1507-1510. [6] Bottke W. F., et al. (2001) *Science* 294, 1693-1696. [7] Bottke, W. F., et al. (2007). *Nature* 449, 48-53. [8] Quantin, C., et al. (2007) . *Icarus* 186, 1-10. [9] Hartmann, W. K., et al. (2007) *Icarus* 186, 11-23. [10] Culler, T. S. et al. (2000). *Science* 287, 1785-1788. [11] Nesvorny, D. et al. (2009). *Icarus* 200, 698-701. [12] Bottke, W. F., et al. (2007). *Icarus* 190, 203-223. [13] Kokubo, E., et al. (2000). *Icarus* 148, 419-436. [14] Canup, R. M., et al. (1999). *Astron, J*. 117, 603-620. [15] Tera F., et al. (1974). *EPSL* 22, 1-21. [16] Hartmann, W. K. (2003). *MAPS* 38, 579-593. [17] Chapman, C. R. , et al. (2007). *Icarus* 189, 233-245. [18] Gomes, R., et al. (2005). *Nature* 435, 466-469. [19] Levison, H. F., et al. (2001) *Icarus* 151, 286-306. [20] Minton, D. A., Malhotra, R. (2009). *Nature* 457, 11090-1111. [21] Agnor, C. B., Lin, D. N. (2007). *BAAS* 39, 537. [22] Strom, R. G., et al. (2005). *Science* 308, 1847-1850. [23] Stoeffler, D., Ryder, G. (2001) *Space Sci. Rev.* 96, 9-54. [24] Ryder, G. (1990). *EOS* 71, 313, 322-323. [25] Cuk, M., Gladman, B. J. (2009). *Icarus* 199, 237-244. [26] Chambers, J. E. (2007). *Icarus* 189, 386-400. [27] Weatherill, G. W. (1975). *LSC Proc.* 2, 1539.

LUNAR RESOURCES AND LRO. M. B. Duke
Affiliation: 1030 Sunset Canyon S., Dripping Springs, TX 78620; 512-535-1671; mikeduke@earthlink.net.

Introduction: Two questions raised by the LRO meeting organizers are: (1) "What do we need to know about in-situ characteristics of potential lunar resources before decisions are made regarding their use or exploitation?"; and (2) "How can LRO data be used to better define lunar resources?" This abstract addresses these questions.

It must be remembered that there are no lunar resources until there are customers or markets for their products. Products could range from lunar rock pieces for collectors; to propellant for lunar and space transportation systems; to ^{3}He for terrestrial fusion reactors. Each of these would have its own base of knowledge, which might be quite small in some cases – e.g., the composition of the local rock types that would be returned for sale to collectors. Although lunar samples sales presently exist (lunar meteorites), markets for the other more sophisticated products do not currently exist. However, a reasonable choice for an initial lunar resource is rocket propellant, hydrogen and oxygen, which would be useful for supporting space transportation from a lunar outpost, surface-transportation systems, and potential export for use in space. The by-products of oxygen extraction systems from lunar regolith and pyroclastics are metals, which could become resources for a lunar outpost. The processes that are utilized for hydrogen extraction from the regolith will also produce carbon, nitrogen, sulfur, and at a larger scale, ^{3}He. Thus, oxygen and hydrogen production from regolith materials can be a forerunner of other resource applications. An exception to this is the possibility that water-ice near the lunar poles can be extracted directly for life support or propellant (though using rare lunar water for propulsion would not be a lunar "green" application). This extraction would not directly produce by-products.

Based upon the above reasoning, two major types of resources will be addressed here: hydrogen and oxygen extracted from the lunar regolith, probably anywhere on the Moon: and water extracted from polar-ice deposits.

It should also be borne in mind is that "profitability" (in a general sense) is determined by a variety of factors, the most important of which is the richness of the ore, and 'yes', water would be an ore. An ore with 1% extractable resources will require twice as much equipment and energy, or time, as one with 2%. Accessibility is important for production processes, as they will inevitably require human-tending. At an early stage, most resources will be extracted from the regolith, with digging representing the chief mechanical process required (little or no crushing) and hauling over relatively short distances. If two products are required, economics could dictate locating an operation where the total return on the process is optimized, rather than going after the highest concentration of a single ore. Processes that minimize power and mass for a given amount of useful product will be sought, because of the large cost of transporting systems to the Moon.

Most lunar resource extraction processes that have been studied (with the exception of extracting water from polar ice) require heating to high temperatures, so power supplies are important. For an equatorial plant that produces resources by electrical heating lunar regolith to 800^{o}C, the energy system (e.g., current technology photovoltaic systems or nuclear systems) typically would constitute 25-50% of the total system mass. In comparison, surface excavation and hauling require significantlysmaller energy sources and smaller equipment masses, as indicated in models built to represent resource extraction processes[1].

What do we need to know about in-situ characteristics of potential lunar resources before decisions are made regarding their use or exploitation? : An initial and principal question to be considered addresses the "grade" or tenor of the ore. For oxygen, the principal choices have focused on pyroclastic glasses and ilmenite-rich or iron-rich mare regolith; the higher the iron content in oxide phases like ilmenite and spinels,, the easier the extraction of a given amount of oxygen. The extent of the ore deposits should not be a serious issue in cases of regolith-derived products, as the composition of the regolith is usually only slowly variable laterally and vertically over the scales accessible to surface mining. Local geological structure should not normally be a serious problem, though recent impact craters that penetrate the regolith should be avoided to avoid local trafficability problems – e.g., boulder fields. Accessibility to a lunar outpost should also not be an issue; mining and processing can be located within a few kilometers of the outpost, where the infrastructure for several base systems can be shared. A systems consideration is that, as one moves away from the equator, solar power systems will require additional mass or complexity for a given power output, so power system masses may be larger.

The hydrogen concentration in typical mare regolith ranges from 50-200 ppm. Although the concentration is low and regolith must be heated to 800^{o}C to extract it, the resource is ubiquitous and much larger

in total quantity than has been suggested for permanently shadowed polar craters. Carbon and nitrogen could also be extracted using the same thermal process, and ^{3}He extraction would require similar, but much larger systems. The ability to find higher concentrations of hydrogen could help determine whether suitable locations exist where hydrogen can be directly extracted from the regolith, profitably.
: The mode of occurrence, concentration and distribution of polar-ice deposits are all critical for resource extraction. As any ice is fundamentally near surface in occurrence, the distribution with depth in the uppermost few meters will be important. Locations where ice is present at 10% concentrations over significant lateral and vertical dimensions would be ideal. Concentrations of 1% ice could be attractive, if accessibility is straightforward. Concentrations of less than 0.5% ice (~500 ppm H_2) are of questionable value as a resource, as the concentration of solar-wind derived hydrogen in locations that are less daunting operationally can reach 100-200 ppm. The physical characteristics of icy regolith (indurated, loose, grain size) will be important for designing extraction systems. If ice is located in steep-walled craters such as Shackleton, significant accessibility problems may occur; however, there are a number of locations where permanently shadowed areas exist in flat-floored craters, which may relieve accessibility issues, if water-ice is located there.

How can LRO data be used to better define lunar resources? (1) Determine the distribution of possible water-ice at the poles; (2) Map extent of icy regolith at highest resolution feasible; (3)Target all regions of permanent shadow in relatively flat-floored craters; (4) If ice is only present in steep-walled craters, obtain high-resolution imaging to plan potential accessibility; (5) Improve iron and titanium maps of the entire Moon, with emphasis on mare locations; (6) **T**arget pyroclastic deposits, particularly those more iron-rich, as to extent, possible maturity, and topography; (7) Devise a means of measuring absolute solar-wind hydrogen content of lunar regolith in general, but mare regolith specifically. (8) Establish remotely sensed soil maturity and particle-size distribution criteria and data, as these provide valuable input for evaluating potential ores.

Reference:

[1] Blair, B. R., J. Diaz, M.B. Duke, E. Lamassoure, R. Easter, M. Oderman, M. Vaucher (2002), Space Resource Economic Analysis Toolkit: The Case for Commercial Lunar Ice Mining, Final Report to the NASA Exploration Team, December 20, 2002.http://www.isruinfo.com//docs/LDEM_ Draft4-updated.pdf

Our Current Understanding of Lunar Polar Hydrogen Deposits. William C. Feldman, Planetary Science Institute, Tucson AZ 85719. Feldman@psi.edu.

Members of the planetary community have been interested in the abundance of hydrogen in planetary bodies for a variety of reasons. First and foremost stems from the realization that water is needed to support life as we know it. A long-standing question is whether life has developed only on Earth, or could it, and has it, developed outside of our earthly environment. This quest has led our community to adopt a 'follow the water' guideline for designing new planetary missions. In addition, the most probable form of hydrogen is water, which is an essential ingredient for the support of manned planetary missions. This necessity has been a major driver in the search for water on the Moon.

The suggestion for the existence of water-ice deposits within permanently-shaded regions near both lunar poles was made a long time ago [1,2]. This suggestion was followed by several studies of thermal conditions near the poles and mechanisms for the redistribution of hydrogen to polar cold traps after its delivery to the Moon by meteorites, dust, and solar wind [3,4,5]. Concurrently, the experimental search for hydrogen in the form of water ice was made using bi-static radar reflection techniques [6,7,8], and the detection of cosmic-ray generated neutrons leaking outward from the Moon [9].

All interpretations of these early experimental results have been questioned, and have spawned lengthy debates. This process is, of course, an essential part of scientific inquiry because none of these experimental techniques measure hydrogen or water ice directly. The radar observations measure the intensity and polarization of back-scattered electromagnetic radiation and the neutron observations measure the intensity of neutrons in the epithermal range of energies. Furthermore, the initial measurements using both techniques did not have the spatial resolution that matched the water-ice deposits expected to exist within a large range of craters that contained significant amounts of permanently-shaded terrain. This situation is evolving quickly on many fronts.

A reanalysis of Lunar Prospector neutron data using a more advanced neutron simulation technique [10] has narrowed possible interpretations of the reduced intensities of epithermal neutrons observed within permanently-shaded regions near both poles to the presence of hydrogen and not to other potential chemical compositions of lunar soil. The sharpening of epithermal neutron maps of both poles using the PIXON spatial-deconvolution technique [11,12] have demonstrated that the origin of the measured reductions in epithermal intensities are consistent with enhanced concentrations of hydrogenous material in some (but not all) of the permanently shadowed cold traps at high latitudes. Yet, recent images of the interior floor of Shackleton crater that borders the south pole of the Moon using the Terrain Camera aboard the Kaguya spacecraft, show no evidence for surface deposits of water-ice [13]. Nevertheless, our best interpretation of the Lunar Prospector epithermal neutron data in terms of many small-area water-ice deposits yields weight fractions ranging anywhere from a few tenths of a percent to perhaps as much as 10% to 20% in

very localized areas existing beneath a thin veneer of hydrogen-free soil [11].

However, we still cannot rule out the possibility that the observed neutron signal is due to the capture and retention of solar wind protons just beneath a very thin skin (less than about 1000 Å) that cover surface grains [14]. Because the retention time in surface skins of regolith grains is sufficiently long within the permanently-shaded craters, implanted protons will form H_2 gas bubbles that will eventually burst to form a very fine powder [9]. It is possible that the skins of these bubbles have sufficiently large areas per unit mass to hold hydrogen at mass fractions (on average, ~1%) that are consistent with the neutron observations [9]. The real question now is: Does the regolith within permanently-shaded craters consist of thick layers of gardened, very thin-skinned bubble material? An answer to this question may require a future robotic lander.

Concurrently, interpretations of the radar results to date in terms of the existence, or nonexistence, of significant deposits of nearly pure water ice have been quite robust. No one disputes that isolated locations of the Moon exist that can backscatter radar having circular polarization in the same sense as that incident on the surface. Normally, rocky planet surfaces backscatter radar having opposite-sense polarization and deposits of nearly pure water ice having thicknesses larger than the wavelength of the radar can have significant intensities of same-sense polarization. A normal interpretation of data showing enhanced same-sense polarization would then identify these terrains as containing water ice. However, some locations on the Moon that receive direct lighting from the Sun have been observed with enhanced same-sense polarized radar reflections. The question then is whether the rocky structure of these sunlit terrains also exist preferentially in permanently-shaded terrains. Future observations will be required to settle this question. Luckily, a synthetic-aperture-radar instrument is aboard the presently orbiting Chandrayaan-1 spacecraft and will also be aboard the forthcoming LRO spacecraft. Preliminary results from the SAR aboard Chandrayaan-1 are providing promising expectations [15]. In addition, the goal of the LEND experiment aboard LRO is to improve the spatial resolution of epithermal neutron maps near both poles to 10 km diameter [16].

References: [1] Watson, K., et al., JGR, 66, 3033-3045, 1961; [2] Arnold, J.R., JGR, 84, 5659-5668, 1979; [3] Butler, B.J., JGR,102,19283-19291, 1997; [4] Vasavada, A.R. et al., Icarus, 141,179-193, 1999; [5] Crider, D.H., R.R. Vondrak, JGR, 108(E7), 5079, doi:10.1029/2002JE002030, 2003; [6] Stacy, N.J. et al., Science, 276, 1527-1530, 1997; [7] Nozette S. et al., JGR, 106, 23253-23266, 2001; [8] Campbell, D.B. et al., Nature, 443, 835-837, doi: 10.1038/nature05167, 2006; [9] Feldman, W.C. et al., JGR, 106, E10, 23231-23251, 2001; [10] Lawrence, D.J. et al., JGR, 111, E08001, doi:10.1029/2005JE002637, 2006; [11] Elphic, R.C. et al., GRL 34, L13204 doi:10.1029/2007GL029954, 2007; [12] Eke, V.R. et al., Icarus, 200, 12-18, 2009; [13] Haruyama, J. et al., Science, 322, 938 doi: 10.1126/science.1164020; [14] Starukhina, L.V., Y.G. Shkuratov, Icarus, 147, 585-587, 2000; [15] Spudis, P.D. et al., LPSC XV, Abstract #1098, 2009; [16] Mitrofanov, I.G. et al., Astrobiology, 8 (#4), 2008.

SMART-1 RESULTS AND TARGETS FOR LRO

B.H. Foing, D. Koschny, B. Grieger, J.-L. Josset, S. Beauvivre, M. Grande, J. Huovelin, H.U. Keller, U. Mall, A. Nathues, A. Malkki, G. Noci, Z. Sodnik, B. Kellett, P. Pinet, S. Chevrel, P. Cerroni, M.C. de Sanctis, M.A. Barucci, S. Erard, D. Despan, K. Muinonen, V. Shevchenko, Y. Shkuratov, M. Ellouzi, S. Peters, A. Borst, F. Bexkens, L. Boche_Sauvan, P. Mahapatra, M. Almeida, D. Frew, J.Volp, D. Heather, P. McMannamon, O. Camino, G.Racca, *SMART1 STWT, ESTEC/SRE-S, postbus 299, 2200 AG Noordwijk, NL, Europe*, (Bernard.Foing@esa.int)

Abstract: We propose number of targets observed with SMART-1 for follow-up studies with LRO. We shall also discuss SMART-1 lunar highlights relevant for science and exploration, in relation with LRO/LCROSS and future lander missions..

Overview of SMART-1 mission and payload: SMART-1 is the first in the programme of ESA's Small Missions for Advanced Research and Technology [1,2,3]. Its first objective has been achieved to demonstrate Solar Electric Primary Propulsion (SEP) for future Cornerstones (such as Bepi-Colombo) and to test new technologies for spacecraft and instruments. The SMART-1 spacecraft has been launched on 27 Sept. 2003, as an Ariane-5 auxiliary passenger and injected in GTO Geostationary Transfer Orbit. The SMART-1 spacecraft reached on 15 March 2005 a lunar orbit 400-3000 km for a nominal science period of six months, with 1 year extension until impact on 3 September 2006. SMART-1 science payload, with a total mass of some 19 kg, features many innovative instruments and advanced technologies [1], with a miniaturised high-resolution camera (AMIE) for lunar surface imaging, a near-infrared point-spectrometer (SIR) for lunar mineralogy investigation, and a very compact X-ray spectrometer (D-CIXS) [4-6] for fluorescence spectroscopy and imagery of the Moon's surface elemental composition. The payload also included two plasma experiments: SPEDE (Spacecraft Potential, Electron and Dust Experiment, PI. A. Malkki) and EPDP (Electric propulsion diagnostic Package, PI G. Noci), an experiment (KaTE) that demonstrated deep-space telemetry and telecommand communications in the X and Ka-bands, a radio-science experiment (RSIS), a deep space optical link (Laser-Link Experiment), using the ESA Optical Ground station in Tenerife, and the validation of a system of autonomous navigation (OBAN) based on image processing.

SMART-1 overall themes and targets: SMART-1 science investigations included overarching themes and sub-themes:
- studies of the chemical composition of the Moon,
- geophysical processes (volcanism, tectonics, cratering, erosion, space weathering) for comparative planetology
- high resolution studies in preparation for future landing sites, lunar bases and exploration.

For each theme, we defined a set of measurement objectives for different instruments, and selection of targets measured along specific illumination conditions and operation modes .
We shall discuss the SMART-1 targets list as well as the coverage coinditions achieved by the mission. Based on these measurements and studies we define a sub-set of targets that are proposed for study with LRO.

SMART-1 instruments lunar results: A package of three spectroscopy and imaging instruments has performed science at the Moon.
SIR (Smart-1 Infra-Red Spectrometer) has been operating in the 0.9-2.6 μm wavelength range and carrying out mineralogical survey of the lunar crust. SIR had high enough spectral resolution to separate the pyroxene and olivine signatures in lunar soils.
SIR data with spatial resolution as good as 400 m permitted to distinguish units on central peaks, walls, rims and ejecta blankets of large impact craters, allowing for stratigraphic studies of the lunar crust.
AMIE (Advanced-Moon micro-Imager Experiment, PI J.L. Josset) is a miniature high resolution (35 m pixel at 350 km perilune height) camera, equipped with a fixed panchromatic and 3-colour filter, for Moon topography and imaging support to other experiments [7,10,11]. The micro camera AMIE has provided high-resolution CCD images of selected lunar areas. It included filters deposited on the CCD in white light + three filters for colour analyses, with bands at 750 nm, 900 nm and 950 nm (measuring the 1 μm absorption of pyroxene and olivine). AMIE images provided a geological context for SIR and D-CIXS data, and colour or multi-phase angle complement. AMIE has been used to map sites of interest, in the South Pole – Aitken basin that are relevant to the study of cataclysm bombardment, and to preview future sites for sampling return.
Lunar North polar maps and South pole (Fig 1)repeated high resolution images have been obtained, giving a monitoring of illumination to map potential sites relevant for future exploration .

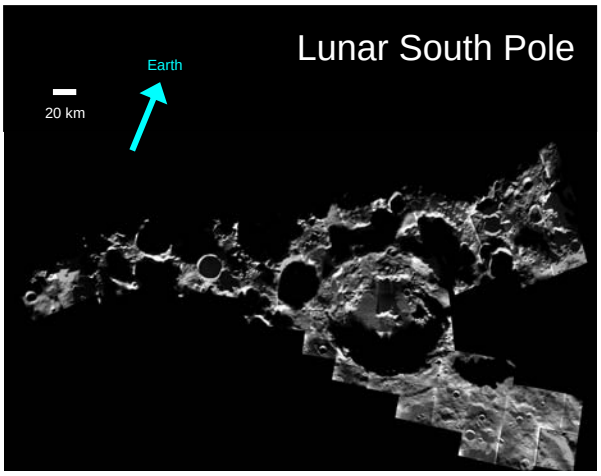

Fig. 1: SMART-1 /AMIE mosaic of the lunar South Pole . The pictures were taken between May 2005 and February 2006, during different phases of the mission.. at a distance of about 400 km, allowing medium-field (about 40 km across) and high-resolution views (40 m/pixel).

D-CIXS (Demonstration of a Compact Imaging X-ray Spectrometer, PI M. Grande) is based on novel detector and filter/collimator technologies, and has performing the first lunar X-ray fluorescence global mapping in the 0.5–10 keV range [4,5,9], in order to map the lunar elemental composition. It was supported in its operation by XSM (X-ray Solar Monitor) which also monitored coronal X-ray emission and solar flares [6]. For instance, D-CIXS measurements of Si, Mg, Al, Si, Ca & Fe lines at 1.25, 1.49, 1.74, 3.7 & 6.4 keV, were made over North of Mare Crisium during the 15 Jan 2005 solar flare, permitting the first detection of Calcium from lunar orbit [9].
Bulk crustal composition has bearing on theories of origin and evolution of the Moon. D-CIXS produced the first global view of the lunar surface in X-ray fluorescence (XRF), elemental abundances of Mg, Al and Si (and Fe when solar activity permitted) across the whole Moon. The South Pole-Aitken Basin (SPA) and large lunar impact basins have been also measured with D-CIXS.

SMART-1 operations and coordination: The Experiments have been run according to illumination and altitude conditions during the nominal science phase of 6-months and 1 yr extension, in elliptical Moon orbit. The planning and co-ordination of the Technology and science experiments operations was carried out at ESA/ESTEC (SMART-1 STOC). The data archiving is based on the PDS (Planetary Data System) Standard.

The SMART-1 observations have been also made in view of future missions coordinated with upcoming missions. SMART-1 has been useful in the preparation of Selene Kaguya, the Indian lunar mission Chandrayaan-1, Chinese Chang'E 1 , and can be used to prepare for targeting of the US Lunar Reconnaissance Orbiter, LCROSS, and subsequent lunar landers. SMART-1 has been contributing to prepare the next steps for exploration: survey of resources, monitoring polar illumination, and mapping of sites for potential landings, international robotic villages and for future human activities and lunar bases.

References: [1] Foing, B. et al (2001) Earth Moon Planets, 85, 523 . [2] Racca, G.D. et al. (2002) Earth Moon Planets, 85, 379. [3] Racca, G.D. et al. (2002) P&SS, 50, 1323. [4] Grande, M. et al. (2003) P&SS, 51, 427. [5] Dunkin, S. et al. (2003) P&SS, 51, 435. [6] Huovelin, J. et al. (2002) P&SS, 50, 1345. [7] Shkuratov, Y. et al (2003) JGRE 108, E4, 1. [8] Foing, B.H. et al (2003) Adv. Space Res., 31, 2323. [9] Grande, M. et al (2007) P&SS 55, 494. [10] Pinet, P. et al (2005) P&SS, 53, 1309. [11] Josset J.L. et al (2006) Adv Space Res, 37, 14. [12] Foing B.H. et al (2006) Adv Space Res, 37, 6.

Links: http://sci.esa.int/smart-1/, http://sci.esa.int/ilewg/

LRO TARGETING OF LUNAR PYROCLASTIC DEPOSITS. L.R. Gaddis[1], M.S. Robinson[2], B.R. Hawke[3], Tom Giguere[3,6], Olaf Gustafson[4], S.J. Lawrence[2], J.D. Stopar[2], B.L. Jolliff[5], J.F. Bell III[4], [1]Astrogeology Program, U.S. Geological Survey, Flagstaff, AZ; [2]School of Earth and Space Exploration, Arizona State University, Tempe, AZ; [3]University of Hawaii, Honolulu, HI; [4]Cornell University, Ithaca, NY; [5]Dept. Earth & Planetary Sciences, Washington University, St. Louis, Missouri 63130; [6]Intergraph Corp., P.O. Box 75330, Kapolei, HI 96707. (lgaddis@usgs.gov).

Introduction: Lunar pyroclastic deposits are high-priority targets for the Lunar Reconnaissance Orbiter (LRO) mission [e.g., 1]. Images from the Narrow Angle Camera (NAC; 0.5 m/pixel images and mosaics) and Wide Angle Camera (WAC; 7-band imager, 100 m/p VIS, 400 m/p UV) subsystems of the LRO Camera (LROC), supplemented by coordinated observations from the Mini-RF [2] and Diviner [3] instruments, will provide information about the lunar surface to address major questions about these deposits. In the first year, the LRO mission will address imaging targets that are of interest to the NASA Constellation (Cx) Program as potential landing sites and for exploration on the lunar surface. In the second year, LRO will move into a science phase that emphasizes scientific targets. Targeting for all sites is underway currently (see http://ser-dev.ser.asu.edu/LSM/targeting.php). This abstract describes the science rationale and status of LRO targets for pyroclastic deposits.

Science Rationale: As volatile- and metallic-element (e.g., S, Fe, Ti) enriched remnants of ancient lunar volcanic eruptions, pyroclastic deposits provide information on the early lunar interior [e.g., 4-6] and the distribution of possible resources [7, 8]. Earth-based telescopic studies of the Moon (0.4-2.4 μm) identified pyroclastic units on the basis of low albedo and absorptions due to iron-bearing volcanic glasses [e.g., 9-11]. These studies provided data on the compositional diversity, distribution, and stratigraphy of unsampled mare and pyroclastic deposits on the near side [e.g., 10, 12]. Recent analyses using Clementine color data demonstrated the compositional heterogeneity of these deposits and expanded our knowledge of pyroclastic deposit types beyond those represented in returned samples [e.g., 13-15].

Exploration Objectives: Several sites within major lunar pyroclastic deposits for the first year (exploration phase) of the LRO mission are included among the 50 'Priority-1' sites specified by Cx. These sites are a subset of possible landing sites from three reference target sets [16-19] that include 75 lunar sites identified as having high scientific, resource utilization, and operational merits and potential [1]. Lunar sites that feature pyroclastic volcanism in the Cx target list include: Alphonsus crater, Apollo 15 near Hadley Rille, Aristarchus Plateau, Rima Bode, Schrodinger crater, and Sulpicius Gallus. LROC coverage for such exploration targets includes (in order of priority): (1) a 10x10 km region of interest (ROI) for complete coverage, including geometric and photometric stereo; (2) a 20 x 20 km ROI 'best effort' target for stereo data products; and (3) a 40 x 40 km 'best effort' ROI for monoscopic mosaic coverage (Figure 1). Nominal exploration image sets will acquire photomosaics of high quality and resolution for hazard and safety assessment and construction of digital elevation models of potential landing sites. Imaging by LROC is subject to a variety of constraints that will determine final coverage and scheduling of image acquisition [20].

Science Objectives: Studies of lunar pyroclastic deposits with LRO data have the potential to address major questions concerning their distribution, composition, volume, eruptive styles, and role in early lunar volcanism. Objectives for LRO observations for lunar pyroclastic deposits include: (1) *Characterization of large, 'regional' deposits.* The presence of volatile elements in sampled pyroclastic glasses suggests that the Moon may not have been totally depleted in volatiles during its formation and magma-ocean phases. We have sampled only two pyroclas-

tic deposits directly (Apollo 15, Apollo 17) but we know from regolith samples that there are many other volcanic glasses for which we have not identified the source deposits [5]. Combined NAC (for mapping extent and thickness) and WAC data (for color and composition) will enable us to characterize the spatial extents, distributions, and compositions of pyroclastic deposits and thus relate them to other sampled glass types and possibly to their associated basalts. (2) *Determination of titanium contents.* The high titanium content of many of the largest lunar pyroclastic deposits (e.g., Rima Bode, Apollo 17/Taurus-Littrow, Mare Vaporum) increase their value as possible economic resources in part because of their association with concentrations of H- and He-rich materials [e.g., 8]. WAC color data will allow us to characterize titanium contents of pyroclastic deposits, to map the diversity of effusive and pyroclastic units with variable titanium contents that are currently not recognized, and to identify which pyroclastic deposits are the best sources of titanium and associated volatile elements. Using NAC stereo data, meter-scale topographic models of the surface will allow us to better constrain emplacement and distribution of possible juvenile materials, the geometry of small pyroclastic eruptions, and models of their eruption. (3) *Assessment of morphology and compositional variation.* Improved knowledge of the morphologic and color characteristics of the lunar pyroclastic deposits from NAC and WAC data will permit refinement of the existing classification of their compositions, with particular attention to intra-deposit compositional variations, identification of juvenile components and evaluation of the distributions and relative amounts of juvenile vs. host-rock components. For each deposit, LROC data will be used to search for small-scale morphologic and compositional variations such as those that might characterize separate eruptive episodes from the same vent, pulses of magma intrusions and/or crustal dikes, and possible changes in composition and volatility of source materials with time.

Targeting Strategy: Seventy-five globally distributed pyroclastic deposits [13] were the focus of our NAC targeting campaign. Additional sites that may feature pyroclastic volcanism have also been targeted, for a current total of ~350 ROIs. At most sites, both high- and low-sun targets (typically 5º-55º and 65º-85º, respectively) were identified, and many targets have been selected for coverage by photometric stereo data to facilitate detailed morphologic analyses.

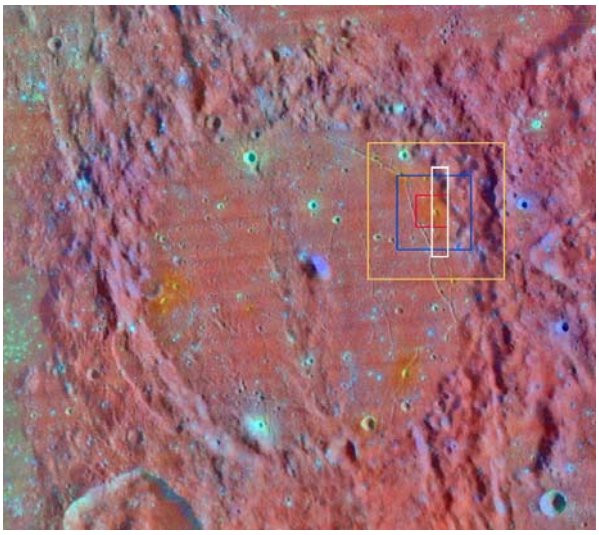

Figure 1. Exploration Target image coverage for LROC superimposed on a merged Lunar Orbiter and Clementine color-ratio (R=750/415 nm; G=750/950; B=415/750) view of Alphonsus crater (80 km dia.; White outline=NAC footprint; red=10x10 'Priority 1' site; blue=20x20 km 'Priority 2' site; yellow=40x40 km 'Priority 3' site.

References: [1] Jolliff et al., 2009, LPS XXXX, abs. #2343. [2] Bussey et al., 2008, LPS XXIX, abs. #2389. [3] Greenhagen and Paige, 2009, LPS XXXX, abs. #2255. [4] Heiken et al. 1974, GCA 38, 1703. [5] Delano, 1986, JGR 91, D201. [6] Shearer et al., 2006, RMG 60, 365. [7] Hawke et al., 1990, PLPSC 20th, 249. [8] Duke et al., 2006, RMG 60, 597. [9] Pieters et al., 1973, JGR 78, 5867. [10] Gaddis et al., 1985, Icarus 61, 461. [11] Hawke et al., 1989, PLPSC 19th, 255. [12] Pieters, 1978, PLPSC 9th, 2825. [13] Gaddis et al., 2003, Icarus 161, 262. [14] Lucey et al., 2006, RMG 60, 83. [15] Wilcox et al., 2006, JGR 111, E09001. [16] ESAS, 2005, NASA TM 2005-214062, 750 p. [17] First Lunar Outpost (FLO) study, NASA Wkshp, Aug. 1990. [18] Taylor & Spudis, Eds., 1990, NASA Conf. Pub. 3070. [19] Ryder et al., 1988, EOS: Trans. AGU, 70, 1495. [20] Lawrence et al., LPS XXXX, abs. #2316.

LUNAR MINING: KNOWNS, UNKNOWNS, CHALLENGES, AND TECHNOLOGIES. L. S. Gertsch[1], [1]Missouri University of Science and Technology (Rock Mechanics and Explosives Research Center, 1006 Kingshighway, Rolla, MO, 65409-0660, United States, GertschL@mst.edu).

Introduction: Humans have mined rock and soil for more than 300,000 years [1]. The first mining technology was digging tools shaped from antler, bone, wood, and rock [2],[3]. Today's mines rely on global positioning satellites, semi-automated machines, and explosives. Lunar and planetary mines will use technology derived from this background and adapted for new environments. All, however, use their technologies for the same purpose: to access the desired material, and separate it from the unwanted material with which it is mixed, using the least energy or economic expenditure possible.

The mining cycle. The mining cycle includes:

- Resource assessment.
- Resource extraction.
- Resource beneficiation.
- Mine closure

Mining unit operations. Every mining method must achieve these unit operations. How they are achieved, and their difficulty, depend on the material of interest, its surroundings, and numerous other environmental characteristics. The unit operations are:

- Fragmentation - breaking material from its *in situ* surroundings.
- Excavation - picking up and loading the fragmented pieces.
- Material handling - hauling as needed.
- Beneficiation - onsite preparation of the mined material for further processing or for use.

Technologies: The technologies used in mining and excavation consist of all the methods by which the fundamental laws of physics can be harnessed in the specific locale of interest to achieve the goals of the project. Even on Earth, there is enough of a range of operational constraints that a correspondingly wide range of technologies has evolved. Expansion to a nonterrestrial location with its significantly different constraints will involve re-examination of the motives for the means, and re-engineering for effective operation there. It will also offer new opportunities for technology development, as well as new difficulties. Many of both are presently unforeseen.

Mining technologies evolved to achieve the unit operations as needed in the various stages of the mining cycle in various types of locations. Workable systems of these are termed "mining methods," which are in turn classified in a variety of ways. This review follows the classification of mining methods on the basis of access: surface methods and underground methods. The choice between approaches is ordinarily made on economic grounds. For lunar operations, the choice will be recast in terms of launch mass and energy in the early stages, and probably in terms of energy alone for later stages.

Surface mining methods. These are operations where personnel are not required to go underground; usually (but not necessarily) all material from the original ground surface to the bottom of the mine is removed. Those that appear most applicable to the Moon consist of open pit mining, area (strip, or opencast) mining, auger (highwall) mining, and dry dredging.

Open pit mining is best applied to thick, irregular deposits expressed on the surface or occurring at shallow depths. It removes all material to create one or more horizontal benches, each successively deeper and covering less area than the preceding one. The unwanted material is stored or disposed of in surface stockpiles nearby.

Area mining is similar except that the unwanted material is piled within previously mined areas. Over time the pit, usually a trench, remains a constant size and area, and appears to march across the landscape. (Open pit mines, on the other hand, grow deeper and/or larger over time.) Area mining is used in horizontally bedded deposits such as coal.

Modern auger mining occurs underground, but is run entirely from the surface. Single or double augers (or other types of excavators) bore into the otherwise unavailable highwalls left when coal seams are mined in mountainous terrain.

Dry dredging, in the form most applicable to lunar operations, is similar to surface versions of the slusher mining methods previously used in some underground mines. A slusher is a drag scraper. Here is an example of the close relationship between methodology and technology.

Underground mining methods. Underground mines are accessed by passages through undesired material to an orebody; mining occurs beneath the cover of overlying formations. The major types are unsupported, supported, and caving. Several methods have been used for underground extraction of near-surface, unconsolidated deposits and thus may be useful initiation points for lunar regolith mining. More mining methods can be found in [4], with more detailed descriptions in [5].

Top-slicing was used to mine placer gold from thick stream gravel deposits before the equipment for modern high-volume methods was available and where contemporary methods such as hydraulic mining could not be used. Similar deposits are mined today either by surface methods (above) or, if in permafrost, by adaptations of methods developed for rock. The most common of the latter approaches is room-and-pillar (below). In the form most suitable for regolith mining, top-slicing consists of

Room-and-pillar mines require the ore to be strong enough to support openings wide enough for the equipment to operate. This method leaves areas of ore (pillars) to support the overlying material, which itself must be strong enough to bridge the gaps between the pillars.

Longwall and shortwall are mechanized adaptations of top-slicing that also permit / require the overlying material to fail and fill the void created by removal of the ore. The main difference between these and top-slicing is that, to date, the ore has had to be strong enough to support excavations without the significant artificial support requirements of top-slicing.

Knowns: The first target of lunar mining and construction will be the regolith. That will expand to include intact rock when operation depths exceed the thickness of the regolith covering.

Many aspects of regolith behavior have been measured from the perspective of soil mechanics, summarized by [6]. The low number of sample sites, and their bias toward mare locations, will be ameliorated by the much greater coverage and resolution of the LRO mission.

Feedstocks for the production of propellants, life-support gases, and basic structural materials probably will require only minimal beneficiation of excavated regolith prior to processing.

Unknowns: The variability and spatial scale of variability, of the regolith properties that affect mining and excavation are not well-characterized in three dimensions. Regolith variability is controlled by its formation mechanisms, which are due primarily to impact processes. Understanding the effects of these processes will enhance understanding of the spatial distribution of material targets, and *vice versa*. It also will improve the development of effective excavation techniques and equipment.

The fourth dimension -- time -- may be of some importance to the determination of potential orebodies and is being studied (*e.g.*, [7], [8]).

Political and legal uncertainty are two unknowns unrelated to science or engineering that nevertheless affect the probability of success. The former speaks directly to government support. The latter controls the willingness of the mining industry to commit.

Challenges: The unknowns listed above lead to engineering challenges expected during lunar mining and excavating.

Regolith *in situ* is tightly compacted and contains varying densities of pebbles, rocks, and boulders. Even without the cementing effect of intergranular ice, undisturbed regolith deposits require some force to fragment and excavate [9]. Mass usually provides the reaction force for surface mining, yet launched mass will be at a premium. Can the materials needed for the pre-manufacturing stage of lunar presence be obtained from the more easily excavated upper layers?

Digging becomes more difficult with depth, possibly plateauing below some critical depth. This, in addition to the presence of oversized particles, will require development of techniques for real-time ahead-of-the-face sensing and machine control. This is part of the challenge of sufficient characterization of the target material, which needs to be more complete than on Earth to offset the difficulty of the additional challenges of remote operation, maintenance, and repair.

Mining and excavation equipment is built to be robust, because it must deal with significant -- and difficult-to-characterize -- ranges of material behavior. This is true in any natural geologic material. Long-term operation of such equipment in the unfamiliar and extreme environment of the Moon adds the difficulties referred to above.

Any prototype technology, or old technology used in a new way or a new place, requires significant development and testing. NASA is familiar with this, but the greatest challenge will be whether humanity yet has the political and financial will to carry the process through well enough to encourage success.

References:

[1] Verri G. *et al*. (2005) *J Archaeological Science, 32,* 207–213. [2] Weisgerber B. and Pernicka E. (1995) *Prehistoric Gold in Europe: Mines, Metallurgy, and Manufacture,* 159-182. [3] Russell M. (2000) *Flint Mines in Neolithic Britain*. [4] Hartman H. and Mutmansky J. (2002) *Introductory Mining Engineering*. [5] Hartman H.L. (1992) *SME Mining Engineering Handbook*, 2nd ed. [6] Heiken G.H. et al. (1991) *Lunar Sourcebook, A User's Guide to the Moon*. [7] Taylor L.A. et al. (2001) *JGR, 106(E11),* 27,985–27,999. [8] Crider D.H. and Vondrak R.R. (2003) *JGR, 108(E7),* 5079. [9] Gertsch L.S. et al. (2006) *GoldenRocks*, 42nd U.S. Symp on Rock Mechanics.

THE LUNAR ATMOSPHERE AND ITS STUDY BY LRO. G. R. Gladstone[1] and K. D. Retherford[1], [1]Southwest Research Institute, 6220 Culebra Road, San Antonio, TX 78238 (rgladstone@swri.edu; kretherford@swri.edu)

Current Understanding: The atmosphere of the Moon is extremely tenuous, with a total mass of only ~10^4 kg (i.e., at STP it would fit inside a large building) [1]. Since it is so thin, the lunar atmosphere is difficult to detect, and has only been partially sampled in situ on the nightside by Apollo pressure gauges & mass spectrometers (these were swamped by contamination on the dayside) [2]. Likewise, remote sensing is only possible using the brightest of atomic resonance lines (e.g., from Na, see Fig. 1) [3,4]. The observed composition of the lunar atmosphere is dominated by noble gases (Ar, He) with a minor (~1%) contribution from alkali species (Na, K); Species expected but not yet observed include CO, H_2O, O, H_2, and S. Despite being hard to measure, the Moon's atmosphere can provide useful constraints on volatile sources (e.g., outgassing, meteroroid & comet impact, solar wind), sinks (e.g., sputtering, photoionization & solar wind pickup, surface adsorption condensation), and transport (ballistic, surface diffusion, implantation of pickup ions).[5,6] .

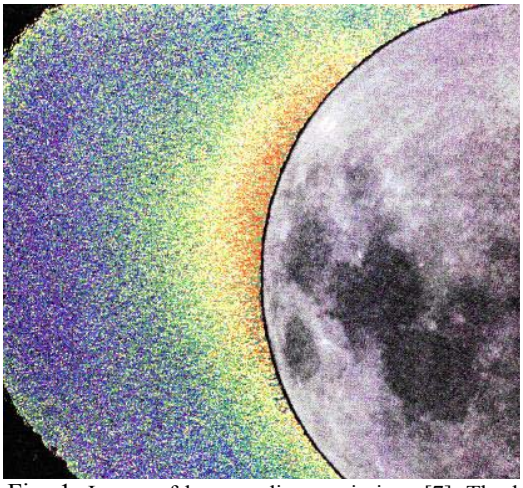

Fig. 1. Image of lunar sodium emissions [7]. The lunar phase angle was 51°. Emissions are brighter near the subsolar point. A coronograph was used to block light from the lunar disk, and the lunar surface is shown for illustration.

LRO Plans: Atmosphere studies are not part of the primary 1-year mission for LRO supported by NASA's Exploration Systems Mission Directorate (ESMD), although some very useful data will be obtained serendipitously. More directed atmospheric observations and campaigns are expected to occur in the planned 1-3 year extension of the LRO mission that will be supported by NASA's Science Mission Directorate (SMD). These will target the NRC-supported objectives of understanding the atmosphere and dust environment of the Moon [8]. Central to these studies will be frequent targeted limb observations, e.g., along the dawn terminator, where the diurnal concentrations of atmosphere are largest, and where horizon glow can be studied for the relative contributions of dust and sodium emissions. Possible campaigns include focused studies of transient phenomena, such as certain meteor showers and crossings of Earth's magnetotail, where atmospheric source rates would be expected to increase.

LAMP Observations: The primary atmospheric observations that will be made with LRO are searches for the resonance and fluorescence emissions of various atomic and molecular species using the Lyman Alpha Mapping Project (LAMP) ultraviolet spectrograph [9] (cf. Fig. 2).

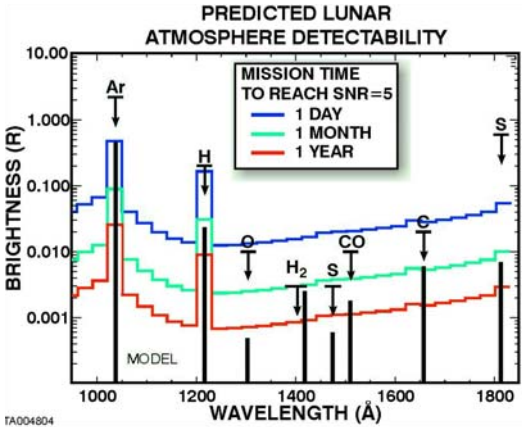

Fig. 2. Upper limits and models of lunar atmospheric far-UV feature brightnesses for atmospheric species of interest. Optically thin emissions are assumed, with nadir viewing near the terminator (as illustrated in Fig. 3). The most constraining upper limits [4]) are shown as downward-directed black arrows. Expected brightnesses are indicated by vertical black bars. LAMP detectable brightnesses with SNR=5 are shown after different mission elapsed times.

Besides just detecting them, LAMP will be used to follow the (possibly already remotely-sensed [10]) atmospheric argon (through its strong resonance lines at 104.8 nm and 106.6 nm) and other species over repeated lunations, to better characterize their sources

and sinks. Argon is particularly interesting, since it mostly comes from the lunar interior and may be tied to outgassing sites that could be of interest to future landing site selections [11,12], some of which may be targeted by LROC. In general, the regional distribution of the observed emissions can be key for understanding important transport processes, e.g., because the atmospheric H distribution itself is a tracer of water vapor transport to the lunar poles [6], observations of the average latitude distribution of H emissions may reveal an H gas deficit ("polar holes") at high latitude which could constrain the rate of water transport to the polar regions.

Although LAMP's sensitivity per unit time is somewhat less than the Apollo 17 UVS, LAMP is a staring spectrograph, whereas Apollo 17's UVS had a single-pixel photometer detector that had to time-share as the grating rotated across the spectral passband [4]. Assuming that only 50% of all possible twilight atmospheric observing opportunities are realized (cf. Fig. 3), LAMP's total lunar atmospheric observing time near the terminator will be ~250 hours/year, more than an order of magnitude increase over what Apollo 17 achieved at any given wavelength. LRO's year-long nominal mission allows LAMP to make a far more extensive survey for neutral species than achieved previously. LRO's orbit near 50 km altitude is well-suited to observing many species in the lunar atmosphere, which have characteristic scale heights of 50-100 km (meaning most of the atmospheric column of these species will be below the spacecraft).

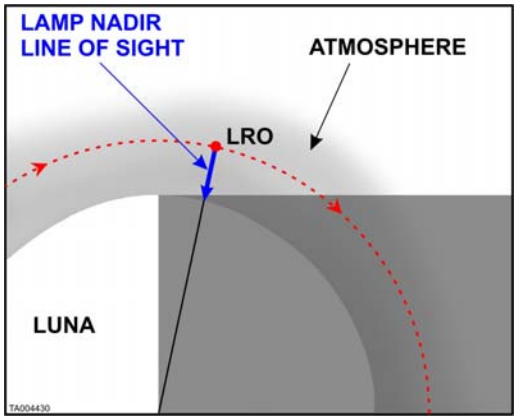

Fig. 3. LAMP will use LRO's nadir-viewing geometry near the terminator to search for resonantly scattered UV sunlight from a variety of atomic species expected in the lunar atmosphere. Monthly limb observations of the atmosphere are also planned.

Most of LAMP's atmospheric observations will be made looking to the nadir near the terminator, as illustrated in Fig. 3. At these geometries, which occur ~6% of the time for LRO, the lunar surface is dark but the atmosphere between the surface and LRO's altitude is sunlit, allowing atoms there to resonantly fluoresce. During these times, normal LAMP data taking will include emissions from the atmosphere along LAMP's line of sight to the surface. Surface background (e.g., from reflected interplanetary Lyα and the interstellar radiation field) can be accurately removed by comparing observations of the same locations made when the surface and atmosphere there are both in shadow.

In addition, about once per month observations will be made with LAMP staring at the atmosphere above the lunar limb. With the largest possible line of sight atmospheric column density, these limb observations will provide LAMP's most sensitive look at the lunar atmosphere. Such limb viewing observations are expected to be made more often during the extended mission and along the dawn terminator, where the largest column densities are expected [1].

LRO's characterization of the lunar atmosphere will also be particularly timely, since this mission will occur before major increases in mission traffic, and therefore rocket motor firings, disturb the natural environment. Even modest human exploration of the Moon will significantly impact the lunar atmosphere [13].

References:

[1] Hodges R. R. et al. (1974) *Icarus*, *21*, 415-426. [2] Stern, S. A. (1999) *Rev. Geophys.*, *37*, 453-491. [3] Potter A. E. and Morgan T. H. (1988) *Science*, *241*, 675-680. [4] Feldman P. D. and Morrison D. (1991) *Geophys. Res. Lett.*, *18*, 2105-2108. [5] Smyth W. H. and Marconi M. L. (1995) *Astrophys. J.*, 443, 839-864. [6] Crider D. H. and Vondrak R. R. (2003) *J. Geophys. Res.*, *108*, doi: 10.1029/2002JE002030. [7] Potter A. E. et al. (2000) *J. Geophys. Res.*, *105*, 15,073-15,084. [8] NRC (2007) *The Scientific Context for the Exploration of the Moon*, National Academies Press, 120pp. [9] Gladstone G. R. et al. (2009) *Space Sci. Rev.*, submitted. [10] Flynn B. C. (1998) *Astrophys. J. Lett.*, *500*, 71-74. [11] Schultz P. H. (2006) *Nature*, *444*, 184-186. [12] Crotts A. P. S. (2008) *Astrophys. J.*, *687*, 692-705. [13] Vondrak R. R. (1988) *LPI Contribution* ***652***, 246.

LUNAR VOLCANISM: TIMING, FORM, AND COMPOSITION. R. Greeley[1], [1]Arizona State University, School of Earth and Space Exploration, Box 87404, Tempe, AZ 85287-1404, greeley@asu.edu.

Introduction: Volcanism has played an important role in the formation and evolution of the lunar surface, providing insight into the history of the surface and interior. The *Lunar Reconnaissance Orbiter* affords the opportunity to advance our knowledge of lunar volcanism by identifying key targets for detailed observations consistent with the overarching scientific goals for lunar exploration. These goals were articulated by the National Research Council (NRC, 2007) and were refined and detailed by NASA at a Lunar Science Workshop (NAC 2008) from which 16 science objectives were defined, three of which related to volcanism: a) *Determine the composition and evolution of the lunar crust and mantle to constrain the origin and evolution of the Moon and other planetary bodies,* b) *Determine the origin and distribution of endogenous lunar volatiles as one input to understanding the origin, composition, and structure of the Moon and other planetary bodies,* and c) *Characterize impact flux over the Moon's geologic history to understand early solar system history*.

Based on the goals and objectives from the NRC and NASA studies, the following specific questions are posed for lunar volcanism:

- What are the morphologic / morphometric characteristics of volcanic vents and effusive lavas, and what do these tell us about origin and emplacement of magmas within the crust and at the surface?
- What is the variety of volcanic structures, styles, and associations and what do they mean for mantle and crustal petrogenesis?
- What is the range of ages of volcanic materials and what do those ages indicate about the volcanic flux over time?
- What is the distribution and what are the characteristics of lunar pyroclastic deposits, and what do these reveal about their origin, eruption and emplacement and the thermal and magmatic evolution of the mantle?
- What is the global distribution and range of ages of "cryptomare" (ancient, mare surfaces buried beneath more recent crater ejecta)?

Targets for LRO should be reviewed and prioritized to address one or more of these key questions. Each target should list specify the instrument or suite of instruments that is needed, along with observation specifications such as incidence angle. The need for coordinated observations for more than one instrument should also be indicated.

References: [1] NAC (2008) *Lunar Science Workshop,* NASA Advisory Council, NP-2008-08-542-HQ. [2] NRC (2007) *The Scientific Context for Exploration of the Moon*, National Research Countil, The National Academies Press.

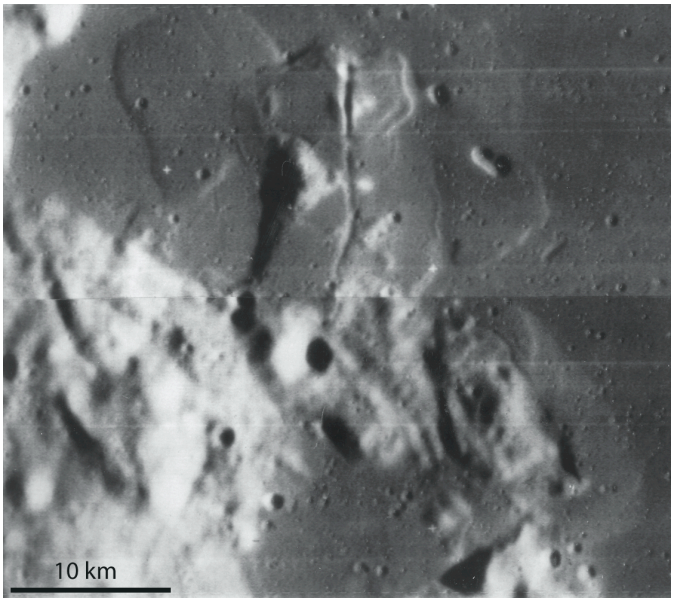

Figure 1. These small shield volcanoes and vent structures were imaged by Lunar Orbiter IV *(illumination from the right) in the mid 1960s in* Lacus Veris, Orientale basin, *but have not been imaged subsequently in better resolution. They could represent a style of lunar volcanism poorly understood on the Moon, and should be a high priority for observations during the* Lunar Reconnaissance Orbiter *mission.*

DIVINER LUNAR RADIOMETER TARGETING CAPABILITIES. B. T. Greenhagen and D. A. Paige, University of California, Los Angeles, Department of Earth and Space Sciences, 595 Charles Young Drive East, Los Angeles, CA 90095 (*greenhagen@ucla.edu*).

Introduction: Diviner (Figure 1) will primarily be operated as a nadir staring, pushbroom mapping radiometer [1]. However, due to its Mars Climate Sounder (MCS) heritage, Diviner has two actuators each with 270° ranges of motion [2]. Therefore Diviner is uniquely capable of targeting independent of the LRO spacecraft. Diviner Observations will include pushbroom nadir mapping, pushbroom off-nadir mapping, and targeted raster imaging. Diviner's approximate field of regard is illustrated in Figure 4.

Diviner Science: Diviner will collect multichannel spectral observations that can be used to constrain lunar surface properties [e.g. 1, 3]. Diviner has nine spectral channels spread unevenly between 0.3 and 400 μm. Diviner will map surface temperatures to investigate the Moon's three thermal environments (daytime, nighttime, and polar) through diurnal and seasonal changes. The temperature data and data from thermal models will be fit to determine thermal-physical properties (e.g. thermal inertia, rock abundance). Diviner's compositional investigation will use solar reflectance and temperature derived infrared emissivity to determine aspects of lunar surface composition [e.g. 3, 4].

Figure 1: Diviner Lunar Radiometer. Diviner's optics are contained in the central drum behind the apertures. The azimuth (red arrow) and elevation actuators (blue arrow) can each rotate 270°. The white surface is the solar calibration target, which is used for photometric calibrations. Blackbody calibration targets, used for radiometric calibrations, are located in the yoke.

Pushbroom Nadir Mapping: Diviner will primarily employ continuous pushbroom nadir mapping to generate a uniform dataset with maximum completeness and consistency. Diviner's pushbroom nadir mapping spatial resolution will be approximately 320 m in track and 160 m cross track at 50 km altitude (6.7 x 3.4 mrad pixel size) with a swatch width of 3.4 km (71 mrad). Due to the relatively narrow swath width and near continuous nadir staring, Diviner will produce image "noodles" that are approximately 3.4 km wide and hundreds to thousands of km in length. Anticipated interruptions to nadir mapping include in-flight instrument calibrations (10 per orbit), LRO off-nadir targeting operations, and Diviner off-nadir mapping and targeted imaging. Diviner's spatial coverage for any given four lunar-hour period (i.e. $1/6^{th}$ of a lunation) is expected to be ~40% at the equator, generally increasing to 100% at the poles for the scheduled one year ESMD mapping orbit. This coverage increases to 80% at the equator for the proposed one year SMD extended mission (90% for two years) [1].

Pushbroom Off-Nadir Mapping: Diviner observations will also include pushbroom off-nadir mapping. Most observations of this type will be caused by LRO off-nadir targeting operations for LROC and Mini-RF. Diviner will "ride-along" on these operations and produce coincident image noodles. Diviner may also perform independent off-nadir pushbroom mapping by slewing in elevation crosstrack in the spacecraft ±y direction (see Figure 2, for examples). These image noodles are parallel to the LRO orbit track with variable emission angle AND lunar local time. Diviner's off-nadir pushbroom mapping spatial resolution varies as a function of emission angle from nadir as shown in Figure 3.

Targeted Raster Imaging: Diviner is also capable of targeted raster mapping. This ability will be used to observe in track emission phase functions (same lunar local time) and targets of interest such as the LRO spacecraft and the Earth. Due to the orientation of the azimuth and elevation actuators, Diviner is incapable of off-nadir in track pushbroom mapping while LRO is in a nadir pointing configuration. When configured for elevation slewing in the in track direction, Diviner's detector arrays are aligned parallel to the orbit track (analogous to MCS limb staring). Therefore it is necessary to raster in azimuth to observe the region of interest for each spectral channel. Figure 2 illustrates the in track "comb" configuration. Targeted raster

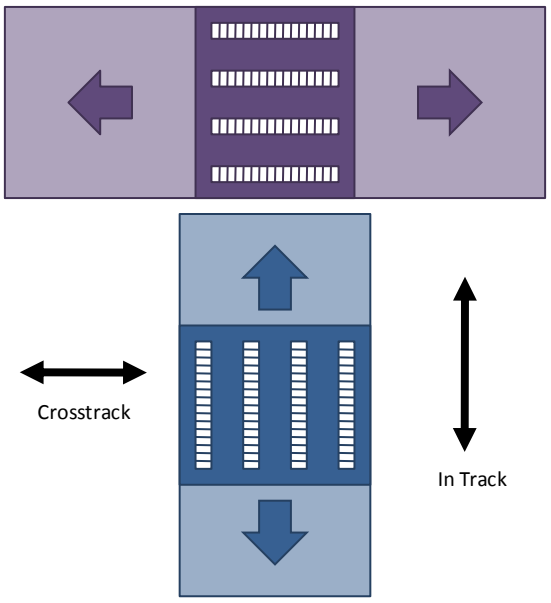

Figure 2: Pushbroom and Comb Configurations. When in pushbroom configuration (top, purple color), slewing with Diviner's elevation actuator results in crosstrack movements. Here, the the detector arrays are perpendicular to the orbit track and the spacecraft motion creates the image. Conversely, elevation slewing in the comb configuration (bottom, blue color) cases in track movemements. However, the detector arrays are parallel to the orbit track and azimuth actuator rastering is required to create an image.

imaging of the spacecraft was tested during thermal vacuum chamber testing at GSFC and will be performed in lunar orbit [4]. Targeted raster imaging of the Earth is also planned.

References: [1] Paige D.A. et al. (2009) *SSR*, in press. [2] McCleese D.J. et al. (2007) JGR, 112, E05806. [3] Greenhagen B.T. and Paige D.A. (2009) LPS XL, Abstract #2255. [4] Greenhagen B.T. (2009) Ph.D. Dissertation, UCLA.

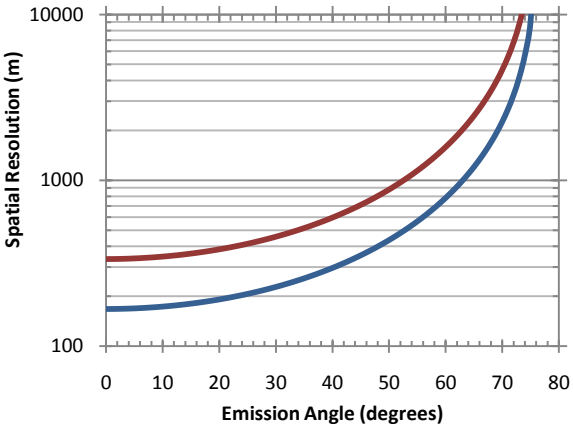

Figure 3: Pushbroom Mapping Spatial Resolution. Diviner's spatial resolution as a function of emission angle for pushbroom mapping. The red and blue traces represent 6.7 and 3.4 mrad respectively.

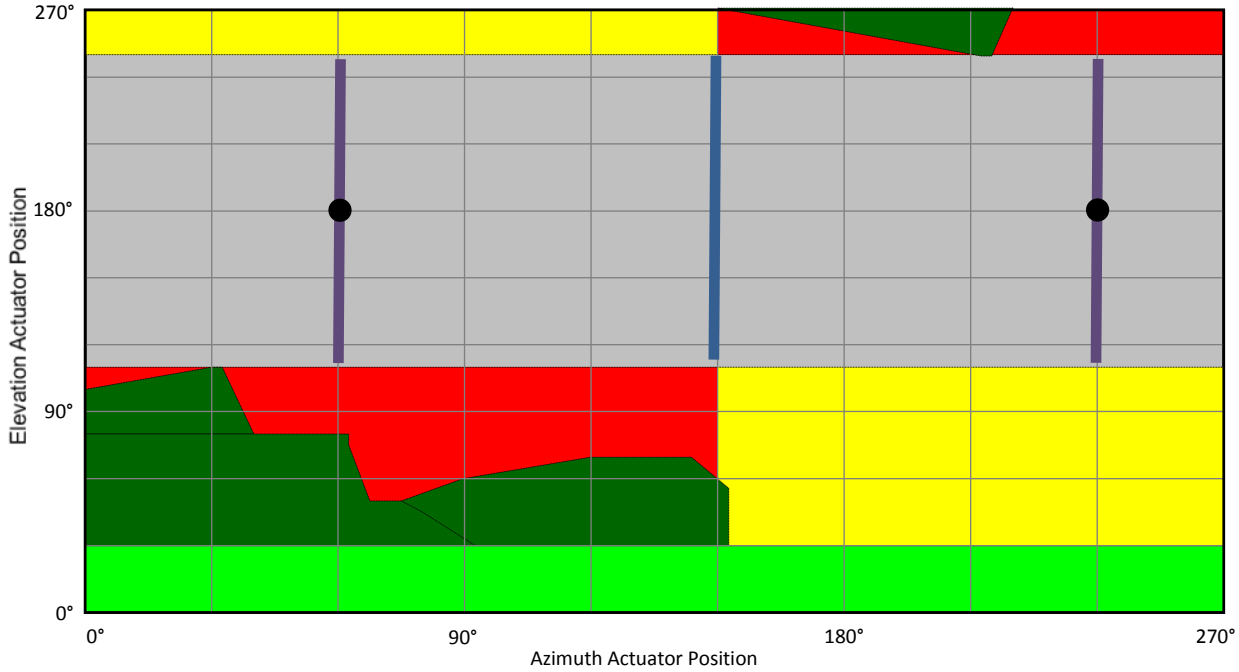

Figure 4: Diviner's Field of Regard. This plot illustrates the positions of the LRO spacecraft, Moon and space relative to Diviner's field of regard. The Moon for 100 km orbit is represented by the gray rectangle. The spacecraft and instruments are dark green and Diviner's yoke is bright green. Space that cannot contain the sun is yellow and space that may contain the sun is red. The positions for pushbroom nadir mapping are represented by the black circles, instrument controlled pushbroom off-nadir mapping are the purple line, and lunar surface targeted comb imaging are the blue line.

NASA Constellation Program Office Regions of Interest on the Moon: A Representative Basis for Scientific Exploration, Resource Potential, and Mission Operations J.E. Gruener[1], B.K. Joosten[2], [1]NASA Constellation Program-Lunar Surface Systems Project Office, Houston, TX 77058, john.e.gruener@nasa.gov, [2]NASA Constellation Program-Office of the Program Systems Engineer

Introduction: The current United States Space Exploration Policy emphasizes a human return to the Moon as a location near the Earth where the nation can learn how to work and live on a planetary body. Major goals for this progarm are to: extend human presence to the Moon to enable eventual settlement; pursue scientific activities that address fundamental questions about the history of Earth, the solar system and the universe - and about our place in them; test technologies, systems, flight operations and exploration techniques to reduce the risks and increase the productivity of future missions to Mars and beyond; provide a challenging, shared and peaceful activity that unites nations in pursuit of common objectives; expand Earth's economic sphere, and conduct lunar activities with benefits to life on the home planet; and use a vibrant space exploration program to engage the public, encourage students and help develop the high-tech workforce that will be required to address the challenges of tomorrow. The National Aeronautics and Space Administration (NASA) is conducting engineering trade studies to develop lunar transportation architectures, lunar surface system concepts, and lunar surface scenarios.

Constellation Program: The Constellation Program Office (Cx) is responsible for the planning of future human missions to the Moon, including long duration missions to a lunar outpost, and possibly shorter duration human-sortie missions to locations other than the outpost location.

The Lunar Reconnaissance Orbiter Camera (LROC) will begin imaging the lunar surface in 2009. Two narrow angle cameras (NACs) will image the Moon at 0.5 cm/pixel. Each individual NAC image frame represents a 2.5 x 25 km surface area, with the NAC pair resulting in a 5 x 25 km area of coverage. In the course of the first year of mapping, this will result in only 8-10% of the Moon's surface being imaged at high resolution. Thus, it is important to make sure priority regions of interest are identified and placed into the NAC targeting plan.

Constellation has identified 50 high priority regions of interest for human exploration of the Moon, based on results from the Clementine and Lunar Prospector missions, and three NASA reports:

1. NASA's Exploration Systems Architecture Study (ESAS), 2005.
2. A Site Selection Strategy for a Lunar Outpost, Science and Operational Parameters, 1990.
3. Geoscience and a Lunar Base, A Comprehensive Plan for Lunar Exploration, NASA Conference Publication 3070, 1990.

The regions of interest identified by Cx are not intended to be, and are not to be interpreted as, a site selection activity for actual landing sites. Rather, they illustrate the diversity of scientific and resource opportunities, and geographic terrains and locations, that togther form a representative basis for scientific exploration, resource development, and mission operations.

The regions of interest were selected based on three criteria:
1. Science rationale - the 50 sites are of unique scientific interest or are scientifically complex requiring intensive field work with human interaction.

2. Resource potential - as a whole, the 50 sites are representative of the type of natural resources available for development and exploitation.

3. Operational perspective - as a whole, the 50 sites are representative of the different terrain types that the Altair lunar lander and the various lunar surface systems may encounter.

The 50 regions of interest have been divided into two tiers, each with 25 locations. Tier 1 regions of interest have a higher priority than tier 2 regions of interest, however, there is no prioritization within each tier.

The images acquired by the LROC NACs will be used by NASA to create image mosaics, topographic maps and digital elevation models, and surface hazard assessments. This data will be used in the design process for the Altair lunar lander (e.g., approach and landing, hazard avoidance), and lunar surface systems such as habitation, surface mobility, power, communications, and navigation.

Constellation has been working with the Lunar Reconnaissance Orbiter (LRO) Project Office and the LROC principal investigator (PI) to develop a plan for imaging the 50 regions of interest identified by Constellation, including the area of coverage for a given loca-

tion that is allowed by orbit parameters and mission constraints. The resulting agreement is illustrated in the figure 1.

For each region of interest, there is a series of nested targets, or a 'box within a box' philosophy, that represent three areas of coverage. The 10 x 10 km 'box' represents an area as described by the LRO Project requirements. This area has a Priority 1 in the LROC prioritization scheme, and a full set of observations will be made for an image mosaic, stereo imaging (geometric and photometric), and hazard identification. The 20 x 20 km 'box' has a Priority 3, and represents a 'best effort' by the LROC PI to acquire a full set of observations. The 40 x 40 km 'box' has a Priority 4, and represents a 'best effort' by the LROC PI to acquire a monochromatic mosaic only.

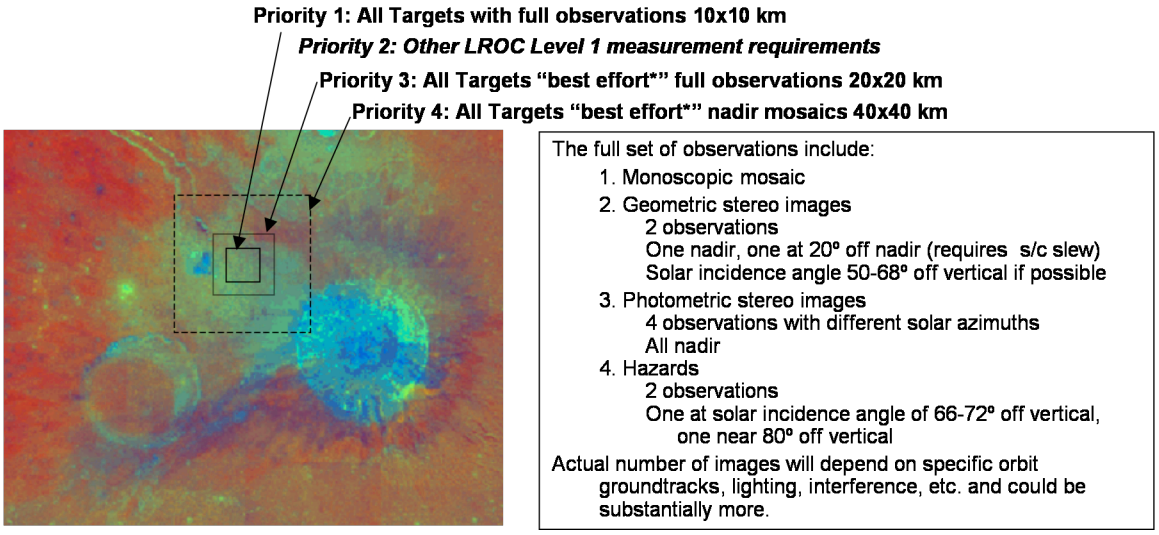

Figure 1. Cx Tageting Philosophy (Note: General LROC targeting prioritization: Priority 1 - Images requested by Cx; Priority 2 - Images needed to satisfy LROC Level 1 requirements; Priority 3 - Images requested by other LROC Co-I or LRO Science Team, Cx requests; Priority 4 - Images requested by lunar science community, Cx requests; Priority 5 - images requested by the public.)

LUNAR VOLCANISM IN SPACE AND TIME: RANGE OF ERUPTION STYLES AND IMPLCATIONS FOR MAGMA ASCENT AND EMPLACEMENT. J. W. Head[1] and L. Wilson[2], [1]Dept. Geol. Sci., Brown Univ., Providence, RI 02912 USA [2]Env. Sci. Dept., Lancaster Univ., Lancaster LA1 4YQ U.K. (james_head@brown.edu).

Introduction: A wide variety of morphologic features representing a range of eruption styles has been documented on the Moon [e.g., 1-2]. We have characterized the nature of numerous steep-sided domes, small shields, cones, dark halo craters of internal origin, dark mantle deposits, linear rille-related deposits, and sinuous rille-related deposits on the Moon using Clementine multispectral, Apollo, and Lunar Orbiter data [2-7]. We have also shown that the main path of the ascent and eruption of magma from mantle source regions is through magma-filled cracks or dikes [2, 8-9]. We have been analyzing additional landforms and synthesizing these results into an overall assessment of the relationship between the nature of dike intrusion to shallow depths within the crust and the resulting landforms and deposits (Fig. 1). These data and this synthesis will be of importance to the general reanalysis of the models of the ascent and eruption of magma [10] and to targeting for the Lunar Reconnaissance Orbiter Mission (LRO).

Analysis: We have revised our theoretical treatment for the penetration of magma-filled cracks (dikes) to the vicinity of the lunar surface (Fig. 1) [10], and we outline here the predicted range of tectonic and associated volcanic features and processes from our analyses [7, 9, 11]. The surface manifestation of a dike that does not actually reach the surface can take a range of forms. If the dike stalls at a sufficiently great depth, there will be some undetectably small amount of surface extension and uplift. If it penetrates to shallower depths there may still be no noticeable topographic effects at the scale of available images, but incipient failure or activation of pre-existing fractures may generate pathways along which gas (probably mainly carbon monoxide) formed by carbon-metal oxide "smelting" reactions [12-13, but see also 14] in magma in the shallowest parts of the dike can reach the surface. Still shallower penetration will lead to a larger volume of melt being exposed to the relatively low pressure environment near the surface and will encourage the generation of a greater mass of CO since the chemical reaction producing it is pressure-dependent. Subsequent loss of this gas, coupled with a magma volume decrease on solidification and cooling, may lead to collapse features (or even explosion craters) forming on the surface above the dike. Very shallow intrusion may lead to further development of a graben and will encourage the formation of small secondary intrusions and possible eruptions; we have developed criteria to distinguish between graben formed by dike emplacement and those resulting from tectonic deformation alone [15]. We have shown how the shallow stalling of a dike wide enough to allow spontaneous convection to occur during the early stages of its cooling can expose so much magma to low pressure degassing that it leads to major gas buildup and propagation of a crack to the surface, resulting in an Io-like eruption plume and the formation of a dark halo deposit ~150 km in diameter [6]. We have also assessed the deep generation of magmatic gas on the Moon and described implications for pyroclastic eruptions [16] as well as the ascent of magma feeding the steep-sided domes [7].

We have further explored the range of morphologies of volcanic vents and landforms and their implications for ascent of magma and behavior of dikes in the near surface zone, emphasizing the range of behaviors related to the four stages shown in Fig. 1. This range of behaviors appears to account for much of the diversity of eruption conditions implied by the morphologies of features seen on the lunar surface, and suggests that the following classes of morphologic features correspond to these several aspects of shallow dike emplacement behavior.

Linear rilles with associated pyroclastic cones: In some cases, a dike may propagate sufficiently near to the surface to create a graben, but still not cause significant eruption of lavas. In this situation, CO generation in the upper part of the dike may produce a region in the dike tip entirely occupied by a continuous gas pocket, behind which is an extended region of magma rich in entrained gas bubbles. As the dike ceases to propagate, the pressure gradient driving magma motion decays to zero over a time interval of a few tens of minutes and the initially low pressure in the dike tip rises to equilibrate with the ambient lithostatic load. Additional pressure and stress changes occur on time scales of tens of hours to a few days as gas bubbles migrate upward through the magma. These changes may force vesicular magma to the surface, producing initial gas venting and one or more relatively low-energy explosive events [9].

Crater chains with no linear rilles: At least some of the crater chains on the Moon which are not associated with linear rilles may be due to the more extensive degassing of dikes too deep to produce near-surface stress fields capable of creating graben, but shallow enough to allow gas production in the magma and venting of gas to the surface to form crater chains (Fig. 1). The pressures at which chemical reactions forming CO operate efficiently range up to ~10-15 MPa, corresponding to lithostatic pressures at depths in the Moon of about 3 km. These data would then suggest that, on average, dikes emplaced to depths between 2 and 3 km below the surface would be too deep to create surface deformation and graben, but shallow enough to allow gas production. Venting of gas to the surface would then form pit craters aligned along the strike of the dike. We have recently examined quantitatively the gas buildup behavior in

large near-surface dikes [6]. A key issue in wide dikes is that spontaneous thermal convection can occur for a considerable length of time before cooling causes the dike to become too narrow for the Rayleigh-Taylor instability to operate. Magma reaching the top of the convection cell is exposed to the low ambient pressure and produces bubbles of CO gas. These drift upward through the magma at a speed dictated by their size and density contrast with the melt. The time available for them to segregate into a continuous gas pocket above the liquid surface depends on the circulation speed of the convecting magma, which will decrease with time. Thus potential scenarios exist in which the gas accumulation rate is initially low (magma flow speed too fast for gas bubble segregation), increases for a time (magma circulation speed decreases) and then decreases again (most of the magma has already been exposed to low pressure and has completed all possible chemical reactions). The Mendeleev crater chain is a candidate example of this eruption type.

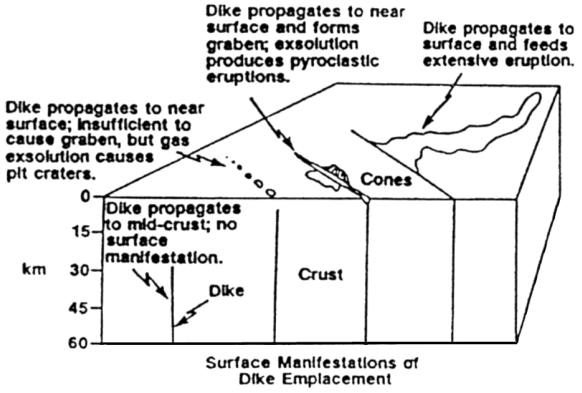

Figure 1. Geometry of shallow dike intrusion and aftermath.

Linear rilles with associated crater chains: The crater Hyginus and the two rilles leading away from it contain pits that are centrally located along the 3-4 km wide linear rilles; some pits appear to have no rims and are interpreted to be collapse craters, but others appear to have partly raised rims and may be explosion craters. The size of the crater Hyginus (9 km) makes it one of the few candidates observed on the Moon for a caldera-like structure associated with a shallow magma reservoir [2]. This is of particular importance because of the general lack of evidence for mare basalt magma stalling in the shallow crust to form reservoirs [17], and the critical nature of such evidence in distinguishing between models of magma ascent and eruption. Thus the radiating graben could be evidence of lateral dike emplacement from a shallow reservoir along a rift zone. Graben width suggests that the depth to the top of the dike is ~1.5-2.0 km, a value within the range of depths where CO gas formation would be expected to occur. Thus the production and explosive venting of the volatiles, with subsequent collapse, may explain the range of features seen here.

Domes and cones: Where these occur in isolation, or in small groups, they represent additional types of features that suggest the presence of unusual conditions giving rise to low effusion rates. We are examining representatives of the full range of domes and cones. The Gruithuisen and Mairan domes are one end member that is spectrally distinct and may be affiliated with early mare deposits or be a candidate for non-mare basalts [5]. We have completed regional multispectral analyses of the domes and their relationship to mare units [5, 18], have established a stratigraphic sequence and obtained crater size-frequency distribution ages [18] and have modeled the ascent and eruption of candidate materials along dikes to produce these features [7]. Variations in magma composition, and hence rheology, are as important as variations in dike geometry in controlling the formation of these features. Small lunar domes and cones (e.g., Marius Hills, Grace and Diana shield volcanoes [3, 4]) represent a range of features involving both effusive and explosive eruptions and we show how fine tuning of dike widths and intrusion depths can lead to the variety observed in these features.

Summary: The range of volcanic eruption features observed on the Moon can be reasonably interpreted in terms of predictions of the consequences of the penetration of magma-filled cracks (dikes) to the vicinity of the lunar surface. Placing these in the context of large-volume, high eruption-rate effusive eruptions [2] provides a much improved picture of the range of characteristics of eruptions and shallow intrusions in the upper lunar crust. The nature and frequency distribution of dike widths, eruption rates, and near-surface intrusions help to distinguish between models in which simple buoyancy forces drive magma to the surface (e.g., 19) and those in which other driving forces play a role (e.g., 11).

LRO: This analysis forms the basis for the systematic targeting of suspected features and structures representing the ascent and eruption of magma: the emplacement of dikes, their stalling and evolution and their extrusion to the surface. The data obtained by the various instruments on board LRO will be essential in testing these hypotheses and further quantifying the processes.

References: [1] J. Head (1976) RGSP 14, 265. [2] J. Head and L. Wilson (1992) G&CA 55, 2155. [3] C. Weitz and J. Head (1999) JGR 104, 18933. [4] C. Weitz et al. (1998) JGR 103, 22725. [5] S. Chevrel et al. (1999) JGR 104, 16515. [6] J. Head et al. (2002) JGR 107, 1438. [7] L. Wilson and J. Head (2003) JGR 108, 5012. [8] L. Wilson and J. Head (1981) JGR 86, 2971. [9] J. Head and L. Wilson (1994) PSS 41, 719. [10] L. Wilson and J. Head (2009) LPSC 40. [11] L. Wilson and J. Head (2001) LPSC 32, 1297. [12] M. Sato (1979) PLPSC 10, 311. [13] R. Fogel and M. Rutherford (1995) G&CA 59, 201. [14] A. Saal et al. (2008) Nature 454, 192. [15] J. Petrycki et al. (2004) LPSC 35, 1123. [16] L. Wilson and J. Head (2003) GRL 30, 1605. [17] J. Head and L. Wilson (1991) GRL 18, 2121. [18] R. Wagner et al. (2002) JGR 107, 5104. [19] M. Wieczorek et al. (2001) EPSL 185, 71.

LUNAR MARE BASALTS: SCIENTIFICALLY IMPORTANT TARGETS FOR LROC. H. Hiesinger[1], K. Klemm[1], C. H. van der Bogert[1], D. Reiss[1], J. W. Head[2]. [1]Institut für Planetologie, Westfälische Wilhelms-Universität, Wilhelm-Klemm-Str. 10, 48149 Münster, Germany. [2]Dept. of Geological. Sciences, Brown University, Box 1846, Providence, RI 02912. Hiesinger@uni-muenster.de

Introduction: The majority of lunar mare basalts are exposed on the lunar nearside within large impact structures, but also occur on the lunar farside, although over a reduced spatial extent [1]. Even after the Apollo and Luna sampling programs, absolute radiometric age data are still absent for most of lunar basalts. Remote sensing techniques allow us to derive relative and absolute model ages for unsampled regions. For example, inspection and interpretation of the superposition of geologic units, including embayment and crosscutting relationships as seen with high-resolution Apollo and Lunar Orbiter images, were used to obtain relative ages for lunar surface units [e.g., 2]. In addition, it has been shown that crater degradation stages and crater size-frequency distribution measurements, calibrated to the landing sites, are useful for the derivation of relative and absolute model ages [e.g., 3-14]. In previous papers, we presented age data based on remote sensing techniques, that is, crater counts [e.g., 11-14]. Our age data represent the most comprehensive data set on lunar mare basalt ages and can help constrain boundary conditions for the thermal and petrologic evolution of the Moon. In particular, our ages can be correlated with Lunar Prospector and Clementine data in order to study the mineralogical evolution of mare basalts with time. In some cases, distinctive kinks in the cumulative crater size frequency distribution can also be used to estimate the thickness of lava flows [14,15]. These thicknesses can be used to estimate the flux of lunar mare basalts over time in order to constrain the thermal evolution of the Moon.

Scientific Questions: ***(1) Mare volcanism in space and time:*** Despite the undisputed scientific value of the returned samples from six Apollo and three Luna landing sites, these data are insufficient to completely explain the thermal evolution of the Moon. For example, based on samples alone, the onset and extent of mare volcanism are not well understood (summarized by [16]). The returned samples indicate that mare volcanism was active at least between ~3.9 and 3.1 b.y. [17,18]. Ages of some basaltic clasts in older breccias point to an onset of mare volcanism prior to 3.9 b.y. [19], perhaps as early as 4.2–4.3 b.y. in the Apollo 14 region [16,20,21]. Early volcanism is also supported by remote-sensing data. For example, dark halo craters have been interpreted as impacts into basaltic deposits that are now buried underneath a veneer of basin or crater ejecta [e.g., 22-24]. These underlying cryptomare basalts might be among the oldest basalts on the Moon, implying that volcanism was active prior to ~3.9 b.y. ago. Early volcanism is also supported by radiometric age dating of the lunar meteorite Kalahari 009, which revealed that volcanism was already active at least 4.35 b.y. ago [25]. On the basis of crater degradation stages, Boyce [6] and Boyce and Johnson [26] derived absolute model ages that indicate volcanism might have lasted from 3.85±0.05 b.y. until 2.5±0.5 b.y. ago. Support for such young basalt ages comes from a recently collected lunar meteorite, Northwest Africa 032, which shows a Ar-Ar whole rock age of ~2.8 b.y. [27]. Indications of late mare volcanism are discussed by Schultz and Spudis [8], who made crater size-frequency distribution measurements for basalts embaying the Copernican crater Lichtenberg, and concluded that these basalts might be less than 1 b.y. old. Our crater counts indicate that lunar volcanism in the large nearside maria started at ~4 b.y. and ended at ~1.1 b.y. ago. Most of the investigated basalts on the lunar nearside erupted during the late Imbrian Period between ~3.3-3.8 b.y. and there is possibly a second period of enhanced volcanic activity at ~2-2.2 b.y. ago. Crater counts of a few basalts on the lunar farside revealed similar results [28].

(2) Mineralogical evolution of the Moon: The presence of basaltic deposits on planetary surfaces is indicative of the thermal activity and volcanic evolution of the body [29-31]. In order to understand the geologic evolution of a planetary body, it is crucial to know when basaltic volcanism was active and how the mineralogy varied with time. Lunar basalts show a large range in TiO_2 content; this broad variation in Ti abundances allows the separation of different basalt types using both laboratory and remote sensing techniques. In the sample collection, three major groups of basalts can be identified: high-Ti (9-14 wt% TiO_2), low-Ti (1-5 wt% TiO_2), and very-low-Ti (< 1 wt% TiO_2) basalts. Laboratory data show a distinctive bimodal distribution of titanium concentrations of basalts in the sample collection with peaks at ~2.5-3 and 12-13 wt% TiO_2, but remote sensing data suggest that there is a continuous distribution of very-low-Ti to high-Ti mare basalts [32]. Early Ti-rich basalts flooded large regions in the eastern lunar hemisphere (Ap11, Ap17) in the early Imbrian Period (3.3-3.8 b.y.) [1]. These basalts were followed by widespread eruptions of less Ti-rich basalts of middle to late Imbrian age (Ap12, Ap15). Finally Ti-rich basalts, which have not been sampled so far, flooded parts of Mare Imbrium and Oceanus Procellarum in the early Eratosthenian Period (2.5-3.0 b.y.). Combining our absolute model ages with mineralogical data from spacecraft (e.g., Clementine, Lunar Prospector), we can study the relationship between the mineralogy and the age of a basalt. Our investigation showed that there is no systematic relationship between the age and the Ti abundance of a lunar basalt, contrary to the results from sample analysis. Based on our investigation of ~220 basalt units in 9 different mare regions we see that Ti-rich basalts can erupt simultaneously with Ti-poor basalts. We do not find any evidence that older basalts are systematically more Ti-rich.

(3) Flux and thermal evolution of the Moon: In order to investigate the volumes and the flux of lunar mare basalt volcanism, it is crucial to know the thicknesses of mare flow units. Previous work on basalt flow thicknesses was based on (1) shadow measurements in high-resolution images that were taken under low-sun conditions in order to enhance subtle surface morphologies of flow units [e.g., 33-35]; (2) in situ observations of Hadley Rille at the Apollo 15 landing site [36], and (3) studies of the chemical kinetic aspects of lava emplacement and cooling [37]. Neukum and Horn [38] showed that endogenic lava flow proc-

esses could be identified by their characteristic effects on crater size-frequency distributions without identifying individual flows directly in the images. For example, emplacement of a young lava flow on top of an old flow results in a preferential destruction of small craters and hence a characteristic deflection in the cumulative crater curve. The crater diameters at which these deflections occur are indicative of the thickness of the flow. Once these diameters are derived, the flow unit height is estimated using the rim height/diameter relationship of [39]. Our measurements of the flow heights of ~70 mare units exposed within the nearside mare revealed an average thickness of ~30-60 m with a variation between 20 and 220 m. Combined with the size of our units, this yields flow volumes in the range of 30 to 7700 km^3, averaging 590-940 km^3.

Targeting Strategy: In June 2009, the Lunar Reconnaissance Orbiter will be launched to investigate the lunar surface in unprecedented detail [40]. On board the spacecraft are two narrow angle cameras (NAC) and a wide-angle camera (WAC), providing global coverage at about 100 m/pixel and coverage of large areas at spatial resolutions of less than 1 m/pixel. The illumination geometry was chosen in order to emphasize subtle morphologic details. Hence, the global WAC and the local/regional NAC data sets will be extremely valuable for crater counts, particularly on the farside. We have specified and entered into the data base more than 1800 targets that cover mare basalts. Our targets were selected based on the count areas of our previous papers [11-14, which in turn were selected to represent spectrally homogeneous areas. Within each of those old larger units, we have now specified several subunits that can realistically be covered with LROC NAC images. We particularly endeavor to avoid secondary craters, wrinkle ridges, ejecta blankets, etc., that could influence our crater counts. Because mare basalts are flat-lying and exhibit rather few morphologic features, we rarely request the acquisition of geometric or photometric stereo images. In order to make full use of the high-resolution capabilities of the NAC to measure small craters, binning of the data should only be applied if necessary.

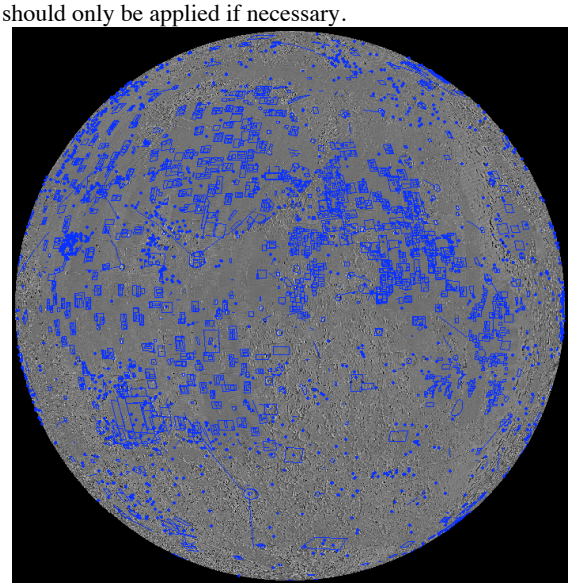

Fig. 1. The lunar nearside with potetial targets for LROC

References

[1] Head, 1976, Rev. Geophys. Space Phys. 14; [2] Shoemaker and Hackman, 1962, in The Moon: IAU Symposium 14; [3] Hartmann, 1966, Icarus 5; [4] Greeley and Gault, 1970, Moon 2; [5] Neukum et al., 1975, Moon 12; [6] Boyce, 1976, Proc. LSC 7th; [7] Neukum, 1983, Habilitation Thesis, Univ. Munich; [8] Schultz and Spudis, 1983, Nature, 302; [9] Wilhelms, 1987, USGS Prof. Paper 1348; [10] Neukum and Ivanov, 1994, in Hazards Due to Comets and Asteroids; [11] Hiesinger et al., 2000, JGR 105; [12] Hiesinger et al., 2001, LPS XXXII, #1815; [13] Hiesinger et al., 2003, JGR 108; [14] Hiesinger et al., 2002, GRL 29; [15] Neukum and Horn, 1976, Moon 15; [16] Nyquist et al., 2001, in The Century of Space Science; [17] Head, 1976, Rev. Geophys. 14; [18] Nyquist and Shih, 1992, GCA 56; [19] Ryder and Spudis, 1980, Proc. Conf. on Lunar Highlands Crust; [20] Taylor et al., 1983, EPSL 66; [21] Dasch et al., 1987, GCA 51; [22] Schultz and Spudis, 1979, Proc. LPSC 10th; [23] Hawke and Bell, 1981, Proc. LPSC 12th; [24] Antonenko et al., 1995, Earth, Moon and Planets 69; [25] Terada et al., 2007, Nature 450; [26] Boyce and Johnson, 1978, Proc. LPSC 9th; [27] Fagan et al., 2002, MAPS 37; [28] Haruyama et al., 2009, Science 323; [29] Solomon and Head, 1984, JGR 89; [30] Solomon and Head, 1980, Rev. Geophys. Space Phys. 18; [31] Head and Solomon, 1981, Science 213; [32] Giguerre et al., 2000, MAPS 35; [33] Schaber, 1973, Proc. LPSC 4th; [34] Schaber et al., 1976, Proc. LPSC 7th; [35] Gifford and El-Baz, 1981; Moon and Planets 24; [36] Howard et al., 1972, Proc. LSC 3rd; [37] Brett, 1975, GCA 39; [38] Neukum and Horn, 1975, The Moon 15; [39] Pike, 1980, USGS Prof. Paper 1046-C; [40] Robinson et al., 2005, LPS XXXVI, #1576.

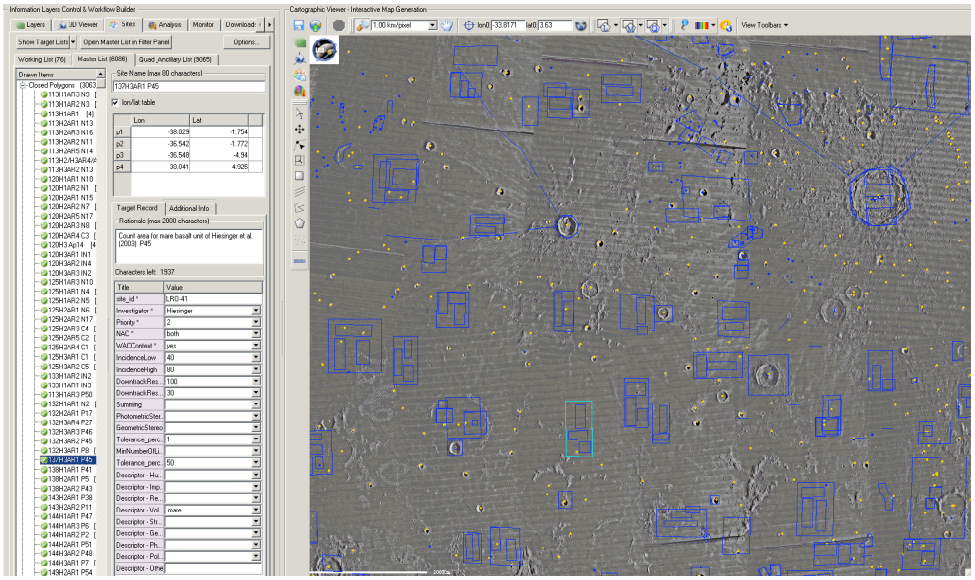

Fig. 2: . Screenshot of the REACT targeting tool with mare basalt targets in Oceanus Procellarum.

LUNAR MAGNETISM. Lon L. Hood[1], [1]Lunar and Planetary Laboratory, University of Arizona, 1629 E. University Blvd., Tucson, Arizona 85721 (lon@lpl.arizona.edu).

Introduction: Lunar crustal magnetism has basic implications for the early history and evolution of the Moon. Some current fundamental and unresolved questions are: (i) Does lunar crustal magnetism require a former core dynamo? (ii) To what extent can impact processes alone explain much or all of the observed crustal magnetization? (iii) What is the origin of unusual surface albedo markings that are closely associated with the strongest individual magnetic anomalies detected from orbit? As will be seen, these questions have general solar system science applications beyond lunar science.

Full answers to these questions will require a combination of refined sample studies and future *in situ* geophysical measurements in orbit and at the surface. However, LRO high resolution imagery and other measurements can provide some useful additional constraints. In particular, it can contribute to a better understanding of the origin and nature of sources of lunar orbital magnetic anomalies. It can also contribute to a better understanding of the unusual Reiner Gamma-type albedo markings.

Constraints on Magnetic Sources: Current evidence suggests that impact processes played a major role in producing the strongest magnetization that is preserved in the lunar crust ([1] and references therein). The largest concentrations of strong magnetization are found antipodal to the youngest and largest impact basins [2] while fields within the youngest basins are relatively weak [3]. Unusual terrain is found in the same antipodal regions that is interpreted to be a consequence of convergence of either seismic compressional waves or basin ejecta (or both) at the antipode. The interaction of vapor-melt clouds produced in basin-forming impacts with an ambient magnetic field (either a solar wind field or a core dynamo field) generates transient magnetic fields with maximum amplitude in the antipodal region [1]. If magnetized materials are entirely surficial and consist, for example, of basin ejecta, then they could have formed quickly enough to have acquired their magnetization only in impact-generated transient fields. However, if sources are deeply buried in the crust, their formation times would be much longer, requiring a steady magnetizing field, i.e., presumably a core dynamo. Verification of a solely impact origin for most or all of lunar crustal magnetism would have basic implications for our understanding of paleomagnetism on other airless silicate bodies in the solar system (e.g., Mercury, asteroids).

High resolution imagery such as will be obtained by the LROC on LRO, combined with future new geophysical measurements and sample returns, can assist in obtaining a better understanding of the origin of lunar magnetic anomaly sources and, therefore, of lunar magnetizing fields. On the geologically less complex near side, correlative studies have previously shown that basin ejecta materials (e.g., the Cayley formation and the Descartes Mountains) [4,5] are likely sources of lunar magnetic anomalies. This hypothesis is consistent with returned sample studies showing that impact-produced materials (e.g., breccias) contain more metallic iron and have much higher magnetization intensities than igneous materials (e.g., mare basalt). In addition, correlative studies on the far side have shown that unusual terrain in basin antipode regions correlates positively with crustal field strength [6]. Any new LRO measurements and high-resolution imagery that would further constrain the geologic origin of these candidate crustal field sources would be very beneficial.

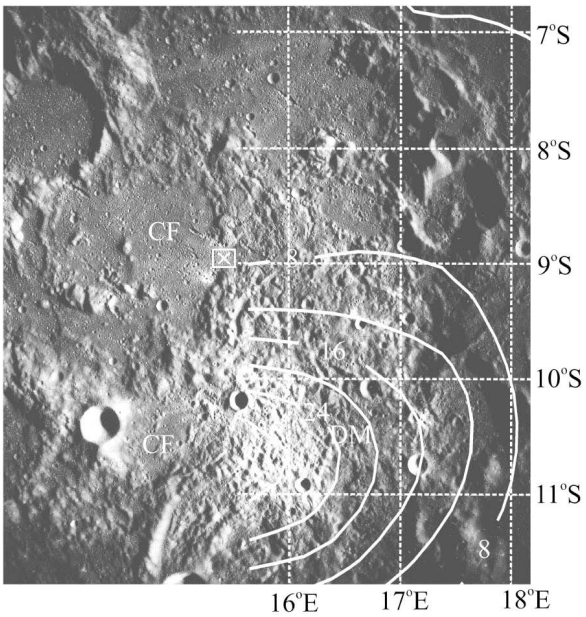

Figure 1. Descartes lunar magnetic and albedo anomaly near the Apollo 16 landing site (×). 2D filtered magnetic field at ~ 19 km altitude is contoured in nT. CF denotes Cayley Formation. Reproduced from [5].

Constraints on Reiner Gamma-Type Albedo Markings: Unusual curvilinear albedo markings correlate with relatively strong and isolated lunar magnetic anomalies ([7] and references therein). It has

been proposed that these albedo markings are, at least in part, a consequence of deflection of the solar wind ion bombardment by the strongest crustal fields. The latter hypothesis assumes that the ion bombardment is an important secondary contributor (in addition to micrometeoroid impacts) to the optical maturation (darkening with time) of lunar surface materials, typified by the gradual disappearance of crater rays. Verification of this hypothesis would have general implications for optical maturation on other airless silicate bodies in the solar system. Alternatively, surface scouring (surficial mass removal) by relatively recent cometary coma impacts [8] or meteorite swarm encounters [9] have been invoked to explain these features. Any additional constraints on the origin of these unusual albedo markings from LROC imagery or other LRO measurements would be beneficial for both lunar magnetism and for the interpretation of lunar surface spectral properties.

Specific Targets of Interest: On the near side, a target of special interest is the Descartes mountains near the Apollo 16 landing site. As indicated in Figure 1, these mountains, which represent primary basin ejecta from Imbrium and/or Nectaris, include the site of the strongest single magnetic anomaly on the near side [5,10]. It is also the site of an unusual albedo anomaly. Future surface magnetometer measurements may confirm that the source of the anomaly is directly exposed at the surface and consists of the Descartes mountains themselves. Any additional LROC or other measurements that would provide constraints on the origin and nature of this part of the Descartes mountains would therefore be a valuable supplement to future surface geophysical measurements and sample returns at this location.

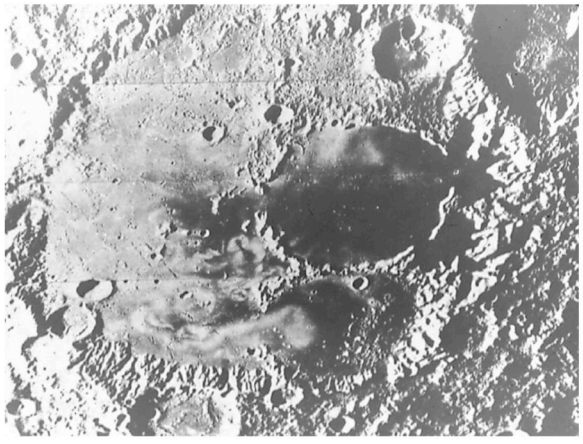

Figure 2. Lunar Orbiter photograph of the Mare Ingenii region on the lunar far side near the Imbrium antipode. Note the unusual modified terrain along the basin walls and the Reiner Gamma-type albedo markings on the mare. Reproduced from [7].

On the far side, exposures of antipodal modified terrain (e.g., Figure 2) would represent especially interesting targets. The northwest periphery of the SPA basin is characterized by both strong magnetic anomalies (antipodal to Imbrium and Serenitatis) and unusual geochemical (thorium) anomalies [11]. Both types of anomalies correlate positively with the distribution of unusual modified terrain [6,12]. Consequently, from a lunar magnetism perspective, more detailed studies of the geologic origin of the modified terrain (seismic and/or ejecta impact) by LRO would be especially useful. Such studies may also be beneficial for understanding the geochemical anomalies. A number of targets within the modified terrain may be identified. These include areas along the rim of the Ingenii basin (Figure 2) near the Imbrium antipode and east of Mare Marginis near the Orientale antipode.

Other obvious targets of interest from a magnetism perspective include Reiner Gamma on western Oceanus Procellarum and within Mare Ingenii on the far side near the Imbrium antipode (Figure 2). Both sites have been designated as Tier 1 targets by Project Constellation according to the LROST meeting web site. Both are characterized by strong magnetic anomalies and easily visible albedo markings. However, both sites are on mare surfaces while the actual anomaly sources are probably beneath the mare [7]. The imagery and radiometry would therefore be mainly beneficial for investigating the origin of the albedo markings (e.g., maximum topographic relief, surface roughness, etc.). Investigations of the magnetic sources themselves probably require other targets as discussed above (Descartes mountains, antipodal modified terrain).

References: [1] Hood L. L. and Artemieva N. A. (2008) *Icarus, 193,* 485-502. [2] Mitchell E. F. et al. (2008) *Icarus, 194,* 401-409. [3] Halekas J. S. et al. (2003) *Meteorit. Planet. Sci., 38,* 565-578. [4] Halekas, J. S. et al. (2001) *J. Geophys. Res., 106,* 27841-27852. [5] Richmond, N. C. et al. (2003) *Geophys. Res. Lett., 30,* doi:10.1029/2003GL016938. [6] Richmond, N. C. et al. (2005) *J. Geophys. Res., 110,* doi:10.1029/2005JE002405. [7] Hood, L. L. et al. (2001) *J. Geophys. Res., 106,* 27825-27839. [8] Schultz, P. H. & L. J. Srnka (1981) *Nature, 284,* 22-26. [9] Srarukhina, L. V. & Y. Shkuratov (2004) *Icarus, 167,* 136-147. [10] Richmond, N. C. & L. L. Hood (2008) *J. Geophys. Res., 113, doi: 10.1029/2007JE002933.* [11] Lawrence et al. (2000) *J. Geophys. Res., 105,* 20307-20331. [12] Wieczorek, M. A. & M. T. Zuber (2001) *J. Geophys. Res., 106,* 27853-27864.

CURRENT UNDERSTANDING OF LUNAR VOLATILE TRANSPORT AND SEGREGATION. D. M. Hurley[1,2], [1]Johns Hopkins University Applied Physics Laboratory (11100 Johns Hopkins Rd, Laurel MD 20723, USA; dana.hurley@jhuapl.edu), [2]Lunar Science Institute (NASA Ames Research Center, Moffett Field, CA, 94035, USA)

Introduction: Volatiles are scarce on the Moon, especially at low latitude. Volatiles sublimate in the lunar high temperature and low pressure environment. Once released, volatiles leave the Moon by Jean's escape or photoionization. Without an active resupply source, the indigenous lunar volatiles have been lost to space. Although it is still unknown whether water ice exists on the Moon, the only place it could possibly persist long-term is in permanently shadowed regions (PSR). We review the data relevant to lunar polar volatiles and their interpretations. Then we describe the processes that control volatile transport and segregation on the Moon. We discuss ongoing and upcoming measurements that will further our understanding of the volatile inventory, sources, losses, and transport. Finally, we summarize the current state of understanding and contribution of LRO to increasing knowledge.

Existing Data: Although data do exist regarding lunar volatiles, none are conclusive.

UVS. Apollo 17 contained an ultraviolet spectrometer (UVS) on the orbiter that measured spectra of atmospheric species in the lunar exosphere [1]. The UVS placed upper limits on the abundances of H_2, H, O, N, C, Kr, Xe, and CO. If solar wind protons were reflected as H, the abundance would exceed the upper limit set by UVS indicating that H is converted to H_2 or other molecules in the regolith before release.

LACE. The Apollo Surface Experiment Package (ALSEP) on Apollo 17 included a neutral mass spectrometer called Lunar Atmospheric Composition Experiment (LACE). LACE measured the argon and helium atmosphere of the Moon for several diurnal cycles [2]. The instrument also detected water group molecules, which were interpreted to be contamination from the descent module [2].

Neutrons. The Lunar Prospector (LP) spacecraft was equipped with a neutron spectrometer (NS). An orbiting NS measures a depletion in epithermal neutrons when flying over enhanced hydrogen concentrations. LPNS detected signatures consistent with hydrogen enhancements over both lunar poles [3]. Neutron measurements are sensitive to atomic composition regardless of the molecular structure. Therefore, the polar hydrogen detected may be water ice deposits in lunar cold traps. However that interpretation is not unique. Other forms include implanted hydrogen and hydrous minerals [4].

Radar. Radar measurement of the Moon are ongoing. Bi-static radar from the Clementine mission indicated an enhanced circular polarization ratio in a region near the south pole about 100 km^2 [5]. Ground based radar also sees some coherent backscatter signals consistent with ice [6]. However, in both ground based and spacecraft based measurements, similar signatures are observed in illuminated regions, where ice is not expected to exist [6,7].

Ground-based spectra. Sodium and potassium are the other constituents that have been observed in the lunar atmosphere, owing to their strong G-factors [8].

Migration, Segregation, and Retention: There are multiple potential sources of volatiles on the Moon. Comets certainly have hit the Moon over the course of time. Micrometeoroids constantly impact the Moon and vaporize material. In addition, the Moon traverses through the solar wind and the Earth's magnetotail. Volatile elements are implanted into the regolith as the plasma, comprised primarily of H+, strikes the surface. Periodic outgassing events might also release volatiles. Radiogenic volatiles diffuse out of the Moon continuously. Each of these processes can liberate volatiles into the lunar exosphere.

Although most of any putative water vapor in the lunar atmosphere would be lost to photodissociation, it is possible to deliver a fraction to the cold traps [9]. Butler has simulated the migration of water and carbon dioxide [10]. Hodges used LACE data to argue that water transport on the Moon is not occurring because migrating water would readily adsorb to the surface on the nightside as Ar does. With both species competing for adsorption sites, Ar would not exhibit the nightside depletion that it does [11].

Just as there are different possible sources that might contribute to the volatile inventory, there are different processes that can remove volatiles from the PSRs. These sinks include Ly-a from scattered light off of the interplanetary hydrogen, earthshine from Earth's UV corona, sublimation, sputtering, and impact vaporization [12]. Sublimation is a very strong function of temperature and is the dominant loss mechanism over most of the Moon. The permanently shaded regions are the only places with a low enough sublimation rate that retention of volatiles is possible [13].

Over time, any volatile condensed in a polar cold trap would be modified by the constant pummeling of meteoroids of all sizes. This gardening can be alternately a source and a sink of volatiles [14]. Impacts vaporize material at the impact site. Those volatiles might recondense within the same cold trap. In con-

trast, a nearby impact will emplace an ejecta layer over exposed volatiles, which would protect the volatiles from UV light. Temperature gradients would drive diffusion within the PSRs as well [15]. We have a model that follows the depth distribution of volatiles in a lunar PSR to understand the retention of volatiles over time in this dynamic environment [14].

Potential Measurements: The purpose of this meeting is to discuss targets of interest for LRO. Those are discussed further below. However, other recent and upcoming missions will also make relevant observations for volatiles. Chandrayaan-1 has a radar experiment, Mini-SAR, which is currently operating. It's radar will be able to detect ice in permanently shadowed regions if the ice has an integrated thickness on the order of the radar wavelength. The SARA instrument on Chandrayaan-1 will detect energetic neutral atoms (ENAs) coming from the Moon. ENAs trace charge exchange processes near the Moon. Onboard Kaguya, the MAP-PACE package is a comprehensive plasma instrument complement. MAP-PACE measures the sputtered ions from the lunar surface and newly ionized particles in the lunar atmosphere. LADEE, a planned NASA mission, will further assay the lunar atmosphere with a UV-VIS camera and a neutral mass spectrometer.

Onboard LRO, several instruments will further understanding of volatiles on the Moon. The combination of LRO and LCROSS has great potential to increase the current state of knowledge.

LAMP will assay the lunar exosphere as a secondary instrument objective. Although the orbital geometry will have most of the lunar exosphere observations be polar observations, occasional limb views will provide data from other lunar local times and latitudes. LAMP will also look for spectral signatures of exposed water frost in PSRs. Scattered UV from interplanetary H provides a light source into PSRs for LAMP to see without direct sunlight. That radiation is also a sink mechanism for exposed volatiles. If LCROSS liberates any water, some of it may recondense nearby and be visible by LAMP. In addition, LAMP will follow the atmospheric evolution after impact.

The sister radar to Mini-SAR, called Mini-RF, will search for water ice in PSRs in 2 wavelength bands.

The LEND instrument will study the distribution of H to expand on the LPNS measurements.

LOLA, LROC, and Diviner will constrain the locations of PSRs to further increase the possible distribution of volatiles in PSRs. Diviner will measure thermal properties, LROC the lighting conditions, and LOLA the topography.

In addition, LROC will target regions of interest for possible recent and ongoing outgassing. This is currently an unconstrained source.

References:

[1] Fastie W. et al. (1973) *Sci. 182*, 710. [2] Hodges R. R. et al. (1973) *J. Geophys. Res. 78,* 8055. [3] Feldman W. C. et al. (1998) *Sci. 281*, 1496. [4] Starukhina I. J. (2002) *LPS XXXIII,* Abstract #1402. [5] Nozette S. et al. (1996) *Sci. 274,* 1495. [6] Campbell D. et al. (2006) *Nature 443*, 835. [7] Simpson R.A. & Tyler G.L. (1999) *JGR 104*, 3845. [8] e.g Stern S. A. (1999) *Rev. Geophys. 37* 453. [9] Watson K. et al. (1961) *JGR 66,* 3033. [10] Butler B. J. (1997) *JGR 102,* 19283. [11] Hodges R. R. (1991) *Geophys. Res. Lett. 18*, 2113. [12] Arnold J. R. (1979) *JGR 84*, 5659. [13] Vasavada A. R. et al. (1999) *Icarus 141*, 179. [14] Crider D. and Vondrak R. (2003) *JGR 108*, 5079. [15] Shorghofer N. and Taylor G. J. (2007) *J. Geophys. Res. 112* E02010.

WHAT NEW CAN LRO TELL US ABOUT LUNAR THERMAL EVOLUTION, INTERIOR STRUCTURE AND DYNAMICS? C. L. Johnson[1], T. R. Watters[2] and S. J. Mackwell[3], [1]Earth and Ocean Sciences, University of British Columbia, 6339 Stores Road, Vancouver, British Columbia, V6T 1Z4, Canada, [2]Center for Earth and Planetary Studies, National Air and Space Museum, Smithsonian Institution, Washington, DC 20560, [3]Lunar and Planetary Institute, 3600 Bay Area Blvd, Houston, TX 77058.

Introduction: Lunar surface features imaged from space can provide important new constraints on lunar structure and dynamics over the history of the Moon. While the surface of the Moon is dominated by impact craters and basins, tectonic landforms attest to basin localized stresses and global crustal contraction resulting from slow cooling of the lunar interior (see [1] and references therein). In addition, seismometers emplaced during the Apollo era recorded numerous moonquakes (see [2, 3] and references therein). While the maximum recorded body wave magnitude is around 5, it is conceivable that surface features associated with known moonquakes may be identified.

Wrinkle ridges, graben and lobate scarps: As shown in the Figure 1, tectonic landforms are mostly concentrated in the mare on the lunar nearside. The wrinkle ridges and graben appear to associated mostly with emplacement and subsidence of mare basalts, while the lobate scarps, although few in number, are less clearly associated with the maria and may express global tectonic stresses.

Lunar wrinkle ridges are complex structures involving thrust faults and folds resulting from compressional stresses in the maria. They are found in mare basalts and consist of a broad arch and a superimposed narrow ridge. While sinuous rilles in the maria are believed to be volcanic in origin, linear and arcuate rilles are graben, resulting from extensional tectonics. The wrinkle ridges and graben appear to result from basin-localized compressional and extensional tectonics associated with subsidence and flexure.

Unlike the wrinkle ridges and graben, the lobate scarps are not directly associated with the mare basins and may have origins similar to those for parallel landforms on Mercury and Mars. Lunar lobate scarps are generally asymmetic and are often lobate and segmented. With lengths of only a few tens of kilometers and maximum relief of only a few tens of meters, they are generally significantly smaller than their counterparts on Mercury and Mars. Lunar lobate scarps appear to be the result of shallow thrust faults, and are sometimes associated with wrinkle ridges, although they are found predominantly in the lunar highlands. The compressional stresses that formed the lobate scarps may have resulted from thermal stresses due to global cooling. If this model is correct, the spatial distribution and scale of the scarps may have important implications for the Moon's thermal history and constrain models for its origin. The relatively small scale of lunar lobate scarps makes identification and characterization of these structures difficult. Because less than about 10% of the lunar surface has been imaged at high enough resolution and optimum illumination conditions to detect small-scale tectonic landforms, the global distribution of the lobate scarps is unknown.

High resolution images from the Lunar Reconnaissance Orbiter Cameras (LROC) will make a global survey of lunar lobate scarps possible. Because of their generally small size, the lobate scarps may not be well characterized by Lunar Orbiter Laser Altimeter (LOLA) data. Thus, stereo derived topography obtained from the LROC Narrow Angle Cameras (NACs) will be used to characterize lobate scarp morphology and relief. LROC high resolution stereo imaging of the larger scale wrinkle ridges and graben will allow much more detailed characterization of associated small-scale structures. Wrinkle ridges and graben and their long wavelength topographic setting in lunar mascons will be well characterized by LOLA data.

Moonquakes: Seismometers were emplaced on the Moon at Apollo sites 12, 14, 15 and 16 as shown by the open triangles in Figure 1. The seismometers form a triangular array with apices around 1100 km apart. The modest geographical coverage limits our ability to see deep within the lunar interior and locate events on the lunar farside. Epicentral locations and moonquake depths are also relatively poorly contrained. During the 8 year history of the seismometers, over 12,500 events were recorded, including 28 shallow and >1360 deep moonquakes. The shallow moonquakes occur at depths up to ~100 km and have been interpreted as tectonic in origin; some of these quakes may occur in the lunar crust. A number appear to be associated with the edges of larger craters or impact basins. The deep quakes occur at depths between 700 and 1000 km and seem to originate in around 100-200 discrete source regions. They appear to be correlated with tidal phases.

Locating surface features that can be directly associated with the deep moonquakes seems highly unlikely. However, it may be possible to correlate shallow quakes with structural features that can be identified from orbit. Analysis of all 28 shallow moonquakes indicates Richter magnitudes in the range from around

1.5 to near 5. Stress drops of around a few MPa to over 100 MPa for the 3 largest events have been calculated. As some of the quakes may be directly associated with crustal faults, it might be possible to correlate epicentral locations and surface manifestations of faults. Such correlation is hindered by poor resolution of epicenter location and rupture depth, and especially by resolution of surface imagery in the region near the epicenter. Higher resolution images of the regions near the epicenters of larger shallow moonquakes may provide evidence for a connection between moonquake generation and pre-existing fault structures, as well as indications of the stress state at depth in the lunar interior. Correlation of moonquake epicenters with increased occurence of slumping and landslides may also provide information on regolith properties.

References:

[1] T.R. Watters and C.L. Johnson, "Lunar Tectonics", in Planetary Tectonics, eds. T.R. Watters and R.A. Schultz, Cambridge University Press, in press. [2] Lognonné, P. and Johnson, C. L. (2007). Planetary Seismology. In *Treatise on Geophysics*, ed. G. Schubert. Elsevier. [3] Wieczorek, M. A., Jolliff, B. L., Khan, A., Pritchard, M. E., Weiss, B. P., Williams, J. G., Hood, L. L., Righter, K., Neal, C. R., Shearer, C. K., McCallum, I. S., Tompkins, S., Hawke, B. R., Peterson, C., Gillis, J. J. Bussey, B. (2006). The constitution and structure of the lunar interior, *Rev. Mineral. Geochem.*, **60**, pp. 221-364.

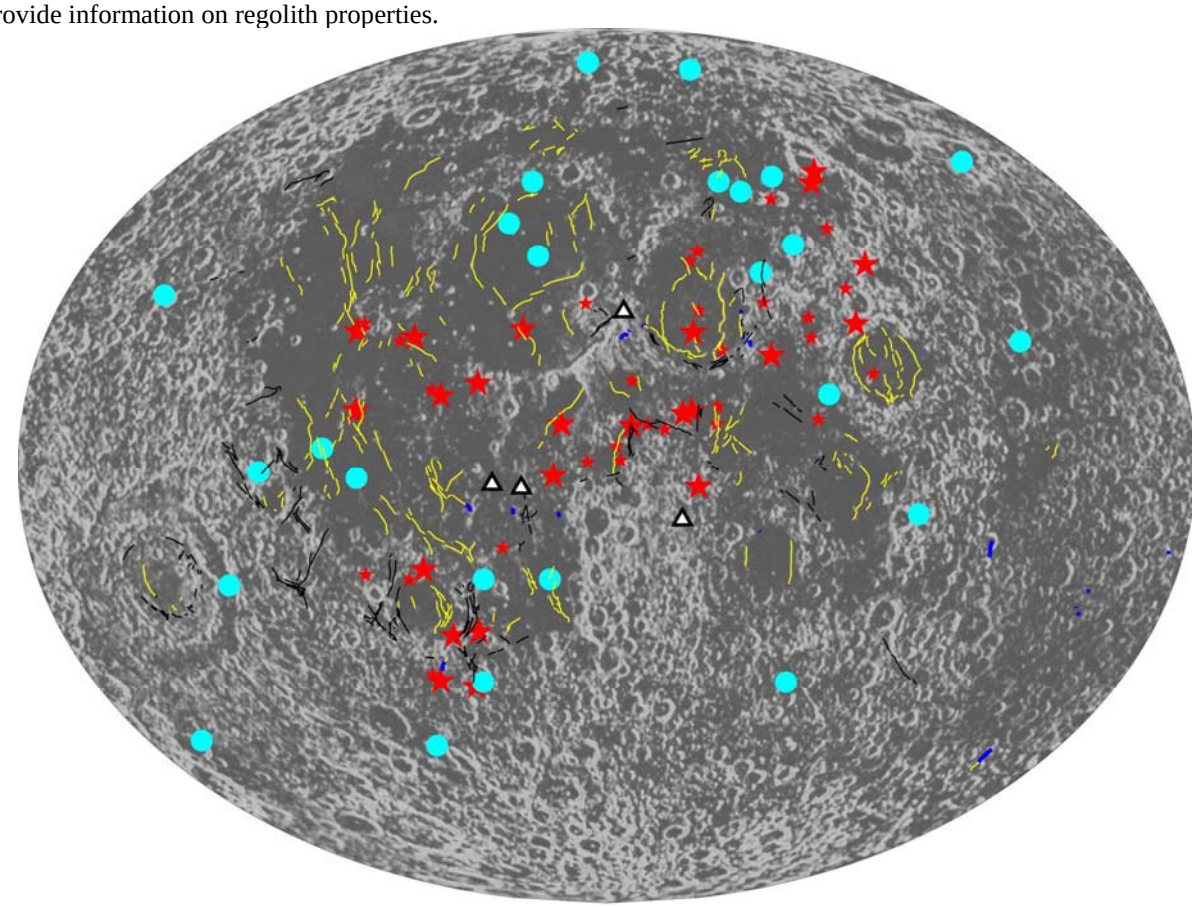

Figure 1: Map of the lunar surface with tectonic features and earthquake epicenters. Hollow triangles are the sites of the Apollo 12, 14, 15 and 16 landings where seismometers were emplaced. Pale blue dots and red stars show the epicenters of shallow and deep moonquakes, respectively. Black lines are graben and yellow lines are wrinkle ridges. The dark blue lines are lobate scarps. Figure from [1].

LUNAR CRUSTAL ROCK TYPES, GLOBAL DISTRIBUTION, AND TARGETING. B. L. Jolliff, Department of Earth and Planetary Sciences and the McDonnell Center for the Space Sciences, Washington University, St. Louis, MO 63130 (blj@wustl.edu)

Introduction. The Apollo samples provide a first-order understanding of the makeup of the lunar crust - its composition, mineralogy, and rock types [1-3]. On the basis of these samples, much has been inferred about the conditions under which these materials formed within the crust as well as the early evolution of the Moon's crust and mantle. Crustal rocks are dominated by three silicate mineral groups: olivine, pyroxene, and plagioclase. Lunar rocks are virtually anhydrous and crystallized at low oxygen fugacity and relatively low pressure. The dominant igneous crustal rock types are thus anorthosite, norite, troctolite, and intermediate types (e.g., anorthositic norite). In lunar crustal rocks, low-Ca pyroxene (orthopyroxene and pigeonite) is more abundant than high-Ca pyroxene (augite) although gabbroic rocks do occur among the samples. Rocks enriched in alkali elements and phosphorous, including alkali anorthosite, alkali norite, alkali gabbronorite, monzogabbro, and granite, are not abundant but are found, especially in samples from the western Apollo sites. Owing to known physicochemical conditions of the lunar crust, these are the rock types expected to occur throughout the Moon's upper crust, even in locations not directly sampled. This inference is supported by the observed mineralogy of lunar meteorites, which arguably provide a random sampling of the Moon's near-surface rock types, and by mineralogical remote sensing of the lunar surface.

Rock compositions, mineral chemistry, and isotopic characteristics allow subdivision of crustal igneous rocks into (1) the ferroan-anorthositic suite (early, primary crust, complementary to the mafic mantle that produced basaltic volcanism later in the Moon's history), (2) the magnesian suite (similar to the products of terrestrial layered mafic intrusives), and (3) the alkali suite, which represents more evolved chemical differentiates of magmatic processes. From these characteristics, an interpretation emerged of a relatively simple lunar crustal formation, with a post-accretion magma ocean solidifying rapidly to produce the ultramafic and dense lunar mantle, and a less dense, plagioclase-rich, buoyant crust. Remelting in the lunar mantle generated partial melts that rose into the crust, ponded, and formed layered mafic intrusions. Extended fractionation of some of these magma bodies produced chemically evolved alkaline rocks, and some may have erupted to form the compositionally distinctive but related KREEP basalts. Impact basin and crater formation melted and mixed these crustal rock types into a variety of impact-melt, fragmental, and granulitic breccias, along with the fine-grained debris that constitutes the regolith.

Global Remote Sensing. Global remote sensing missions of the 1990s – Clementine and Lunar Prospector – extended what was known from the Apollo and Luna landing sites and the narrow swaths of Apollo remote sensing to a global perspective, and the paradigm of the lunar crust changed significantly. These missions filled in details only hinted at by Apollo remote sensing. The data showed that surface expressions of crustal composition vary strongly and broadly across the lunar surface. The northern far-side highlands were found to be highly anorthositic (low-Fe, high-Al), even more so than the "type" highlands landing site, Apollo 16. The region where most of the Apollo landing sites occurred lay within the compositional influence of the Imbrium basin and its ejecta, and the global view provided by Lunar Prospector showed this region to be anomalously rich in chemically evolved crustal components and characterized by the compositionally distinctive KREEP signature. Further studies of the Apollo samples revealed a relationship between the magnesian- and alkali-suite rocks, and the suggestion arose that perhaps these rocks formed mainly in the Procellarum-Imbrium region, or the *Procellarum KREEP Terrane*. This area also appears to be a locus of crustal magmatism and extended volcanic activity, featuring some of the youngest surfaces on the Moon [4].

Another major terrane of the Moon is the area of the southern far side that is associated with the giant South Pole-Aitken Basin. Remote sensing shows that the interior of the basin still retains a distinct compositional signature that is relatively mafic (rich in Fe and Mg) and exhibits modest Th concentrations, although the latter are significantly less than concentrations found in the Procellarum KREEP Terrane. According to the size of the SPA Basin, we might expect contributions from upper-mantle as well as crustal components in its rocks, which may be impact-melt rocks or differentiated products of deep impact melt that now resemble rocks of igneous derivation.

Remote Sensing Approaches. Multispectral data from Clementine were used to investigate rock types in fresh exposures across the Moon in the form of central peaks of impact craters that mainly sample the upper crust [5]. Spectral characteristics of immature surfaces have also been used to map mineralogy globally [6]. These approaches complement global compositional remote sensing (gamma-ray) and provide a framework

for the global distribution of crustal rock types. These methods rely heavily on the Fe^{2+} content of mafic silicates; however, Mg is not determined directly, and this is important to determine the distribution of ferroan vs. magnesian rock types. Recently spectral modeling by Lucey and Cahill [7,8] has been used to estimate Mg' globally; although promising, these results need further validation.

Despite efforts to deconvolve Mg contents (or Mg/Fe) from the remotely sensed data, the distribution of *ferroan* vs. *magnesian* rocks remains poorly known and one of the key remaining petrologic problems. Ferroan anorthosite as a rock type is well known; however, magnesian anorthosite, which is found mainly as a clast component in lunar meteorites, is much less common among the samples and its mode and place of origin in the lunar crust is not known [9]. Similarly, the origin (location and igneous rock precursors) of magnesian granulitic breccias, which are common among the Apollo samples, is not well understood [10]. Furthermore, most of the crustal rocks types appear to have shallow origins, so the composition of deep crustal rocks is not well known, either.

Another key lunar petrologic mystery is the distribution and extent of the more chemically evolved lunar crustal magmatic differentiates, the alkali-suite rocks, including granite and monzogabbro. To date, these rock types are found only as minor components in breccias and small rocks or rock fragments in regolith, mainly from Apollo 12, 14, and 15. Whether these rock types are concentrated in areas such as the Aristarchus region [11,12] and nonmare volcanic domes or spectral "red sots" [13,14] remains speculative.

What can the Lunar Reconnaissance Orbiter do to improve knowledge of lunar crustal rock types and their distribution? The main advances in furthering knowledge of rock-type distribution from fresh rock exposures is coming from high spectral- and spatial-resolution remote sensing by multi- and hyperspectral imagers (on Kaguya and Chandrayaan). LRO, through its camera systems, will contribute to these advances. The narrow-angle cameras (NACs) will provide the highest spatial resolution terrain imaging to date (0.5 m/pixel in targeted locations and perhaps 2 m/pixel global resolution if there is an extended mission with an appropriate orbit). These images will provide context for remote compositional data that can be used to better understand and deconvolve sources of variation in the data. Stereo images will enable high-resolution slope determinations and normalization of slope-induced illumination geometry effects [15]. Images taken at the boundaries between distinctive units will aide efforts to better understand mixing relationships.

The wide-angle camera (WAC) will extend multispectral data at a similar spatial scale to Clementine throughout the visible region (415 to 680 nm) and into the UV (315 and 360 nm); however, these data will be mainly applicable to the mineralogy of basaltic rocks (better determination of ilmenite content and possibly improved olivine detection, and to mapping out the distribution of volcanic glass deposits that span a range of Tiand color). WAC coverage will be global and targeted NAC images will include WAC color for context imaging. The main concern here is for targeting the NACs so as to best support compositional remote sensing of geologic features that are key to understanding compositional diversity of the lunar crust.

Important targets for the NACs in this regard include crater structures that reveal fresh rocks such as central peaks, crater walls and terraces, melt sheets, and impact ejecta deposits. Of particular interest are massifs that occur in the ring structures of impact basins as these – along with central peaks – reveal rock types exhumed from some depth in the crust. Other important targets include nonmare volcanic domes and contacts between compositionally distinctive units.

Acknowledgements: Funding for BLJ's work on lunar sample and remote sensing relationships is from the NASA PG&G program, NNG05GI38G.

References: [1] *Lunar Sourcebook* (1991) Chap. 5 (Papike et al.) and Chap. 6 (G. J. Taylor et al.), 121-284, Cambridge Univ. Press. [2] Papike et al. (1998) Lunar samples (Ch. 5), in *Planetary Materials*, 1-234, *RiM-G* **36,** Min. Soc. Am. [3] Wieczorek et al. (2006) The constitution and structure of the lunar interior. Chap. 3, *New Views of the Moon, RiM-G* **60**, Min. Soc. Am. & Geochem. Soc. [4] Hiesinger & Head (2003) Ages and stratigraphy of mare basalts in Oceanus Procellarum.., *JGR*, **108** (E7), 5065. [5] Tompkins & Pieters (1999) Mineralogy of the lunar crust.., *Met. Planet. Sci.* **34**, 25-41. [6] Lucey (2004) Mineral maps of the Moon. *Geophys. Res. Lett.,* **31**, L08701. [7] Cahill & Lucey (2007) Radiative transfer modeling of lunar highlands.. *JGR,* **112**, E10007. [8] Lucey & Cahill (2009) The Composition of the lunar surface relative to lunar samples. *Lunar Planet. Sci. Conf.* **40**, #2424. [9] Korotev (2006) Geochemistry of a .. lunar meteorite .. a crystalline impact-melt breccia dominated by magnesian anorthosite. *Lunar Planet. Sci*. **39**, #1402. [10] Korotev & Jolliff (2001) The curious case of the lunar magnesian granulitic breccias, *Lunar Planet. Sci*, **32**, #1013. [11] Lucey et al. (1986) A compositional study of the Aristarchus region of the Moon.., *JGR* **91**, D344-D354. [12] Jolliff B. L. (2004) Evolved lithologies and their inferred sources in the northwestern Procellarum region.., *Lunar Planet. Sci. 35*, #2032. [13] Hawke et al. (2002) Remote sensing studies of geochemical and spectral anomalies on the nearside.., *Lunar Planet. Sci. Conf.*, *33*, #1598. [14] Hagerty et al. (2006) Refined thorium abundances for lunar red spots.., *JGR.* **111**, E06002. [15] Robinson and Jolliff (2002) Apollo 17 landing site: Topography, photometric corrections.., *JGR*, **107**, 20-1–20-30.

MOON ZOO: UTILIZING LROC LUNAR IMAGES FOR OUTREACH AND LUNAR SCIENCE. K. H. Joy[1], P. M. Grindrod[1], I. A. Crawford[1], C. T. Lintott[2], A. Smith[2], D. Roberts[3], L. Fortson[3], S. Bamford[4], A. C. Cook[5], R. Bugiolacchi[6], M. R. Balme[7], P. Gay[8].[1]UCL-Birkbeck Research School of Earth Sciences, Gower Street, London, WC1E 6BT, UK, (k.joy@ucl.ac.uk). [2]Oxford University, UK. [3]Adler Planetarium, Chicago, USA. [4]Nottingham University, UK. [5]Aberystwyth University, Wales, UK. [6]Max Plank Institute for Solar System Research, Germany. [7]The Open University, UK. [8]Southern Illinois University Edwardsville, USA.

Introduction: Moon Zoo will be an online lunar citizen science project. It is one of the latest incarnations of the highly successful Galaxy Zoo project (http://www.galaxyzoo.org/), which harnesses the power of the Internet to classify galaxies to support astrophysics research.

In the first instance, Galaxy Zoo users were presented with ground based telescopic images of almost a million galaxies, given the choice to classify their shape and — if the galaxy was a spiral — record the rotation direction of the arms. Using the data the project provided, the Galaxy Zoo science team was able to prove that the citizen classifications were as good as those completed by professional astronomers. In the words of the Galaxy Zoo team "In fact, the Galaxy Zoo data has an advantage over traditional expert classification; obtaining a large number of multiple independent classifications allows the team to quantify the uncertainty in their results."

Numerous papers have been published [e.g. 1-4] using the Galaxy Zoo database to address key questions about the formation and evolution of galaxies, and to follow up on serendipitous discoveries of new and unusual celestial objects made by Galaxy Zoo users.

The second Galaxy Zoo project (Galaxy Zoo 2) has just been launched, and within the first two months of operation has received over 220,000 registered users completing 27 million individual user classifications.

The Moon Zoo Concept: Moon Zoo, due to be launched in late summer 2009 (initially with archive data), will be a similar online citizen science project that will ask users to identify, classify and measure the shape of features on the surface of the Moon using a specially designed graphical interface. The interface will be available in several languages to ensure that this is a truly international lunar science project.

Moon Zoo Outreach Potential: We expect Moon Zoo to be even more popular than Galaxy Zoo in engaging the public with modern day space exploration. The Moon captures the interest and imagination of all generations as it is seen as a constant presence in peoples' lives and it is therefore accessible to everyone. We plan to tap into this awareness by providing a free and easy to access device for studying the Moon's surface, whilst harnessing this user power to conduct high quality lunar science.

Moon Zoo Data: The project will initially utilize PDS released high spatial resolution images (with associated metadata) from NASA's Lunar Reconnaissance Orbiter Camera (LROC) instrument, which is due to be launched on the LRO mission in June 2009 [5].

Statistical analysis of the Moon Zoo user data will allow us to address interesting lunar science topics, and will also aid the planning of future exploration of the Moon by robotic and manned missions.

Moon Zoo Science Case: The Moon Zoo lunar science team has identified three preliminarily Moon Zoo user projects [6] that can be readily addressed by registered Moon Zoo users utilizing LROC data. These projects address a variety of important lunar science and exploration themes [7], and are briefly described below:

Project 1a. Count the number of and measure the dimensions of impact craters on the Moon (yielding both crater diameter and ellipticity) with the aim of improving the precision of lunar crater counting statistics. Crater counting allows us to calculate the apparent age of the lunar surface, by comparing the number of impact craters on different lunar surfaces (i.e. lava flows, crater ejecta blankets etc.). Technical issues such as classifying primary vs. secondary craters are beyond the scope of user classification tasks and so will form an important component of subsequent database exploitation and scientific interpretation.

Understanding the age of different lunar lava flows and crustal surfaces will shed new light on the temporal thermal and magmatic history of the Moon, and will have important implications for understanding heating processes of small rocky planetary bodies.

Project 1b. Users will also be asked to assess a scale of blockiness state (ejected boulder concentration) of crater rims, to classify them and help to determine local regolith thickness variation [8].

We will also ask Moon Zoo users participating in both Project 1a and 1b to identify, and therefore catalogue, the location of interesting lunar features such as lava channels (rilles), crater chains, lava flooded impact craters, volcanic eruptive centers (pyroclastic deposits), volcanic domes and unusually shaped craters within the scale size of the LROC images, for further analysis by the science team.

Project 2. Users will assess the degree of boulder hazards on the lunar surface by comparing two images

(of similar scale at similar illumination conditions), and identifying the one with the higher boulder density. These results will produce relative boulder density hazard maps to help identify the most suitable locations for sending future robotic and manned missions to the Moon.

Project 3. Identify recent (in last 40 years) changes on the lunar surface by comparing new LRO images with older Apollo photographs (of similar image resolution and illumination conditions). We hope to identify the locations of recent impact craters or landslides or even volcanic eruptions [9,10] on the lunar surface.

By counting the number of 'new' impact craters we can calculate the current impact flux rate of the Earth-Moon system, which is of great interest for assessing the risk to humans from asteroid and meteoroid impacts and to help constrain planetary chronology based on impact crater counting.

All Moon Zoo Projects: Moon Zoo users will also be asked to identify the location of space mission hardware on the Moon (i.e. Apollo lunar landers, Russian Luna rovers, crashed US, European and Chinese probes and rocket stages etc.), to build up a database that can be made available to the worldwide science community to be used as positional landmarks for lunar cartographic mapping.

Moon Zoo Current Status:

Science Team and Goals: The Moon Zoo Science Team is being assembled and we are refining our project goals through discussion within the team and with the LROC Science Team.

Software: The Moon Zoo software database 'back-end' is being developed by the team at Oxford University, based on their experience with storing and analyzing large amounts of citizen science data. The 'front-end' user interface is being designed to fulfill the science goals and development will be in progress over the next few months, once the science projects have been finalized.

Outreach and public engagement: Lunar science outreach information and links on the Moon Zoo website are being developed by a team led by Pamela Gay (Southern Illinois University Edwardsville). The Moon Zoo team is also working closely with Adler Planetarium to promote the project through their 'Moon Wall' interface and other outreach activities.

Website: The Moon Zoo website will be tested with PDS released Apollo image data and then will go live with PDS released LROC data as soon as this is available. User data will be assessed and software updates made accordingly after the website launched. Moon Zoo lunar science database mining and scientific interpretation will begin approximately six months after going live.

Validation: The Galaxy Zoo project utilizes a variety of statistic analysis tools to study the quality of user classifications (i.e. how often they get the 'correct' answer compared to an expert classification; how varied the classification result is between users; identification of potentially malicious classifications etc.). Similar tools will be employed for exploiting the Moon Zoo user databases.

A variety of data reduction techniques will be employed to turn raw data collected by the Moon Zoo website into science-ready outputs. For example, it is possible to 'weight' users according to their degree of agreement with expert classifications (or other results), and then iterate these results through the database. This technique has proved to be effective in obtaining high fidelity results even for apparently difficult citizen science tasks [1-4].

We also expect the validation process to produce additional science results in itself, for example, analysis of the standard deviation of the crater diameter histogram can help to reveal craters with degraded rims through slight variations in user measurements, because these will be the most difficult to measure.

Concluding Statement: All new Zoo projects must be capable of delivering peer-reviewed science. Moon Zoo is poised to do just this by providing high quality data to address key questions in lunar science. At the same time, Moon Zoo will be an excellent outreach tool to help promote lunar science and exploration and engage the public in learning about the process of science discovery.

The Moon Zoo Science Team, welcome comments and feedback from the lunar science community on the project science goals defined in this abstract.

References: [1] Lintott C.J. et al. (2008) *MNRAS, 389*, 1179. [2] Land K. et al. (2008) *MNRAS, 388*, 1686. [3] Bamford S.P. et al. (2008) *MNRAS, 393*, 1324. [4] Slosar A. et al. (2008) *MNRAS, 392*, 1225. [5] Jolliff et al. (2009) *LPS XL*, Abstract #2345. [6] Joy et al. 2009. *Science Priorities for Moon Zoo v4.* Moon Zoo internal report. [7] NRC (2007) *Report on the Scientific Context for the Exploration of the Moon*. [8] Wilcox et al. (2005) *MAPS 40*, 695–710. [8] Schulz et al. (2006) *Nature 444*, 184-186. [10] Crotts (2008). *The Astrophysical Journal 687*, 692-705

IMAGING RILLES AND FLOOD LAVAS WITH LROC. L. P. Keszthelyi[1], [1]U.S. Geological Survey, Astrogeology Science Center, 2255 N. Gemini Dr., Flagstaff, AZ 86001 (*laz@usgs.gov*).

Introduction: The origin of sinuous rilles on the Moon remains enigmatic. While originally considered to have been carved by flowing water [1-3], the Apollo missions showed the rilles to be volcanic. However, it is still unclear if they are predominantly constructional or erosional and whether the lava was transported through stable lava tubes or largely open lava channels.

More generally, the mode in which the mare lavas were emplaced is not well constrained. These large flood lavas inundate major impact basins with thick stacks of dense basalt but the eruption rates are unknown. These rates are of interest because they can be linked to the plumbing system and thus has implications for the crustal structure and magma source region.

Targeting Rilles: I have entered select locations along all the named rilles (rimae) [4] into the LRO targeting database. The reasoning behind targeting these specific locations should be discussed with the lunar science community and modified as appropriate.

Perhaps the most diagnostic information on the formation of rilles comes from the nature of the locations where they appear and disappear. If they are partially collapsed lava tubes, these locations may reveal caves. Such caves have been suggested to be desirable sites for human habitats [5].

LROC NAC imaging (especially rolling off-nadir to image the sunlit wall at ~0.5 m/pixel) could provide the straightforward proof of such caves. The closest analogs may be the search for caves in pit craters seen on the Martian shield volcanoes in HiRISE images [6]. However, it is worth noting that the visible wavelength images were targeted on the basis of THEMIS IR data showing thermal anomalies in these locations. Currently, a number of LROC targets cover potential tube entrances but additional targets should be entered based on LRO Diviner results. As is, we are relying in part on serendipity, like with the first example of a natural bridge on Mars discovered by HiRISE (Fig. 1) [7].

Vent locations may also provide extremely useful information on the style of eruptions that formed rilles. There are hints of edifices at some vents, perhaps indicative of perched lava ponds. Again, the best analogs are low shields on Mars that feed open channels (Fig. 2) [7]. In such cases, stereo imaging by LROC NAC is essential since the scale of these features may be too small to be well resolved by LOLA. A perched lava pond should have a rim that is at a constant elevation (except where breached). Alternatively, vent constructs could be spatter or cinder cones. Lava ponds would point to more gentle and longer-lived eruptions while edifices containing large quantities of pyroclastics are more suggestive of high effusion rates and shorter durations. The vent area for the Athabasca Valles flood lavas on Mars could be a good analog if the rilles were formed by turbulent floods of lava [7,8].

To investigate the role of erosion, it will be important to ascertain whether the rilles cut through preexisting rocks. This is most likely to have ocurred where rilles appear to traverse highlands or other topographic highs. Several such locations have been entered as LROC NAC stereo targets. While very high-resolution color would have been desired to help differentiate rock types in the walls of the rilles, combining LRO panchromatic NAC and 100-400 m/pixel color WAC data may provide additional clues. An important calibration will come from imaging the section of Rima Hadley that was observed by the Apollo 15 astronauts.

Targeting Flood Lavas: Few targets aimed at the emplacement of mare lavas. This is primarily because the basemaps in the REACT software do not include low-sun data that allow the identification of flow margins and other lava features. The best images were acquired by Apollo and are currently being digitized at ASU. However, they are not (yet?) integrated into the LROC targeting tool.

One of the major objectives would be to determine if the mare were produced by true flood volcanism or their close kin, plains volcanism [9]. The distinguishing characteristic is the presence of shallow volcanic edifices in plains volcanism. As MOLA did for Mars, LOLA should be able to answer this question.

Well targeted LROC images would be more important for identifying the style of emplacement of individual lava flows. Were they pahoehoe, aa, or rubbly pahoehoe flows? The diagnostic features used on Earth are only visible at the outcrop or hand sample scale. However, a link has been made between these features and meter- to decameter-scale features visible in orbital imagery [7,10]. Unfortunately, on the Moon, such features are highly degraded by impacts. Still, it is likely that topographic suggestions of channels, lobe fronts, tumuli, inflation pits, and rafted plates should persist and be identifiable in LROC stereo images. Since it is impractical to blanket the mare with stereo imaging much of the target selection must await the release of a LOLA basemap. In the interim, a few sample sites will be collected.

References: [1] Urey H. C. (1967) *Nature, 216*, 1094-1095. [2] Peale S. J. et al. (1968) *Nature, 220*, 1222-1225. [3] Lingenfleter R. E. et al. (1968) *Science, 161*, 266-279. [4] http://planetarynames.wr.usgs.gov/ [5] Coombs C. R. and Hawke B. R. (1992) Conf. Lunar Bases Space Activities 21st Cent. 1, 219-229. [6] Cushing G. E. et al. (2008) LPSC XXXIX Abstract #2447. [7] Keszthelyi L. P. et al. (2008) JGR 113, 2007JE002968. [8] Jaeger W. L. et al. (2007) Science 317, 1709-1711. [9] Greeley R. (1982) JGR 87, 2705-2712. [10] Keszthelyi L. et al. (2000) JGR 105, 15027-15050.

Figure 2. Low shield on the Tharsis volcanic rise. Anaglyph from HiRISE observations PSP_002328_2080 and PSP_002605_2080. The drained perched lava pond at the top of this shield could be analogous to the vents of some lunar sinuous rilles. In this case the lava that exited the lava pond fored a lava fan instead of a large channel, but other nearby vents do feed channels.

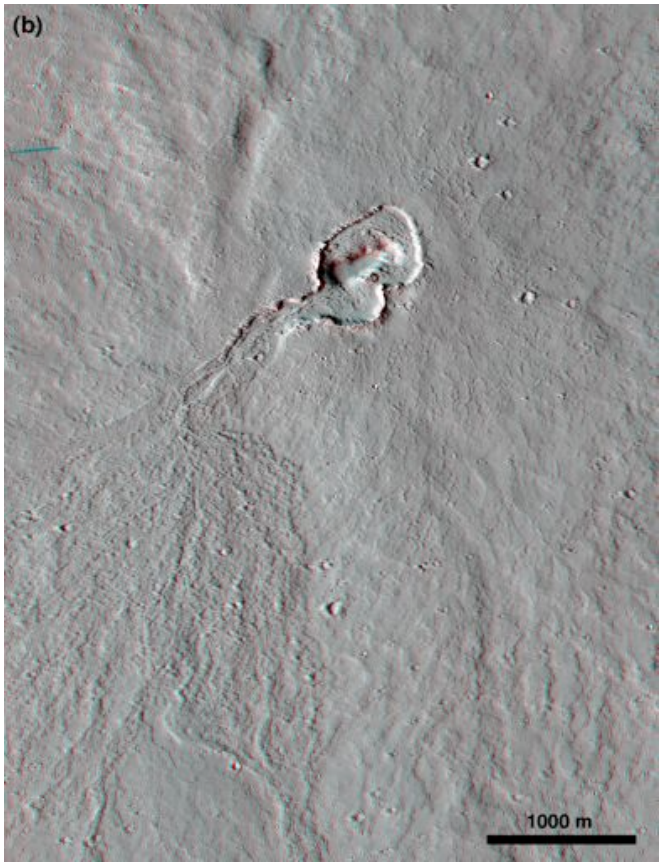

Figure 1. Roofed channel seen in HiRISE image PSP_001420_2045 of the Tartarus Colles.

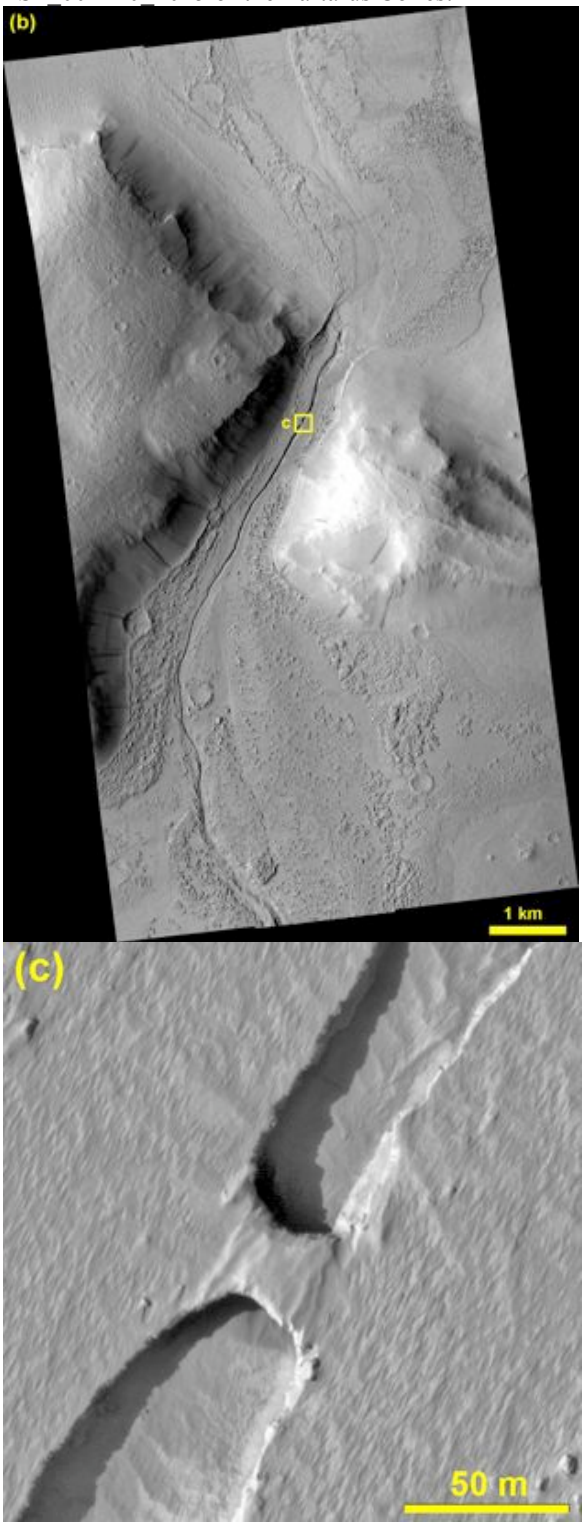

CENTRAL UPLIFT FORMATION IN COMPLEX IMPACT CRATERS – COMPARISON OF LUNAR AND TERRESTRIAL CRATERS. C. Koeberl[1] [1]Department of Lithospheric Research, University of Vienna, Althanstrasse 14, 1090 Vienna, Austria (e-mail: christian.koeberl@univie.ac.at).

Introduction: The exact mechanism of the formation of central peaks and central uplifts in impact structures is still not clear. On Earth, most craters are either deeply eroded or covered, and thus not accessible or not in pristine condition. A high resolution study of lunar craters woulkd be highly desirable to provide data on structural elements of central uplifts of iimpact craters of various sizes.

Complex craters: Impact craters (before post-impact modification by erosion and other processes) occur on Earth in two distinctly different morphological forms – simple and complex craters (the exact change-over diameter between simple and complex crater depends on the composition of the target). On the Moon the changeover diameter is at about 15-20 km crater diameter, and very large craters are multi-ring basins, which are rare on Earth.

Complex craters are characterized by a central uplift. Craters of both types have an outer rim and are filled by a mixture of fallback ejecta and material slumped in from the walls and crater rim during the early phases of formation. Such crater infill may include brecciated and/or fractured rocks, and impact melt rocks. Fresh simple craters have an apparent depth that is about one third of the crater diameter. For complex craters, this value is closer to one fifth or one sixth. The central structural uplift in complex craters consists of a central peak or of one or more peak ring(s) and exposes rocks that are usually uplifted from considerable depth.

Uplift Formation: The formation of the Major readjustments of the transient cavity occur for the formation of complex craters, while the bowl-shaped transient crater is quasi not modified in the case of simple craters. Two competing processes act during the modification stage; downward-directed gravitational collapse of the inner rim and uplift of the transient crater floor. The initially steep walls of the transient crater collapsed under gravitational forces forming characteristic terraces. Concerning the development of the central uplift, the formation is thought to occur by displacements along faults as a brittle component in the case of moderately sized impact structures (such as for Bosumtwi, see below), whereas in the case of larger impact structures central uplifts involve fluidization and/or large differential movements of target blocks.

A Terrestrial Example: Recent work in our group [1] characterized the shock wave attenuation in the uppermost part of the central uplift of the Bosumtwi impact structure, a moderately sized (10.5-km-diameter) and well preserved complex impact structure that was recently the target of a multidisciplinary and international drilling project. The data acquired in the couse of the drilling, the related geophysical (e.g., seismic) investigations, and subsequent drill core studies were used by [1] to reconstruct the original position of the sampled section in the target prior to crater modification. This was done by combining petrographic investigations (at the micro-scale) with modeling of inelastic rock deformation (at the meso-scale) and modification processes during uplift (at the mega-scale). This approach allowed to constrain shock wave attenuation and rock deformation during central uplift formation. An example is given in Fig. 1.

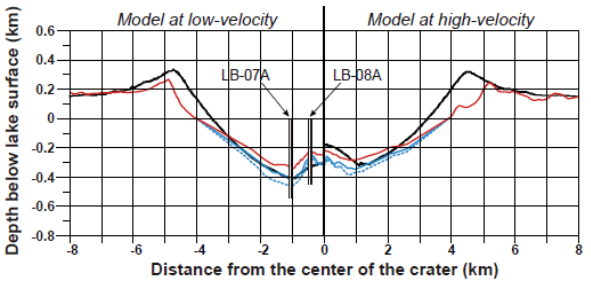

Fig. 1. Model crater profiles (black; using ANEOS granite equation of state for target and projectile) versus observed (i.e., actual) crater profile (red and solid blue lines for the apparent and true crater profiles, respectively, and dashed blue line for the lower limit of the monomict impact breccia).

Only few craters on Earth have been studied by this method. Our results imply that for moderately sized impact craters, the rise of the central uplift is dominated by brittle failure, whereas in the case of larger impact structures, and also depending on rock proprieties, the uplifted, relatively stronger shocked rocks may behave in a more ductile manner.

I am proposing a detailed photogeological study of a series of relatively fresh lunar impact craters near the simple/complex changeover, and of large (100-km-diameter-range) craters to determine of the block-uplift (brittle failure) vs. fluidization models can be distinguished. This would also have important implications for the understanding of impact crater formation in different types of target rocks, especially as a result of layering in the target.

References: [1] Ferriere, L., Koeberl, C., Ivanov, B., and Reimold, W.U. (2008) *Science 322*, 1678–1681.

LUNAR SURFACE GEOCHEMISTRY AND LUNAR METEORITES. R. L. Korotev, Campus Box 1169, Dept. of Earth and Planetary Sciences, Washington University, Saint Louis MO 63130; korotev@wustl.edu

Since 1979, about 136 lunar meteorite stones from ~65 meteorites representing not more than ~45 craters on the Moon have been found of Earth. The meteorites provide a different type of information than the rocks of the Apollo collection because the derive from randomly distributed locations over the whole Moon whereas the Apollo samples all derive from in or near the geochemically anomalous PKT (Procellarum KREEP Terrane). For none of the lunar meteorites is the source crater actually known [1–3]. Presumably because of the global sampling provide by the meteorites, they demonstrate that the lunar crust is more diverse than can be easily inferred from the Apollo collection.

Ten of the meteorites are, or contain large clasts of, unbrecciated basalt. Three others are breccias consisting nearly entirely of basalt. In detail, none of basaltic lunar meteorites is a compositional match to any of the basalts from the Apollo and Luna collections, although some are similar to the basalts of Apollo 12 and, to a lesser extent, Apollo 15. None is a high-Ti basalt (>6% TiO_2), such as those from Apollo 11 and 17 (Fig. 1b). Some of the basaltic meteorites are very different from any in the Apollo and Luna collections [4–8]. The NWA 773 clan of lunar meteorites includes some stones that are dominated by cumulate olivine gabbro, a lithology that does not occur in the Apollo collection [9,10].

All other lunar meteorites are breccias, i.e., they are mechanical mixtures of more primary rock types. More than half of the lunar meteorites are regolith or fragmental breccias. Such breccias are, in effect, sedimentary rocks in that they are composed mainly of shock-lithified material that existed near the surface of the Moon. As such, their compositions and mineralogies likely reflect the material that would be sensed remotely from orbit in the vicinity of their respective source craters. Others are impact-melt and granulitic breccias that may represent material from deeper in the crust. (The author suspects that many of the lunar meteorites that have been classified as impact-melt breccias are not, in fact, crystalline or glassy melt breccias as defined by [11] in that the matrix was never largely molten. Many of the nominal "impact-melt breccias" may well also represent near-surface material.)

More than half the lunar meteorites have composition that are consistent with derivation from the feldspathic highlands in that they have low concentrations of FeO (Fig. 1c) and incompatible elements (Fig. 1e). Nearly all have concentrations of incompatible elements that are lower than those of Apollo 16 soils (Fig. 1f) because of the Apollo 16 site's proximity to the PKT [12,13]. On average, feldspathic lunar meteorites (somewhat arbitrarily, those with <7.7% FeO) have compositions that corresponds to noritic anorthosite with 78 mass % plagioclase (Table 1). On average, the proportion of iron carried by pyroxene is about the same as that carried by olivine. The principal compositional difference among the feldspathic lunar meteorites is the ratio of MgO to FeO (Fig. 1a). *Mg´* (mole % Mg/[Mg+Fe]) is highly variable, ranging from 57 to 78 and averaging 67. *Mg´* tends to increase with normative olivine [12]. The high *Mg´*, compared to ferroan anorthosite, of feldspathic lunar meteorites, indicates that magnesian anorthosites exist somewhere in the lunar crust [12–15]. Whether the *Mg´* variation is primarily lateral or vertical in the feldspathic highlands is a first order question.

Table 1. Mean of 36 feldspathic lunar meteorites, with normative mineral abundances (mass %) and calculated volume abundances.

	mass %		mass %	vol. %
SiO_2	44.7	plag	78	82
TiO_2	0.25	opx	9	7
Al_2O_3	27.9	cpx	5	4
Cr_2O_3	0.11	ol	8	7
FeO	4.76	ilm	0.5	0.3
MnO	0.07		100.5	100.3
MgO	5.50			
CaO	16.2	from Antarctic CaO/Al_2O_3 ratio		
Na_2O	0.37			
K_2O	0.03	Antarctic only		
P_2O_5	0.03	Antarctic only		
	100.0	mean *Mg´* = 67%		

Lunar meteorites with intermediate concentrations of FeO are the most compositionally and petrographically diverse. Three (5% of total) are almost certainly from the PKT (Fig. 1e). None of the three breccias has a composition that matches any of the Apollo soils (Fig. 1f). Some intermediate FeO meteorites clearly derive from a region of mare-highlands mixing because they consist of both basalt and feldspathic breccias. Others, however, do not obviously have a significant basalt component and may represent mafic areas in the highlands or perhaps some type of nonmare volcanism. At least one lunar meteorite has composition and mineralogy consistent with derivation from the South Pole-Aitken basin [3,16].

This work was funded by NASA grant NNG04GG10G.

References: [1] Warren (1994) *Icarus* **111**, 338–363. [2] Korotev (2005) *Chemie der Erde* **65**, 297–346. [3] Korotev et al. (in press) *M&PS*. [4] Warren & Kallemeyn (1989) *GCA* **53**, 3323– 3300. [5] Anand et al. (2003) *M&PS* **38**, 485–499. [6] Zeigler (2005) LPSC 36, #2385. [7] Zeigler et al. (2007) *LPSC 38*, #2109. [8] Sokol et al. (2008) *GCA* **72**, 4845–4873. [9] Fagan et al. (2003) *M&PS* **38**, 529–554. [10] Jolliff et al. (2003) *GCA* **67**, 4857–4879. [11] Stöffler et al. (1980) *Proc. Conf. Lunar Highlands Crust*, 51–70. [12] Korotev et al. (2003) *GCA* **67**, 4895–4923. [13] Korotev et al. (2006) *GCA* **70**, 5935–5956. [14] Arai et al. (2008) *Earth, Planets and Space* **60**, 433–444. [15] Treiman et al. (2008) *NLSI Lun. Sci. Conf.*, #2112. [16] Jolliff et al. (2009) PLPSC 40, #2555.

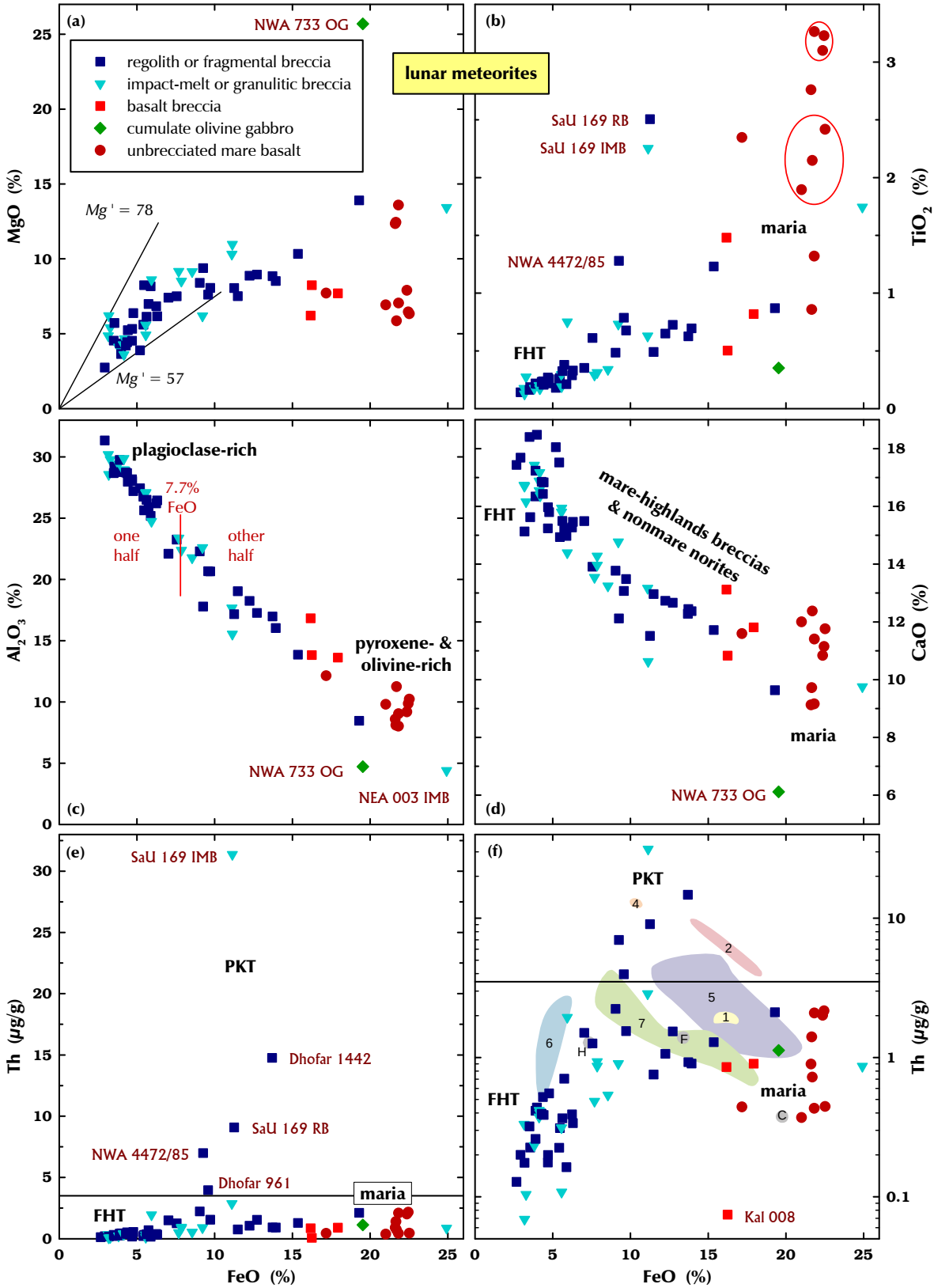

Figure 1. Compositions of lunar meteorites. (a) Diagonal lines show the range of *Mg´* for feldspathic lunar meteorites. (b) Ellipses enclose meteorites from the same source crater. (c,d) Plagioclase – pyroxene+olivine+ilmenite mixing. (e, linear) Most meteorites with >3.5 µg/g Th likely come from the Procellarum KREEP Terrane; Dhofar 961 may be from South Pole-Aitken [x]. (f, logarithmic) Comparison to soils from the Apollo (1=11, etc.) and Luna (F=16, H=20, C=24) missions.

TARGETING COMPLEX CRATERS AND MULTI-RING BASINS TO DETERMINE THE TEMPO OF IMPACT BOMBARDMENT WHILE SIMULTANEOUSLY PROBING THE LUNAR INTERIOR. David A. Kring[1,2], [1]Center for Lunar Science and Exploration, USRA Lunar and Planetary Institute, 3600 Bay Area Blvd., Houston, TX (kring@lpi.usra.edu), [2]NASA Lunar Science Institute.

Introduction: Ages of thermally altered Apollo samples indicate impact cratering was particularly severe in the Earth-Moon system during the first billion years of its evolution. A concentration of ages *c*. 3.9-4.0 Ga suggests there may have been a spike in the impact flux in an event called the lunar cataclysm [1,2]. Hints of impact events at that same time among meteoritic samples of several planetesimals and Mars suggest the lunar cataclysm is really an inner solar system cataclysm [3,4]. Not only may the bombardment have affected the geologic evolution of terrestrial planets, it may have also influenced the origin and evolution of life on the Earth and potentially Mars [*e.g.*, 5]. Because the impact flux to the inner solar system is both accessible and uniquely preserved on the lunar surface, additional samples to further evaluate the impact flux are among the highest lunar science priorities [6].

Target Requirements: To determine that flux and any variations in it, we need to

- Target impact craters and multi-ring basins that are representative of the flux in both time and geographic location on the lunar surface.

To provide a temporally broad chronometer, we also need to

- Target impact craters that provide surfaces (*e.g.*, crater floors) that can be used to calibrate crater counting chronologies and/or
- Target impact craters that provide stratigraphic horizons (*e.g.*, ejecta blankets) that can be used for relative chronologies, even for events that may occur too close in time to be discernable using radiometric techniques.

I have applied these targeting requirements to an inventory of complex craters and multi-ring basins on the lunar surface [7] and identified a subset of those impact sites as potential landing sites for sampling. To better evaluate that potential, this subset of impact sites should be integrated into the imaging campaign by the Lunar Reconnaissance Orbiter.

Exploring the Basin-forming Epoch: The most intense period of bombardment produced dozens of >300 km-diameter impact basins. The duration of this activity is uncertain. Thus far, we only have one solid age and five tentative ages for the 15 basins produced during the Nectarian and Early Imbrian periods of time. Based on those ages, estimates for the duration of a lunar cataclysm range from 20 to 200 Ma. We have no ages for ≥29 older, pre-Nectarian basins and, thus, no idea if they are part of a lunar cataclysm or are instead part of an extended period of bombardment that may have lasted ~500 million years.

As discussed elsewhere [6,8], the highest priority target is unaltered impact melt from the ***South Pole-Aitken (SPA) Basin***. Because SPA is the oldest and largest basin, it will define the beginning of the basin-forming epoch. If this basin is part of the cataclysm, then the magnitude of the lunar cataclysm event is far greater than previously proposed, involving ~3 times the number of basin-forming impact events. If SPA has instead a much older age (say 4.4 Ga), then pre-Nectarian basins with successively younger relative ages need to be sampled to determine if a cataclysm began in the pre-Nectarian and, if so, when it began in that basin-forming sequence. Candidate targets include the ***Nubium Basin*** (middle pre-Nectarian), ***Smythii Basin*** (slightly younger), and ***Apollo Basin*** (the last of the pre-Nectarian basins).

The timing of the latter third of the basin-forming events is better understood because of the availability of Apollo and Luna samples, but links between samples of known ages with specific basins is still fraught with uncertainty. For that reason, better documented samples of impact melt or impact-metamorphosed samples from the ***Nectaris***, ***Serenitatis***, ***Crisium***, ***Schrödinger***, and ***Orientale*** basins are recommended. Orientale Basin is a particularly attractive target because it is the youngest basin and exquisitely preserved, so that the geological relationships between target rocks and impact lithologies can be mapped. That clarity will dramatically assist with investigations of samples from older basins.

Determining the Post-basin Impact Flux: After the formation of Orientale, the impact flux declined at a still-uncertain rate. To quantify the flux we need precise analyses of impact ages from a moderate number of post-3.8 Ga impact craters and an accurate determination of the relative number of impact events that occurred between those absolute benchmarks. We currently have no ages for Late Imbrian and Eratosthenian impact craters. To begin constraining the Late Imbrian, samples are needed from craters that meet target requirements, such as ***Humboldt***, ***Tsiolkovskiy***, ***Antoniadi***, and ***Archimedes***. Eratosthenian craters

that meet target requirements include ***Hausen***, ***Pythagoras***, ***Theophilus***, ***Eratosthenes***, and ***Maunder***.

The ages of younger impact events during the Copernican Period are also ill-defined, although tentative ages of 1.29 Ga, 0.8 Ga, and 0.1 Ga have been suggested for Autolycus (or Aristillus), Copernicus, and Tycho, respectively, based on samples that are interpreted to be distal ejecta and an impact-generated landslide. To confirm those ages and to further refine the flux during the Copernican, well-documented impact melt samples from ***Kepler***, ***Aristarchus***, ***King***, ***Copernicus***, and ***Tycho*** are recommended.

Scientific Multipliers: In addition to solving several chronological problems, these same impact melt samples can be used to (i) determine the source of projectiles and their chemical compositions. This will, in turn, (ii) test proposed mechanisms for the impact flux. These data can also be used to (iii) calculate the delivery of biogenic elements during the bombardment and (iv) the environmental consequences of the impact events. In many cases, sampling sites associated with the craters identified above will also (v) provide access to impact melt samples from additional craters. For example, samples of pre-Nectarian Nubium Basin melt may coexist with samples from the younger (Nectarian) Humorum Basin.

Complex craters and multi-ring basins are also excellent probes of the lunar interior. Normal faults in the modification zones of these craters (vi) expose subsurface lithologies and their stratigraphic relationships. Uplifted central peaks and peak rings in the centers of these craters (vii) expose even deeper levels in the Moon's crust. Furthermore, (viii) clasts of subsurface lithologies are entrained in impact melt breccias deposited within the crater and beyond the crater rim. Thus, by combining observations of modification zones, central uplifts, and impact breccias, one can (ix) generate a cross-section of the lunar crust that may be kilometers to 10's of kilometers deep. The volume of material beneath an impact site that is melted extends to an even deeper level than the material that is excavated. Because that melt is mixed, samples of it will provide (x) an average chemical composition of the crustal (and potentially upper mantle) volume affected by an impact event. Consequently, while collecting samples to determine the impact flux to the lunar surface, one is also collecting samples of the lunar interior.

Many of the impact craters that satisfy the target requirements above are also associated with other geological processes. The floors of impact craters were often flooded by mare basalts (*e.g.*, Nubium, Nectaris, Serenitatis, and Tsiolovskiy). Thus, missions designed to collect impact melt from those craters can also (xi) provide access to volcanic samples that help clarify the magmatic evolution of the lunar interior.

As outlined recently [9], the ***Schrödinger Basin*** is an example of a location where the impact flux can be evaluated while also uncovering information about magmatic activity and the lunar interior. Schrödinger Basin is ~320 km in diameter and is the second youngest basin on the Moon. It is located, however, within the SPA, the oldest basin on the Moon. Because the Schrödinger event excavated and uplifted impact melted material from the SPA event, one may be able to collect samples at a single landing site that provides the ages of both events. That outcome would virtually bracket the entire basin-forming epoch.

In addition, the floor of the Schrödinger Basin is partially covered with several younger volcanic units [10] that appear to be Eratosthenian and/or Copernican in age. Because the style of eruption varies, the volcanic units may have tapped sources from different depths in the lunar interior. Thus, collectively, by targeting the impact melts in Schrödinger Basin, one might simultaneously bracket the duration of the entire basin-forming epoch, expose upper crustal units in the walls of the basin, expose deeper crustal units in the peak ring, expose fragments of crustal units in impact breccias, provide an average chemical composition of the crust (and potentially upper mantle) beneath the point of impact, provide magmatic products from several episodes of volcanic activity, and provide a mineralogical and chemical window into subsurface magmatic processes.

Imaging Guidelines: Wide-angle imaging of the targets described above will often be sufficient for evaluating the gross distribution of impact melt-bearing lithologies. Narrow-angle camera imaging will be required, however, for specific landing site selection and traverse planning. The locations for that type of spatically-focused imaging can be deduced from existing imaging and from preliminary studies of potential landing sites. For example, the recent study of the Schrödinger Basin described above identified three specific locations for a possible landing site that are sufficiently precise to guide narrow-angle camera targeting.

References: [1] Turner G. et al. (1973) *Proc. 4th Lunar Sci. Conf.*, 1889-1914. [2] Tera F. et al. (1974) *Earth & Planet. Sci. Letters, 22*, 1-21. [3] Bogard D. D. (1995) *Meteoritics, 30*, 244-268. [4] Kring D.A. and Cohen B.A. (2002) *J. Geophys. Res., 107*, doi: 10.1029/2001JE001529. [5] Kring D.A. (2000) *GSA Today*, *10*(8), 1-7. [6] NRC (2007) *The Scientific Context for Exploration of the Moon*, 107p. [7] Losiak A. et al. (2009) *LPS XL*, Abstract #1532. [8] Kring D.A. (2008) *LPS XXXIX*, Abstract #1251. [9] Kohout T. et al. (2009) *LPS XL*, Abstract #1572. [10] Shoemaker E.M. (1994) *Science*, *266*, 1851-1854.

LEAG REVIEW OF CONSTELLATION PROGRAM REGIONS OF INTEREST FOR HUMAN EXPLORATION OF THE MOON P. G. Lucey[1], J.T. Gillis-Davis[1], B.R. Hawke[1], L.A. Taylor[2], M. B. Duke[3], T. Brady[4] and T. Mosher[5]; [1]University of Hawaii, Institute for Geophysics and Planetology, 1680 East-West Road, Honolulu Hawaii, 96822, lucey@higp.hawaii.edu, [2]Dept. of Geological Sciences, Planetary Geosciences Institute, 402 GS Building, University of Tennessee, [3] Colorado School of Mines, 1500 Illinois St., Golden, CO 80401.Knoxville, TN 37996-1410, [4]Draper Laboratory 555 Technology Square, MS27 Cambridge, MA 01239, [5]Sierra Nevada Corporation Space Systems 8130 Shaffer Parkway Littleton, CO 80127

Introduction: The National Aeronautics and Space Administration (NASA) Constellation Program Office (CxPO) requested the Lunar Exploration Analysis Group (LEAG) to form a special action team to review and comment on targets and regions of interest identified by CxPO for imaging by the Lunar Reconnaissance Orbiter Narrow Angle Camera. These are intended to be representative of regions of future human lunar exploration activities and are meant to provide valuable scientific, operational and resource information.

Background: The Lunar Reconnaissance Orbiter Camera (LROC) will begin imaging the lunar surface in 2009. Two narrow angle cameras (NACs) will image the Moon at 0.5 m/pixel. Each individual NAC image frame represents a 2.5 x 25 km surface area, with the NAC pair resulting in a 5 x 25 km area of coverage. In the course of the first year of mapping, this will result in only 8-10% of the Moon's surface being imaged at high resolution. Thus, it is important to make sure priority regions of interest are identified and placed into the NAC targeting plan. The Constellation Program Office (CxPO) is responsible for the planning of future human missions to the Moon, including long duration missions to a lunar outpost, and shorter duration human-sortie missions to locations other than the outpost location. CxPO has identified 50 high priority regions of interest for human exploration of the Moon, based on three past NASA reports[1,2,3].

The 50 regions of interest have been divided into two tiers to aid planners in the case of LROC operational conflicts, each with 25 locations. Tier 1 regions of interest have a higher priority than Tier 2 regions of interest; there is no prioritization within each tier.

The regions of interest were selected based on three criteria:

1. Science rationale - the 50 sites are of unique scientific interest or are scientifically complex requiring intensive field work with human interaction.
2. Resource potential - as a whole, the 50 sites are representative of the type of natural resources available for development and exploitation.
3. Operational perspective - as a whole, the 50 sites are representative of the different terrain types that the Altair lunar lander and the various lunar surface systems may encounter.

The images acquired by the LROC NAC will be used by NASA to create image mosaics, topographic maps and digital elevation models, and surface hazard assessments. These data will be used in the design process for the Altair lunar lander (e.g., approach and landing, hazard avoidance), and lunar surface systems such as habitation, surface mobility, power, communications, and navigation.

CxPO has been working with the Lunar Reconnaissance Orbiter (LRO) Project Office and the LROC principal investigator (PI) to develop a plan for imaging the 50 regions of interest identified by Constellation, including the area of coverage for a given location that is allowed by orbit parameters and mission constraints.

For each region of interest, there is a series of nested squares, or a 'box within a box', that represent three areas of coverage. The 10 x 10 km 'box' represents an area as described by the LRO Project requirements. This area has a Priority 1 in the LROC prioritization scheme, and a full set of observations will be made for an image mosaic, stereo imaging (geometric and photometric), and hazard identification. The 20 x 20 km 'box' has a Priority 3, and represents a 'best effort' by the LROC PI to acquire a full set of observations. The 40 x 40 km 'box' has a Priority 4, and represents a 'best effort' by the LROC PI to acquire a monochromatic mosaic only.

Request to LEAG by Constellation: The review and comment on the 50 regions of interest identified by Constellation will include:

1. Reprioritization between Tiers 1 and 2, if deemed appropriate.
2. Adjustment of the target coordinates if deemed appropriate.
3. Additional suggested targets and regions of interest that could replace those identified by CxPO.
4. Suggested additional regions of interest for a lower priority ranking (i.e., “Tier 3”).

Rationale will accompany all comments and suggestions, based on Constellation's criteria of scientific rationale, resource potential, and operational perspective.

TIER ONE TARGETS		
Feature Name	Lat	Long
Alphonsus Crater	-2.16	-12.56
Aristarchus 1	-48.95	24.56
Orientale 1	-95.38	-26.2
Apollo 15	3.66	26.08
Aristarchus 2	-52.9	25.68
Ingenii	164.42	-35.48
Ina ('D-caldera')	5.29	18.65
Flamsteed Crater	-43.22	-2.45
Reiner Gamma	-58.56	7.53
Copernicus Crater	-20.01	9.85
Tycho Crater	-11.2	-42.99
Orientale 2	-87.91	-18.04
South Pole	-130	-89.3
North Pole	76.19	89.6
Van De Graaf Crater	172.08	-26.92
Malapert Massif	-2.93	-85.99
Gruithuisen Domes	-40.14	36.03
Mare Tranquillitatis	22.06	6.93
Rima Bode	-3.8	12.9
Marius Hills	-55.8	13.58
South Pole-Aitken Basin Interior	-159.94	-50.76
Tsiolkovsky Crater	128.51	-19.35
Mare Smythii	85.33	2.15
Montes Pyrenaeus	40.81	-15.91
Dante Crater	177.7	26.14

TIER TWO TARGETS		
Feature Name	Lat	Long
Aitken Crater	173.48	-16.76
Anaxagoras Crater	-9.3	73.48
Apollo 16	16.47	-9
Apollo Basin	-153.72	-37.05
Balmer Basin	69.82	-18.69
Bullialdus Crater	-22.5	-20.7
Compton/Belkovich Th Anomaly	99.45	61.11
Hertzsprung	-125.56	0.09
Hortensius Domes	-27.67	7.48
Humboldtianum Basin	77.14	54.54
King Crater	119.91	6.39
Lichtenberg Crater	-67.23	31.65
Mare Crisium	58.84	10.68
Mare Frigoris	40.74	55.45
Mare Moscoviense	150.47	26.19
Mendel-Rydberg Cryptomare	-93.07	-51.14
Murchison Crater	-0.42	4.74
Mutus Crater	30.85	-63.77
Plato Ejecta	-5.21	53.37
Riccioli Crater	-74.28	-3.04
Rimae Prinz	-41.72	27.41
Schickard	-53.96	-44.05
Schrödinger	138.77	-75.4
Stratton	166.88	-2.08
Sulpicius Gallus	10.37	19.87

References: 1. Exploration Systems Architecture Study (ESAS), 2005. 2. A Site Selection Strategy for a Lunar Outpost, Science and Operational Parameters, 1990. 3. Geoscience and a Lunar Base, A Comprehensive Plan for Lunar Exploration, NASA CP 3070, 1990.

THE COMPOSITIONAL CONTRIBUTION OF LRO. P. G. Lucey[1], S. J. Lawrence[2], M.R. Robinson[2], B. T. Greenhagen[3], D.A. Paige[3], M. B. Wyatt[4], and A. R. Hendrix[5] [1]University of Hawaii, Institute for Geophysics and Planetology, 1680 East-West Road, Honolulu Hawaii, 96822, lucey@higp.hawaii.edu, [2]School of Earth and Space Exploration, Arizona State University, Tempe, AZ,. [3]University of California, Los Angeles, Department of Earth and Space Sciences, 595 Charles Young Drive East, Los Angeles, CA 90095 (*greenhagen@ucla.edu*), [4]Brown University, Department of Geological Sciences, Box 1846, Providence RI, 02912, michael_wyatt@brown.edu, [2]JPL/Caltech, 4800 Oak Grove Dr. Pasadena, CA 91109, arh@jpl.nasa.gov.

Introduction: LRO will provide measurements of the Moon in the ultraviolet and thermal infrared spectral regions that are little explored, and provide these data at unprecedented spatial resolution. At these new wavelengths, important lunar minerals and processes are manifest in phenomena that are independent of the well-developed and sampled near-IR wavelengths provided by prior and on-going missions. Radar and laser measurements will also contribute compositional information.

Despite the successes of visible and near-IR spectroscopy and multispectral imaging, independent LRO measurements can address inherent shortcomings in the current measurements, and confirm important discoveries. In addition, LRO will provide new information either inaccessible to near-IR techniques, or not well-established.

LRO Compositional Contribution to Lunar Science

Lunar Science Application	LRO Contribution	LRO Data Sets
Lunar Maria		
Titanium Contents	Independent measurements of ilmenite content	LROC WAC, LAMP, mini-RF
Olivine and aluminum contents	Independent measurements of olivine and feldspar abundances	Diviner
Lunar Highlands		
Anorthosites	Sodium content of feldspar, distinguish ferroan anorthosite from alkali anorthosite	Diviner
Mafic rocks	Feldspar-mafic ratio	Diviner, LOLA
Evolved Rocks	Detect quartz, alkali feldspars	Diviner
Space Weathering	Independent measurement	LAMP

Lunar Maria: LRO measurements will address the ilmenite (titanium), olivine and iron contents of the lunar maria. In current measurements there are known high uncertainties, or the measurements lack corroboration or are model dependent.

Ilmenite and Titanium: Since the 1970's near-UV-visible color has been used as a proxy for titanium content of the lunar maria, with "blue" maria thought to indicate high titanium and "red" maria indicating low titanium. However, comparison of Lunar Prospector gamma-ray and neutron measurements of Ti to UV-visible color measurements shows a poor correlation between color and Ti [1]. At the extremes of color, very blue maria are Ti rich and very red maria are Ti-poor according to LP data, but maria of intermediate color can exhibit any Ti-content. For example, the very low Ti Mare Crisium has intermediate color values. Because the compositional controls on UV-visible color are not known, at resolutions much higher than Lunar Prospector, even extreme color values must be treated as highly uncertain in Ti content.

LRO contributes to this problem with three measurements. The LAMP (Lyman-Alpha Mapping Project) will obtain spectra in the lunar maria between 100 and 190 nm where ilmenite is spectrally distinct from other minerals. While acceptable signal to noise ratios will force co-adding to km scale resolutions, this experiment will still greatly excced LP resolutions at the close of the SMD phase of operations. Mini-RF measurements are sensitive to the extreme loss-tangent values of ilmenite and will have very high spatial resolution, and can measure farside maria not accessible to ground-based radar.

The LRO Camera, Wide Angle Camera (LROC WAC) features two UV and five visible bands that characterize a diagnostic spectral feature of ilmenite that is incompletely covered by existing data [2]. The two UV bands especially capture a strong spectrally blue slope that is diagnostic of opaque Fe-Ti bearing oxides. The spatial resolution of the WAC is sufficient to allow direct calibration of these data to Apollo sampling stations and Luna sample return sites.

Olivine and Low-iron Basalts: Olivine basalts were discovered spectroscopically in western Oceanus Procellarum [3] and their distribution mapped [4]. The

Diviner thermal IR multispectral radiometer is sensitive to the ratios of olivine, pyroxene and feldspar [5] and can independently determine if these reported olivine-rich maria do contain anomalous amounts of olivine. Mare Frigoris has high albedo which causes NIR FeO algorithms to return low values (and interpretations of aluminous basalts), however, [4] pointed out that small craters in this mare have very strong bands indicating high iron. Diviner will measure the ratio of of feldspar to the Fe-carrying mafic minerals to indepently estimate the abundance of iron and provide improved mineralogical constraints on these maria.

Lunar Highlands: LRO Diviner will contribute to three major issues in lunar highlands studies: Distinguishing alkali from ferroan anorthosites; determining the feldspar-mafic ratio in mafic lunar rocks; and exploring for large (500-m) exposures of evolved rocks.

Anorthosites: In the lunar samples, the famous rock type anorthosite (>90% plagioclase) comes in two varieties: ferroan (thought to be an essential magma ocean product), and alkali (thought to originate from differentiation of KREEP-related magma in small magma bodies). Both Selene and Chandryaan-1 spectrometers have shown the presence of large exposures of anorthosites with exceedingly low mafic mineral contents, with firm upper limits of 3 wt. % mafic mineral abundance. Elsewhere, areas with very low iron contents but elevated Th contents (Aristarchus and Compton-Belkovitch Th anomaly) have been attributed to alkali anorthosites. Recent laboratory work has shown that in samples with low mafic mineral contents, the alkali content of the feldspar can be determined with sufficient accuracy to easily distinguish ferroan from alkali anorthosite [6].

Mafic rocks: Rocks other than anorthosites make up an important fraction of the lunar highlands samples returned from the Moon and show that extrusive and intrusive igneous activity was vigorous early in lunar history. How widespread or volumetrically important this activity was is poorly known. The ratio of plagioclase to mafic rocks (together with the magnesium to iron ratio) is a key indicator of the type of lunar rock. At present, this ratio is estimated from visible and near-IR data, but the quality of this estimate is not well validated, and the presence of feldspar is inferred from albedo measurements that can be contaminated by many other factors.

LRO Diviner is more directly sensitive to feldspar through measurement of the position of the thermal IR Christiansen feature [5]. That spectral feature is a strong function of feldspar content, so Diviner surveys will provide independent measurements of this key ratio, and determine the relative importance of magma ocean processes and secondary crust formation in the formation of the lunar crust.

In addition to Diviner, LOLA will make independent measurements of low-Ca pyroxene abundances by taking advantage of the temperature sensitive albedo of this mineral. By comparing LOLA shots of nearby or targeted regions taken during both the day and night, changes in the reflected return will be proportional to the abundance of pyroxene and space weathering, with the latter controlled using other data sets.

Evolved rocks: The lunar samples contain rare examples of silica-rich rocks including granites, some of which appear to have formed in modest (km) scale magma bodies. The existence of localized Th anomalies (especially Aristarchus and the Compton-Belkovitch Th anomaly) also indicate the presence of differentiated rocks, these related to KREEP. Finally, some geologic features on the Moon (e.g. Gruithuisen Domes and Hansteed Alpha) have constructional morphologies suggestive of silicic lava features.

Diviner thermal IR multispectral radiometry is sensitive both to the presence of quartz and alkali feldspars leading to possible confirmation of these candidate regions as true differentiated rock types.

Space Weathering: Space weathering can be estimated by near-IR methods because of the strong effect of nanophase iron and dark agglutinate glass on that wavelength region. LRO LAMP UV measurements will provide independent estimates of space weathering based on strong relationships observed between soil maturity and UV spectral properties in lunar samples [7].

In a larger sense, space weathering includes all aspects of regolith evolution, and Diviner measurements of thermal inertia will provide estimates of rock abundances to 500-m resolution, a strong indicator of the macroscopic maturity of the surface [5].

References: [1] Gillis-Davis, et al. Geochimica et Cosmochimica Acta, Volume 70, Issue 24, p. 6079-6102.(2006) [2] Chin et al. Space Science Reviews 129, no. 4 (April 21, 2007): 391-419; Robinson M.S. et al. (2005), LPS XXXVI, Abstract #1576. [3] Pieters (1978) *Proc. Lunar Sci. Conf. 9th*, 2825-2849. [4] Staid, M. et al (1996) *J. Geophys. Res.* **101**, 23,213-23,228. [5] Paige et al. Space Science Reviews, in press; Greenhagen, B. T., PhD. Dissertation, University of California, Los Angeles, 2009. [6] Donaldson Hanna, K. L, et al., 40th LPSC, #2286, 2009. [7] Hendrix, A. NLSI Lunar Science Conference, held July 20-23, 2008 at NASA Ames Research Center, Moffett Field, California, LPI Contribution No. 1415, abstract no. 2151.

Do Lunar Pyroclastic Deposits Contain the Secrets of the Solar System?

David S. McKay, Mail Code KA, NASA Johnson Space Center, Houston TX 77058, david.s.mckay@nasa.gov

Introduction: A new lunar exploration program should have a broad scientific basis, going much beyond the lunar focus of the Apollo program. Part of the new program should include regolith studies, but these studies should have much broader implications beyond understanding the development of the lunar regolith. The concept of using the lunar regolith as a tape recorder containning a broad but complex record of solar system history can be the basis for some fundamental science. Answers to a number of important questions may be preserved in the lunar regolith, some of which have significance for the evolution of the Earth and even for the development of life on Earth:

- How long did planetary objects bombard the Moon and Earth the rate of bombardment decrease finally allowing life to catch hold on Earth?
- Did life start independently on Earth and can we find still preserved Earth-derived meteorites from the earliest billion years or so, a record destroyed on the Earth by geologic processing and resurfacing?
- Or did life come via meteorite transport from a more quiet Mars where impacts were less severe and life could start earlier, allowing Mars life to become implanted on Earth in welcoming nutrient-rich oceans and ponds?
- Did the solar system undergo occasional bursts of severe radiation from the sun, from other stars, supernovas, black holes, or from unknown mysterious sources?
- Were these this radiation bursts strong enough to kill early life on Earth or to blast away the ozone layer causing major mutations in the development of life?
- If so, is a record of these strong radiation bursts still preserved in ancient regolith samples on the Moon?

The answer to these and other solar system history questions may already be recorded in the lunar regolith and be waiting for us to develop the tape reader allowing this history channel to be played. The lunar regolith has, in theory, recorded the history of the early Moon, the early Earth, and the entire solar system back through time. While much of that record has been destroyed by continuous impact bombardment, some may still preserved in pockets of ancient regolith, fortuitously buried and preserved by subsequent protective deposits. This recording may consist of impact remains from large and small meteorites that can be identified by their chemistry and possible remnant fabrics, textures, and mineralogy just as they are on Earth. The meteorite type and chemistry may have changed over time as different populations of impactors became dominant or disappeared. It is entirely possible that meteorites generated on early Earth may be preserved in ancient regolith pockets, and even meteorites from Venus, Mercury, the satellites of Jupiter and Saturn may be present on the Moon. Ejecta from large impact may have left lunar ray material or marker beds preserved in ancient regolith. Whether or not such ejecta can be traced to specific craters, age dating of ejecta from larger impacts should still provide us with statistically useful impact data. How frequent were large impacts? What was the relative frequency of large to small impactors and how did that ratio vary over time? Do early preserved regolith samples have agglutinates? Or are agglutinates a characteristic of much younger regoliths? The lunar regolith also contains a history of the sun and possibly other stars and supernova in the form of implanted and trapped solar wind, solar flare materials, and radiation damage and cosmogenic isotope changes resulting from energetic gamma rays.

This impact history is preserved as mega-regolith layers dating back to the lunar cataclysm or earlier, ejecta layers, impact melt rocks, ancient impact breccias, and perhaps most valuable, buried and well-preserved ancient regolith. A major goal of the developing lunar exploration program should be to find and sample existing fragments of that taped record in the form of carefully located and sampled pockets of preserved ancient regolith. Burial of existing regolith by a hot basalt flow, a hot impact-generated melt flow, or even an impact-produced base surge of impact debris is one set of possibilities, and such burial from any of these events could preserve ancient regolith. However, for each of these scenarios the upper exposed regolith layers may be mechanically and thermally disrupted by the basalts and impact melt or debris flows. ***By contrast, it is likely that coverage of ancient regolith by fine-grained pyroclastic deposits was the most gentle and least destructive process for sealing off and preserving the detailed history of the moon and the solar system up to the moment in time of the pyroclastic eruption event. On earth, deposits of pyroclastic ash falling from an eruption may preserve the underlying soil and stratigraphy in complete detail and without significant disruption.*** The equivalent lunar sandwich filling, bounded on top and bottom by precisely datable lunar pyroclastic deposits, has likely been trapped and removed from further processing at many places and constitutes a buried time capsule perhaps containing well-preserved ancient regolith, including recoverable records of solar wind, giant solar flares, supernova events, and ejection debris layers or marker beds from impacting bodies such as comets and asteroids. It is entirely possible that some

areas contain pyroclastic deposits from multiple eruption events and that these deposits were each exposed to space weathering for short periods of time until they were covered by a subsequent ash deposits. This scenario would create multiple time capsules or snapshots, each preserving a unique slice of the record of the moon and solar system. Detailed study of materials in a cross section or trench through such deposits should show us how the solar system has evolved and changed over time and provide us with detailed snapshots of specific portions of solar system history.

Large areas of presumed pyroclastic dark mantle are found on the front side of the moon, and small dark mantle regions have been identified on the back side. The Aristarchus Plateau is one of the most studied areas, and estimates for the thickness of those deposits range from 10s of meters to 100s of meters. If these thicknesses represent multiple eruptions extending over significant time, the probability is that layers of space-weathered pyroclastics have been encapsulated and preserved by each subsequent pyroclastic deposit. Close examination by LRO might spot evidence for multiple eruptions separated by layers of space-weathered regolith.

While we should not expect large expanses of pristine impact ejecta layers or marker beds, or pristine or even continuous pyroclastic deposits to be preserved intact, discontinuous fragments of such layers may be found in many places protected from destruction or gardening by burial by subsequent pyroclastic deposits. In general, the thicker the covering blanket, the greater the chance that covered ancient regolith will be preserved intact and escape subsequent gardening, and the relatively thick large dark mantle deposits such as those on the Aristarchus Plateau may be the best place to look.

The lunar regolith is the only readily accessible place in the solar system for finding and revealing the detailed record of solar system history. The tape recorder aspect of the moon may ultimately turn out to be its single most valuable scientific asset, and we need to focus a major exploration effort in this direction. This focus is readily understood by the public and can be the underlying scientific basis of much of our lunar program. The recovery, sample return, and decoding of pristine ancient regolith may be one of the most important scientific discoveries of the new lunar era.

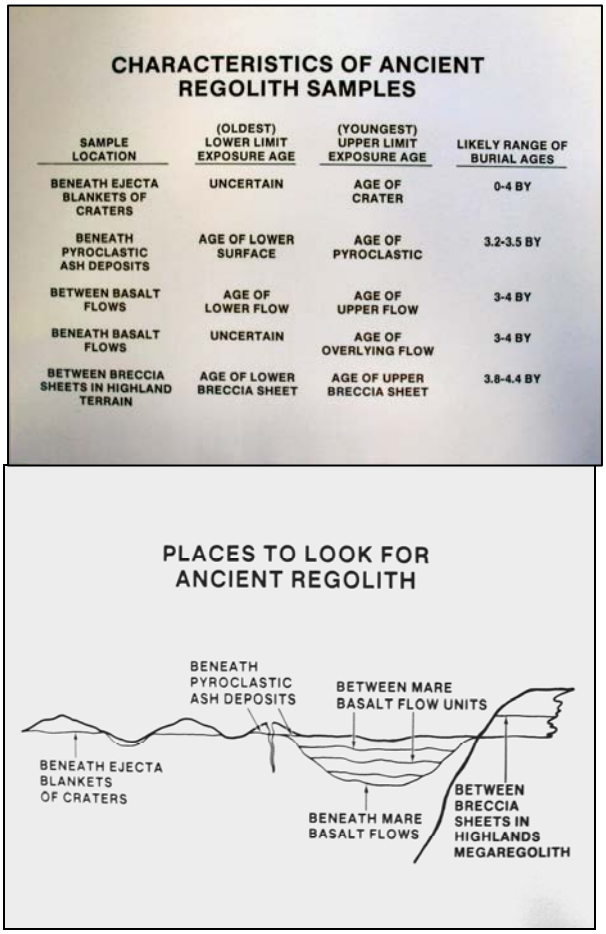

THE LUNAR REGOLITH AS A REMOTE SENSING TARGET FOR THE LUNAR RECONNAISSANCE ORBITER (LRO) W. W. Mendell, NASA Johnson Space Center, Houston, TX 77058, <wendell.mendell@nasa.gov>.

Introduction: Of the 6 instruments and one technology demonstration aboard the LRO, only CRaTER does not measure some kind of interaction of particles with the lunar regolith. LEND detects neutron fluence that contains information about the number density of protons in the upper regolith. To infer the presence of protons, the PI must assume a model that characterizes the surface as a collection of atoms. Thus, LEND does not sense the regolith as a structure.

LROC, LOLA, and LAMP sense reflected photons whose wavelength is much shorter than the median particle size in the regolith. The photons inteact with electrons, either in atomic shells or in chemical bonds. These intractions occur within a nanometer or so of the surface of a particle. Thus, the particles are macroscopic objects and models of the reflection process invoke ray-tracing optics.

DIVINER senses photons that have been emitted by surface particles through thermal phonon processes. The wavelengths detected by the instrument are of the same order as the median particle size, and the photons contain information on particle dimensions as well as the molecular bonds in the constituent compounds.

The Mini-RF synthetic aperture radar generates and detects photons of a few centimeters wavelength that interact with the regolith as a dielectric, the dielectric properties of the particulate component being described through effective medium theory. However, the interaction with "rocks" (macroscopic objects of interest to geologists) can be characterized using Fresnel or Mie models of electromagnetic properties.

Regolith Structure: The great majority of lunar scientists come from geologic sciences and gravitate to the LROC images for their data on the regolith. These cameras are surrogates for our eyes, and the morphologies and textures in the images can be interpreted in terms of canonical geologic process models.

On the Moon, rocks have a significance in the process of regolith formation and maturation. The textbook narrative of regolith formation starts with a large impact that buries pre-existing regolith under an ejecta blanket. Large boulders are deposited on the rim and smaller blocks go larger distances. One of the attributes of a "fresh" crater is a blocky ejecta blanket; and conversely a surface block population is usually taken as evidence for a fresh ejecta blanket.

Over geologic time, the blocks are fractured and comminuted until, over time scales of hundreds of millions of years, the blocky ejecta blanket is transformed into a mature regolith.[1]

A block on a particulate surface will maintain a positive thermal contrast after lunar sunset. Large blocks are positive thermal anomalies throughout the lunar night, but rocks on the order of 10 cm will become indistinguishable from background by midnight.

The Apollo 17 Infrared Scanning Radiometer (ISR) detected these thermal enhancements, which provide a measure of the level of degradation (i.e., age) by the level of enhancement.[2] DIVINER should be able to provide an approximate age sequence for Copernican Age craters., analogous to, but more quantitative than, the Pohn and Offield [3] visual degradation scheme.

The ISR and the Apollo X-ray spectrometer showed that the tops of massifs such as the Apennines are rocky even though they are old. This mass wasting phenomenon may imply that regoliths on basin and (large) crater rims evolve differently from regoliths on flat plains. DIVINER should provide information on this phenomenon, which might have implications for potential outpost sites.

The Epiregolith: Rarely considered are the variations in regolith properties more closely associated with the physics of the photonic interactions sensed by the LRO instruments. Can non-trivial differences be detected in the *epiregolith*, the term I use for the interaction zone at the upper surface of the Moon? To discuss this possibility, I will discuss the history of the current knowledge base.

Scientific literature on optical and thermal properties of the pre-NASA Moon was written by astronomers using techniques, instruments, and concepts from stellar astronomy. Radio technology from the Second World War led to passive microwave thermal measurements and radar probing of the surface. The combination of these observations produced mathematical models of the upper meter of the surface and of the epiregolith. The model of the upper meter was a reasonable representation of the physical reality, but the epiregolith has never really been studied *in situ*.

Prior to 1960, the source of the lunar photometric function was an enigma. All Earth-based data indicated that the lunar surface reflected sunlight in an odd manner at all locations. In 1963, Bruce Hapke [4] published a model that reproduced the photometric function mathematically and that gave some insight into the physical mechanism responsible for it. Starting from the Lommel-Seeliger 19th-Century model for reflec-

tance from collections of particles, Hapke postulated a complex, highly porous, interconnected surface configuration that allowed reflected photons to escape the surface preferentially if they happened to reflect back along the path by which they entered the structure. He referred to the structure as a "fairy castle". Hapke further refined his model in later years, and it survived at least two major challenges from competitors. Although the reflectance spectroscopy community resisted employing the Hapke concepts for at least two decades, the model is now regularly cited and utilized.

In 1930, Pettit and Nicholson [5] demonstrated that thermal emission from the Moon was directional in the infrared. Sinton [6] and Montgomery, et al. [7] confirmed the behavior decades later. Bastin and Gough [8] first modeled the directionality successfully with a completely artificial geometric construction. The model consisted of thermally isolated elements exchanging heat only by radiation, and the temperature of each class of element was determined by its view factor of space. The important characteristic of the construction was that the spacing between the elements was about the same dimension as the elements themselves. A Hapke fairy castle fits this description, and Winter and Saari [9] succeeded in matching the directionality using sparse arrays of cubes. In these particulate constructs, the particles perched at the very top have a large view factor of space and are cooler than particles one or two layers down. A detector looking straight down at the collection sees a mixture of temperatures and overestimates the average temperature of the collection because of the Planck function nonlinearity. Conversely, a detector looking along a slant path at the exact same surface element at the exact same time will see more of the cool particles on top and report a lower temperature.

I plan to discuss other observations consistent with this conception of the epiregolith. In particular, the directionality effect should decrease with wavelength throughout the thermal infrared to the submillimeter because the median particle size in a mature regolith is about 50 micrometers. At longer wavelengths, the thermal contrasts become averaged out, and the indivicual particles become more transparent to the radiation. I think data exists in various places that could test this prediction.

Enigma of the Epiregolith: As far as we know, the epiregolith exists everywhere on the Moon, a belief consistent with the idea that regolith processes are the same everywhere. The directionality of reflected and emitted radiation was documented by Earth-based observations of low spatial resolution. However, the photometric function appears to apply at scales appropriate to orbital imaging and to surface operations.

The fairy castle structure described by Hapke need not be more than several particles (~mm) thick and must be quite fragile. How does it survive over geologic time? It must regenerate after being disrupted. Why is it so tenuous, modeled at 90% porosity?

I suggest it has something to do with the charging of the surface. The local charge densities do not generate fields large enough move "average" particles in a regolith, but the accumulation of like charge on the surface particles should produce a repulsion that could result in a fairy castle. If that is so, then the surface structure may change near the terminators and may be different on the day and night sides. Such shuffling among the surface particles would have significance for thermal models because the upper layer dictates the directionality of emissivity and is important in the coupling to the solar insolation.

Thre may be regions of the surface where this effect is muted or enhanced for some reason. Such regions could show unusual thermal behavior. The ISR data detected a small region near the craters Bessarion A and B that was anomalously cool during the lunar night. [2] Positive nighttime thermal anomalies are easy to explain; negative ones are not in the context of a mature regolith.

In principle, DIVINER might detect a rearrangement of the surface particles. In practice, it almost certainly will not because the thermal modeling is not at the correct level of accuracy. Nevertheless, scientists ought to be alert to optical or thermal measurments that seem unusual.

References: [1] Hörz, F. (1977) *Phys. Chem. Earth, X*, 3-15. [2] Mendell, W. (1976) Ph.D. Thesis, Rice Univ. [3] Pohn, H. A. and Offield, T. W. (1969) USGS Interagency Rpt.: Astrogeol. 13. [4] Hapke, B. (1963) *JGR, 68*, 4571-4586. [5] Pettit, E. and Nicholson, S. (1930) *Ap. J., LXXI*, 102-135. [6] Sinton, W. (1959) *Lowell Obs. Bull, 4*, 260. [7] Montgomery, C. et al. (1966) *Boeing Dcmt. D1-82-0568.* [8] Bastin, J.A. and Gough, D. O. (1969) *Icarus, 11*, 289-319. [9] Winter, D. F. and Saari, J. M (1969) *Ap. J., 156*, 1135-1151.

LUNAR EXPLORATION NEUTRON DETECTOR FOR NASA LRO MISSION. I. G. Mitrofanov[1] , A. S. Sanin[1], M. I. Mokrousov[1], M. L. Litvak[1], A. S. Kozyrev[1], A. A. Malakhov[1], V. I. Trety'akov[1], A. V. Vostrukhin[1], V. N. Shvetsov[2], R. Sagdeev[3], W. Boynton[4], K. Harshman[4], H. Enos[4], J. Trombka[5], T. McClanahan[5,] L. Evans[6] and R. Starr[7], [1]Institute for Space Research, Moscow 117997, Russia, [2] Joint Institute for Nuclear Research, Dubna, Russia, [3] University of Maryland, Collage Park, USA, [4] University of Arizona, Tucson, USA, [5] NASA Goddard Space Flight Center, Greenbelt, [6] USA, Computer Science Corporation, Greenbelt, USA, [7] Catholic University, Washington DC, USA.

Introduction: The concept of Lunar Exploration Neutron Detector is presented, which is Russian contributed instrument for NASA's Lunar Reconnaissance Orbiter [1]. The measurements of this instrument will allow to continue studies of neutron emission from the Moon started by Lunar Prospector [2], but with much higher spatial resolutions about 10 km for the orbit with altitude of 50 km.

Instrument objectives: Three main objectives of LEND experiment will be discussed, as the following:

- mapping of hydrogen content over the entire surface of the Moon;
- testing the presence of water ice deposits within polar craters with permanent shadow from sun sight;
- characterization of neutron component of lunar radiation environment.

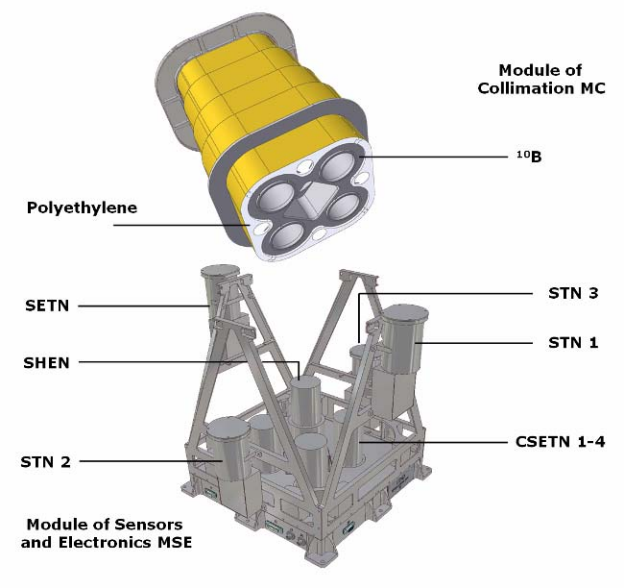

Figure 1. Schematic view of LEND with removed Module of Collimation MC. This module contains the absorbing substance of ^{10}B and layers of polyethylene. Module of sensors and electronics (MSE) has collimated sensors CSETN 1-4 of epithermal neutrons and sensor SHEN of high energy neutrons. It also has four omni-directional sensors of epithermal neutrons SETN and thermal neutrons STN 1 – 3.

Design of the instrument: Design of LEND will be described (Figure 1), as the suite of 9 individual sensors of thermal, epithermal and high energy neutrons. All of them are integrated within the module of sensors and electronics (MSE). Details on neutron module of collimation (MC) will be presented together with results of physical calibrations of its collimation efficiency. Major parameters of flight unit of the instrument will be presented (Figure 2).

Data products from LEND: All four levels of data products will be discussed: from level-0 data with rough counting data up to the level-3 data with maps of hydrogen distribution and estimations quantity or upper limits of water ice deposits. Time schedule to data product development will also be presented.

Figure 2. General view of LEND flight unit

LEND support for LCROSS. The program of LEND data analysis will be presented for creation of the list of the most probable polar regions with water ice deposits.

References: [1] Mitrofanov I.G. at al. (2008) *Astrobiology* v. 8, issue 4, p. 793. [2] Spudis P.D. et al. (1998) *Solar System Research*, v. 32, p. 17.

LUNAR ANORTHOSITES AS TARGETS FOR EXPLORATION. M. D. Norman[1,2], [1]Lunar and Planetary Institute, Houston TX 77058 USA, [2]Research School of Earth Sciences, Australian National University, Canberra ACT 0200 Australia (Marc.Norman@anu.edu.au).

Introduction: The discovery of anorthosite was arguably the second major surprise to come from the first sample return mission to the Moon, the first being the extraordinarily high TiO_2 contents of Apollo 11 mare basalts. The juxtaposition of these two extreme lithologies formed the cornerstone of our current understanding of the Moon as a highly differentiated body composed predominantly of igneous cumulates.

In the context of a global exploration program, it will be useful to distinguish two fundamental classes of anorthositic lithologies on the Moon: (1) igneous anorthosites and (2) polymict breccias with anorthositic mineralogy and bulk compositions. The occurrence and distribution of these two types lithologies can be used to address distinct processes and a variety of science questions.

Igneous anorthosites. Despite the mineralogical simplicity of igneous lunar anorthosites (most are >99% plagioclase+pyroxene), their geochemistry is surprisingly complex in major and trace element compositions. A simplified generic classification of igneous lunar anorthosites might recognize (1) ferroan anorthosites, and (2) anorthosites associated with the Mg-suite of highlands cumulates and related lithologies.

Ferroan anorthosites are the quintessential highlands crustal cumulate. Type examples, collected mainly at the Apollo 15 and 16 sites, are composed of ≥98% plagioclase with a narrow range of anorthite contents (An_{95-98}). Mafic phases are predominantly opx although some examples have olivine > pyroxene. In contrast to the plagioclase compositions, mafic phases have a relatively broad range of major element compositions with Mg# ~50-75.

In addition to the highly anorthositic type examples, the 'ferroan anorthositic suite' also includes a variety of related, generally more mafic lithologies. James [1] recognized two varieties of troctolitic anorthosite, one with 10-20% mafics having Mg# at the upper end of the range for ferroan anorthosite (66-75), and a second, somewhat less-mafic variety with lower Mg# (50-63). A troctolitic anorthosite clast in the Dhofar 489 lunar meteorite with Fo_{79} olivine [2] may represent an extension of James' high-Mg# group. Noritic anorthosites with px > olivine and relatively abundant cpx have also been recognized and linked to the ferroan anorthositic suite using major and trace element compositions [3, 4, 5]. James [1] also recognized a slightly sodic variety of ferroan anorthosite based on their slightly lower An contents of the plagioclase (An_{94-95}).

Ferroan anorthosites are the best candidates for a primitive flotation crust from a lunar magma ocean [6, 7], but we do not yet have a detailed petrogenetic model that explains the petrologic and geochemical diversity of the ferroan anorthositic suite. Trace elements that are concentrated in plagioclase (Sr, Eu, Ba, Ga), and therefore likely to be robust against subsequent disturbance, are broadly consistent with crystallization from an evolving magma ocean having initially chondritic relative abundances of refractory lithophile elements [5, 8, 9]. The REE compositions of 'typical' or 'main group' ferroan anorthosites are also consistent with accumulation from a moderately evolved magma ocean [7], despite potential complications from disturbance by shock and/or metamorphic re-equilibration during slow cooling.

The petrogenesis of other subgroups of the ferroan anorthositic suite appears to be more complex. The more mafic varieties tend to have anomalously high contents of REE and other incompatible elements [5,7], possibly indicating a greater proportion of trapped melt or contamination with more evolved melts. Cooling rates estimated from pyroxene exsolution lamellae also indicate a range of emplacement conditions within the lunar crust. At least some of the ferroan anorthosites likely formed depths of 10-20 km [10] whereas others cooled much more rapidly [5], possibly in localized, near-surface plutons [4].

Crystallization ages of ferroan anorthosites are not well established. Their Sr isotopic compositions are consistent with early crystallization from a primitive magma but redistribution of Rb by impact metamorphism has obscured this record [11]. ^{147}Sm-^{143}Nd mineral isochrons are restricted to examples with atypically high abundances of mafic minerals, and have yielded a range of apparent ages extending from 4.29-4.54 Ga [5]. The petrologic or geochronological significance of this range is also not well understood. If the isochron ages are real they may reflect a complex petrogenesis of ferroan anorthositic suite rocks that includes post-magma ocean magmatism [11] or compositional modification during tectonic emplacement and/or re-crystallization [12]. Alternatively, the apparent range of Sm-Nd isochron ages may be an artifact of impact metamorphism. A preferred age of 4.46 $\pm$ 0.04 Ga can be calculated based on Sm-Nd systematics of mafic phases, on the assumption these are more resistant to disturbance than the coexisting plagioclase [5]. However, this analysis assumes that the four samples for which Sm-Nd mineral data exists are related to a

common magmatic system. A peculiar characteristic of some ferroan anorthosites is the apparent disequilibrium between REE abundances in plagioclase and coexisting pyroxene [7]. The reason for this decoupling is not understood, but it may have significant implications for attempts to obtain Sm-Nd crystallization ages of ferroan anorthosite, using mineral isochrons.

Alkali and Mg-suite anorthosites. Other types of igneous lunar anorthosite have mineral and chemical characteristics indicating crystallization from KREEP-rich or Mg-suite magmas. These include the highly evolved alkali anorthosites [13] and small samples of anorthosite that have petrologic and geochemical affinities with Mg-suite troctolites [14]. These types of anorthosite are most abundant in the Apollo 12 and 14 collections, consistent with a close petrogenetic association with KREEP.

Alkali suite anorthosites are distinguished from ferroan anorthosites by their more sodic plagioclase (An_{76-86}), compositional zoning in the plagioclase (normal and reverse), and igneous textures indicating predominantly near-surface crystallization [12,14]. Mafic phases are sparse and have relatively low Mg# (50-70). The Mg-suite anorthosites have mineral compositions similar to those of Mg-suite troctolites (An_{94-97}, Fo_{84-90}) [14]. These small fragments may represent fine-scale layering within an Mg-suite pluton rather than bodies of anorthosite [14].

Parental magmas for the alkali anorthosites and the Mg-suite anorthosites have evolved trace element characteristics (high Eu/Al, low Sc/Sm, high REE abundances) but the alkali and Mg-suites cannot be related by simple closed-system crystallization of a common parental magma [7,8,14]. Their petrological and geochemical characteristics apparently require a diverse set of igneous processes including assimilation and magma mixing. By analogy with cooling rates inferred from Mg-suite gabbronorite, sodic ferrogabbro, and quartz monzodiorite, the alkali anorthosites were probably emplaced at relatively shallow depths in the uppermost lunar crust (0.2-0.5 km) [10].

Another variant of sodic anorthosite that also has relatively ferroan mafic phases but plagioclase compositions intermediate between those of ferroan and alkali anorthosites (An_{91-94}) was described by Norman et al. [15]. These sodic anorthosites also have unusually high Sr and Eu contents, and mineral compositions suggesting affinities with Mg-suite gabbronorites, but their petrogenesis has not been clearly elucidated.

Polymict anorthositic breccias with feldspathic bulk compositions close to that of anorthosite (~30 wt% Al_2O_3) were collected at the Apollo 16 site and have been found as lunar meteorites (e.g. Dhofar 081 and 489). These feldspathic polymict breccias generally have low contents of incompatible trace elements and may be difficult to distinguish from igneous anorthosite based on remote sensing data alone. Metamorphosed polymict breccias with granoblastic textures also have mineralogy and bulk compositions similar to some igneous anorthosites.

Such lithologies may be relatively common at the lunar surface. Large regions of the farside, north of the South Pole-Aitken basin, have bulk compositions very close to that of anorthosite (<2% FeO) [16]. The lithologic affinity of these regions is unclear, but they may represent either SPA ejecta, or a veneer of SPA ejecta over primary anorthositic upper crust [16]. The Apollo 16 feldspathic fragmental breccias may represent ejecta from either the Imbrium or Nectaris basins.

Targets and Questions. The anorthosite massifs observed in the rings of several lunar basins [16] are obvious targets for closer inspection by LRO. High-value targets might include the Inner Rook ring of Orientale, described as a "mountain range of anorthosite" [16], the eastern rings of Grimaldi near the contact with Oceanus Procellarum, and the northwestern region of Nectaris near Theophilus and the Kant Plateau. These large bodies of anorthosite apparently occurred at pre-excavation depths similar to those obtained form the cooling rate calculations on ferroan anorthosites [10], sandwiched between layers of more mafic material [16]. Questions that might be addressed by closer observation of these regions include: (1) The nature of the contacts between mid-crustal anorthosite and the more mafic layers above and below the anorthosite. Are the contacts igneous or depositional? Is there evidence for diapiric emplacement of the anorthosite? (2) Can highly feldspathic breccia despoits be recognized and if so, can they be linked with confidence to basin ejecta? What is the fraction of locally reworked vs. transported ejecta in these deposits?

References: [1] James et al. (1989) PLPSC 19, 219-243. [2] Takeda et al. (2006) EPSL 247, 171-184. [3] McGee (1993) JGR 98, 9089-9105. [4] Jolliff et al. (1995) GCA 59, 2345-2374. [5] Norman et al. (2003) MAPS 38, 645-661. [6] Warren (2005) Treatise on Geochemistry, vol. 1, 559-599. [7] Shearer and Floss (2000) In: Origin of the Earth and Moon, 339-359. [8 Warren and Kallemeyn (1984) PLPSC 15, C16-C24. [9] Floss et al. (1998) GCA 62, 1255-1283 [10] McCallum and O'Brien (1996) Am. Min. 81, 1166-1175. [11] Borg et al. (1999) GCA 63, 2679-2691. [12] Haskin et al. (1981) PLPSC 12, 41-66. [13] Warren and Wasson (1980) PLPSC 11, 431-470 [14] Shervais and McGee (1999) JGR 104, 5891-5920. [15] Norman et al. (1991) GRL 18, 2081-2084 [16] Hawke et al. (2003) JGR 108, 10.1029/2002JE00890.

JOINT LROC – MINI-RF OBSERVATIONS: OPPORTUNITIES AND BENEFITS. S. Nozette[1], D.B.J. Bussey[2], B. Butler[3], L. Carter[4], J. Gillis-Davis[5], J. Goswami[6], E. Heggy[7], R. Kirk[9], T. Misra[6], G.W. Patterson[2] , M. Robinson[8], R. K. Raney[2], P. D. Spudis[1], T. Thompson[7], B. Thomson[2], E. Ustinov[7] 1. Lunar and Planetary Institute, Houston TX 77058 (Stewart.Nozette-1@nasa.gov) 2. Applied Physics Laboratory, Laurel MD 20723 3. NRAO, Socorro NM 4. NASM, Wash- ington DC 5. Univ. Hawaii, Honolulu HI 96822 6. ISRO, Bangalore, India 7. JPL, Pasadena CA 8. ASU, Tempe AZ 9. USGS, Flagstaff AZ

Introduction: Mini-RF is a lightweight Synthetic Aperture Radar (SAR) instrument set to fly on the Lunar Reconnaissance Orbiter (LRO). A sister instrument is currently imaging the Moon aboard the Indian Chandrayaan-1 spacecraft. Mini-RF on LRO has three primary functions:- 1. Communications demonstration. 2. SAR-mapping. 3. Interferometric mapping.

Mini RF measures the properties of the lunar regolith at two wavelength scales; S band (12cm) and X band (3 cm) and at two spatial resolutions, 150 meters and 30 meters.

LRO-LROC Operations: Mini RF and LROC share common LRO spacecraft support assets (e.g. power, bandwidth) which requires operating one of the two instruments at any given time. Mini-RF can operate during periods when LROC observations are not useful, for example during dawn-dusk orbits with low sun angles or when LRO is traversing above the unilluminated lunar surface. In addition to the planned Mini-RF observations of the permanently shadowed polar regions, additional Mini-RF observations may be possible of scientifically interesting non-polar areas during the LRO primary and extended missions. Joint planning of these observations with LROC should be explored. Such planning will produce operational benefits allowing for a more streamlined Mini-RF commanding, data collection and distribution, and provide unique science observations.

Non-Polar Targets: Mini RF probes beneath the surface at scales comparable to each wavelength. The size and distribution of surface and subsurface blocks, regolith bulk density, and in some cases regolith composition may be inferred from Mini-RF data. When combined with higher resolution LROC images additional knowledge of regolith albedo, structure, and physical properties may be derived, leading to new geologic insight and interpretation. This was recently demonstrated using data from LRO Mini-RF's forerunner, Mini-SAR on Chandrayaan 1. The location and distribution of pyroclastic deposits is a long-standing lunar science objective recently endorsed by the NAS. Mini-SAR obtained images of the Schrödinger impact basin (Figure 1). Schrödinger shows an unusual, keyhole-shaped crater along a long fissure on the basin floor. This crater is surrounded by optically dark material, which has been interpreted as volcanic ash deposits. The new Mini-SAR image shows that this material is also dark in radar reflectivity, exactly what would be expected from a fine-grained, block-free deposit. Mini-SAR radar images confirm the geological interpretation first derived in 1994 from Clementine images. Additional observations will benefit from higher resolution LROC and Mini RF images acquired in a coordinated manner.

The goal of Mini-Rf on LRO during the scince-driven extemded mission is to image areas of scientific interest, such as pyroclastic deposits. Co-ordinated studies using targeted-data of other LRO instruments will enhance the scientific return.

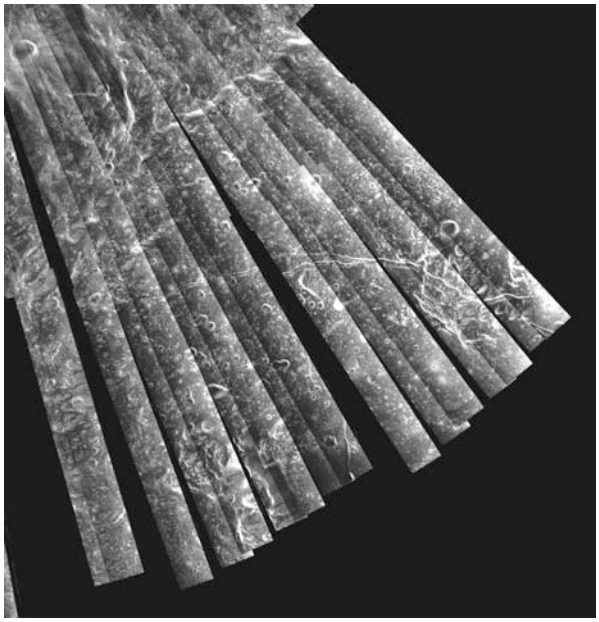

Figure 1. Mosaic of mini-Rf data covering a portion of Schrödinger basin, including the pyroclastic vent.

LOCATIONS AND MORPHOLOGY OF SPACECRAFT IMPACT CRATERS FOR RE-CALIBRATION OF APOLLO SEISMIC DATA. J. Oberst[1], M. Wählisch[1], S. Hempel[1], and M. Knapmeyer[1], [1]German Aerospace Center, Institute of Planetary Science, Rutherfordstr. 2; D-12489 Berlin; Germany (Juergen.Oberst@dlr.de).

Introduction: We propose to investigate the sites of man-made impacts on the Lunar surface to derive their precise coordinates and sizes of impact craters that have formed. Improved impact coordinates and derived ranges from the Apollo stations will warrant a re-investigation of the Apollo seismic data for improvements in our knowledge of seismic velocity structure. Measured impact crater sizes will help to improve the available scaling laws that relate impact energy to seismic amplitudes.

Lunar Seismic Data: The Lunar 4-station seismic network operated on the Lunar surface from November 1969 to September 1977 [1]. Several thousand seismic events were recorded, including Deep Moonquakes, Shallow Moonquakes, as well as large numbers of Meteoroid Impacts. The seismic data were used to study the Lunar seismic velocity structure by inversion of seismic wave arrival times at the 4 stations. However, in the inversion, the coordinates of natural seismic sources must be determined along, thus leaving only little data to solve for parameters of Lunar structure.

Man-made Impacts: Impacts of the spent Saturn V Boosters and the ascent stages of the LMs (Lunar Models) constituted crucial "calibration data". The impact times and the coordinates of the impact sites [2] were fairly well known from radio tracking of the spacecraft up to impact (Table 1). Therefore, the recordings represented unique data of seismic travel times over known distances. Unfortunately, the acccuracy of the tracking data was limited, and thus, impact coordinates suffered from uncertainties. While some of the early impacts sites have been identified in images of Apollo missions that followed, the geodetic control of such images and the coordinate knowledge is limited. Moreover, for the impact of the Apollo 16 booster, the tracking signal was lost before impact, and impact coordinates were only re-constructed from the seismic data [3]. Impacts that followed later have not been identified in any image data at all. We propose to revisit the impact areas, identify the impact sites, and to measure impact coordinates and ranges to the Apollo seismic stations carefully.

Scaling Laws: Data on size of the impact craters can be used as ground truth for seismic scaling laws, i.e. to find relationships between impact parameters via crater sizes to seismic amplitude. The impact energies and impact angles of the Saturn boosters and the LEMs differed substantially and therefore cover most parts of the parameter space of interest. Improved scaling laws will greatly help in our understanding of the population of seismically observed meteoroid impacts and their relationship to Lunar impact flashes and impact crater statistics.

Impactor	Time [UT]	Lat. N [°]	Lon. E [°]
LM-12	20. Nov 69 22:17:17.7	-3.94	-21.2
LM-14	07. Feb 71 00:45:25.7	-3.42	-19.67
LM-15	03. Aug 71 03:03:37.0	26.36	0.25
LM-17	15.Dec.72 06:50:20.8	19.96	30.5
S4B-13	05. Apr 70 01:09:41.0	-2.75	-27.86
S4B-14	04. Feb 71 07:40:55.4	-8.09	26.02
S4B-15	29. Jul 71 20:58:42.9	-1.51	-11.81
S4B-16	19. Apr 72 21:02:04 ± 4	1.3±0.7	-23.8±0.2
S4B-17	10.Dec.72 20:32:42.3	-4.21	-12.31

Table 1: List of Impact times and sites [2]. Apollo 16 S4B entries are estimated from seismic data [3].

References: [1] Bates, J. R., et al. (1979), ALSEP Termination Report; NASA Reference Publication 1036, NASA Scientific and Technical Information Office. [2] Toksöz, M. N. et al., (1974), Structure of the Moon ; Rev. Geophys. and Sp. Phys., Vol. 12, No. 4, pp.539-567. [3] Apollo 16 Mission Report (1972), NASA Manned Spacecraft Center, Houston, TX, MSC-07230. [4] Stooke, P.J. (2007), The International Atlas of Lunar Exploration, , Cambridge Univ. Press.

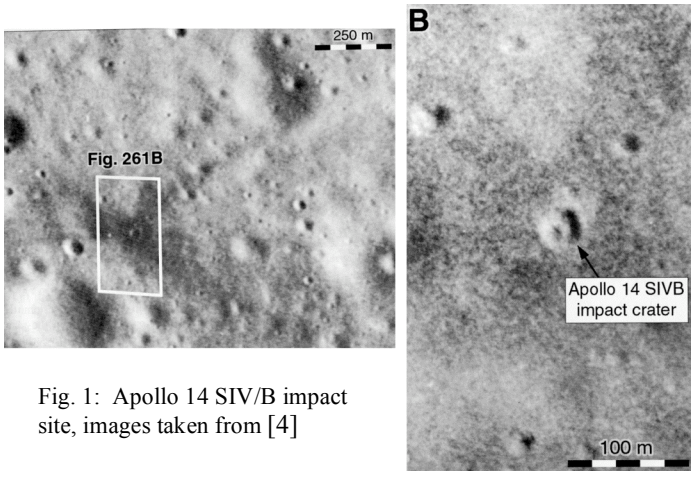

Fig. 1: Apollo 14 SIV/B impact site, images taken from [4]

CHARACTERIZATION OF LUNAR MINERALOGY: THE MOON MINERALOGY MAPPER (M^3) ON CHANDRAYAAN-1. C. M. Pieters[1], J. Boardman[2], B. Buratti[3], R. Clark[4], J-P Combe[5], R. Green[3], J. W. Head III[1], M. Hicks[3], P. Isaacson[1], R. Klima[1], G. Kramer[5], S. Lundeen[3], E. Malaret[7], T. B. McCord[5], J. Mustard[1], J. Nettles[1], N. Petro[8], C. Runyon[9], M. Staid[10], J. Sunshine[11], L. Taylor[12], S. Tompkins[13], P. Varanasi[3] [1]Dept. Geological Sciences, Brown University, Providence, RI 02912 (Carle_Pieters@brown.edu), [2]AIG, [3]JPL, [4]USGS Denver, [5]Bear Fight Center, WA, [6]ISRO-PRL, [7]ACT, [8]NASA Goddard, [9]College of Charleston, [10]PSI, [11]Univ. MD, [12]Univ. Tenn., [13]DARPA.

The Moon Mineralogy Mapper (M^3, pronounced "m-cube") is a state-of-the-art high spectral resolution imaging spectrometer that is orbiting the Moon on Chandrayaan-1, the Indian Space Research Organization (ISRO) mission to the Moon. M^3 is one of several foreign instruments chosen by ISRO to be flown on Chandrayaan-1 to complement the strong ISRO payload. M^3 is a NASA Discovery Mission of Opportunity selected through peer-review as part of the SMD Discovery Program.

The type and composition of minerals that comprise a planetary surface are a direct result of the initial composition and later thermal and physical processing. Lunar mineralogy seen today is a direct record of the early evolution of the lunar crust and subsequent geologic processes. Specifically, the distribution and concentration of individual minerals or groups of minerals is closely tied to magma ocean products, lenses of intruded or remelted plutons, basaltic volcanism and fire-fountaining, and any process (e.g. cratering) that might redistribute or transform primary and secondary lunar crustal materials. The primary *science* goal of M^3 is to characterize and map lunar surface mineralogy in the context of its geologic evolution, and the primary *exploration* goal is to assess and map lunar mineral resources at high spatial resolution to support planning for future, targeted missions.

M^3 is first and foremost a near-infrared spectrometer designed to accurately measure diagnostic mineral absorption features. To meet the above science and exploration goals, M^3 acquires spectra in image format (all spectral channels co-registered to < 0.1 pixel). M^3 operates in two measurement modes as summarized below.

M^3 Measurement Modes

All M^3 Spectroscopic data (from 100 km orbit)**:**
40 km FOV, contiguous orbits
0.70 to 3.0 μm [0.43 to 3.0 μm achieved]

***Targeted Mode*: Full Resolution Science targets**
70 m/pixel spatial (600 pixel crosstrack)
10 nm spectral [260 bands]

***Global Mode*: Lower Resolution Global Coverage**
140 m/pixel spatial (300 pixel crosstrack)
20 & 40 nm selected (85 bands, averaging)

In February 2009, Chandrayaan-1 completed its primary commissioning phase. During this initial period M^3 operated principally in Global Mode. The low resolution Global Mode M^3 coverage achieved for the nearside is shown in Figure 1. A closer view of one band of several neighboring M^3 swaths is shown in Figure 2. Both images are compressed to meet abstract requirements. Pre-calibration assessment of these data (over one billion spectra) indicates they are of excellent quality, meeting all instrument requirements for science. Early results are presented in [1, 2]; a descriptive overview of M^3 is found in [3] along with other Chandrayaan-1 instruments.

At least three full optical imaging periods are planned over the next two years. For M^3, we have two prime measurement periods in each imaging period. Our plans are to complete M^3 coverage for the entire Moon using the 140 m Global mode and to then acquire optimum full resolution data (Target mode) for the highest priority science targets.

References: 1) Pieters et al., 2009, *LPSC40* #2052 2) Green et al., 2009, *LPSC40* #2307. 3) Pieters et al., 2009, *Current Science*, Vol. 96, No. 4.

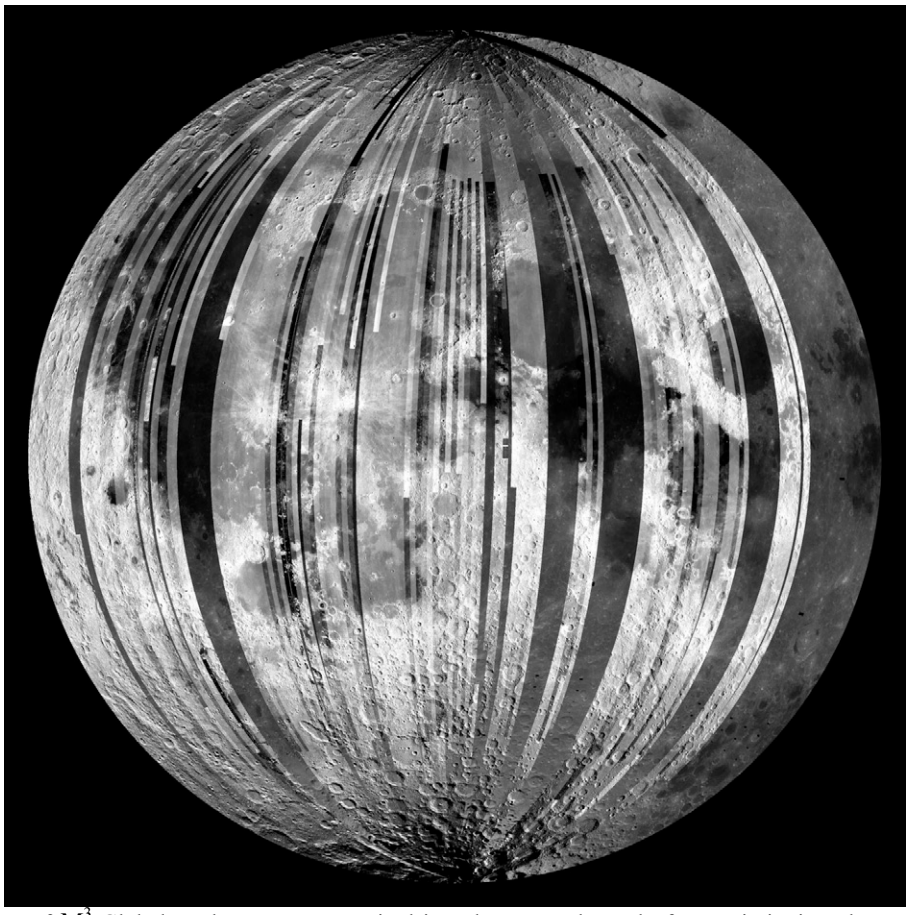

Figure 1. Overview of M^3 Global mode coverage acquired in February at the end of commissioning phase of the first optical period of Chandrayaan-1. Each M^3 data swath is 40 km wide. Shown is one channel of M^3 data. No photometric corrections have been made, but since each swath is scaled independently, swath boundaries are evident. (Background is Clementine)

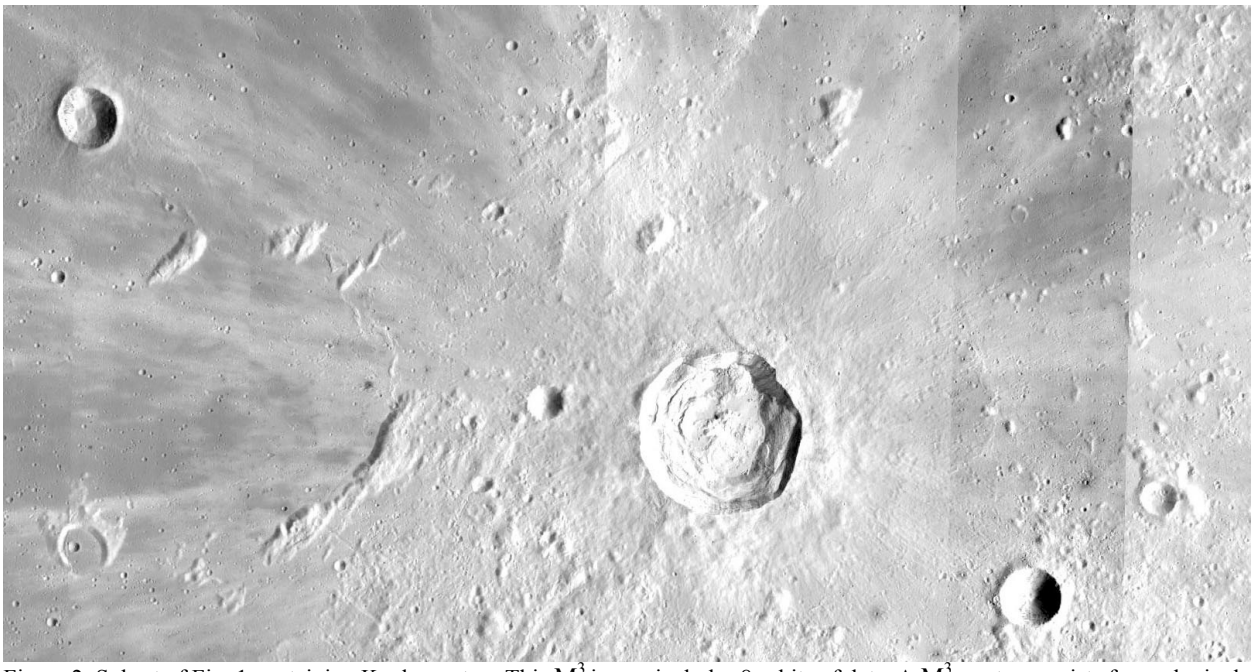

Figure 2. Subset of Fig. 1 containing Kepler crater. This M^3 image includes 8 orbits of data. A M^3 spectrum exists for each pixel.

UNDERSTANDING THE PHYSICAL EVOLUTION OF THE LUNAR REGOLITH USING LRO DATA.
J. B. Plesica, The Johns Hopkins University, Applied Physics Laboratory, 11100 Johns Hopkins Road, Laurel, MD 20723; jeffrey.plescia@jhuapl.edu.

Introduction: The lunar surface is covered by a layer of fragmental debris – the regolith – produced over billions of years by the physical disintegration of the surface materials by micro- to macroscopic scale impacts [1]. To first order, the process is mechanical, unlike the chemical processes that produce soils on the Earth. Because the lunar regolith is ubiquitous, it is the prism through which virtually all aspects of the Moon are seen. The regolith is also the surface on which lunar operations will be conducted and may serve as a resource. Thus, a detailed understanding of its properties and its evolution are necessary.

Background: Our understanding of the origin and evolution of the regolith is derived from remote sensing data (orbital and Earth based) and from *in situ* samples and analysis (Apollo and Luna). The physical, chemical, and mineralogic properties are summarized by [1-7]. While a general understanding of the physical properties exists [3], much remains poorly defined.

Questions: A series of questions can be posed for the regolith, some can be addressed by data from the Lunar Reconnaissance Orbiter (LRO) and from the Japanese Kaguya, Indian Chandrayaan-1, and Chinese Chang'e missions.

What is the variation in thickness of the lunar regolith? How does thickness vary with surface age, maturity, and composition.

Are there significant local variations in regolith thickness in the mare or highlands; if so what does this imply for regolith formation?

Is the regolith in areas of permanent shadow fundamentally different from regolith elsewhere?

Can a fossil regolith be located?

How do rays from recent impact events modify the regolith such that they are visible and what is the mechanism for the disappearance of rays?

What Do We Know: Regolith analysis began with data from Ranger, Lunar Orbiter (LO) and Surveyor. Ranger and LO provided variable resolution images allowing the regional properties to be defined; Surveyor and Apollo provided higher resolution local views.

Regolith Thickness: Mare regolith is estimated to be a few meters thick; the highlands megaregolith is considerably deeper, up to tens of meters thick. Original estimates of regolith thickness were made using crater morphology [8-10]. The model assumed the crater morphology changes from simple to concentric or flat floored when the crater excavates to the top of an underlying strong layer (i.e., bedrock). The diameter at which blocks first appeared was also used to estimate thickness. Later, Apollo seismic data [11] and radar data have also been used to estimate the thickness [12]. Using such methods, regolith was estimated to be 8.5 m thick at the Apollo 14 site; 12.2 m at the Apollo 16 site, and 7-32 m at the Apollo 17 site.

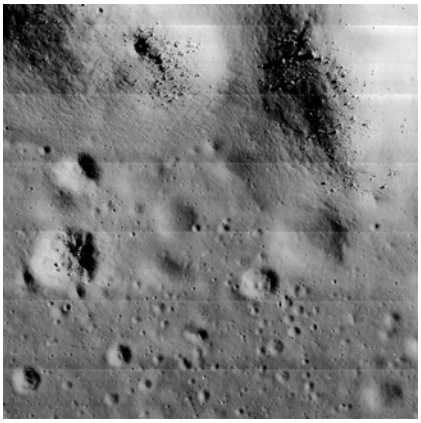

Figure 1. Variations in crater morphology and abundance of rocks can be seen in this LO image of a portion of Flamsteed Ring and adjacent mare..

Wilcox *et al*. [13] show that such a simple model may not always be applicable. For example, similar diameter craters can have different morphology, some have blocks whereas others do not. These differences indicate that the regolith formation process is complex.

Rocks: Craters which excavate into bedrock will distribute blocks. As the regolith is thinner on the mare than in the highlands, blocks will be excavated at relatively smaller diameters (shallower depths) on the mare. Block populations around fresh craters and on the intercrater areas have been measured [13-20]. Using LO images, blocks around craters 30-100 m typically are 1-3 m. Apollo and Surveyor sites have rocks >30 cm of 1 to >30 / 100 m^2. At Apollo 16, rocks >10 cm range from <1% at Sta. 1 to ~16% near WC crater. [13] found 10% of craters 50-100 m have blocks; 100% of craters >300 m have blocks on the mare. Some correlations between surface and orbital data have been made; radar data have also been used to assess surface block populations, although in a statistical sense.

Crater Size Frequency: The size frequency distribution of craters has been measured with orbital data (LO and Apollo) to diameters of a few meters and

from Surveyor images to cm scale [24-31]. LROC data will allow data to diameters of perhaps 2-3 m at numerous locations to be collected allowing for a better understanding of the small projectiles flux, local variations in the surface ages, and the extent to which surfaces are saturated with craters at diameters <200-300 m [32].

Ejecta Thickness: Ejecta thickness can be measured using the LOLA data or geometric or photometric topography from images. This will allow better constraints on ejecta thinning as a function of radial distance and azimuth, and the net bulking of the regolith by the impact process.

Morphometry: Various morphometric relations (e.g., depth / diameter, rim height / diameter, etc.) will be developed using both the LOLA and stereo topography data. This will allow existing data bases [33-39] to be examined and extended to much smaller diameters than was previously possible.

Slopes: Previous studies [40-41] show that slope distributions are a function of the baseline over which they are measured. LOLA data can be used to address slope variations at scales ranging from the distance between shot points (25 m) to kilometers. Topography derived from stereo can be used to address the slope distribution to baselines of ~1 m.

New Data: LROC narrow angle (NAC) targeted observations provide images with ground surface distances (GSD) of 0.5 m/pixel. These images allow very high spatial assessment of the parameters noted above. However, the amount of surface covered by NAC is very limited. Therefore, targeted observation and a statistical sample are critical. Stereo imaging data from Kaguya and Chandrayaan-1 (GSDs ~5-10 m/pixel) are also important. LOLA and altimeters from the other missions provide very high resolution (horizontal and vertical) topography. In addition, LOLA data provide estimates of surface roughness and albedo. These data, supplemented by geometric and photometric stereo, will provide critical topographic data.

Radars on Chandrayaan-1 and LRO will image permanently shadowed areas and provide data on surface roughness and volume scattering. Instrument resolution is too low to resolve individual blocks, but the data do provide a statistical estimate.

Maturity: Over time, the regolith matures due to space weathering – exposure to radiation and the effects of micrometeoroid bombardment [7]. Color images have been used to estimate the optical maturity of the regolith [43-44]. LROC wide angle camera, as well as the spectral instruments form other missions, will provide better calibrated data that can be correlated with high resolution images of the surface and other data sets to better understand the maturation process.

Summary: LRO and other missions will provide a suite of key data sets at varying resolution and coverage to address problems of the lunar regolith. For the instruments with high spatial resolution (LROC, radar) targeted observations are critical to ensure the relevant data are collected. Using these data sets, the processes by which the regolith forms, evolve and mature will be better understood. Spatial variations in the physical properties of the regolith that will affect surface activity (landing, construction, mining, roving) will be better defined to allow better planning and system design.

References: [1] Shoemaker, E., et al. (1968) NASA SP-173. [2] McKay, D., et al. (1991) Lunar Source Book, 285-356. [3] Carrier, W., et al. (1991) Lunar Source Book, 475-594. [4] Taylor, G., et al. (1991) Lunar Source Book, 183-284. [5] Haskin, L., and Warren, P. (1991) Lunar Source Book, 357-474. [6] Papike, J., et al. (1998), *Rev. Mineral., 35*, 5-1–5-234. [7] Lucey, P., et al. (2006), *Rev. Mineral., 60*, 83-219. [8] Quaide, W. and Oberbeck, V. (1968) *JGR, 73*, 5247-5270. [9] Oberbeck, V., and Quaide, W. (1968) *Icarus, 9*, 446-465. [10] Oberbeck, V., et al. (1973) *Icarus, 19*, 87-107. [11] Watkins, J., and Kovach, R. (1973) *Proc. 4th Lunar Sci. Conf.*, 2561-2574. [12] Shkuratov, Y., and Bondarenko, N. (2001) *Icarus, 149*, 329-338. [13] Wilcox, B., et al. (2005) *Met. Planet. Sci., 40*, 695-710. [14] Shoemaker, E., and Morris, E. (1970) *Icarus, 12*, 188-212. [15] Morris, E., and Shoemaker, E. (1970) *Icarus, 12*, 173-187. [16] Bart, G., and Melosh, H. (2005) LPSC XXXVI, Abstract 2022. [17] Bart, G., and Melosh, H. (2007) LPSC XXXVIII, Abstract 1501. [18] Bart, G. (2007) Dissertation, University of Arizona. [19] Cintala, M., and McBride, K. (1995) NASA TM 104804. [20] Thompson, T., et al. (1979) *Moon and Planets, 21*, 319-342. [21] Moore, J. (1971) NASA SP 232, 26-27. [22] Muehlberger, W., et al. (1972) NASA SP-315, 6-1 to 6-81, 1972. [23] Swann, G., et al. (1971) NASA SP-272, 39-86. [24] Swann, G., et al. (1972) NASA SP-289, 5-1 to 5-112. [25] Morris, E., and Shoemaker, E. (1970) *Icarus, 12*, 167-172. [26] Schultz, P., et al. (1977) *Proc. Lunar Sci. Conf 8th*, 3539-3564. [27] Boyce, J. et al. (1974) *Proc. Lunar Sci. Cong. 5th*, 11-23. [27] Chapman, C. et al. (1970), *JGR, 75*, 1445-1466. [29] Greeley, R., and Gault, D. (1970) *The Moon, 2*, 10-77. [30] Hartmann W. et al. (1981) Basaltic Volcanism on the Terrestrial Planets, 1049-1127. [31] Hiesinger, H., et al. (2000) *JGR, 105*, 29239-29275. [32] Hiesinger, H., et al. (2003) *JGR, 108*, doi:10.1029/2002JE001985. [33] Gault, D. (1970) *Radio Science, 5*, 273-291. [34] Pike R. (1977) *Proc. Lunar Sci. Conf. 8th*, 3427-3436. [35] Pike, R. (1974) *GRL, 1*, 291-294. [36] Pike, R. (1980) USGS Prof. Paper 1046-C. [37] Pike, R. (1985) *Meteoritics, 20*, 49-68. [38] Pike, R., (1971) *Icarus, 15*, 384-395. [39] Smith, E. (1976) *Icarus, 28*, 543-550. [40] Soderblom, L. (1970) *JGR, 75*, 2655-2661. [41] Moore, H., and Tyler, G. (1973) NASA SP-330, 33-17 to 33-26. [42] Tyler, G., et al. (1971) *JGR, 76*, 2790-2795. [43] Lucey, P. (2004) *GRL, 31*, doi;10.1029 / 2003GL019406. [44] Lucey, P., et al. (2000) *JGR, 105*, 20377-20386.

LRO/LAMP Expected Data Products: Overview of FUV Maps and Spectra. K. D. Retherford[1], G. R. Gladstone[1], S. A. Stern[2], D. E. Kaufmann[2], J. Wm. Parker[2], A. F. Egan[2], T. K. Greathouse[1], M. H. Versteeg[1], D. C. Slater[1], M. W. Davis[1], A. J. Steffl[2], P. F. Miles[1], D. M. Hurley[3], W. R. Pryor[4], A. R. Hendrix[5], P. D. Feldman[6], [1]Southwest Research Institute (6220 Culebra Rd. San Antonio, TX 78228; kretherford@swri.edu), [2] Southwest Research Institute (1050 Walnut St., Suite 300, Boulder, CO 80302), [3] The Johns Hopkins Applied Physics Laboratory (11100 Johns Hopkins Rd., Laurel, MD 20723), [4]Central Arizona College (8470 N. Overfield Rd., Coolidge, AZ 85228), [5]Jet Propulsion Lab. (4800 Oak Grove, Dr., Pasadena, CA 91109), [6]The Johns Hopkins University (3400 N. Charles St., Baltimore, MD 21218).

Introduction: The Lunar Reconnaissance Orbiter (LRO) Lyman-Alpha Mapping Project (LAMP) is a UV spectrograph (Figure 1) designed to address how water is formed on the moon, transported through the lunar atmosphere, and deposited in permanently shaded regions (PSRs)[1]. Its main objectives are to 1) identify exposed water frost in PSRs, 2) characterize landforms and albedos in PSRs, 3) demonstrate the feasibility of using natural starlight and sky-glow illumination for future lunar surface mission applications, and 4) assay the lunar atmosphere and its variability.

The production and transport of lunar atmosphere constituents (e.g., H, Ar, and potentially others) will be investigated by observation of their resonantly scattered FUV emissions. LAMP albedo maps of PSR landforms and potential surface water ice will be used to investigate the intriguing processes that occur within PSRs. Potential sites of active outgassing such as the Aristarchus crater and the Ina structure [2] are targets of special interest for LAMP spectral map products.

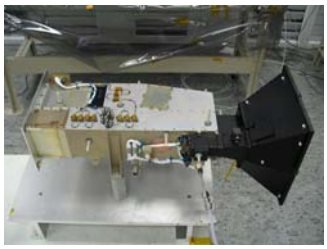

Figure 1. LAMP instrument prior to shipment.

Data Products: LAMP high-level data products (Table 1) include brightness maps (global and of selected features) over specific wavelength ranges, similarly constructed albedo maps (i.e., brightness maps normalized by the illumination), band depth maps (i.e., maps of the ratio between albedo maps for wavelength ranges on and off important absorption bands such as water frost), and atmospheric spectra of global and specific features (e.g., the dawn terminator, the LCROSS impact site, regions of possible outgassing).

The maps use low-level pixel lists from which individual FUV photon events are selected for inclusion based on criteria such as timing, wavelength, emission and incidence angles, and spacecraft location. The mapping products follow the polar stereographic and equirectangular projections planned for the LOLA instrument. Each surface element is populated for the conditions of the selected criteria. Wavelength information is maintained by storing the maps as spectral data cubes (i.e., [X,Y,λ]).

For the albedo and band depth maps, an important intermediate product is the sky illumination as a function of wavelength and time for each surface element of interest. On the nightside these include Lyman-α sky-glow, UV starlight, and, for near-terminator regions, scattered sunlight. On the dayside the illumination is the solar FUV flux, with crater shadowed regions removed from the compilation maps. The high-level data products will be produced regularly during the nominal mission, but will be refined after the end of the nominal mission to include important inputs from other LRO instruments (e.g., surface roughness and slope estimates from LOLA).

Name	Description
Engineering Level Data	Instrument value science data (raw photon events, pixel list & spectral images)
Science Level Data	Calibrated value science data (tabulated pixel list & spectral images)
Far-UV Brightness Map	2D lunar surface map of UV brightness
Landform Albedo Map	2D lunar surface map of UV albedos
H_2O Absorption Feature Depth Map	2D lunar surface map of H_2O absorption feature depths, first-order H_2O surface mixing ratios
Atmospheric Nadir Spectra	Near-terminator spectra of atmospheric constituents
Atmospheric Limb Spectra	Atmosphere limb brightness profiles

Table 1. LAMP data products to be archived in the PDS Imaging Node.

References: [1] Gladstone, G. R., and 15 coauthors (2009) *submitted to Space Sci. Rev.* [2] Schultz, P.H., Staid M. I., and Pieters C. M. (2006) *Nature*, *444*, 185-186.

Lunar basalts as probes of the Moon's mantle and recorders of crustal growth. C.K. Shearer, Institute of Meteoritics, Department of Earth and Planetary Sciences, University of New Mexico, Albuquerque, New Mexico 87131 (cshearer@unm.edu).

Introduction: Secondary crust that was added to the primary lunar crust was a product of melting of a lunar mantle that was already processed during the initial stages of lunar differentiation (most likely through a planetary-scale magma ocean (LMO)). Lunar secondary crust formation is essentially basaltic in nature, started soon after the formation of the primary crust and continued for approximately 3.5 billion years. The distribution, mineralogy, composition (elemental and isotopic), and chronology of basaltic lithologies making up the secondary crust provides a record of the composition and chemical evolution of the mantle, thermal history of the Moon, and growth of the lunar crust. In this presentation, we will examine the diversity of the Moon's secondary crust, provide examples of its usefulness in reconstructing the history of the lunar mantle, and suggest potential sites on the lunar surface that may provide additional insights into unresolved problems related to the thermal and magmatic history of the Moon.

Diversity of lunar magmatism: Although the Moon is a relatively simple body compared to many of the terrestrial planets, the composition of the secondary crust generated from it's mantle is extraordinarily diverse. The earliest stages of post-LMO magmatism are preserved in the magnesian suite. These are plutonic rocks (dunites, troctolites, norites, gabbronorites) that represent basaltic magmas that were emplaced into a primary crust consisting of ferroan anorthosites. These plutonic rocks exhibit an interesting dichotomy of geochemical signatures that include mafic silicates with high Mg#, low Ni and high incompatible elements (KREEP geochemical fingerprint). These petrologic contrasting mineralogical and geochemical signatures may reflect mixing of distinctly different LMO cumulate horizons within a dynamic lunar mantle [1-3]. The alkali suite of plutonic rocks has more evolved mafic silicate (lower Mg#) and plagioclase (lower An) compositions with elevated incompatible element abundances. Samples that represent this suite have crystallization ages that generally overlap or are younger than the magnesian suite [4,5]. The earliest periods of lunar volcanism (3.84-4.3 Ga) are represented by the high-Al basalts and the Apollo 15 and 17 KREEP basalts [summaries in 6,7]. The KREEP basalts have been petrogenetically linked to the both the magnesian and alkali plutonic suites [4-7]. Basaltic magmatism with a KREEPy geochemical signature should not be ascribed to only early periods of lunar magmatism. In lunar meteorites, basalts with KREEPy signatures have crystallization ages of approximately 3 Ga and remotely sensed data suggests young lunar basalts (≈ 1 Ga) are associated with lunar terrains with high Th (and presumably high-KREEP) [7-9]. Mare volcanic effusive activity reached a peak in output between 3.8-3.5 Ga [7,9,10]. The volcanic output of mare magmas prior to 3.8 Ga is not well documented, whereas after 3.5 Ga smaller pulses of mare basalts erupted into basins as late as 1.2 Ga. One of the most striking compositional characteristics of the crystalline mare basalts and their pyroclastic equivalents (i.e. picritic volcanic glasses) is the variation in TiO_2. TiO_2 ranges from 0.2 wt. % in very low-Ti crystalline basalts and volcanic glasses to almost 17% in volcanic glasses associated with pyroclastic deposits [6,7,11]. By far, this exceeds the range observed in planetary basalts on all other terrestrial planets that have been sampled. The volcanic glasses associated with pyroclastic deposits implies eruption and fragmentation driven by volatiles derived from the lunar interior.

Reconstructing the thermal and magmatic evolution of the Moon: Samples of lunar basaltic magmas provide significant insights into the nature of the lunar interior. Observations such as nearly ubiquitous negative Eu anomalies, positive ε_{Nd} values, large range of TiO_2, and very low CaO and Al_2O_3 indicate that the mare basalts were derived from the melting of LMO cumulates produced during early lunar differentiation [7]. Some of the geochemical dichotomy observed in both the magnesian suite and mare basalts suggests cumulate source mixing or "fertilization" prior to melting [7,12-14]. One mechanism for this mixing/fertilization is overturn of LMO cumulates in response to density and temperature variations in the LMO cumulate pile. Experimental data can be interpreted as indicating that some the mare basalts were produced by melting initiated deep in the lunar mantle (>500 km), the mantle sources were "undersaturated" with regards to plagioclase, high-Ca pyroxene, and ilmenite, and (combined with compatible elements) the low Ti basalts were derived from a limited stratigraphic section of a olivine-orthopyroxene dominated LMO cumulates.

What is the nature and origin of lateral asymmetry in the Moon's mantle and its relationship to the well-defined crustal asymmetry: *Magnesian suite:* As stated above, plutonic rocks that make up this

suite represent the earliest phases of secondary crust formation. Further, their KREEP signature has been interpreted as indicating that the petrogenesis of their parent magmas is intimately related to KREEP and heat-producing elements. Following this line of reason, it would be expected that these plutonic lithologies should be geographically restricted to the Procellarum-KREEP terrane (PKT). Alternatively, the generation of the magnesian suite magmas may be unrelated to KREEP in other terranes outside the PKT. In this case, the KREEP is not the "driver" of magnesian suite petrogenesis but only the "passenger". Understanding this association is fundamental to deciphering the relationship among heat producing elements in the lunar interior, thermal history, and the generation of the first episode of secondary lunar crustal growth. Exploring central peaks outside of the PKT terrane that consist of dunites, troctolites, or norites [15,16] would be an important step in deciphering the relationship between heat-generating elements and thermal history.

Mare magmatism: A fundamental observation is that near side basalts are widespread, diverse, span a range of ages, and are spatially associated with crustal terranes with high abundances of heat-producing elements, whereas far side basalts are few, spotty, occur primarily in basin such as SPA, Moscoviense, and Tsiolkovskiy [7,9,10]. This correlation may be attributed to lower heat production in the far side mantle due to the migration of radioactive elements (K, U, Th) toward the near side mantle and the PKT. There are two other alternatives to this model. First, the heat sources in the far side mantle may be just as abundant as in the near side mantle, but lie deeper or are more diffuse than in the near side mantle, leading to differences in mantle dynamics and/or the volume of magma generated. A second alternative is that the same volume of basalts were produced in the far side mantle but a thicker overlying lithosphere allowed only a small volume of rather fractionated magmas to erupt.

What is the nature of volatiles in the lunar mantle, their role in driving mare volcanism, and their potential as a resource: The general consensus among lunar scientist has long been that the bulk composition of the Moon is depleted in volatile elements [17]. However, pyroclastic deposits sampled by Apollo 15 and 17 missions provided evidence for volatile-driven fire-fountaining on the lunar surface. Orbital observations indicate that these deposits are not unusual in occurrence or insignificant in volume (>2500 km^2) [18]. Volatile element coatings on volcanic glass surfaces from these deposits hint at the nature of eruptive mechanisms and potential volatile reservoirs in the lunar mantle. For example, stability of chlorides (such as $ZnCl_2$) on volcanic glass surfaces and the fractionation of Cl isotopes suggest HCL and the HCl/H_2S may play roles in the eruptive process [11,19-21]. More recently, the role of H_2O in lunar fire-fountaining has been explored [22]. The occurrence of large volatile-rich pyroclastic deposits may be a future resource for human occupancy and sustainability on the Moon. Exploring large pyroclastic deposits would provide scientific value (i.e. origin of the Earth-Moon system, volatile reservoirs in the lunar interior) and an assessment of the scale and economic potential of available resources. Potential targets for further exploration could be the large pyroclastic deposit identified on the Aristarchus Plateau or at Rima Bode [18].

How do lunar basalt compositions changes with time: Lunar basalts provide a 3.5 billion year record of the thermal-magmatic evolution of the Moon. Yet, over half of this record is missing in the sample collection. We only have a limited glimpse of the style of magmatism that preceded the large eruptive pulse of mare volcanism at 3.8 Ga. What are the petrogenetic linkages between this large pulse of mare magmatism and earlier periods of lunar magmatism? What is the relationship between the high-Al and older KREEP basalts indentified in the Apollo sample collection and the cryptomare identified by orbital observations? The small volumes of basalts erupted after 3.1 Ga have a limited representation in the meteorite collection. Yet, these missing basalts are fundamental to understanding mantle sources and melting processes as the lunar thermal-magmatic system winds down. Targeting both the youngest (e.g. Lichtenberg) and oldest lunar basalt (e.g. Balmer-Kapteyn) would allow a richer understanding of the thermal-magmatic history of the Moon.

References: [1] Warren, P.H. (1988) PLPSC 18, 233-241. [2] Shearer, C.K. and Papike, J.J. (2005) GCA 69, 3445-3461. [3] Longhi, J. et al. (2009) GCA 73, in press. [4] Snyder, G.A. (1995) GCA 59, 1185-1203. [5] Warren, P.H. and Wasson, J.T. (1979) PLPSC 10, 583-610.[6] Papike, J.J. et al. (1998) in Planetary Materials (ed. J.J. Papike) 5-1 - 5-234. [7] Shearer et al. (2006) In New Views of the Moon (eds. B.L. Jolliff, M.A. Wieczorek, C.K. Shearer, C.R. Neal) 365-518 [8] Borg, L.E. et al. (2004) Nature 432, 209-211.[9] Hiesinger, H. et al. (2003) JGR 108, doi 10.1029/2002JE001985. [10] Head, J.W. and Wilson, L. (1992) GCA 56, 2155-2175. [11] Delano, J.W. (1986) PLPSC 16, D201-D213. [12] Snyder, G.A. et al. (2000) In Origin of the Earth and Moon (eds. R.M. Canup and K. Righter) 361-396. [13] Hess, P.C. (1991) GRL 18, 2069-2072. [14] Shearer et al., (1991) EPSL 102, 134-147. [15] Pieters, C.M. and Tompkins, S. (1999) JGR 104, 21935-21949. [16] Cahill, J.T (2008) LPSC XXXIX, abst.# 1398. [17] BVSP (1981) Section 1.2.9. [18] Gaddis, L.R. et al. (1985) Icarus 61, 461-489. [19] McKay, D. et al. (1973) PLSC 4, 225-238. [20] Colson, R.O. (1992) PLPSC 22, 427-436. [21] Sharp, Z. (2009) LPSC XL, abst.#2351. [22] Saal et al. (2008) Nature 454, 192-195.

LROC TARGETING OF LUNAR DOMES, CONES, AND ASSOCIATED VOLCANIC FEATURES.

J. D. Stopar[1], B. R. Hawke[2], S. J. Lawrence[1], M. S. Robinson[1], T. Giguere[2], L. R. Gaddis[3], B. L. Jolliff[4], [1]School for Earth and Space Exploration, Arizona State University, Tempe, AZ. [2]Hawaii Institute for Geophysics and Planetology, University of Hawaii, Honolulu, HI. [3]Astrogeology Program, U.S. Geological Survey, Flagstaff, AZ. [4]Dept. Earth and Planetary Sciences, Washington University, St. Louis, MO. (jstopar@asu.edu)

Introduction: The Lunar Reconnaissance Orbiter Camera (LROC) is one of seven instruments aboard the Lunar Reconnaissance Orbiter (LRO). The first year of the LRO mission is focused on exploration objectives enabling future human exploration and utilization of the Moon; it is expected that the nominal exploration mission will be followed by a multi-year extended mission with a focus on scientific objectives. The LROC cameras are ideally suited to these tasks with the two Narrow-Angle Camera (NACs) providing ~0.5m/pix resolution in a combined 5×25-km swath, and the Wide-Angle Camera (WAC) providing ~100m/pix resolution in five VIS bands and ~400m/pix in two UV bands with 60-km wide footprints (in color imaging mode) for context imaging and composition [1]. Occasional stereo image sets (both geometric and photometric) are possible with the NACs but will be limited to select sites due operational constraints [2]. Domes, cones, and associated volcanic features (e.g., sinuous rilles, depressions, vents, and collapsed lava tubes) are important as potential exploration sites, in part because of the potential for resources associated with these features, and because they represent a high-viscosity volcanic end-member that may yield information about the volcanic history of the Moon. Several prominent domes (e.g., Marius Hills, Gruithuisen Domes, and Rümker Hills) appear on the preliminary Project Constellation (Cx) "Priority 1" targeting list as possible sites for future human exploration [3].

The Marius Hills Example: The Marius Hills region is a volcanic plateau in Oceanus Procellarum that contains the highest concentration of low-relief domes, cones, sinuous rilles, and depressions, which may provide clues to the lunar interior, evolution, and volcanic history. Because these types of volcanic features are relatively rare on the Moon, they have immense scientific value that makes them important targets for the LROC cameras.

Previous studies of the Marius Hills utilized telescopic, Lunar Orbiter, Apollo, and Clementine imagery to study the morphology and composition of the volcanic features in this region [e.g., 4-12]. The discussion focused on the method of formation for the domes and cones. One theory suggests that the domes are of different composition (more silicic) than the surrounding mare [6]. The opposing (and now favored) theory suggests that the domes formed via eruptions with a lower effusion rate (i.e., a low-temperature, high crystal-content lava) rather than with lava of a more silicic composition [7-10, 12]. Two different types of domes have been identified in Marius Hills: low domes and steep-sided domes [6]. The range in dome morphologies might imply a range of eruption styles and effusive events over a long period of time [10-11]. In addition to the domes, cones with a "classic cone" morphology, possibly constructed from pyroclastic materials, are present in the Marius Hills (e.g. Fig 1). LROC will contribute to previous studies by providing new high-resolution NAC (~0.5m/pix) images that may resolve dome flow-fronts and cone details as well as WAC multispectral UV/VIS imaging for regional context imaging and compositional information.

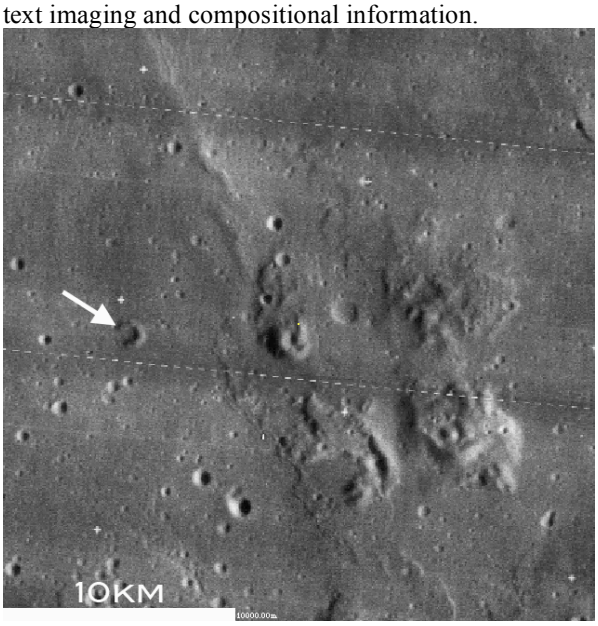

Figure 1: Example of domes and a cone (arrow) in the Marius Hills (14.77°N, -56.55°E). [Lunar Orbiter basemap, USGS]

Targeting Strategy: In the Marius Hills alone, more than 80 domes and 15 cones were identified for NAC imaging (~50 sites are shown in Fig 2) from [4, 10-12]. The Marius Hills targets cover the morphologic array from low dome, to steep-sided dome, to the "classic" cone, and include features with central pits. Additional targets focus on sinuous rilles, depressions, and possible lava tubes. The bulk of the LROC NAC requested observations favor morphology (with incidence angles typically between 45° and 80°) in order to study flow fronts, layering, dome and/or cone structure, and su-

perposition relationships with the surrounding basalts. In addition, several key LROC NAC targets request geometric and photometric stereo for morphological dome and cone archetypes. These requested stereo observations could provide image sets with m-scale topography [1].

Other Lunar Domes: Many domes and related volcanic features are found in areas other than the Marius Hills region on both the lunar near- and farsides [11-14]. These domes could result from a wide variety of extrusive or intrusive eruption mechanisms and may consist of a wide range of materials.

Targeting Strategy: Several hundred domes, cones, and associated volcanic features are currently targeted by the NACs, with more being added every week. These domes extend over a wide latitude distribution, and the lighting conditions available at each location will vary during imaging. In general, LROC NAC domes and other volcanic feature targets will be imaged at both high and low sun angles to emphasize both morphology and albedo variations. In addition, each location will have associated multispectral WAC imaging.

Summary of Targeting Objectives: Studies of lunar domes and related volcanic features with LROC images may provide clues into the interior and evolution of the Moon as well as the composition of the lunar crust. LROC NAC images have the potential to provide new insight into the structure of lunar domes and cones including lava or pyroclastic layering, flow fronts, and vent morphology. In addition, NAC images can be used to search for small, short-lived pyroclastic deposits that did not result in cone formation [e.g., 10] and investigate the nature of "dark spots" that may be associated with lunar cones [e.g., 9]. Finding these small features would provide important insight into how domes and cones form. LROC WAC multispectral data (particularly in the UV) will provide a measurement of the color variations within and amongst deposits and possibly allow interpretations of the composition of lunar volcanic features [1].

The scientific importance of the Marius Hills region makes it a prime candidate for future human exploration. The Marius Hills offer considerable resource potential, including easy access to Ti-rich mare regolith, the potential presence of easy-to-process pyroclastic materials, and the inferred presence of lava tubes that could be used as convienent locations for human habitats [15]. LROC data will be used to place important constraints on the availability and accessibility of these exploration-enabling resources.

LROC NAC and WAC images will complement Apollo and Lunar Orbiter imagery as well as the multispectral global Clementine dataset, which are the basis for much of our current knowledge about morphology and distribution of domes and volcanic features on the Moon. Spacecraft imagery has been greatly aided by recent Earth-based telescopic and radar efforts [13-14, 16]. Interpretations of domes and associated volcanic features will also be greatly aided by new imagery and multispectral datasets from Kaguya and Chandrayaan-1 [e.g., 17-20].

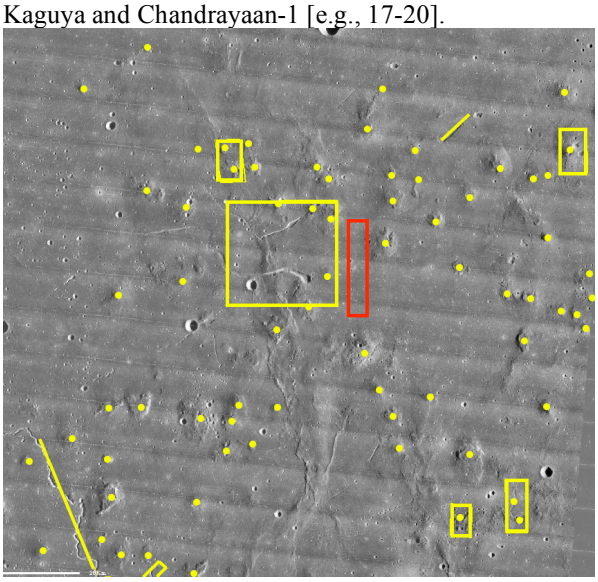

Figure 2: A portion of the Marius Hills region (centered at 13.36°N, -55.75°E) showing NAC target requests (yellow) and dual NAC 5×25-km NAC footprint (red) for scale. Small boxes outline geometric and photometric stereo requests. Yellow lines and the large box just off-center highlight NAC target requests for rilles and depressions. [Lunar Orbiter basemap, USGS]

References: [1] Robinson M. S. et al. (2005) *LPSC XXXVI* #1576. [2] Lawrence S. J. et al. (2009) *LPSC XL* #2316. [3] Jolliff B. L. et al. (2009) *LPSC XL* #2343. [4] Greeley R. (1971) *Moon, 3,* 289-314. [5] Guest J. E. (1971) *Geol. and Phys. of the Moon*, Elsevier, p. 41-53. [6] McCauley J. F. (1967) *USGS Geologic Atlas of the Moon*, Sheet I-491. [7] Head J. W. et al. (1978) *LPSC IX* 488-489. [8] Gillis J. J. and P. D. Spudis (1995) *LPSC XXVI* 459-460. [9] Weitz C. M. and J. W. Head (1999) *JGR, 104,* 18933-18956. [10] Heather D. J. et al. (2003) *JGR*, doi:10.1029/2002JE001938. [11] Whitford-Stark J. L. and J. W. Head (1977) *Proc. LSC VIII*, 2705-2724. [12] Head J. W. and A. Gifford (1980) *Moon and Planets 22,* 235-258. [13] Wohler C. et al. (2006) *Icarus, 183*, 237-264. [14] Wohler C. et al. (2007) *Icarus, 189*, 279-307. [15] Coombs C. R. and Hawke B. R. (1992) *2nd Conf. Lun. Base and Space Act. 21st Cent., 1,* 219-229. [16] Campbell B. A. et al. (2009) *JGR*, doi:10.1029/2008JE003253. [17] Haruyama J. et al. (2009) *Science, 323,* 905-908. [18] Bussey D. B. J. et al. (2008) *Lunar Sci Conf* #2083. [19] Pieters C. M. et al. (2007) *LPSC XXXVIII* #1295. [20] Matsunaga T. (2008) *Geophys Res. Lett.* doi:10.1029/2008GL035868.

LUNAR SINUOUS RILLES: REASSESSING THE ROLE OF EROSION BY FLOWING LAVA. D. A. Williams[1], W. B. Garry[2], L. P. Keszthelyi[3], R. C. Kerr[4], W. L. Jaeger[3], [1]School of Earth & Space Exploration, Arizona State University, Tempe, AZ 85287-1404 (David.Williams@asu.edu), [2]Center for Earth & Planetary Studies, Smithsonian Institution, Washington, D.C. (GarryW@si.edu), [3]Astrogeology Team, U.S. Geological Survey, Flagstaff, AZ (laz@usgs.gov, wjaeger@usgs.gov), [4]Research School of Earth Sciences, Australian National University, Canbera, Australia (Ross.Kerr@anu.edu.au).

Introduction: Erosion by flowing lava is known to incise relatively shallow (meter-scale) troughs into substrates ranging from basalt to carbonatite and sulfur [e.g., 1-3], and is thought to have carved larger (tens to hundreds of meters deep) channels in some historic basalt lava tubes [4] and prehistoric komatiite lava channels [5-6]. Previous workers suggested that low-viscosity lunar mare lavas, rheologically similar to terrestrial komatiites, could have produced the lunar sinuous rilles by lava erosion, either under the turbulent [7] or laminar [8] flow regimes. Two of us have developed more rigorous analytical-numerical models to constrain erosion by lava in either flow regime [9, 10] which, when constrained by appropriate field data (e.g., flow thickness, channel dimensions, lava and substrate compositions and degrees of consolidation), can provide useful estimates of erosion depth, degrees of contamination, and other parameters as a function of flow rate and distance downstream. We propose that the *Lunar Reconnaissance Orbiter* Camera's (LROC) Narrow Angle Camera (NAC) target portions of selected lunar sinuous rilles to obtain stereo images of channel widths and depths, and potential outcrop layer thicknesses, in specific sinuous rilles to constrain lava flow rates for our modeling. In this abstract we discuss our approach, focusing on one already high-priority LROC target, Schröter's Valley on the Aristarchus Plateau (**Fig. 1**), which can be used to assess erosion by mare lava over both highlands and pyroclastic substrates.

Previous Modeling: Our analytical-numerical models were developed to assess the degree of erosion by low-viscosity, turbulently-flowing terrestrial komatiites [9, 11] and laminarly-flowing basalts and carbonatites [10, 12] lavas over a variety of substrates. The turbulent flow model of *Williams et al.* was adapted to assess erosional lava channel formation on Io, Mars, and for the Moon, in the latter case focusing on erosion by mare basalt lavas on mare basalt substrate [13]. An aspect of lunar sinuous rille formation that has not been studied is the nature of erosion by a mare basalt lava flowing over highlands material of different composition, or erosion of a glassy pyroclastic deposit. Our models were previously adapted to examine these scenarios on Earth [11, 12], and can be modified relatively easily to assess these scenarios on the Moon. Previous analyses of *Apollo* samples can provide physical and chemical constraints on lunar highland materials and pyroclastic glasses.

LROC Imaging: The key parameter to evaluate better the nature of erosion in lunar sinuous rilles via our models is an estimate of the range of lava flow thicknesses, which serve as a proxy for lava flow rates. These thicknesses can be estimated from images of lava flow outcrops exposed on the sides of the lunar sinuous rilles, such as that seen in Hadley Rille by *Apollo 15* astronauts (**Fig. 2**).

Outlook: Topographic data derived from LROC NAC stereo pairs will have the potential to provide additional information on lava flow thicknesses in lunar sinuous rilles, as well as on the morphological structure of the rilles. This information will serve as key input data for our models of the lava erosion process, which will provide further constraints on the styles, duration, and extents of lunar mare volcanism.

References: [1] Peterson, D.W. and Swanson, D.A. (1974) *Stud. Speleol. 2*, 209-222; Kauahikaua, J. et al. (1998) *JGR 103*, 27,303-27,324. [2] Dawson, J.B. et al. (1990) *Geology 18*, 260-263. [3] Harris, A.J.L. et al. (2000) *Geology 28,* 415-418. [4] Greeley, R. and Hyde, J.H. (1972) *Geol. Soc. Am. Bull. 83,* 2397-2418. [5] Lesher et al. (1984) in *Sulphide Deposits in Mafic and Ultramafic Rocks*, Inst. Min. and Metall., London, 70-80. [6] Barnes, S.J., et al. (1988) *J. Petrol 29*, 302-331. [7] Hulme, G. (1973) *Mod. Geol. 4*, 107-117. [8] Carr, M.H. (1974) *Icarus 22*, 1-23. [9] Williams, D.A. et al. (1998) *JGR 103, B11*, 27,533-27,549. [10] Kerr, R.C. 2001) *JGR 106*, 26,453-26,465. [11] Williams, D.A., et al. [2002] *JVGR 110(1-2)*, 27-55. [12] Kerr, R.C. (2009) *JGR*, in review. [13] Williams, D.A. et al. (2000) *JGR 105*, 20,189-20,206.

Figure 1. *Apollo 15* Metric camera image of the Aristarchus Plateau on the lunar nearside. For scale, crater Aristrachus at left is 40 km in diameter. The Aristarchus Plateau is about 200 km across, and is thought to be composed of crustal material uplifted, tilted, and fractured by the Imbrium impact event. At center right is Schröter's Valley, a rille that is about 160 km long, up to 11 km wide and 1 km deep, and contains an inner sinuous rille. The plateau is cover by a pyroclastic deposit thought to be composed of Fe-rich glass spheres, visible in multispectral data. High-resolution LROC-NAC imaging at 50 cm/pixel could reveal outcrops in the walls of Schröter's Valley, which can constrain our models of lava erosion and lava flow emplacement. Photo AS15-M-2610.

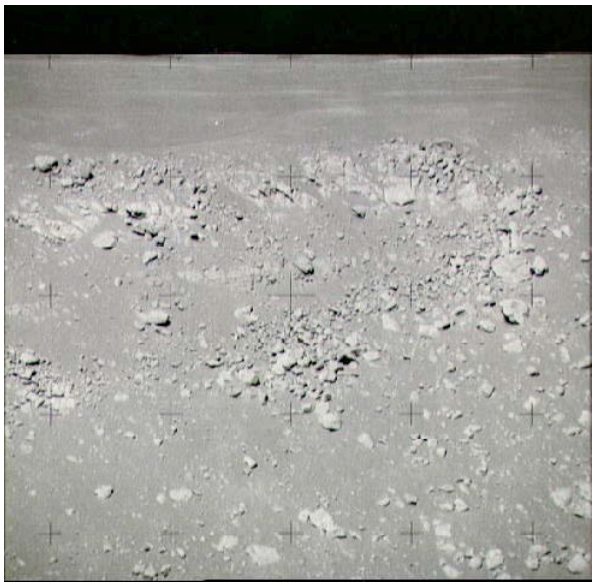

Figure 2. A telephoto lens view looking across Hadley Rille, photographed during the third *Apollo 15* lunar surface extravehicular activity (EVA-3) at the Hadley-Apennine landing site on the lunar nearside. The blocky outcrop at the top of the west wall of the rille is about 1.9 kilometers from the camera. About one-half of the debris-covered wall is visible in the photograph. Smaller outcrops of lava flows could be exposed in other sinuous rilles and can be imaged by LROC-NAC (spatial resolution 0.5 m/pixel). Photo AS15-89-12157.

COORDINATING LOIRP ENHANCED LUNAR ORBITER AND LUNAR RECONNAISSANCE ORBITER HIGH RESOLUTION IMAGES FOR SELECTED SCIENCE AND EXPLORATION TARGETS. D. R. Wingo[1] and C. A. Lundquist[2], [1]Skycorp Incorporated, NASA Ames Research Park, Building 596, Moffett Field, CA 94035 (wingod@earthlink.net), [2]University of Alabama in Huntsville, 500 North Sparkman Drive, Huntsville, AL 35899

Introduction: The Lunar Orbiter Image Recovery Project (LOIRP), located at the NASA Ames Research Park is in the process of digitizing the original analog tapes of the Lunar Orbiter (LO) image database. This new resource of 43 year old LO images are being digitized in a manner that will foster their utility for comparison with the output of the Lunar Reconnaissance Orbiter Camera (LROC)

In order to meet on of the LROC's main exploration goals of ascertaining the hazards of small meteors for crew operations, the oldest and highest resolution datasets must be used. The LOIRP recovered images from the five Lunar Orbiters meet this criterion.[1]

LO 35mm Film vs Analog Tape Derived Quality: The five LO spacecraft, who's missions were flown in the period of August 1966 to August of 1967 are still to this day the highest resolution visible light images taken of the lunar surface in the near side equatorial region of the Moon as well as other selected regions.[2]

The LO spacecraft used SO-243 70 millimeter film coupled to a 610mm optical system for high resolution imaging. The SO-243 film, with a granularity for LO of 286 lines/mm provided images with four lines per meter on the lunar surface.[3] The LO spacecraft, flying at a periselene altitude of ~40 km on the near side equatorial region photographed several thousand square kilometers at this resolution.

The existing imagery in the Planetary Data System (PDS) and other archives are based upon a 35mm film reconstruction of the LO 70mm film. The 70mm film was electronically scanned on the spacecraft, transmitted to the Earth as an analog signal, demodulated, and reconstructed through three generations of equipment to arrive at the 35mm filmsets. These filmsets have subsequently been scanned by various efforts over the years to arrive at our current datasets.

While these digital datasets are the best that can be derived from the 35mm film, the film itself was not the best representation of the quality of the data. A group of ~1500 2" analog tapes were made in parallel with the 35mm film from the predetected (before baseband conversion and demodulation) analog data stream. In 2008 LOIRP project successfully restored an Ampex FR-900A tape drive of the same type that originally recorded these images. We have also successfully reconstructed the LO demodulator and have confirmed the higher dynamic range of the analog tape based data.[4] The following image shows a comparison between the LPI LO-III-162-H3 and the LOIRP image recovered from the undemoulated analog tapes:

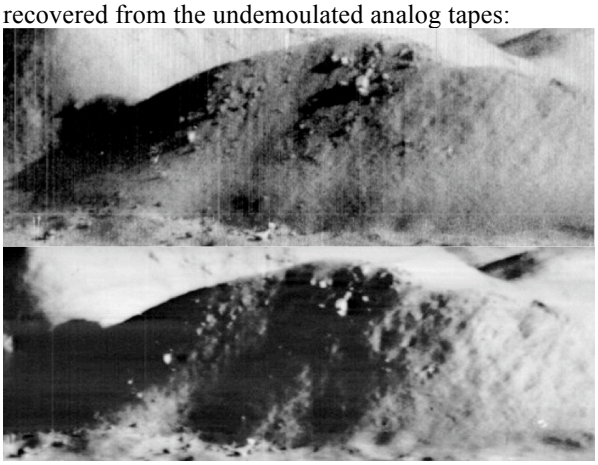

LOIRP (top) vs GRE Copernicus Uplift Image

The reason for the striking difference in the grey scale values in the above images is that during the reconstruction process, the whitest whites and blackest blacks were clipped due limitations in the 35mm film based Ground Reconstruction Equipment (GRE).[5] This is shown below:

Gray Step No.	SO-243 R/O Density Range	Reassembled Record Density Range
1	0.21 - 0.29	Clipped by GRE
2	0.26 - 0.34	1.89 - 2.11 (clipped if R/O density below 0.30)
3	0.34 - 0.42	1.64 - 1.82
4	0.45 - 0.57	1.33 - 1.49
5	0.61 - 0.73	0.99 - 1.13
6	0.82 - 0.94	0.66 - 0.80
7	1.05 - 1.21	0.50 - 0.60
8	1.32 - 1.48	0.42 - 0.50 (may be clipped)
9	1.40 - 1.56	Clipped by GRE

Dynamic Range Clipping of LO 35mm Film

The above gray step data is derived from the calibration blocks on each framelet of LO data and represent the difference in dynamic range between the 35mm GRE film and the analog data on the 2" LO tapes. As can be readily seen above, as well as in the full images, the increased dynamic range brings out subtle details (shadows emanating from boulders on the central uplift of Copernicus for example) that are simply impossible to see on the 35mm film, no matter how expertly reprocessed and digitized.

LOIRP Images as Applied to LROC Mission Goals: One of the six primary goals of the LROC camera is *"Meter-scale coverage overlapping with Apollo era Panoramic images (1-2 m/pixel) to document the number of small impacts since 1971-1972, to ascertain hazards for future surface operations and interplanetary travel".*[6] The LOIRP image database, as it is digitized will allow a direct mapping of the LROC images to the corresponding LO images. The LOIRP software team are currently working with Apple computer to develop the software and methodology for automated creation of LO images from the analog tapes. A follow on to this will be to develop the automated means of integrating LROC images with our reprocessed LO database and targeting known impacts that occurred after the LO missions.

One example of a significant historical impact was recorded on May 13, 1972 by the seismic array placed on the Moon by the Apollo missions. The impact coordinates derived from the seismic data are 1.1 N latitude and 16.9 W longitude with an uncertainty of 0.2 degrees.[7] The area of this impact was imaged by the LO imaging system to ~1 meter resolution and would be a perfect calibration target for the LROC imaging system. It is estimated that this impactor created a crater on the order of 50-100 meters, which was below the threshold of detection from Clementine. Images of this area have not been released by other nations so this will be a great test and an ideal calibration test for the LROC camera. Other impacts, such as the one personally witnessed by astronaut Dr. Harrison Schmidt during the Apollo 17 mission could also be reimaged.[8]

The LOIRP project is, as of this writing, digitizing images from LO missions I,II, and III. This includes the Apollo landing sites as well as the area of the impact identified by the Apollo seismographs. Automated methods for identifying differences between the LO other missions are being developed that will seamlessly integrate with the LROC imaging products.

By using a known post LO impact, along with others surely to be found, it is expected that the risk to the crew of small impactors can be quantified. Additionally, with the multispectral capability of the LROC camera, and with known lunar regolith color maturation rates, the number of impacts in the recent geological epoch can be estimated with a much higher confidence than before the LROC mission, when coupled with the LO analog tape dataset.

References: [1] Wingo, D.R., Cowing, K Abstract 2517 LPS XD, [2] Lunar Orbiter Catalog (1970) (TWP-70-047) October, [3][4] Ibid [1][5][6] http://lunar.gsfc.nasa.gov/lroc.html, accessed 4/22/09, [7] Latham, G.V, Ewing, M, Press, F, Sutton, G. et al, (1972) NASA SP 315, , [8] Schmidt H, Personal Communication. etc. References should then appear in numerical order in the reference list, and should use the following abbreviated style:

[1] Author A. B. and Author C. D. (1997) *JGR, 90,* 1151–1154. [2] Author E. F. et al. (1997) *Meteoritics & Planet. Sci., 32,* A74. [3] Author G. H. (1996) *LPS XXVII,* 1344–1345. [4] Author I. J. (2002) *LPS XXXIII,* Abstract #1402.

Targeted search near lunar poles for potential alteraltion products resulting from impact cratering into volatile-"rich" terrains S.P. Wright and H.E. Newsom, Institute of Meteoritics, University of New Mexico, Albuquerque, NM 87131, spwright@unm.edu

Introduction: Whereas the Moon is cold and dry, there is evidence for water ice deposited in "permanent" shadows near the poles [1]. These deposits are of interest as water reservoirs for future manned missions to the Moon, of which planning for such is a primary goal of the Lunar Reconnaissance Orbiter (LRO) [2]. As the search for water ice continues, including LCROSS [3], we propose to use LRO instrumentation to search for potential alteration products resulting from the interaction of target lunar rocks, water/ice, and heat associated with melt formation during the impact cratering process.

Proposed Processes and Targets: The study of lunar impact craters provided the early impetus to investigate terrestrial impact craters, leading to many classic studies of impact craters like the Meteor Crater [4], Ries [5,6], Manicouagan [7] and Lonar [8,9]. While most of the Moon is considered to lack volatile elements in any significant amount, there is a distinct possibility that the lunar poles contain volatile reservoirs including water ice that originally collected in permanently shadowed craters [10,11] (*e.g.*, **Figures 1-3**). The most definitive observation suggesting water ice at the lunar poles is the evidence for epithermal neutron depletions attributed to the hydrogen in the form of water molecules. The lunar poles exhibit epithermal neutron depletions attributed to the presence of water molecules [1]. The continuing processes of impact cratering at all scales, including regolith gardening by small impacts may have resulted in the formation of alteration minerals and the formation of water-bearing impact melts that could represent a substantial reservoir. In addition to being scientifically interesting, the extreme value of water as a resource for oxygen and fuel for future human solar system exploration makes the study of this potential volatile reservoir a priority. The favorable environmental conditions at the lunar poles, including the availability of continuous solar energy has led to proposals to build a lunar base on the rim of a permanently shadowed crater as part of the effort to return humans to the Moon.

A lunar base at the poles will provide unique challenges for construction, operation and scientific study related to volatile elements. In contrast to the nearly volatile-free lunar regolith at the equator, the lunar regolith at the poles may contain a completely new assemblage of volatile-bearing phases, including impact melt glasses and alteration minerals. Modeling of recent ion probe analyses of lunar glasses suggest minor amounts of indigenous water (745 ppm) may be present in the lunar interior [12]. Analysis of terrestrial impact melts and experiments has shown that substantial amounts of water (as high as 16 to 24 wt%) can be trapped in silica-rich melts [13]. Kieffer and Simonds [14] also suggested that the alteration minerals, including phyllosilicates found in the matrices of some impact ejecta blankets, such as at the Ries crater were formed by pencontemporaneous alteration during the impact process.

Radar evidence for water ice at the lunar poles has been somewhat controversial [15], though disseminated grains of ice at the 1-2% level are suggested from radar [16]. The most definitive observation suggesting water ice at the lunar poles is the evidence for epithermal neut-

Figure 1. Smart-1 image of the 19 km diameter Shackleton Crater near the lunar south pole. The south pole is about on the center of the left rim of Shackleton. The rim of Shackleton has been proposed as a possible site for a lunar base.

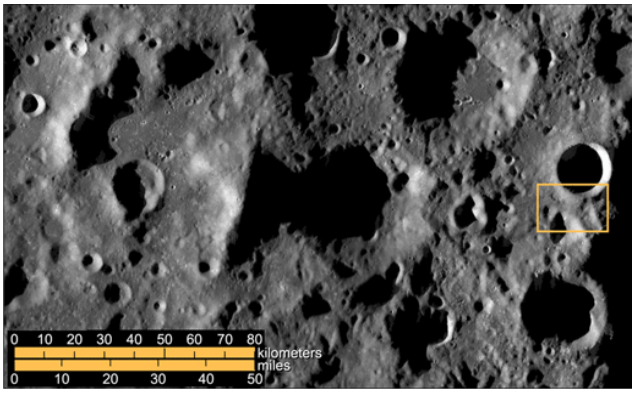

Figure 2. Radar image of the moon's rugged highly cratered south polar region, with a resolution to 20 meters per pixel, illumination is from the Earth to the left [16].

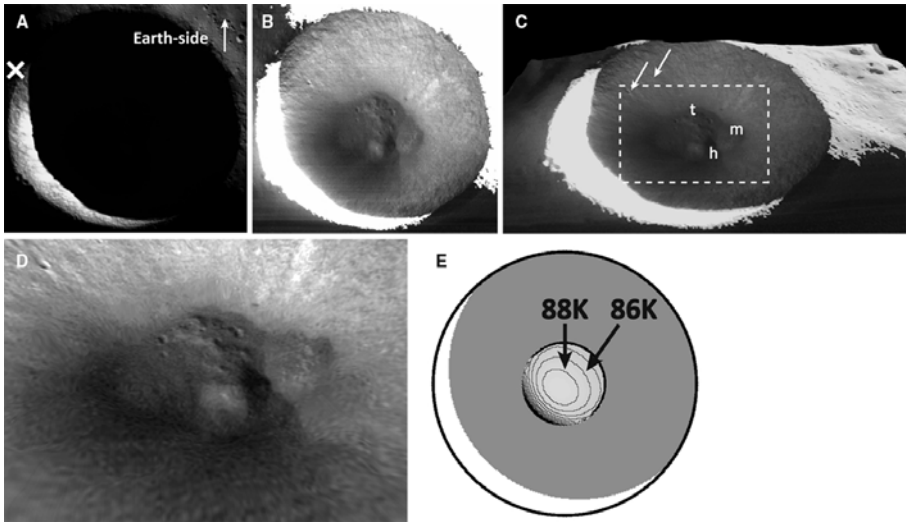

Figure 3. The ~ 19 km diameter Shackleton Crater near the lunar south pole [19]. (**A**) Image taken by the SELENE Terrain Camera (TC) on 19 November 2007. The Lunar South Pole is indicated by an 'X'. (**B**) Enhanced image of (A) with the shadowed area inside Shackleton lit by scattered light from the illuminated portion of the upper wall. (**C**) A perspective view of the Shackleton Crater. A few craters on the order of hundred of meters in diameter exist on the inner wall. Mound-like feature (m) (~300-400m in thickness) is probably the result of down-slide movements of materials from the inner wall. Central hill (h) is ~200m in height and is associated with a terrace-like terrain (t) with several hundred meters scale craters. (**D**) A closer view of the rectangular area marked in (C). (**E**) The maximum temperature of the floor is ~ 88 K near the center, which is cold enough to retain water-ice, though we note that temperature information alone does not settle the problem of presence of water-ice on the lunar poles.

-ron depletions attributed to the hydrogen in the form of water molecules. The lunar poles exhibit epithermal neutron depletions attributed to the presence of water molecules [1]. Lunar Prospector data shows that the largest concentrations of hydrogen overlay regions in permanent shade. Near the South Pole, the inferred hydrogen content is enhanced within several 30-km-scale craters that are in permanent shade. Vilas et al. [17] found evidence for Fe-bearing phyllosilicates near the lunar South Pole that could have been formed by impacts into an ice-rich regolith. The formation of impact craters when H_2O is available can result in hydrated minerals and mobile element transport on the lunar poles [18]. Hydrated minerals could represent an important resource for future exploration of the solar system.

Remote Sensing w/ LROC, Diviner, etc.: Remote sensing may provide some clues, but only of the uppermost lunar surface. Whereas clays have distinct spectral features in the VNIR and TIR [*e.g.*, 20,21], water ice shares some of these features – hence, some are known as "hydration bands". However, we propose that whereas the water ice may be sparse or difficult to detect in the uppermost surface, alteration products might be found in the suevite layers of lunar ejecta blankets or inner-crater melt sheets. Whereas the South Pole and specifically Shackleton is listed as an LROC [2] and Mini-RF RADAR target [22], we propose that Diviner [23] target these regions with its three ~8 μm bands. Clays and glassy impact melts have different Christiansen Features than those of primary silicate minerals [23,24].

Summary: The possible existence of volatiles at the lunar poles has implications for future exploration. These sites may be of interest for future robotic or manned investigations where ejecta and soil geochemistry can be sampled in detail. Rather than a positive detection of water, the presence of phyllosilicates and other alteration minerals uncommon in lunar samples may provide constraints on water content in the lunar polar regolith.

References: [1] Feldman et al., *JGR-Planets*, 106, 23231-23251 [2] Joliff et al. (2009) *LPSC 40*, #2343 [3] Bart & Colaprete (2008) *LPSC 39*,#2225 [4] Shoemaker (1960) Impact mechanics at Meteor Crater, AZ, 55 pp., Princeton Univ., NJ [5] Pohl et al. (1977), in: *Impact and Explosion Cratering*, Pergamon Press, NY, pp. 343-404 [6] Hörz et al. (1983) *Rev. Geophys. Space Phys.*, 21, 1667-1725 [7] Grieve et al. (1977) in: *Impact and Explosion Cratering*, Pergamon Press, NY, pp. 791-814 [8] Fredriksson et al. (1973) *Science*, 180, 862-864 [9] Kieffer et al. (1976) *LPSC 7*, 1391-1412 [10] Watson et al. (1961) *JGR*. 66, 3033–3045 [11] Arnold (1979) *JGR*, 84, 5659–5668 [12] Saal et al. (2008) *Nature* 454, 192-195 [13] Harris et al. (2007) Bridging the Gap II, #8051 [14] Kieffer & Simonds (1980) *Rev. Geophys. Space Phys. 18*, 143-181 [15] Nozette et al. (1996; 2001) *Science* 274, 1495-1498; *JGR 106*, 106, 23253–23266 [16] Campbell & Campbell (2006) *Icarus 180*, 1–7 [17] Vilas et al. (1998; 1999) *Wrkshp New Views Moon*, #73*; LPSC 30*, #1343 [18] Stewart et al. (2001) *LPSC 32*, #2092 [19] Haruyama et al. (2008) *Science* doi:10.1126/science.1164020 [20] Poulet et al. (2005) *Nature*, *438*, 623-627 [21] Michalski et al. (2006) *EPSL 248*, 822– 829 [22] Bussey et al. (2008) *LPSC 39*, #2389 [23] Greenhagen and Paige (2009) *LPSC 40*, #2255 [24] Wright et al. (2009/10) *JGR*, submitted

DIVINER CONSTRAINTS ON PLAGIOCLASE COMPOSITIONS AS OBSERVED BY THE SPECTRAL PROFILER AND MOON MINERALOGY MAPPER. M. B. Wyatt[1], K. L. Donaldson Hanna[1], C. M. Pieters[1], J. Helbert[2], A. Maturilli[2], B. T. Greenhagen[3], D. A. Paige[3], and P. G. Lucey[4], [1]Brown University, Department of Geological Sciences, Box 1846, Providence, RI 02912 (michael_wyatt@brown.edu), [2]Institute for Planetary Research, German Aerospace Center DLR, Rutherfordstr. 2, Berlin-Adlershof, Germany, [3]University of California, Los Angeles, Department of Earth and Space Sciences, 595 Charles Young Drive East, Los Angeles, CA 90095, [4]University of Hawaii, Institute for Geophysics and Planetology, 1680 East-West Road, Honolulu, HI 96822.

Introduction: Near-infrared observations from the SELENE Spectral Profiler (SP) have been used to identify iron-bearing crystalline plagioclase in the central peaks of several large highland craters [1]. Recent image-cube data from the Chandrayaan-1 Moon Mineralogy Mapper (M^3) acquired across the Orientale Basin have also been used to identify iron-bearing crystalline plagioclase [2]. These observations are significant because they validate the near-infrared identification of plagioclase on the Moon.

Shocked plagioclase had been previously inferred from a lack of Fe^{2+} absorptions [3-5] in near-infrared measurements of high albedo locations as plagioclase can become sufficiently disordered with shock to lose its absorption bands [6]. The identification of iron-bearing crystalline plagioclase in the near-infrared comes from a broad absorption band at ~ 1.3 μm due to electronic transitions of Fe^{2+}. Near-infrared laboratory studies of this feature have suggested its band depth and center position may vary with Fe and An content respectively [7-9].

DIVINER: The upcoming Diviner Lunar Radiometer Experiment (DLRE) on the Lunar Reconnaissance Orbiter (LRO) will provide the first global coverage maps of thermal-infrared derived compositions on the Moon. Extensive thermal-infrared laboratory studies of plagioclase minerals and plagioclase-rich rocks indicate that both plagioclase abundances and compositions can be determined by linear deconvolution of mixed spectra [10-11]. However, Diviner has only three mineralogy spectral channels centered at 7.8, 8.2, and 8.6μm, so it is important to investigate the applicability of Diviner data for plagioclase composition studies.

In this study, we review thermal-infrared laboratory spectra of mineral endmembers, a mineral mixture, Apollo highlands, and Apollo mare soil samples convolved to Diviner spectral bands [12] and focus on the ability of Diviner data to distinguish plagioclase compositions.

Samples and Methods: Laboratory emissivity spectra of < 25 μm and > 90 μm grain size fractions of plagioclase, low- and high-Ca pyroxenes, olivine, and ilmenite used in this work are from the Berlin emissivity database (BED) [13]. A 50/50 wt% mineral mixture of endmembers anorthite and olivine is also examined.

Lunar soil samples are characterized by the Lunar Soil Characterization Consortium (LSCC) [14-15]. Apollo mare soil samples chosen for this study include 10084, 12001, 12030, 15041, 15071, 71061, 71501, 70181, and 79221 [14] and Apollo 16 highlands soil samples include 61141, 61221, 62331, 64801, 67471, and 67481 [15]. Apollo lunar soils are plotted in Figure 1 on a plagioclase-orthopyroxene-clinopyroxene ternary diagram [16]. Brown University's RELAB FTIR spectrometer was used to measure thermal-infrared spectra of each lunar soil sample for the 10 – 20 μm grain size fraction [17]. Thermal-infrared RELAB spectra are converted to emissivity using the approximation to Kirchoff's relation E=1-R. All thermal-infrared spectra are convolved to Diviner's three spectral bands using ENVI's spectral resampling tool.

The Diviner spectral bands were chosen specifically to measure the location of the Christiansen Feature (CF). The CF is an emission maximum, or reflectance minimum, first described as an indicator of compositions by [18]. The CF shift to shorter wavelengths for particulate materials in a vacuum environment is well constrained [19-20]. In this study, we calculate band ratios for each spectrum, assume that the CF shift applied to each spectral band is the same, and apply the ratios to accurately identify lunar compositions.

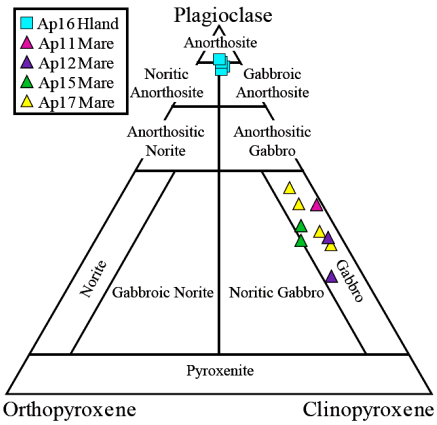

Figure 1. Highland soils are classified as anorthosite and mare as gabbro. It is important to note that anorthosite soils are not pure plagioclase, but contain small abundances of mixed pyroxenes (~ 4-10 total vol. %).

Thermal-Infrared Data: Recent work by [12] explored how to use Diviner band ratios for distinguishing fine-grained (< 25 μm) minerals, mineral mixtures and lunar soil samples. Figure 2 shows the 7.8/8.6 versus 8.6/8.2 Diviner band ratios for plagioclase, orthopyroxene, clinopyroxene, olivine, ilmenite, a 50/50 wt% plagioclase-olivine mixture, and lunar soil spectra [12]. Each mineral group is clearly distinguished using the 8.6/8.2 ratio with plagioclase plotting in the upper left (CF at shorter wavelengths) and olivine plotting in the lower right (CF at longer wavelengths). Mixture endmembers anorthite and olivine plot within their respective mineral groups, however the 50/50 mixture is indistinguishable from orthopyroxene and clinopyroxene. Work by [12] demonstrated that integrating Diviner thermal-infrared data with near-infrared spectral parameters (e.g. spectral curvature, integrated band depth, and band depth position) resolves these mineral mixture uncertainties. The Apollo highlands spectra plot closer to the plagioclase mineral group compared to Apollo mare spectra, consistent with its classification of anorthosite.

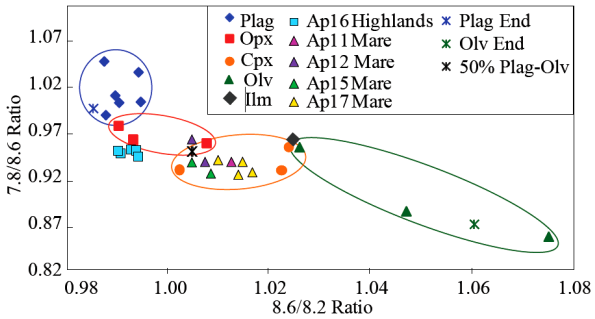

Figure 2. Simple band ratios 7.8/8.6 and 8.6/8.6 plotted against one another for individual minerals, a mixture of minerals, and lunar soils.

Plagioclase Focused Studies: The regions where crystalline plagioclase have been identified with SP and M^3 data are ideal locations on the Moon for Diviner data analysis. We now investigate the utility of Diviner data to distinguish different plagioclase compositions. It should be noted that this analysis is only applicable to the pure plagioclase regions on the Moon.

Figure 3 (top) shows a 7.8/8.6 ratio versus 7.8/8.2 ratio for coarse- (> 90 μm) and fine-grained (< 25 μm) plagioclase endmembers. The coarse- and fine-grained fields are distinguished due to the unique position and shape of the CF for each mineral composition. The middle and bottom sections of Figure 3 separate the coarse- and fine-grained fields to maximize the differences between each plagioclase composition. The 7.8/8.6 ratio versus 7.8/8.2 ratio clearly sets apart the plagioclase series with the Ca-rich anorthite plotting on the left and the Na-rich albite and oligoclase plotting on the right for both particle sizes. Intermediate compositions plot in the middle.

While it is not possible to determine the An # with these ratios, it is possible to distinguish Ca-rich, intermediate, and Na-rich compositions. This will be significant for constraining plagioclase compositions in the feldspathic highlands, specifically the distributions of ferroan anorthosite and alkali-suite materials.

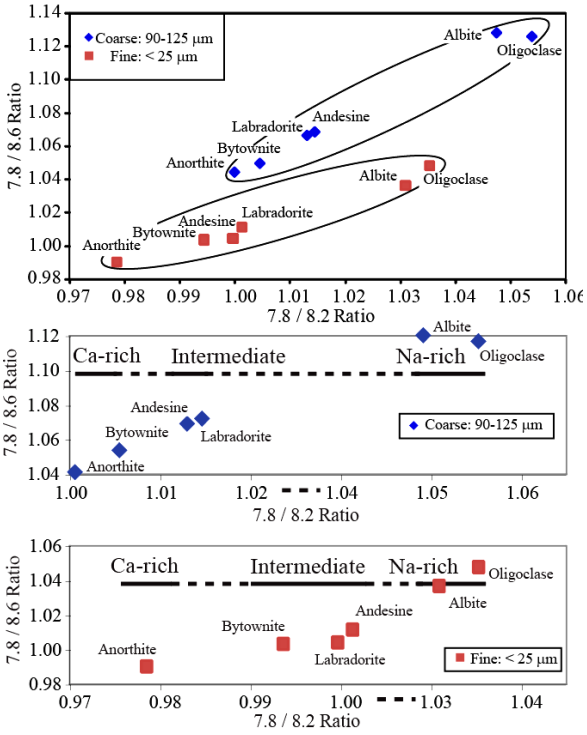

Figure 3. Simple band ratios 7.8/8.6 and 7.8/8.2 plotted against one another for plagioclase minerals.

References: [1] Matsunaga T. et al. (2008) *GRL, 35,* L23201. [2] Pieters C. et al. (2009) *LPSC XL*, Abstract #2052. [3] Spudis P. et al. (1984) *JGR, 89,* C197-C210. [4] Hawke B. R. et al. (2003) *JGR, 108,* (E6). [5] Tompkins S. and Pieters C. (1999) *Met. & Planet. Sci., 34,* 25–41. [6] Johnson J. and Horz F. (2003) *JGR, 108,* 5120. [7] Adams J. B. and McCord T. B. (1971) *PLPSC 3,* 2183-2195. [8] Bell P. M. and Mao H. K. (1973) *GCA, 37,* 755-759. [9] Cheek L. C. et al. (2009) *LPSC XL,* Abstract #1928. [10] Ruff S. W. (1998) *Ph.D. dis. ASU.* [11] Milam K. et al. (2004) *JGR, 109,* 4001. [12] Donaldson Hanna K. L. et al. (2009) *LPSC XL*, Abstract # 2286. [13] Maturilli A. et al. (2008) *Planet. & Space Sci., 56,* 420–425. [14] Taylor L. et al. (2001) *Met. & Planet. Sci., 36,* 285–299. [15 Taylor L. et al. (2003) *LPSC XXXIV,* Abstract #1774. [16] Stoffler D. et al. (1980) In *Proc. Conf. Lunar High. Crust,* 51-70. [17] Pieters C. and Hiroi T. (2004) *LPS XXXV,* Abstract #1720. [18] Conel J. (1969) *JGR, 74,* 1614-1634. [19] Logan L. M. et al. (1973) *JGR, 78,* 4983-5003. [20] Salisbury J. and Walter L. (1989) *JGR, 94,* 9192-9202.

NOTES

NOTES